

ELASTIC PLASTIC BEHAVIOUR OF A
SAND-BENTONITE MIXTURE

by

JAMES M. OSWELL

A Thesis
Submitted to the Faculty of Graduate Studies
in Partial Fulfillment of the Requirements for the Degree of
DOCTOR OF PHILOSOPHY

Department of Civil Engineering
University of Manitoba
Winnipeg, Manitoba

© March 1991



National Library
of Canada

Acquisitions and
Bibliographic Services Branch

395 Wellington Street
Ottawa, Ontario
K1A 0N4

Bibliothèque nationale
du Canada

Direction des acquisitions et
des services bibliographiques

395, rue Wellington
Ottawa (Ontario)
K1A 0N4

Your file *Votre référence*

Our file *Notre référence*

The author has granted an irrevocable non-exclusive licence allowing the National Library of Canada to reproduce, loan, distribute or sell copies of his/her thesis by any means and in any form or format, making this thesis available to interested persons.

L'auteur a accordé une licence irrévocable et non exclusive permettant à la Bibliothèque nationale du Canada de reproduire, prêter, distribuer ou vendre des copies de sa thèse de quelque manière et sous quelque forme que ce soit pour mettre des exemplaires de cette thèse à la disposition des personnes intéressées.

The author retains ownership of the copyright in his/her thesis. Neither the thesis nor substantial extracts from it may be printed or otherwise reproduced without his/her permission.

L'auteur conserve la propriété du droit d'auteur qui protège sa thèse. Ni la thèse ni des extraits substantiels de celle-ci ne doivent être imprimés ou autrement reproduits sans son autorisation.

ISBN 0-315-86070-7

Canada

ELASTIC PLASTIC BEHAVIOUR OF A SAND-BENTONITE MIXTURE

BY

JAMES M. OSWELL

A thesis submitted to the Faculty of Graduate Studies of
the University of Manitoba in partial fulfillment of the requirements
of the degree of

DOCTOR OF PHILOSOPHY

© 1991

Permission has been granted to the LIBRARY OF THE UNIVERSITY OF MANITOBA to lend or sell copies of this thesis. to the NATIONAL LIBRARY OF CANADA to microfilm this thesis and to lend or sell copies of the film, and UNIVERSITY MICROFILMS to publish an abstract of this thesis.

The author reserves other publication rights, and neither the thesis nor extensive extracts from it may be printed or otherwise reproduced without the author's written permission.

ABSTRACT

Two aspects of sand-bentonite behaviour are developed in this thesis. The first is an examination of the effective stress theories as they apply to this soil. A series of tests was carried out that showed that many rheological mechanisms can be characterized using the apparent effective stress (σ'), without direct knowledge of either the true effective stress (σ^*) or the repulsive/attractive stress balance ($R - A$). They are related by: $\sigma' = \sigma^* + (R - A)$.

The second aspect of the thesis is a study of the elastic plastic behaviour of a 50:50 sand-bentonite mixture. The dry densities of the specimens were either 1.49 Mg/m^3 or 1.67 Mg/m^3 . Triaxial compression tests were performed to determine the elastic moduli, the yield locus, flow rule and plastic potential, hardening law, and failure criterion.

The elastic behaviour of specimens in this study is isotropic (or only slightly anisotropic) in shear. It is believed that swelling prior to shear removes the anisotropy reported by other researchers that is initially induced by forming the specimens in a rigid mold.

The yield locus was examined in a variety of normalized stress-strain spaces. For the first time, this yield locus is normalized in volume space. The yield locus is the same for both specimen densities, and lies completely below the failure envelope in q, p' -plots.

Data showed evidence of early yielding in some specimens. This concept was developed based on similar behaviour observed in a natural clay. Early yielding suggests that two distinct, but essentially elastic (linear) regions exist.

The flow rule is non-associated: the plastic potential is different from the yield locus.

The hardening law was developed for both densities from end-of-consolidation data from 63 tests from this study and from previous researchers.

The shear data from this study is consistent with that of previous researchers.

Evidence of visco-plastic swelling is presented, from which a model is developed that predicts the effects of OCR and time on volume strain following isotropic stress release.

ACKNOWLEDGEMENTS

I wish to thank my advisor, Dr. James Graham, for his impetus and support for this research. His continuous encouragement, understanding and friendship helped immensely.

Others at the University of Manitoba helped me in many ways. Fellow graduate students F. Saadat, J.-H. Yin, and B.E. Lingnau provided helpful suggestions and discussions. Technical support was provided by N. Piamsalee, E. Lemke, and I. Trestral.

Useful discussions were held with staff at Atomic Energy of Canada, Pinawa - namely, A. Wan, B. Kjartanson, D. Dixon, and M. Gray.

Financial support during the three years of research was provided by a research contract from AECL, a Post-Graduate Scholarship (Natural Sciences and Engineering Research Council of Canada), the W.M. Stephens Memorial Fellowship (Manitoba Hydro), the John W. Davies Memorial Award (Society of Naval Architects and Marine Engineers - Arctic Section), and a Graduate Fellowship (University of Manitoba).

Finally, and most importantly, I would like to express my gratitude and love to my family who helped me in my studies. In particular, my wife Donna and sons Adam, Thomas, and Alexander; my father Michael Oswell; and parents-in-law Peter and Diane Tchir provided continuous encouragement and support. At the end of the day, they re-affirmed for me that family and friends are always the most important.

TABLE OF CONTENTS

	Page
ABSTRACT	i
ACKNOWLEDGEMENTS	ii
TABLE OF CONTENTS	iii
LIST OF FIGURES	viii
LIST OF TABLES	xiv
LIST OF SYMBOLS AND ABBREVIATIONS	xv
1. INTRODUCTION	1
1.1 General	1
1.2 Hypotheses	2
1.3 Objectives and Proposed Methodology of Research	3
1.3.1 Effective Stress Testing	3
1.3.2 Elastic Plastic Behaviour	4
1.4 Organization of Thesis	6
2. LITERATURE REVIEW	9
2.1 Introduction	9
2.2 Overview of Active Clay Structure and Behaviour	9
2.3 The Concept of Effective Stress	12
2.3.1 The Classical Concept of Effective Stress	12
2.3.2 Modification to the Effective Stress Principle	13
2.3.3 Synthesis of Literature	17
2.4 Elastic Plastic Soil Mechanics (EPSM)	18
2.4.1 General	18

2.4.2	Elastic Plastic Model Development	21
2.4.3	An Application of Elastic Plastic Theory	28
2.4.4	EPSM and Laboratory Studies	33
2.5	Review of Buffer Research	35
3.	EXPERIMENTAL EQUIPMENT, TEST MATERIALS AND SPECIMEN PREPARATION/INSTALLATION/REMOVAL	52
3.1	Equipment - Triaxial Cells	52
3.1.1	Standard Triaxial Cells	52
3.1.2	GDS Triaxial Testing System	53
3.1.3	High Pressure Isotropic Consolidation Cell	54
3.2	Equipment Peripherals	55
3.2.1	Axial Displacement Measurement (Non GDS Equipment)	55
3.2.2	Load Measurement	55
3.2.3	Pressure Measurement	56
3.2.4	Volume Change Measurement (Non GDS Equipment)	56
3.2.5	Data Acquisition System	56
3.3	Test Materials	57
3.4	Specimen Preparation and Installation Techniques	57
3.4.1	Specimen Preparation	57
3.4.2	Side Drain Permeability Study	58
3.4.3	Specimen Installation	59
3.5	Overconsolidation Procedure for Yielding Specimens	60
3.6	Post-Test Procedures	61
4.	EFFECTIVE STRESSES IN THE BUFFER	67
4.1	Introduction	67

4.2	Experimental Evidence in Support of the Effective Stress Concept	68
4.2.1	Undrained Stress-Change Tests	68
4.2.2	Drained-Isotropic Tests	70
4.2.3	Other Experimental Evidence	75
4.3	Discussion	76
5.	PRESENTATION OF YIELD AND END-OF-TEST DATA	89
5.1	Introduction	89
5.2	Incremental Stress Controlled Tests	92
5.3	Constant Rate of Strain Tests	94
5.4	Constant Rate of Stress Tests	95
5.5	Yield States of the Buffer	96
5.5.1	Analysis of Yield Data	96
5.5.2	Yield Locus and End-of-Test Data in q, p' -Space	98
5.5.3	Yield Locus and End-of-Test Data in V, p' -Space	103
5.6	Discussion and Summary	106
6.	EVALUATION OF ELASTIC PLASTIC PARAMETERS OF THE BUFFER	122
6.1	Introduction	122
6.2	Elastic Behaviour	122
6.2.1	Elasticity in Drained Shear	122
6.2.2	Elasticity in Undrained Shear	126
6.2.3	Elasticity in Swell under Isotropic Stress Conditions	129
6.2.4	Elasticity during Unload/Reload in Shear	130
6.3	Plastic Potential and Flow Rule	131
6.4	Hardening Law	134
6.5	Summary	135

7.	REVIEW AND MODIFICATIONS TO THE ELASTIC PLASTIC MODEL	156
7.1	Introduction	156
7.2	Review of the Original Model	157
	7.2.1 Elasticity	157
	7.2.2 Yielding	158
	7.2.3 Flow Rule and Plastic Potential	158
	7.2.4 Hardening Law	159
	7.2.5 Failure Criteria	160
7.3	Porewater Behaviour in the Buffer	160
	7.3.1 Porewater Behaviour with Isotropic Stress Application	161
	7.3.2 Porewater Pressure Behaviour during Shear	162
7.4	An Alternative Yielding Concept	164
	7.4.1 Introduction	164
	7.4.2 The Concept of Early Yielding	165
7.5	Visco-Plastic Swelling of the Buffer	167
	7.5.1 Introduction	167
	7.5.2 Conceptual Model of Visco-Plastic Swelling	168
	7.5.3 Implication for the Elastic Plastic Model	170
7.6	Concluding Remarks	172
8.	CONCLUSIONS AND SUGGESTIONS FOR FUTURE RESEARCH	182
8.1	Conclusions	182
8.2	Suggestions for Future Research	183
	REFERENCES	185
	APPENDIX A Specimen Dry Density, Moisture Content Data	193

APPENDIX-B The Use of Side Drains in Triaxial Testing at Moderate
to High Pressures

197

APPENDIX C Deviator Stress *versus* Shear Strain Data for Yield Tests

212

LIST OF FIGURES

	Page	
FIGURE 1.1	Components of the Canadian concept for nuclear fuel waste disposal (after Kjartanson and Gray 1987) (a) Schematic diagram of the underground vault for nuclear waste disposal. (b) Borehole emplacement sequence (all dimensions in millimeters).	8
FIGURE 2.1	Drucker-Prager yield criterion in 3-dimensional space (from Chen and Baladi 1985).	38
FIGURE 2.2	Flow rule concept.	39
FIGURE 2.3	Isotropic hardening in $\sigma_1, \sigma_2, \sigma_3$ -space (from Scott 1985).	40
FIGURE 2.4	Hardening law for modified cam-clay constitutive model.	41
FIGURE 2.5	Mohr-Coulomb failure criterion represent in 2-dimensions.	42
FIGURE 2.6	Mohr-Coulomb failure criterion in 3-dimension $\sigma_1, \sigma_2, \sigma_3$ -space.	43
FIGURE 2.7	Yield function predicted by Cam-clay constitutive model.	44
FIGURE 2.8	One dimensional consolidation of Winnipeg clay (from Graham and Au 1985).	45
FIGURE 2.9	Yield data for Winnipeg clay (a) in q, p' -space and (b) in normalized q, p' -space (from Graham, Noonan and Lew 1983).	46
FIGURE 2.10	Normalized yield envelope and plastic strain increment vectors for Winnipeg clay (from Graham, Noonan, and Lew 1983).	47
FIGURE 2.11	Normalized yield envelope for Winnipeg clay showing low stress strength, overconsolidation strength, and critical state strength (from Graham and Li 1985).	48
FIGURE 2.12	Normalized stress-strain data for buffer specimens. (a) T927 and (b) T931 (from Saadat 1989).	49
FIGURE 2.13	Normalized porewater pressure response <i>versus</i> normalized total mean pressure change (from Saadat 1989).	50
FIGURE 2.14	Swelling equilibrium pressure <i>versus</i> clay specific volume (Hardening Law) for buffer (from Graham <i>et al.</i> 1986).	51

FIGURE 3.1-	Photograph of Triaxial equipment. (a) Wykeham Farrance and Brainard Kilman equipment, (b) GDS stress path cell and controllers.	63
FIGURE 3.2	Schematic diagram illustrating the use of a differential pressure transducer as a volume change device.	64
FIGURE 3.3	Sieve analysis of blended sand used in buffer specimens.	65
FIGURE 3.4	Swelling equilibrium pressure <i>versus</i> moisture content of buffer (from Wan 1987).	66
FIGURE 4.1	Total (cell) and porewater pressures <i>versus</i> time under undrained conditions. Buffer specimen T1127.	78
FIGURE 4.2	Total (cell) and porewater pressures <i>versus</i> time under undrained conditions. Buffer specimen T1131.	79
FIGURE 4.3	Total (cell) and porewater pressures <i>versus</i> time under undrained conditions. Buffer specimen T1142.	80
FIGURE 4.4	Total pressure and apparent effective stress <i>versus</i> time under undrained conditions. Buffer specimen T1127.	81
FIGURE 4.5	Total pressure and apparent effective stress <i>versus</i> time under undrained conditions. Buffer specimen T1131.	82
FIGURE 4.6	Total pressure and apparent effective stress <i>versus</i> time under undrained conditions. Buffer specimen T1141.	83
FIGURE 4.7	Total (cell) and porewater pressure <i>versus</i> time during consolidation and undrained conditions. back pressure (top) during consolidation was 200 kPa. Buffer specimen T1199a.	84
FIGURE 4.8	Apparent effective stress <i>versus</i> specific volume of clay: buffer specimens (1100 series).	85
FIGURE 4.9	Apparent effective stress <i>versus</i> specific volume of clay: illite specimens.	86
FIGURE 4.10	Apparent effective stress <i>versus</i> specific volume of clay: Wyoming bentonite specimens.	87
FIGURE 4.11	Normalized stress-strain data for undrained triaxial compression test. T927 and T932. (from Saadat 1989).	88
FIGURE 5.1	The classical elastic plastic soil model in q, p' -space.	108

- FIGURE 5.2 Stress-strain parameters showing yielding for low density specimen (T1134). (a) q versus ϵ_s (b) σ_1' versus ϵ_1 (c) Work versus LSSV. 109
- FIGURE 5.3 Stress-strain parameters showing yielding for high density specimen (T1141). (a) q versus ϵ_s (b) σ_3' versus ϵ_3 (c) σ_1' versus ϵ_1 (d) Work versus LSSV. 110
- FIGURE 5.4 Schematic diagram illustrating potential errors in shear strain at yield associated with the yield deviator stress. 111
- FIGURE 5.5 Graphical method to determine p_y' at a pre-determined value of shear strain. (a) low density specimen T1134 (b) high density specimen T1141. 112
- FIGURE 5.6 Yield and end-of-test data for low density specimens. Failure envelope from Wan (1987) is shown for comparison. The solid lines are incremental stress controlled tests, the dashed lines are strain controlled tests, and the dash-dot lines are constant rate of stress tests. 113
- FIGURE 5.7 Yield and end-of-test data for high density specimens. Peak strength (short dashed line) and failure (long dashed line) envelopes from Saadat (1989) is shown for comparison. 114
- FIGURE 5.8 Normalized yield data for low and high density specimens with interpreted yield locus. The solid line is the yield locus assuming anisotropic elasticity. The dashed line is the yield locus portion assuming isotropic elasticity. 115
- FIGURE 5.9 Conceptual model for swelling of buffer on effective mean stress release. 116
- FIGURE 5.10 Yield locus for low and high density specimens in q, p' -space, normalized with respect to p_c' . An elliptical yield locus is shown. 117
- FIGURE 5.11 Yield and end-of-test data for low density specimens, plotted in V_c, p' -space. Critical state lines from Saadat *et al.* (1989) and Wan *et al.* (1990) are shown for comparison. 118
- FIGURE 5.12 Yield and end-of-test data for high density specimens, plotted in V_c, p' -space. The critical state line from Saadat *et al.* (1989) is shown for comparison. The light dashed line represents the peak strength line based on the data presented. 119

FIGURE 5.13	Yield locus for low density and high density specimens in $V_c, p_y/p'_c$ -space. The slope lines represent the yield loci for the different densities. The dashed lines represent interpolated yield loci based on limited data.	120
FIGURE 5.14	Normalized yield locus for high and low density specimens in $V_c, p_y/p'_c$ -space.	121
FIGURE 6.1	Predicted and measured elastic strain vectors for low density buffer. The predicted stains marked with arrows were removed from the error estimates in Table 6.2.	137
FIGURE 6.2	Predicted and measured elastic strain vectors for high density buffer. The predicted stains marked with arrows were removed from the error estimates in Table 6.2.	138
FIGURE 6.3	Normalized porewater response <i>versus</i> normalized total mean pressure change during undrained stress controlled shear. Buffer specimen T1125.	139
FIGURE 6.4	Normalized porewater response <i>versus</i> normalized total mean pressure change during undrained stress controlled shear. Buffer specimen T1128.	140
FIGURE 6.5	Normalized porewater response <i>versus</i> normalized total mean pressure change during undrained stress controlled shear. Buffer specimen T1130.	141
FIGURE 6.6	Normalized porewater response <i>versus</i> normalized total mean pressure change during undrained stress controlled shear. Buffer specimen T926 (unreported data from Saadat (1989)).	142
FIGURE 6.7	Shear strain <i>versus</i> volume strain during 3 day swelling under isotropic stress. Low density specimens (1100 series).	143
FIGURE 6.8	Shear strain <i>versus</i> volume strain during 3 day swelling under isotropic stress. High density specimens (1100 series).	144
FIGURE 6.9	Graphical method to determine plastic strains by separation of elastic strains (a) deviator stress <i>versus</i> shear strain, (b) effective mean pressure <i>versus</i> volume strain. Buffer specimen T1136.	145

FIGURE 6.10	Graphical method to determine plastic strains by separation of elastic strains (a) deviator stress <i>versus</i> shear strain, (b) effective mean pressure <i>versus</i> volume strain. Buffer specimen T1141.	146
FIGURE 6.11	Plastic strain increment vectors originating from yield stresses. Low density specimens, normalized with respect to p'_c . The dashed arrows denote initial interpretation of strain vectors for that test.	147
FIGURE 6.12	Plastic strain increment vectors originating from yield stresses. High density specimens, normalized with respect to p'_c . The dashed arrows denote initial interpretation of strain vectors for that test.	148
FIGURE 6.13	Plastic strain increment vectors for low and high density specimens.	149
FIGURE 6.14	Deviation of strain vectors from normality on the yield locus (normalized with respect to p'_c , as a function of stress path angle. (a) for low density specimens, (b) for high density specimens.	150
FIGURE 6.15	Plastic strain increment vectors originating from yield stresses. Low density specimens, normalized with respect to p'_c .	151
FIGURE 6.16	Plastic strain increment vectors originating from yield stresses. High density specimens, normalized with respect to p'_c .	152
FIGURE 6.17	Deviation of strain vectors from normality on the yield locus (normalized with respect to p'_c , as a function of stress path angle. (a) for low density specimens, (b) for high density specimens.	153
FIGURE 6.18	Proposed plastic potential for buffer data, normalized with respect to p'_c .	154
FIGURE 6.19	Hardening function for the buffer. Specific volume of clay fraction <i>versus</i> effective mean pressure (natural log scale). Additional data from Wan (1987) and Saadat (1989).	155
FIGURE 7.1	Pressure <i>versus</i> time data for (a) T1134, low density, and (b) T1141 high density specimens.	173

- FIGURE 7.2 Pressure *versus* time data for low and high density specimens. (a) T1145 and (b) T1136, low density, and (c) T1137 and (d) T1147, high density. The inset q, p' plots show the approximate stress path of each specimen during shear. 174
- FIGURE 7.3 Pressure *versus* time data for low and high density specimens during undrained shear. (a) T1128, low density, and (b) T1130, high density. 175
- FIGURE 7.4 Pressure *versus* time data for T1119, low density specimen. 176
- FIGURE 7.5 Yield locus and plastic potential for the buffer based on analysis from Chapters 5 and 6. The region subject to early yielding is denoted by the dashed section of the yield locus. 177
- FIGURE 7.6 Yield data (early) and rupture data in q, p' -space. The solid yield locus is the original "first" early locus developed in Chapter 5. The dashed yield locus is the "second" rupture locus. 178
- FIGURE 7.7 Conceptual model for visco-plastic swelling of the buffer due to large increment isotropic stress release. (same as Fig. 5.9) 179
- FIGURE 7.8 Volume strain *versus* overconsolidation ratio of the buffer, showing the effect of swell time. 180
- FIGURE 7.9 Deviator stress *versus* shear strain for high density specimens - T1130 undrained, and T1140 drained. 181

LIST OF TABLES

	Page	
TABLE 3.1	Statistical Data on Specimen Preparation of "Yielding" Specimens	58
TABLE 4.1	Effective Stress Tests: Undrained	70
TABLE 4.2	Effective Stress Tests: Drained	71
TABLE 5.1	Incremental Stress Controlled Tests	93
TABLE 5.2	Strain Controlled Tests	94
TABLE 5.3	Constant Rate of Stress Tests	95
TABLE 5.4	Yield Stresses for Buffer Specimens	99
TABLE 6.1	Elastic Parameters for the Buffer and Winnipeg Clay	124
TABLE 6.2	Errors between Predicted and Measured Elastic Strain Vectors	125
TABLE 6.3	Isotropic Elastic Moduli from Unload/Reload Data	131

LIST OF SYMBOLS AND ABBREVIATIONS

A	Total interparticle attractive force per unit area
a	Fraction of the total interparticle contact area. Subscripts: m = mineral-to-mineral contact; a = air phase; w = water phase
D_{10}, D_{85}	Particle diameter for which 10%, 85% of the material has a small diameter
CSL	Critical state line
c'	Effective Mohr Coulomb cohesion intercept
E	Elastic Young's modulus
f	Yield function
G, G^*	Elastic shear modulus, isotropic and anisotropic
H	Hardening function
I_1	First stress invariant
J	Elastic anisotropic coupling modulus
J_2	Second invariant of deviator stress
K, K^*	Elastic bulk modulus, isotropic and anisotropic
LSSV	Length of the stress vector
M	Invariant stress ratio at critical state
m	Porewater pressure parameter, $\Delta u/\Delta p$
N	Equilibrium specific volume corresponding to unit effective mean stress
NCL	Normal consolidation line
OCR	Overconsolidation ratio
p	Total mean stress $(\sigma_1 + 2\sigma_3)/3$
p'	Effective mean stress $(\sigma'_1 + 2\sigma'_3)/3$
Q	Plastic potential
q	Deviator stress $(\sigma_1 - \sigma_3)$

R	- Total interparticle repulsive force per unit area
R	Error between predicted and measured elastic strains
R^2	Correlation coefficient
SEL	Swelling equilibrium line
u	Porewater pressure
u_a, u_w	Average stress acting on the air and water phases
V, V_c	Specific volume, specific volume of the clay fraction
W	Work
w	Moisture content
γ_d	Dry density
ϵ	Strain
η	Stress ratio = q/p'
κ	Slope of unload/reload line in $V, \ln p'$ -space
λ	Slope of normal consolidation line in $V, \ln p'$ -space
ν	Poisson's ratio
σ	Stress
$\bar{\sigma}$	Average stress acting on the mineral phase
τ_{oct}	Octahedral shear stress
ϕ'	Effective Mohr Coulomb friction angle
ψ	State parameter for sands
Subscripts	
1,2,3	Principle, intermediate and minor (stresses)
c	Consolidation pressure (ie: p'_c)
c	Clay fraction (ie: V_c)
e	Equivalent (ie: p'_e)

m,p	Measured, predicted (elastic strains)
o	Initial conditions (prior to shear, ie: p'_0)
s,v	Shear, volume (strains)
y	Yield

Superscripts

e,p	Elastic, plastic (stresses and strains)
'	Apparent (effective stress)
*	True (effective stress)

CHAPTER 1 INTRODUCTION

1.1 General

The Canadian proposal for long term disposal of radioactive waste calls for the emplacement of the waste in underground vaults (Bird and Cameron 1982). See Fig. 1.1. The waste containers will be placed in large diameter boreholes in plutonic rock surrounded by several engineered barriers.

The barrier that will be placed between the container and the rock is a mixture of sand and sodium montmorillonite (also commonly called "bentonite"). This mixture was developed and "defined" at the Whiteshell Nuclear Research Establishment of Atomic Energy of Canada Ltd. (AECL) as the Reference Buffer Material (RBM or buffer) (Dixon and Gray 1985; Dixon and Woodcock 1986). The RBM comprises a 50:50 mix by weight of silica sand and Avonseal bentonite (produced by Avonlea Mineral Industries, Regina). The dry density to be used is 1.67 Mg/m^3 with a moisture content of approximately 21%. The dry density corresponds to an ASTM Modified Proctor Dry Density of 95%.

The buffer has several functions. One of the most important is to inhibit the migration of radionuclides from a leaking waste container to the surrounding bedrock. The buffer should also be "self-healing" so that any cracks or fractures that form will close themselves. The buffer should be easy to install and provide sufficient support for the waste containers. Finally, the buffer should be able to withstand or transmit to the bedrock, thermal gradients emitted from the containers. A complete review of the functions and desirable attributes of the buffer are found in Lopez (1985), Bechai, Mansson and Rao (1986), and Dixon and Woodcock (1986).

Computer modelling and simulation of the disposal scheme is part of the overall research program undertaken by AECL. To create the models, appropriate constitutive relationships for each component in the scheme (for example: containers, buffer, and bedrock) must be developed. Recent research at the University of Manitoba examined the use of a hypoelastic constitutive

model to represent the rheology of the buffer (Yin, 1990). Another potential relationship is based on elastic plastic soil mechanics, a powerful method of describing the stress-strain behaviour of clay soils. To use this model it is first necessary to determine the elastic plastic material parameters.

The buffer is likely to reach a saturated condition sometime after emplacement in the underground vault (Selvadurai and Au 1988). The role of porewater pressure, and its influence on the buffer will become important, particularly to the analysis and understanding of the strength and deformation behaviour. In "well behaved" soils, the concept of effective stress has been used to rationalize volume change and strength data that would otherwise appear unrelated. However, the role of effective stresses in active clays such as bentonite is a matter of some debate.

The primary objectives of this study are an examination of the buffer as an elastic plastic material, and an examination of the effective stress concept as it relates to active clays.

1.2 Hypotheses

Previous research on the buffer examined, in a general way, the role of porewater pressures and the applicability of the classical principle of effective stress. However, a critical appraisal of the previous work and its implication to buffer behaviour has not been fully documented. The thesis will therefore examine the hypothesis that a modified version of the classical theory of effective stress is generally applicable to the buffer under certain specified conditions.

Strength data for the buffer collected by previous researchers (Wan 1987, Saadat 1989) showed several characteristics typical of elastic plastic soil behaviour. However, the tests that were performed did not investigate all features of the elastic plastic model. As a starting point for this thesis, the hypothesis is made that the buffer behaves as an elastic plastic material and that the necessary parameters for an elastic plastic model can be determined from carefully

controlled laboratory tests. A major component of the thesis will be the presentation and discussion of data that assesses the applicability of elastic plastic modelling to buffer behaviour.

1.3 Objectives and Proposed Methodology of Research

Examination of the hypotheses that some form of effective stress theory can be used to rationalize buffer stress-strain data, and that the buffer behaves as an elastic plastic material provides the main goals for the research described in this thesis. The hypotheses will be examined using carefully controlled laboratory tests. The general approach used in this work is discussed below.

1.3.1 Effective Stress Testing

The applicability of the effective stress theory will be considered on several levels. Chapter 2 presents the classical theory and several modifications to the classical theory of effective stress. Modifications have been proposed when the soil has a large physico-chemical component that influences its behaviour. This is the case for bentonite. However, the direct application of many of the modified concepts implicitly (and sometimes explicitly) requires a knowledge of the magnitude of the physico-chemical forces acting at the microscopic level.

There are a number of indirect methods of checking the validity of the "effective stress" theory under equilibrium conditions. (Quotation marks around the term effective stress are used to avoid explicitly defining it as classical or modified.) Some introductory tests were performed by Wan (1987) and Saadat (1989). New tests have been designed and conducted in this program.

In one test series, specimens were subjected to high total confining pressures, under undrained conditions. That is, no volume change was permitted. Porewater pressures were measured at the top and base of the specimen. The total confining pressure was maintained until the porewater pressure reached a steady-state. The confining pressure could then be changed and

the porewater pressure response observed. Thus the "effective stress" within the specimen could be compared to the different total pressures applied.

A second test series examined the development of "effective stress" as a function of moisture content or specific volume of clay. Specimens with very high moisture content were built into triaxial cells and then subjected to a high total confining pressure. No drainage was permitted initially, and transducers measured the internal porewater pressures at the top and base of the specimens. After porewater pressures had stabilized, drainage (consolidation) of the specimen was permitted from the top and the specimen consolidated under the influence of the isotropic stress. The change in "effective stress" could be followed using the base porewater pressure transducer. This test was repeated for specimens at a variety of moisture contents that were formed in several different ways.

Some researchers suggest that the classical effective stress theory is inadequate to deal with high-swelling clays. On the other hand, the theories that require quantification of the physico-chemical forces at the molecular level may be unnecessarily complicated. The data from these two test series and data collected by Wan (1987) and Saadat (1989) will be used to show that a slightly modified classical effective stress concept rationalizes the rheological behaviour of the sand bentonite mixture.

1.3.2 Elastic Plastic Behaviour

The cornerstone of any elastic plastic model is the concept of yielding. Yielding is the limit of purely elastic behaviour, the boundary which separates recoverable elastic deformation from non-recoverable plastic deformation. All other considerations of the model stem from this concept.

Saadat (1989) presented data from several undrained strain controlled unload-reload compression tests. These data indicated an abrupt change in behaviour when the pre-existing

maximum shear stress was reached on reloading. This is interpreted as a first indication of yielding behaviour in the buffer. To examine the behaviour in more detail a series of tests was designed to determine the parameters needed in an elastic plastic model. These include elastic moduli such as bulk and shear moduli, the yield locus, the hardening law, the flow rule, and the failure criterion. The yield locus in q, p' -space and the more general State Boundary Surface are determined from stress probe tests. To achieve a particular stress probe (or "path") the cell pressure in a drained triaxial test is changed in a selected way relative to a change in the axial stress.

There are three methods of shearing specimens in triaxial tests. They are: (1) strain controlled tests, (2) constant rate of stress tests, and (3) incremental stress controlled tests. In strain controlled tests the axial strain rate is fixed, and the axial load is measured as a response to the strain. This test has the advantage that strain softening behaviour can be followed after the peak strength is reached. The disadvantage is that constant monitoring of the load and cell pressure must be carried out to achieve the desired stress path. (The concept of strain softening and other features of these tests are discussed in Chapter 5.)

In constant rate of stress tests, the specimen is sheared at a fixed rate of axial stress. Axial strain is a response to the applied stress. These tests also require constant monitoring and adjustment of the cell pressure to achieve the desired stress path. Because the test will continually seek a higher stress the axial strain rate will accelerate toward rupture. Therefore, strain softening behaviour will not be observed.

Incremental stress controlled tests are the easiest tests to perform. They are the tests traditionally used for examining yielding behaviour. Dead weights are added to the axial ram and the axial strain response measured. As with constant rate of stress tests, the axial strain rate is uncontrolled and will increase towards rupture. Strain softening behaviour is not observable. Although strain softening behaviour in these tests can not be examined with this procedure, the

yield stress for any stress path can still be found. Generally, the stress that produces sudden rupture is taken as the yield stress. In the case of strain hardening behaviour, several additional load increments can be added above the yield stress before the specimen is brought to rupture.

The elastic plastic parameters are obtained from a suite of yielding tests. The elastic moduli come from the pre-yield stress strain behaviour. The yield curve comes directly from the stresses at yield. The flow rule is found by examining the direction of the plastic strain increment vectors after yielding. The hardening law comes from performing consolidation tests under post-yield isotropic stresses. The failure criterion comes from the rupture and/or large strain end-of-test shear data.

1.4 Organization of Thesis

This thesis is organized as follows: Chapter 2 reviews literature pertinent to this research study. It begins with a brief discussion of clay mineralogy and behaviour. It describes possible volume change and stress transfer mechanisms in terms of mechanical or physico-chemical processes. Effective stress theories are discussed next. Shortcomings of the original theory as it relates to active clays are presented. Then modifications are introduced that attempt to incorporate the physico-chemical aspects of active clay behaviour. These modifications usually originate from double layer theory. A synthesis of effective stress literature is presented.

Elastic plastic soil mechanics (EPSM) is introduced and the constitutive parts defined. Application of one particular elastic plastic model to clays is described. Following sections relate EPSM to laboratory data.

Chapter 2 concludes with a review of buffer research as it relates to this program.

In Chapter 3, the experimental equipment, test materials, and general specimen preparation/installation/removal procedures are described. Initial moisture contents, dry densities, and saturations of the specimens are tabulated. A subsidiary study is presented on the efficiency

of side drains in triaxial testing.

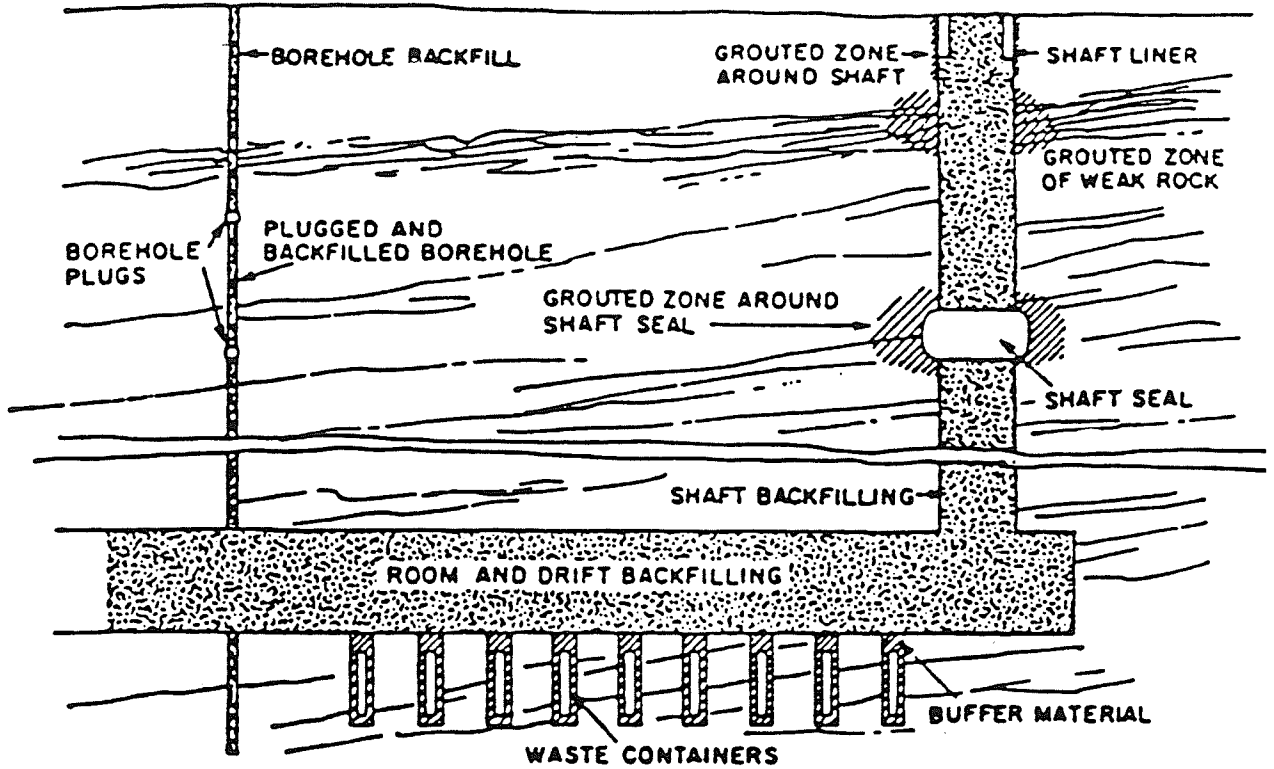
In Chapter 4, two series of newly developed effective stress tests are described and the results presented in detail. Data from other research on the buffer are used, together with this new data to show that a modified classical effective stress equation provides a rational approach to understanding stress-strain behaviour under certain limiting conditions. It will be shown that understanding or quantifying the physico-chemical forces in the buffer are not necessary.

The yielding tests used to develop the elastic plastic parameters are described in Chapter 5. The testing procedures and experimental design are given. Specimens of two densities have been tested. Examination of the test data has shown, for the first time, the existence of a yield locus in the buffer. Different sets of stress-strain parameters are used to examine the yielding behaviour. The yield locus is presented in q, p' -space and V_c, p' -space. New normalizing techniques are used to normalize specific volume data, and to examine the yield locus as a constant volume section of the state boundary surface. The failure or end-of-test data is also discussed.

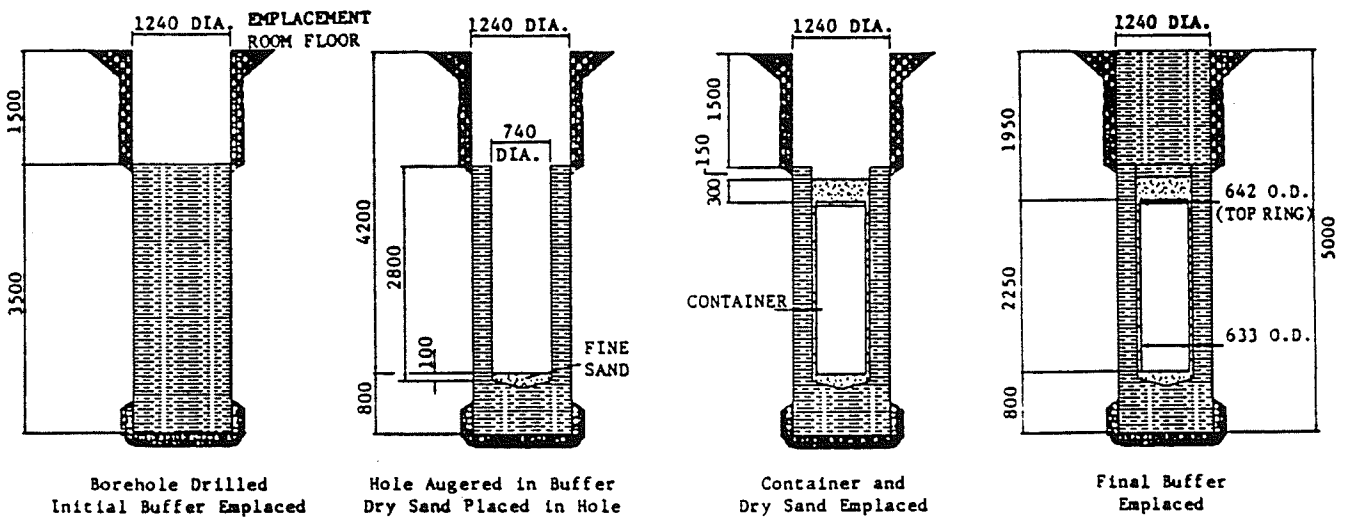
Chapter 6 evaluates the remaining elastic plastic parameters for the buffer. This section includes new, original work on determining the elastic moduli, the flow rule and plastic potential, and the hardening law.

The complete elastic plastic model is reviewed in Chapter 7. In following sections specific topics, identified in Chapters 5 and 6 will be expanded. These include porewater pressure behaviour, an alternate yielding criterion, and visco-plastic swelling behaviour of the buffer.

Chapter 8 presents conclusions and suggestions for further research.



(a) Schematic diagram of the underground vault for nuclear waste disposal.



(b) Borehole emplacement sequence (all dimensions in millimeters).

FIGURE 1.1 Components of the Canadian concept for nuclear fuel waste disposal (after Kjartanson and Gray 1987)

CHAPTER 2 LITERATURE REVIEW

2.1 Introduction

Chapter 1 presented two hypotheses about the behaviour of the sand bentonite buffer. Briefly, they stated that porewater pressures and strength behaviour can, in general terms, be interpreted using an effective stress principle, and that the buffer can be characterized as an elastic plastic material.

This chapter discusses the background of each hypothesis. In the case of effective stresses, different theories available from the literature will be discussed. The classical theory adequately describes the behaviour of granular soils and non-active clays. For active clays, modifications have been proposed to account for the apparent physico-chemical forces acting in their adsorbed water layers.

For elastic plastic theory, the general requirements of the theory will be given, followed by a mathematical development of a general elastic plastic model. One particular soil model based on elastic plastic theory will be discussed in detail. Elastic plastic theory will then be shown to be useful for interpreting and understanding laboratory test data. A major portion of this thesis will investigate if the buffer can be modelled as an elastic plastic material.

Chapter 1 stated that the sand and bentonite represent equal portions of the mixture by weight. However, it is the bentonite that dominates the rheological behaviour of the buffer (Dixon, Gray, Baumgartner, and Rigby 1986). The behaviour of bentonite is complex and it is useful at the beginning of this thesis to overview its nature and properties.

2.2 Overview of Active Clay Structure and Behaviour

This section presents only those features of clay structure and behaviour that relate to the porewater pressure, or the stress strain behaviour of bentonite. More detailed treatments of clay mineralogy and clay properties are presented elsewhere, for example by Yong and Warkentin

(1975) and Mitchell (1976).

Bentonite (also known as sodium montmorillonite) is an active clay belonging to the smectite group of minerals (Gillott 1987). Active clays have a high ratio of plasticity index to the fraction of clay size particles. For comparison, smectites have activities of 1 to 7 compared to kaolinites, which have activities of about 0.5 (Mitchell 1976). The most notable property of bentonite is its ability of absorb large volumes of water.

Smectite clay particles possess a net negative surface charge as the result of ionic substitutions in the crystal lattice. (The edges possess a positive charge.) A montmorillonite platelet has a thickness of approximately 10 Å (Yong and Warkentin 1975). Individual platelets are not tightly bonded to each other and will easily separate when water is available. This behaviour contrasts with that of kaolinite, which have platelet thicknesses of 7.2 Å that are well bonded to each other. Kaolinite units may be up to 1000 Å thick (Bailey 1965).

When dry bentonite at low confining stress is exposed to water, the individual platelets will hydrate, permitting water molecules to enter between the platelets. Water is a polar molecule; hence the positive side of the water dipole will be attracted to the negatively charged clay surface. In addition, hydrogen atoms in the water will try to form hydrogen bonds with any exposed oxygen atoms on the clay surface (Yong and Warkentin 1975).

Water can exist in a clay in three different forms (Cheung, Gray, and Dixon 1985). The water layer immediately adjacent to the clay surface is called the "Stern" or "surface water" layer. This layer may be only several water molecules thick. The water molecules in this layer are tightly bound to the clay and the layer is highly viscous. Water molecules are free to move laterally, but have difficulty moving away from the clay surface (Yong and Warkentin 1975).

Between the clay platelets, beyond the surface layer, is "interlayer" water. This water is less tightly bound to the clay mineral, less viscous than the surface water, but more viscous than normal free water. This layer is also called the "double layer". The Stern layer, together

with the double layer is called the "adsorbed water layer". The adsorbed water layer is important in understanding clay behaviour, and will be discussed in greater detail in following paragraphs.

Water occupying the larger pores, and unaffected by the clay mineralogy is called "free" or "interstitial" water. Its behaviour and properties are the same as porewater in granular soils.

Stress transfer and volume change behaviour are controlled by the crystalline structure of the clay particles and the surrounding water layers. These two phenomena are closely linked. To understand stress transfer in active clays, it is first necessary to understand the swelling and volume change mechanisms. The discussion will be restricted to isothermal conditions.

Olson and Mesri (1970) identified two processes that control volume changes in clays. One is the "mechanical" process. This includes volume changes that result from particle diminution (crushing at high pressures), particle deformation (bending of platy particles), and particle reorientation (rotation and translation) (Bailey 1965; Balasubramonian 1972). The mechanical process acts in the same manner in clays as in granular soils.

The second process is "physico-chemical". In this case volume change is explained by changes in double layer thicknesses. Olson and Mesri (1970) examined the swelling of several pure clays. They concluded that one or the other of these two processes usually dominated volume change behaviour. For kaolinite, mechanical processes controlled volume change. In smectites (Na montmorillonite), they found that physico-chemical processes dominated behaviour. Illite is mineralogically between kaolinite and montmorillonite, and its behaviour appeared to be a mixture of the two processes. Taken individually the processes fail to explain clay behaviour in many situations. The two-process volume change theory provides a clearer picture of swelling or compression behaviour.

Physico-chemical volume changes in clay depends on the thickness of the double layer. Double layer theory was developed originally by Chapman (1913) and Gouy (1919). The theory assumes a parallel, widely spaced platelet structure. Estimates of the double layer thickness, and

the repulsive force acting between two platelets can be made using the theory. Implicit in the application of the theory is that the magnitude of the attractive forces (A) in the double layer is small compared to that of the repulsive forces (R).

Bailey (1965) reviewed the source of the repulsive and attractive forces. The repulsive forces arise from several sources. One is the repulsion of dissolved anions from the negatively charged clay surface. A second is due to osmotic forces. Since the cation concentration varies in the water layers surrounding the platelets, a gradient is set up that attempts to equalize the concentration of ions. Hence an osmotic pressure gradient is induced between the clay platelets, which tries to force the platelets apart.

The attractive forces between adjacent clay platelets are attributed primarily to London-van der Waals forces (Bailey 1965). These forces are proportional to the inverse cube of the particle half space (d^{-3}). As the particles get closer together, the attractive forces rise sharply.

Examination of the double layer theory reveals several factors that influence the thickness of the double layer. These factors include absolute temperature, cation valency, cation concentration in the interlayer and free pore fluids, and the dielectric constant of the pore fluids. Data by Olson and Mesri (1970), Mitchell (1976), Sridharan and Venkatappa Rao (1973), and others show the effects of many of these factors on volume change behaviour.

2.3 The Concept of Effective Stress

2.3.1 The Classical Concept of Effective Stress

The importance of pore fluid pressure on the rheological behaviour of soils was first recognized by Terzaghi in the 1920's (see for example Terzaghi 1936). Terzaghi's understanding of effective stress grew over a number of years during his research on the consolidation of clays. The concept, now often upgraded to a "principle", was implicit in his writings of 1921, but was

not formally expressed until 1924 (Skempton 1960a). ("Principle" will be used in following sections.)

The principle of effective stress for saturated soils, as it is generally accepted today, has two parts. The first part states that the total stress imposed on a soil is carried by the tensor sum of the average stress carried by the soil skeleton, and the hydrostatic pressure within the soil voids. The former stress is called the effective stress. Hence,

$$[2.1] \quad \{\sigma\} = \{\sigma'\} + u\{I\}$$

where σ is the total stress, σ' is the effective stress, u is the porewater pressure and $\{I\}$ is the identity matrix. (A list of symbols is given on page xv.) Stress in the context of this discussion is defined as the force supported by a small finite area of the total material, including both soil particles and water. If the force transmitted through the area is carried by the soil particles, the corresponding stress is the "effective stress". If the force transmitted through the area is carried by both the soil particles and the water, the corresponding stress is the "total stress".

The second part of the principle states that the effective stress, not the total stress, controls shear strength and volume change behaviour.

Modern soil mechanics is, in large part, founded on the principle of effective stress. Simple experiments show that the classical principle is valid within the degree of accuracy required for most design applications (Mitchell 1976). Skempton (1960b) showed however, that the classical relationship is only an approximation. The relative compressibility of the solid phase to the whole soil should be considered. Skempton concluded that for saturated soils this was of little significance, but needed to be considered in the case of rock and concrete.

2.3.2 Modifications to the Effective Stress Principle

In the 1950's the applicability of the classical effective stress principle to active clays was questioned. Lambe and Whitman (1959) reviewed the evidence at the time and concluded that

for active clays the classical equation required an additional term to account for the physico-chemical behaviour. This new term would account for the molecular repulsive and attractive pressures within the double layer.

Lambe (1958) introduced the repulsive/attractive pressure balance (R - A) into the effective stress equation. His original formulation was:

$$[2.2] \quad \sigma = \sigma' + u = I + (R - A)$$

where σ = total stress, σ' = effective stress, u = pore pressure, I = interparticle contact pressure through the Stern layer, and (R - A) = net balance of long range repulsive and attractive pressures.

Equation [2.2] was succeeded (Lambe 1960) by a form that considered equilibrium over a unit area:

$$[2.3] \quad \sigma = \underline{\sigma}a_m + u_a a_a + u_w a_w + (R - A)$$

where a_m , a_a , a_w = ratio of cross sectional areas of the mineral, air and water phases respectively. $\underline{\sigma}$, u_a , u_w = average stresses acting on the mineral, air and water phases respectively.

For saturated soils [2.3] reduces to:

$$[2.4] \quad \sigma = \underline{\sigma}a_m + u_w(1 - a_m) + (R - A)$$

For the case where a_m is very small and $u_w a_m$ approaches zero,

$$[2.5] \quad \sigma = \underline{\sigma}a_m + u_w + (R - A)$$

In this equation $\underline{\sigma}a_m$ represents the stress transfer by interparticle contact, u_w represents the porewater pressure and (R - A) represents the amount of stress transfer by physico-chemical processes.

Balasubramonian (1972) rewrote [2.5] as:

$$[2.6] \quad \sigma = \sigma' + u = \sigma^* + u + (R - A)$$

$$[2.7] \quad \sigma' = \sigma^* + (R - A)$$

Here σ' is the "apparent" effective stress and σ^* is the "true" effective stress.

Balasubramonian (1972) separated mechanical volume change processes from physico-chemical processes. He extended the work of Olson and Mesri (1970), who earlier recognized the importance of the two processes on active clay behaviour.

The (R - A) term in [2.6] and [2.7] represents the effect of changes in the physico-chemical environment. The (R - A) term changes when factors such as cation concentration, salinity or dielectric constant of the pore fluids, or temperature change. Changes in these factors will create gradients that will try to equalize throughout the system. This equalization process will manifest itself as a change in the double layer thickness and hence a change in clay volume. When equilibrium in the physico-chemical environment is re-established, the clay platelets will generally have a different average spacing. (R - A) is a fixed value (constant) whenever the physico-chemical environment is in equilibrium. As well, when external loading is accompanied by the opportunity to absorb or expell water, the average particle separation changes and so does the (R - A) term. When (R - A) diminishes to zero, as in the case of granular soils, the apparent and true effective stresses as defined by Balasubramonian are the same.

The net repulsive pressure (R - A) can be calculated using Gouy-Chapman theory. (see for example Mitchell 1976). This approach was used by both Balasubramonian (1972), who studied two western Canadian clays, and Chattopadhyay (1972), who studied the residual strength of several pure clays.

Equations [2.6] and [2.7] represent the combination of two distinct mechanisms that control volume change and stress transfer. Bailey (1965) said that the two mechanisms could be separated according to particle spacing. The short range mechanism was the interparticle contact, or the true effective stress (σ^*) given by Balasubramonian. The long range mechanism was the (R - A) balance. Bailey treated the mechanisms as independent, and essentially "on/off" in

nature. Moreover, he strongly suggested that the two mechanisms do not overlap. This belief was also shared by Balasubramonian (1972). The author does not share this position. Bailey's view seems to be a convenient simplification of the problem. There is no *a priori* reason that the two mechanisms should not overlap, particularly in a real soil where clay platelets are not arranged in a convenient parallel fabric.

The change of stress transfer mechanism from one to the other has been generally based on particle spacing. Many researchers (for example Leonards and Andersland 1960; Bailey 1965; Balasubramonian 1972) used a particle spacing ($2d$) of 20 \AA as the criterion to separate the ranges of the two mechanisms. Intuitively it is understandable that the true effective stress might act only at close particle spacings, and would be inoperative at large particle spacings. It is much less certain that the (R - A) pressure acts only in the long range but not at very close particle spacings. The implication of this latter statement is that at very close spacings $R = A$. Although Bailey in his review of the literature attempted to support this line of thought, his support was rather tenuous.

Recently, Barbour (1987) and Barbour and Fredlund (1989) discussed osmotic consolidation in terms of changes in (R - A). They found that (R - A) could be indirectly measured during one dimensional consolidation. The soils they tested were Regina clay and a sand-bentonite mixture (different from the mixture used in the present research program). They then attempted to calculate (R - A) as a function of vertical stress. At first glance the experimental and calculated results are remarkably similar. In order to calculate (R - A) the specific surface area of the soil is needed. For the bentonite alone, a specific surface area of 700-840 m^2/g is reported. For the sand-bentonite mixture a specific surface area of 140-168 m^2/g is given. However in the calculation of the theoretical (R - A), a specific surface area of 580 m^2/g was used for the sand-bentonite mixture. If the reported specific surface area of 140-168 m^2/g was used in the calculations the correlation between the experimental and theoretical curves

would be much lower.

2.3.3 Synthesis of Literature

In spite of all the research done in the past several decades the question of the applicability of the classical effective stress principle to active clays remains confused. The work by Olson and Mesri (1970), Balasubramonian (1972), Sridharan and Venkatappa Rao (1973), Barbour (1987) and others link changes in physico-chemical factors to volume change and shear behaviour. However, if an active clay remains in physico-chemical equilibrium during changes in applied external stress, then any changes in volume or strength are due to the true effective stress. Furthermore, if $\Delta(R - A) = 0$ then $\Delta\sigma' = \Delta\sigma^*$.

Diffuse double layer theory assumes a parallel plate structure. This assumption is not appropriate for many clays, most notably natural clay deposits. In reality, clay platelets in most natural and laboratory prepared samples would have a semi-flocculated, card house structure. Some adjacent platelets would be parallel, but many would be in end-to-side, or end-to-face contact. Particles may be parallel in discrete "packets" or "peds" in the soil but the packets may not all have the same alignment. Such a random arrangement requires that any calculation of particle spacing be of a gross average. There would likely be a very wide range of actual spacings.

A variation in particle spacing implies that stress transfer by interparticle contact and physico-chemical forces act at the same time. Some stress transfer will be by long range physico-chemical pressures, while the rest will be short range interparticle contact. So long as the physico-chemical environment remains at equilibrium, a change in Balasubramonian's true and apparent effective stresses will have the same effect on the specimen. That is, the classical and modified effective stress equations will predict the same behaviour of a specimen when the $(R - A)$ pressure is fixed, and the "base line" physico-chemical pressure previously established.

If the base line physico-chemical pressure changes due to a change in the physico-chemical environment, then the change in $(R - A)$ must be accounted for if any comparisons of behaviour of pre- and post-change conditions are to be made.

The discrepancy between the theoretical and experimental data for $(R - A)$ reported by Barbour (1987) and Barbour and Fredlund (1989) illustrates a serious flaw in the physico-chemical approach to effective stresses. To be fair, their selection of variables to achieve the desired results is perhaps more common than not. True class A predictions (Lambe 1973) are rare. The point to be made is that engineers and scientists do not have the means to accurately measure the variables by which $(R - A)$ can be calculated. Instead of examining effective stresses on a micro-scale, as inferred by the physico-chemical approach, it seems more reasonable to examine this problem on a wider, macro-scale. This examination will be presented in Chapter 4.

2.4 Elastic Plastic Soil Mechanics (EPSM)

2.4.1 General

Elastic plastic constitutive models were first applied to metals and later extended to soils. The premise is that strains and stresses are composed of two parts; an elastic component and a plastic component, that can be added together to give the total stress or strain. Further, it is assumed that there exists in stress and strain space a region where straining is essentially elastic. The region is bounded by a yield surface on which plastic deformations will occur.

If the stress state of a specimen lies within the yield surface all strains are considered to be elastic, and therefore recoverable. If the stress state lies on the yield surface then the total strain has both elastic and plastic components. Plastic strains are by definition, permanent and non-recoverable. States of stress outside the yield surface cannot exist.

There are important differences between metal plasticity and soil (clay) plasticity. The

first difference concerns "virgin loading". When a piece of metal, fresh from the foundry is initially loaded its response will be elastic. If the load is less than its yield stress then unloading will produce no permanent deformation. The metal will, as a result of its smelting, have a predetermined yield stress. Clay behaves differently. A clay laid down by sedimentation, either as a river carrying sediment enters a lake, or from a laboratory prepared slurry, is termed normally consolidated. That means it has no history of higher stresses, just as with the "virgin" metal. However, when loaded the clay will immediately begin accumulating plastic strains. If the clay is then unloaded the elastic component of the total strain will be recovered, while the plastic strain will not be recovered. If the clay is reloaded, all strains up the previous maximum load will be elastic. Straining of clays depends on the previous history of stressing. The general behaviour of metals and clays after initial loading is similar. Clays that have experienced unloading are termed overconsolidated.

A second difference between metals and soils has to do with the application of hydrostatic stress. For metals it is generally accepted that application of a hydrostatic stress ($\sigma_1 = \sigma_2 = \sigma_3$) will not result in either yielding or failure. Theoretically, a metal specimen can withstand infinite hydrostatic stress. On the other hand, overconsolidated soils (especially in a drained condition) will yield when the hydrostatic stress reaches a pre-defined yield stress.

A third difference between soils and metals is in their constitutive phases. Metals are essentially single phase - solid. Soils have usually two (and sometimes three or more) phases - solid soil minerals, liquid water, and air or water vapour. The compressibilities of the solid and liquid phases are very low compared to that of the gaseous phase(s).

The final difference deals with composition. Metals are usually considered to be isotropic in composition. Thus the stress-strain behaviour is the same regardless of the axis of loading or orientation. Soils on the other hand are usually considered isotropic only for analytical convenience. In fact, very few natural deposits or laboratory prepared specimens are isotropic.

In the horizontal plane the behaviour may indeed be isotropic. However, the behaviour on the horizontal plane compared to the vertical plane is different. This special case of anisotropy is called "transverse" isotropy or cross anisotropy (Barden 1963).

In spite of these differences, the basic concepts of elastic plastic theory apply equally to both soils and metals. The differences are in details, not fundamentals.

Scott (1985) described the development of plasticity theory and its introduction to soil mechanics. Drucker, Gibson and Henkel (1955) first developed a comprehensive plasticity theory for soils. A few years later a series of soil plasticity models was developed at Cambridge University. One feature of these models was the concept of a unique condition (the so-called "Critical State") achieved by shear straining to high displacements. At high strains, the changes in porewater pressure, volume strain, and deviator stress relative to shear strain are zero. The Cambridge elastic plastic models have been grouped together to form Critical State Soil Mechanics (Roscoe, Schofield and Wroth 1958; Schofield and Wroth 1968; Roscoe and Burland 1968). This group of soil models is being increasingly used today in computer modelling of geotechnical problems.

Several other plasticity models have been developed in recent years. There are essentially two other common variations of the Drucker theme (Iwan and Chelvakumar 1988). They are multiple yield surface models (the Critical State models are single yield surface models) and bounding surface models. The multiple yield surface models incorporate several yield surfaces that can expand or shift position in stress space. As one inner yield surface moves and encounters an outer yield surface the parameters controlling the model become those of the outer yield surface.

Bounding surface models permit non-recoverable strains to occur while lying within the boundary surface. This is achieved by utilizing a plastic modulus that is a function of the distance from the current stress state to the bounding surface (Dafalias and Herrmann 1980).

There are four requirements for an elastic plastic model. They are: knowledge of the elastic parameters (for example, Young's modulus and Poisson's ratio), a yield surface, a flow rule, and a hardening law. In addition, it is convenient to have knowledge of a failure criterion, but it is not, strictly speaking, necessary. In the next section each of these parts will be developed for the general case.

2.4.2 Elastic Plastic Model Development

To begin, it is necessary to define a system of stresses and strains. The principal stresses acting on a specimen are denoted as $\sigma_1, \sigma_2, \sigma_3$ where, unless otherwise noted, σ_1 represents the major stress, σ_2 represents the intermediate stress, and σ_3 represents the minor stress.

The principal strains produced as a result of changes in stress are given as $\epsilon_1, \epsilon_2, \epsilon_3$ occurring in the same direction as $\sigma_1, \sigma_2, \sigma_3$ respectively.

Compressive stresses and strains are considered positive; tensile stresses and expansive or dilative strains are considered negative.

The mean stress acting on a specimen is given by $p = (\sigma_1 + \sigma_2 + \sigma_3)/3$. In a triaxial condition where $\sigma_2 = \sigma_3$ this reduces to $p = (\sigma_1 + 2\sigma_3)/3$. This is a variation of the first stress invariant (I_1) used in continuum mechanics. In terms of classical effective stresses where $p' = p - u$ (where u is the porewater pressure), $p' = (\sigma_1' + 2\sigma_3')/3$.

The deviator stress in a triaxial condition is given as $q = q' = \sigma_1 - \sigma_3$. The deviator stress is a variation of the second deviator stress invariant.

The volume strain for a triaxial condition is $\epsilon_v = \epsilon_1 + 2\epsilon_3$. The shear strain for a triaxial condition is then defined by $\epsilon_s = 2(\epsilon_1 - \epsilon_3)/3$ to retain an appropriate specification of energy absorption in the specimen.

The premise of elastic plastic theory is that strains may be divided into two components comprising recoverable elastic strains and non-recoverable plastic strains. All other

considerations in the theory, including yielding, stem from this premise. Using the notation defined above, $\epsilon = \epsilon^e + \epsilon^p$ in general; and $\epsilon_v = \epsilon_v^e + \epsilon_v^p$ and $\epsilon_s = \epsilon_s^e + \epsilon_s^p$ in particular. The superscripts e and p represent elastic and plastic strains respectively. The subscripts v and s represent volume and shear strains respectively.

2.4.2.1 Elastic Parameters

Elastic strains are recoverable. When an elastic stress increment is removed, the specimen will return to its initial size and shape. For an ideal elastic material, the specimen has no "memory" of its loading and unloading experience. Linear isotropic elastic behaviour is most commonly described by Hooke's Law, using the elastic constant Young's Modulus (E) to relate stress and strain. As the specimen is stressed it might change shape. Poisson's ratio (ν) relates the radial strain to the axial strain.

Two alternative elastic constants often used in soil mechanics are the bulk and shear moduli, denoted K and G respectively. These moduli are related to E and ν by:

$$[2.8] \quad K = \frac{E}{3(1 - 2\nu)}$$

$$[2.9] \quad G = \frac{E}{2(1 + \nu)}$$

The isotropic bulk and shear moduli relate changes in volume and shear strains to the mean stress and deviator stress respectively. Written in matrix notation the relationship for isotropic materials is:

$$[2.10] \quad \begin{bmatrix} p' \\ q \end{bmatrix} = \begin{bmatrix} K & \\ & 3G \end{bmatrix} \begin{bmatrix} \epsilon_v \\ \epsilon_s \end{bmatrix}$$

The moduli are uncoupled in linear isotropic elasticity.

The bulk modulus in [2.10] is given in terms of effective stresses. This is because the modulus is different for drained and undrained conditions, and because volume straining in soils cannot be systematically related to total stress changes. By setting ϵ_v to zero in [2.10], it can be shown that for an undrained case, the bulk modulus (K_u) is infinite, or in practice equal to the bulk stiffness of water. Conversely, changes in the mean effective stress clearly produce finite volume strains, so K' must likewise be finite.

The preceding discussion of elastic behaviour applies only to isotropic materials. Soils however are usually anisotropic. Graham and Houlsby (1983) developed a set of three elastic parameters for a transversely isotropic (or cross anisotropic) natural clay. They modified [2.10] to account for shear strains produced by changes in the effective mean stress and volume strains produced by changes in the deviator stress. The revised formulation was:

$$[2.11] \quad \begin{bmatrix} p' \\ q \end{bmatrix} = \begin{bmatrix} K^* & J \\ J & 3G^* \end{bmatrix} \begin{bmatrix} \epsilon_v \\ \epsilon_s \end{bmatrix}$$

The asterisks emphasize that these bulk and shear moduli are different from their isotropic counterparts. The cross anisotropic modulus is J . As a minimum, two drained triaxial tests of different slopes in stress space (q, p') are required to solve for the constants in [2.11]

2.4.2.2 Yield Criteria

Yielding is the state of stress such that plastic strains occur. For an ideal plastic material, yielding is a function of stress level alone, and not of the stress increment that produced yielding. Mathematically the function is written as $f(\sigma_{ij}) = 0$. In more general conditions, yielding may be a function of stress, strain and energy (work) absorbed by the specimen. Thus, $f(\sigma_{ij}, \epsilon_{ij}^p, W^p) = 0$. If the stress state of a specimen is in the elastic region, then $f(\sigma_{ij}) < 0$. Conditions where $f(\sigma_{ij}) > 0$ are not possible.

Numerous yield criteria have been proposed. Most were developed for metal plasticity. The Tresca (1868) and von Mises (1913) criteria are two of the most common. Drucker and Prager (1952) developed a yield criterion for soils.

Tresca (1868) proposed that metal yields when the maximum shear stress exceeds a threshold level. In its simplest form the yield criterion is:

$$[2.12] \quad f(\sigma_{ij}) = \frac{(\sigma_1 - \sigma_3)}{2} = k \quad (\text{constant})$$

The intermediate stress is not considered in this criterion.

The von Mises (1913) criterion is based on the second deviatoric stress invariant reaching a threshold value (Valliappan 1981). Based on the derivation by Spencer (1968) the criterion is:

$$[2.13] \quad (\sigma_1 - \sigma_2)^2 + (\sigma_2 - \sigma_3)^2 + (\sigma_3 - \sigma_1)^2 = \text{constant}$$

Using the concepts of continuum mechanics the above criterion is a function of the second invariant of the deviator stress (J_2). In terms of principal stresses,

$$[2.14] \quad \frac{1}{6}[(\sigma_1 - \sigma_2)^2 + (\sigma_2 - \sigma_3)^2 + (\sigma_3 - \sigma_1)^2] = k^2$$

This criterion can also be written in terms of the octahedral shear stress as: $\tau_{\text{oct}}^2 = \frac{2J_2}{3} = \frac{2}{3}k^2$.

The von Mises criterion has two advantages over the Tresca criterion. First, the intermediate stress (σ_2) is included and thus it is more general. Second, because each of the stresses is squared the convention that $\sigma_1 > \sigma_2 > \sigma_3$ need not apply.

These two criteria can be mapped on to principle stress space ($\sigma_1, \sigma_2, \sigma_3$). The Tresca criterion is a hexagonal cylinder centred around the space diagonal ($\sigma_1 = \sigma_2 = \sigma_3$). The von Mises criterion maps as a circular cylinder centred around the space diagonal. For these two criteria, it is observed that a hydrostatic stress ($\sigma_1 = \sigma_2 = \sigma_3$) does not affect the yield function. While this may be generally true for most metals, it is not true for soils. Thus the classical yield

criteria are poorly suited for use in soil plasticity.

Drucker and Prager (1952) recognized this shortcoming and modified the von Mises criterion to account for the effect of the mean stress on yielding. The modified criterion is known as the extended von Mises or the Drucker-Prager criterion. Using continuum mechanics notation, the yield criterion is:

$$[2.15] \quad f(\sigma_{ij}) = J_2^{1/2} - \alpha I_1 - k = 0$$

where α and k are material parameters, J_2 is the second invariant of deviator stress, and I_1 is the first invariant of stress.¹ The material parameters are functions of the friction angle and the cohesion (Valliapan 1981):

$$[2.16] \quad \alpha = \frac{2 \sin \phi}{\sqrt{3} (3 - \sin \phi)}$$

$$k = \frac{6c \cos \phi}{\sqrt{3} (3 - \sin \phi)}$$

When this criterion is mapped in principal stress space (Fig. 2.1) the result is a cylindrical cone with a cap centred about the space diagonal.

Lade and Kim (1988) and Lade (1990) developed a yielding criterion for soils based on a condition of constant plastic work. The yield surface is an "asymmetric teardrop", centred about the hydrostatic axis when mapped in the triaxial $(\sigma_1, \sqrt{2}\sigma_3)$ plane.

Tests of metals have shown that the von Mises criterion usually fits experimental data better than the Tresca criterion (Mendelson 1968). The von Mises criterion has also been used in the study of ductile frozen soils and ice (Salençon 1977).

1

$$J_2 = \frac{1}{6}[(\sigma_{11} - \sigma_{22})^2 + (\sigma_{22} - \sigma_{33})^2 + (\sigma_{33} - \sigma_{11})^2 + 6(\sigma_{12}^2 + \sigma_{23}^2 + \sigma_{31}^2)]$$

$$I_1 = \sigma_{11} + \sigma_{22} + \sigma_{33}$$

2.4.2.3 Flow Rule

The flow rule relates the components of plastic strain (ϵ_v^p and ϵ_s^p) to the state of stress (p_y' and q_y) at the yield surface. Mathematically the flow rule is written as:

$$[2.17] \quad d\epsilon_{ij}^p = d\phi \frac{\delta Q}{\delta \sigma_{ij}}$$

where $d\phi$ is a scalar that depends on whether the yield surface is expanding or contracting. Q is a function of the stress state (Chen and Baladi 1985). Fig. 2.2 illustrates the flow rule concept.

If the strain increment vectors are plotted in $\epsilon_s^p, \epsilon_v^p$ -space it would be possible to join each of the vectors by a curve such that each vector is normal to the curve. This curve is the function Q , in [2.17]. It is called the plastic potential.

For the general case illustrated in Fig. 2.2, the plastic potential Q and the yield function F are different. In this case, the flow rule is termed non-associated. When the plastic strain increments are perpendicular to the yield function, that is the plastic potential and the yield surface are identical, the flow rule is termed associated. There are many advantages in assuming an associated flow rule. The most important advantage is that a single function can be used to describe the yield surface and the flow rule. This leads to savings in computational efforts when it is used in numerical analyses.

The flow rule defines the relative proportion of plastic shear strain to plastic volume strain. The rule gives no indication of the magnitude of the total plastic strain: that is determined from the hardening law.

2.4.2.4 Hardening Law

When plastic flow (yielding) occurs it is important to know how much the yield surface will expand (plastic work harden) or contract (plastic work soften) in response to the stress increment. Hardening laws are used to describe the change in position of the yield surface in

stress space. In general terms, the function may be written as: $f(\sigma_{ij}, h) = 0$, where h is a scalar hardening parameter, and is a function of the plastic strain.

There are two variations that a hardening law may take to describe the movement of the yield surface (Prager 1959). They are isotropic hardening and kinematic hardening. The simplest form is isotropic hardening. In this case the yield surface is assumed to change size without changing shape or alignment. That is, if the yield surface is taken to be an ellipse centred on a particular axis, then during plastic flow the yield surface may change position but will remain an ellipse centred on the original axis. A 3-dimensional illustration of isotropic hardening is shown in Fig. 2.3.

In kinematic hardening, the yield surface can change position and move off its original axis, but remains a fixed size. This type of hardening is reasonably consistent with metal behaviour (Scott 1985). It is however, much more difficult to develop a mathematical formulation.

The hardening function may be any relationship that follows the changing position and/or shape of the yield surface. In one particular application (Section 2.4.3) the hardening law has been taken as a relationship between volume strain and the first stress invariant, I_1 . The function is written as:

$$[2.18] \quad \epsilon_v^p = \frac{\lambda - \kappa}{V} \ln p'$$

where λ and κ are slopes of virgin loading and unload/reload lines in $V, \ln p'$ -space respectively, and V is the specific volume of the soil (see Fig. 2.4). The term λ represents the total volume strains, and the κ represents the pure elastic volume strain. Thus the difference is the plastic volume strain.

2.4.2.5 Failure Criterion

In many textbooks on plasticity and soils, the Mohr-Coulomb relationship is often referred to as a yield criterion. In fact, the Mohr-Coulomb relationship defines the onset of plastic straining without any increase in deviator stress. Therefore it is more properly termed a failure or rupture criterion. Only in the case of elastic perfectly plastic materials could the Mohr-Coulomb relationship be interpreted as a yield (and simultaneously a failure) criterion. In plastic strain hardening (or softening) materials yielding and failure are separate phenomena.

The Mohr-Coulomb failure criterion is widely used in soil plasticity, and failure in the Critical State Model (Section 2.4.3) is based on such a condition. The criterion requires two material parameters that represent respectively the cohesion and frictional resistance of the material. A 2-dimensional illustration of the failure surface is shown in Fig. 2.5. In its most general form the criterion is written as (Yong and Warkentin 1975):

$$\begin{aligned}
 [2.19] \quad & [(\sigma_1 - \sigma_2)^2 - \{2c \cos\phi + (\sigma_1 + \sigma_2)\sin\phi\}^2] \cdot \\
 & [(\sigma_2 - \sigma_3)^2 - \{2c \cos\phi + (\sigma_2 + \sigma_3)\sin\phi\}^2] \cdot \\
 & [(\sigma_3 - \sigma_1)^2 - \{2c \cos\phi + (\sigma_3 + \sigma_1)\sin\phi\}^2] = 0
 \end{aligned}$$

As with yield criteria, it is possible to map the 3-dimensional failure criterion in general stress space. The result is an irregular hexagonal cone centred on the space diagonal, as shown in Fig. 2.6.

2.4.3 An Application of Elastic Plastic Theory

The Cam-clay soil model (Roscoe, Schofield and Wroth 1958, Schofield and Wroth 1968) is a plasticity model that permits post-yield strain hardening and strain softening behaviour. Several assumptions were made in developing this model (Atkinson and Bransby 1978). The first was that the yield surface and the plastic potential were coincident. That is, the flow rule was associated. This had the advantage that the yield surface and the plastic potential were described

by the same mathematical function. Second, in developing the yield criterion, it was assumed that there was no elastic (recoverable) shear strain. Third, it was assumed that volume change data can be plotted in e (void ratio) or $V(1 + e)$, $\ln p'$ -space (Fig. 2.4). Two straight lines result, representing virgin loading and unload/reload behaviour. The virgin loading (normally consolidated) line with slope λ represented the elastic plastic hardening law. The unload/reload (overconsolidated) line with slope κ represented elastic behaviour.

By considering the work done on a specimen during loading, a yield curve was developed. The yield function plotted as a 'bullet' in q, p' -space (Fig. 2.7).

The Cam-clay model was the first comprehensive soil model that linked stress and strain behaviour. It provided a relatively simple framework that described, in general terms, the behaviour of a normally consolidated or lightly overconsolidated clay mass. However, the model had a number of problems that were mainly attributed to the shape of the yield curve (Ko and Sture 1981). The model over predicted the amount of strain at small deviator stresses. More importantly, the model predicted shear strains during isotropic consolidation.

In the mid 1960's a modified Cam-clay model was proposed (Roscoe and Burland 1968). It differed from the original Cam-clay model in several respects. First, and most important was a change in the yield function. The yield curve was assumed to be an ellipse and the yield function was derived from the assumed curve (this was in contrast from the original model where the yield function was derived from work considerations). A second difference was that elastic shear strains could occur and were calculated from a relationship based on equation [2.10].

The equation of the yield function is:

$$[2.20] \quad q = [M^2(p_o' p' - p'^2)]^{0.5}$$

where p'_0 is the mean pressure at $q = 0$, that is, at the end of isotropic consolidation. The associated flow rule is assumed to apply, hence [2.20] can also be used to define the plastic potential.

Since the associated flow rule applies, a simple relationship between strain increments and stress increments evolves. Referring also to Fig. 2.2 it is seen that:

$$[2.21] \quad \frac{\delta \epsilon_s^P}{\delta \epsilon_v^P} = -\frac{\delta p'}{\delta q}$$

The yield function can also be written in differential form. Using the notation $\eta = q/p'$ we get:

$$[2.22] \quad \frac{\delta p'_0}{p'_0} = \left[\frac{M^2 - \eta^2}{M^2 + \eta^2} \right] \frac{\delta p'}{p'} + \left[\frac{2\eta}{M^2 + \eta^2} \right] \frac{\delta q}{p'}$$

If [2.22] is set to zero, the ratio $\delta p'/\delta q$ can be determined. Solving and setting this into [2.21] gives:

$$[2.23] \quad \frac{\delta \epsilon_s^P}{\delta \epsilon_v^P} = \frac{2\eta}{M^2 - \eta^2}$$

This ratio represents the flow rule.

One of the assumptions of Cam-clay models is that the consolidation behaviour produces a straight line in V (specific volume), $\ln p'$ -space, such as illustrated in Fig. 2.4. The equation of the normal consolidation line (on which yielding occurs) is:

$$[2.24] \quad V = N - \lambda \ln p'$$

The equation of the elastic unload-reload line is:

$$[2.25] \quad V = V_{\kappa} - \kappa \ln p'$$

where V_{λ} and V_{κ} are the intercepts of the lines at $p' = 1$ kPa. The use of $p' = 1$ kPa is simply a scaling convention established at Cambridge University, England.

Figure 2.4 shows the change in specific volume of a specimen as the mean pressure is increased from p'_1 to p'_2 . The total change is made up of an elastic component and a plastic component. Using [2.24] and [2.25] the change in the plastic component is found to be:

$$[2.26] \quad \Delta V^P = -(\lambda - \kappa) \ln \left[\frac{p'_2}{p'_1} \right]$$

In the limit, as p'_1 approaches p'_2 [2.26] becomes:

$$[2.27] \quad \partial V^P = -(\lambda - \kappa) \frac{\partial p'_o}{p'_o}$$

A change in the specific volume may be equated to a change in volume strain by dividing ∂V^P by the initial specific volume. Thus:

$$[2.28] \quad \frac{\partial V^P}{V} = \partial \epsilon_v^P = -\frac{(\lambda - \kappa)}{V} \frac{\partial p'_o}{p'_o}$$

Equations [2.27] and [2.28] show the effect on the specific volume and volume strain produced by changing the mean pressure. The maximum consolidation pressure increases as the mean pressure moves from p'_1 to p'_2 . The yield locus is "anchored" by the maximum consolidation pressure - therefore the yield locus also increases. Hence [2.28] represents the hardening law for this model.

To review, the yield function and plastic potential are given by [2.20]. The flow rule is given by [2.23], and the hardening law is given by [2.28].

In the elastic zone the strains may be calculated using the inverse of [2.10]. Thus:

$$[2.29] \quad \begin{bmatrix} \delta\epsilon_v^e \\ \delta\epsilon_s^e \end{bmatrix} = \begin{bmatrix} \frac{1}{K'} & 0 \\ 0 & \frac{1}{3G} \end{bmatrix} \begin{bmatrix} \delta p' \\ \delta q \end{bmatrix}$$

When plastic flow occurs, the plastic strain increments may be written as (Wood 1991):

$$[2.30] \quad \begin{bmatrix} \delta\epsilon_v^p \\ \delta\epsilon_s^p \end{bmatrix} = \frac{(\lambda - \kappa)}{Vp'(M^2 + \eta^2)} \begin{bmatrix} M^2 - \eta^2 & 2\eta \\ 2\eta & \frac{4\eta^2}{M^2 - \eta^2} \end{bmatrix} \begin{bmatrix} \delta p' \\ \delta q \end{bmatrix}$$

The final requirement for the Cam-clay model is a failure criterion. The Cambridge University group used the term "critical state" to describe the condition in a specimen when there is no change in deviator stress, mean stress, porewater pressure, or volume strain relative to shear strain. That is:

$$[2.31] \quad \frac{\partial q}{\partial \epsilon_s} = \frac{\partial p'}{\partial \epsilon_s} = \frac{\partial \epsilon_v}{\partial \epsilon_s} = \frac{\partial u}{\partial \epsilon_s} = 0$$

The specimen will continue to deform without any increase or loss in strength. The condition $\partial \epsilon_v / \partial \epsilon_s = 0$ arises from the associated flow rule (Wood 1991).

When a specimen is sheared, the ratio η ($= q/p'$) changes continuously. When failure occurs q/p' will remain constant. The ratio η at failure is denoted by M . This represents the slope of the failure line or Critical State Line in q, p' -space. The ratio M may be related to the conventional Mohr-Coulomb angle of internal friction ϕ by the relationships:

$$\begin{aligned}
 [2.32] \quad M_c &= \frac{6\sin\phi}{3 - \sin\phi} \quad \text{for compression} \\
 M_e &= \frac{6\sin\phi}{3 + \sin\phi} \quad \text{for extension}
 \end{aligned}$$

Referring to equation [2.23] it is seen that as η changes during a test, so does the ratio of shear strain to volume strain. As a consequence of the associated flow rule and the shape of the yield surface, it is seen that at the critical state the strain vector $(\partial\epsilon_g^p/\partial\epsilon_v^p)$ is vertical.

2.4.4 EPSM and Laboratory Studies

The parameters that constitute an elastic plastic model have been considered in preceding paragraphs in mathematical form. One role of a soil model is to provide a rational framework for interpreting field and laboratory test data. The data presented below will show that natural clay soils can be interpreted using an elastic plastic model. This lends support to the hypothesis that the buffer will also fit a similar model.

Although there is a large amount of laboratory data available in the literature, there is much less data that considers all the necessary elements of an elastic plastic model. The data on natural Winnipeg clay (Graham, Noonan and Lew 1983; Graham and Houlsby 1983; Graham and Li 1985) is some of the most comprehensive data published. Another complete data base comes from tests on kaolin clay (by Balasubramaniam 1969 and Loudon 1967).

The elastic properties of Winnipeg clay were presented by Graham and Houlsby (1983). The isotropic bulk modulus was determined from a plot of effective mean pressure *versus* volume strain. The isotropic shear modulus was determined from a plot of deviator stress *versus* shear strain. The data indicates that the moduli are stress path dependent, and that the elastic behaviour of the clay would be better predicted by assuming anisotropic elasticity, rather than isotropic elasticity. Errors in prediction reduced by about 32% when an anisotropic fabric was assumed.

The one dimensional consolidation test is one of the most common tests performed on clay soils. For a lightly overconsolidated clay (Winnipeg clay) a typical plot is shown on Fig. 2.8. The point where there is a maximum change in slope is termed the preconsolidation pressure (p'_c). In EPSM the preconsolidation pressure is a yield point. The deformation of the specimen in the portion of the curve when p' is less than p'_c is "elastic". The deformation in the portion of the curve when p' is greater than p'_c comprises both elastic and plastic components. The yield point is observed as a change from relatively stiff behaviour to less stiff behaviour.

By performing a number of stress controlled drained triaxial tests with different stress paths (dq/dp') a number of yield points in q, p' -space can be found. When joined together the points define a yield curve in q, p' -space. Yield curves for Winnipeg clay are shown in Fig. 2.9a. If all the stresses are normalized with respect to a common stress parameter such as the preconsolidation pressure (p'_c), a single normalized yield curve is produced (Fig. 2.9b).

The one-dimensional consolidation data shown in Fig. 2.8 represents graphically a hardening law. The ordinate is vertical strain, which can easily be converted to volume strain. The abscissa is the effective vertical pressure (logarithmic scale).

The Cam-clay model assumes an associated flow rule. It may be asked if an associated flow rule is reasonable in the case of Winnipeg clay. Graham, Noonan, and Lew (1983) superimposed plastic strain increment vectors on a plot of the normalized yield curve for Winnipeg clay (Fig. 2.10). Although the average apparent deviation between the vectors and the normal to the yield curve is small (less than 1°) Graham, Noonan and Lew showed a systematic pattern that suggested the flow rule was not completely associated.

The final requirement of the model is a failure criterion. At large strains after failure the specimens should be at critical state. However due to processes such as bifurcation where distinct shear bands form, only the soil along the shear bands may be at critical state. Graham and Li (1985) published a plot of normalized critical states for Winnipeg clay (Fig. 2.11).

2.5 Review of Buffer Research

In the past six years, research on the stress deformation characteristics of the sand bentonite buffer used in the Canadian Nuclear Fuel Waste Management Program has been centred at the University of Manitoba and at Atomic Energy of Canada's Whiteshell Nuclear Research Establishment.

Wan (1987) and Saadat (1989) considered the applicability of the classical effective stress principle for describing the stress-strain behaviour of the buffer. This was done by using a corollary of the principle that stated that only changes in effective stress would produce changes in volume. Wan and Saadat performed several experiments where the total (cell) pressure and back pressure were increased by equal amounts (thus keeping the "effective" stress constant). The resulting volume changes were essentially unaffected by the changes in effective pressures. Saadat also performed undrained shear tests on two specimens at the same "effective" stress, but where the cell pressure differed by 5.2 MPa. The shear behaviour was essentially the same for each specimen. Wan and Saadat concluded separately that the classical effective stress principle applied to the buffer. This work will be discussed in more detail in Chapter 4, in light of new data presented in this thesis.

Elasticity and yielding have both been observed during shearing. Saadat (1989) determined tentative values for the elastic bulk and shear moduli assuming isotropic elasticity. Both moduli were approximately proportional to the consolidation pressure, although their variability was quite large.

In two undrained tests by Saadat, specimens were unloaded and reloaded after shearing had progressed for several days. In one test, (Fig. 2.12a) two unload-reload cycles were conducted after peak strength occurred in a strain controlled undrained shear test. In the other test an unload-reload cycle took place (Fig. 2.12b) before reaching peak strength in drained shearing at constant p' . A well defined "yield" point was observed and elastic behaviour was

apparent in the unload/reload sections of both tests. No data has yet been collected that examines yielding during first time loading. This will be done in the present research program.

Saadat (1989) found evidence of anisotropic elastic behaviour during shearing. Fig. 2.13 is a plot of normalized porewater pressure ($\Delta u/p'_c$) increase *versus* normalized total mean pressure ($\Delta p/p'_c$). A straight line relationship is apparent in the early part of the test. Graham and Houlsby (1983) showed that if the soil were isotropic, the elastic portion of the plot would be linear and of slope 1 ($\Delta u = \Delta p$). Deviation of the ratio ($\Delta u/\Delta p'$) from unity in the figure indicates anisotropy ($\Delta u/\Delta p = 2.13$).

Wan (1987) and Graham *et al.* (1986) presented data showing a relationship for the hardening law (Fig. 2.14). While this relationship is for specimens at swelling pressure equilibrium, it was asserted by Graham *et al.* (1989a) that the swelling equilibrium line is the same as the normal consolidation line. Thus any mathematical equation used to describe the swelling equilibrium line would apply equally as a hardening function.

The strength envelope and failure criterion have been developed over a number of years as the testing program was extended to higher pressures. Wan (1987) reported data for a range of specimens prepared at a dry densities between 1.32 Mg/m^3 and 1.63 Mg/m^3 at moisture contents ranging from 38% to 23%. The failure envelope for this data had an effective cohesion intercept (c') of 40 kPa and an angle on internal friction of 14° . Saadat (1989) reported the most recent data for specimens prepared at a dry density of 1.66 Mg/m^3 and a moisture content of about 21%. (He also reported some new data for low density specimens.) The failure envelope was curved in q, p' -space at low effective mean pressures (less than 1500 kPa). At higher pressures the slope M of the straight line portion of the failure envelope in q, p' -space was 0.53. This corresponds to a Mohr-Coulomb angle of internal friction of about 14° .

In conclusion, some data have been reported that confirms the applicability of the classical effective stress principle under certain restrictive conditions. This data will be used

together with new data reported in this thesis to develop a more rational approach to the use of effective stresses in active clays. Several of the parameters necessary for an elastic plastic model of the buffer have been determined. These are, the bulk and shear moduli necessary to describe elastic behaviour (based on limited data from drained and undrained tests), the hardening law and the failure envelope. The parameters that remain to be found are the yield surface, flow rule, and plastic potential.

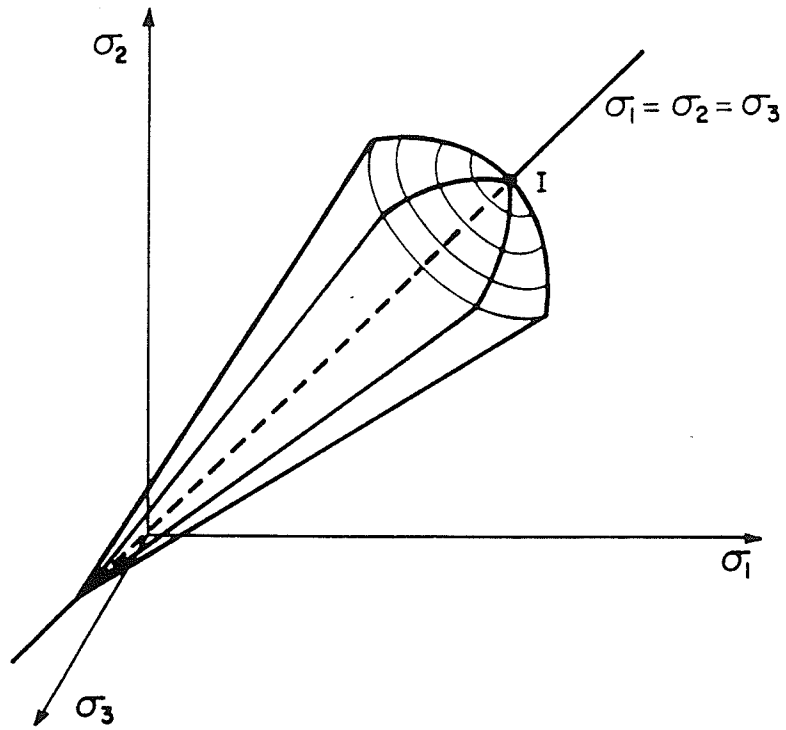


FIGURE 2.1 Drucker-Prager yield criterion in 3-dimensional space (from Chen and Baladi 1985).

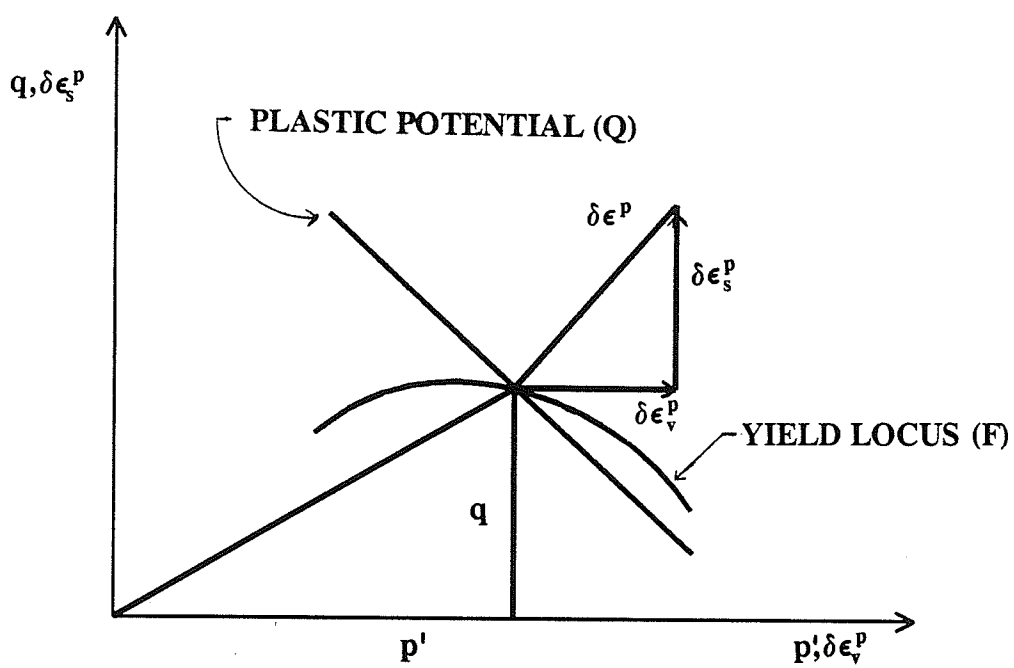


FIGURE 2.2 Flow rule concept.

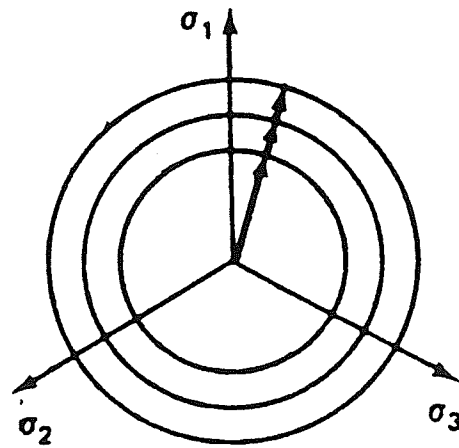
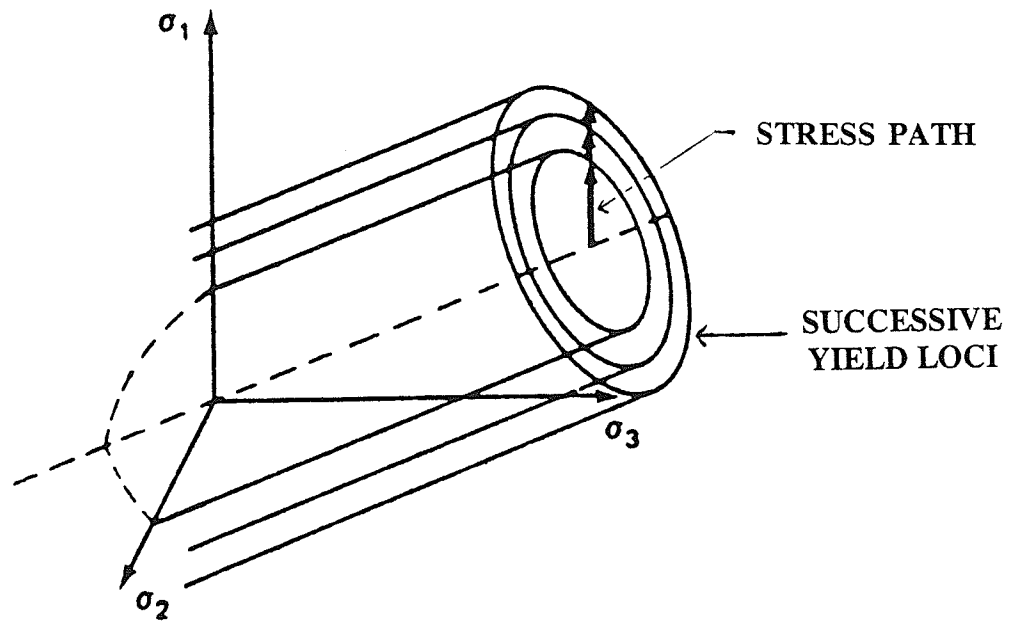


FIGURE 2.3 Isotropic hardening in $\sigma_1, \sigma_2, \sigma_3$ -space (from Scott 1985).

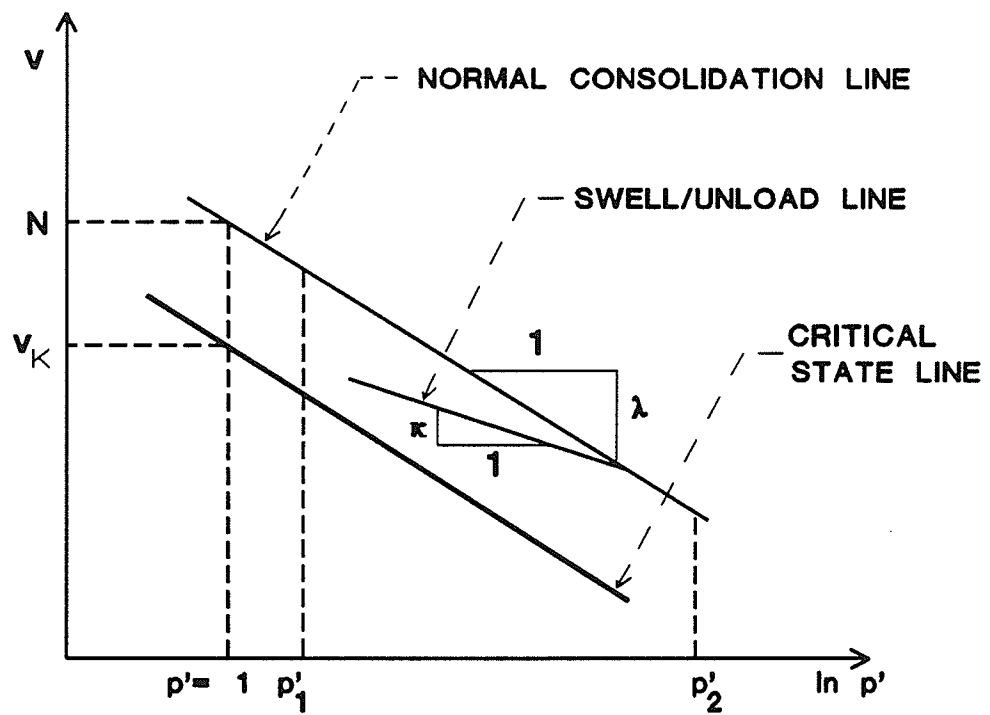


FIGURE 2.4 Hardening law for modified cam-clay constitutive model.

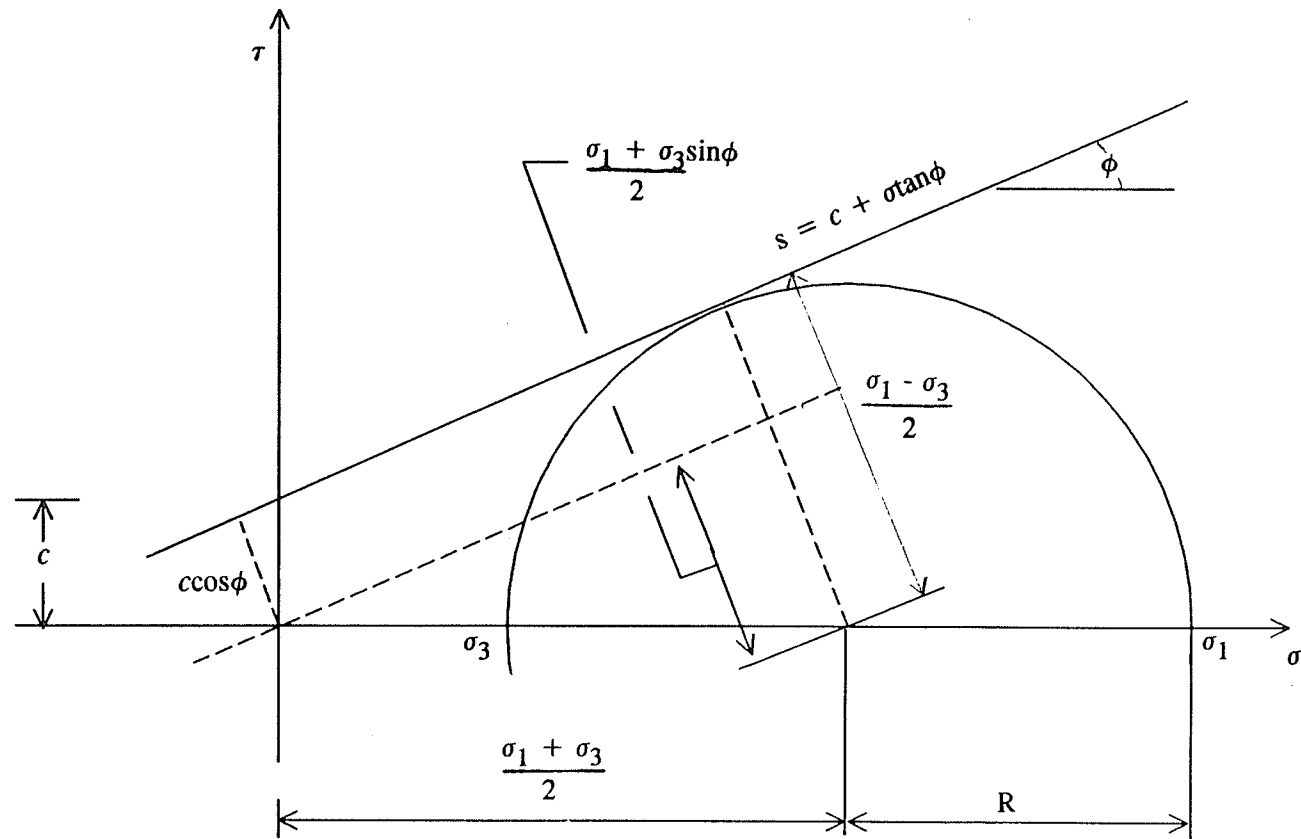


FIGURE 2.5 Mohr-Coulomb failure criterion in 2-dimensions.

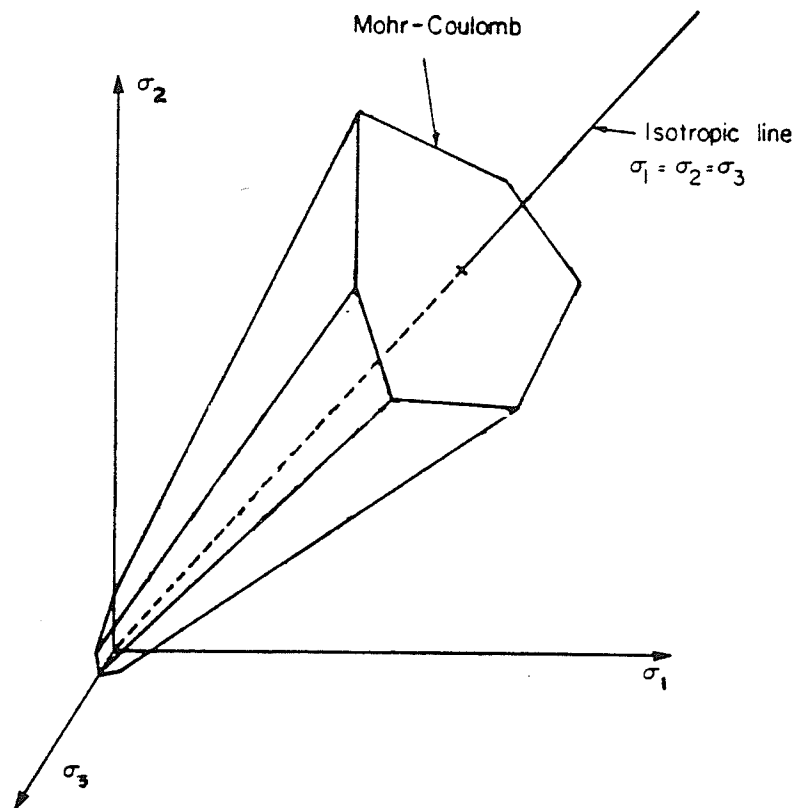


FIGURE 2.6 Mohr-Coulomb failure criterion in 3-dimension $\sigma_1, \sigma_2, \sigma_3$ -space.

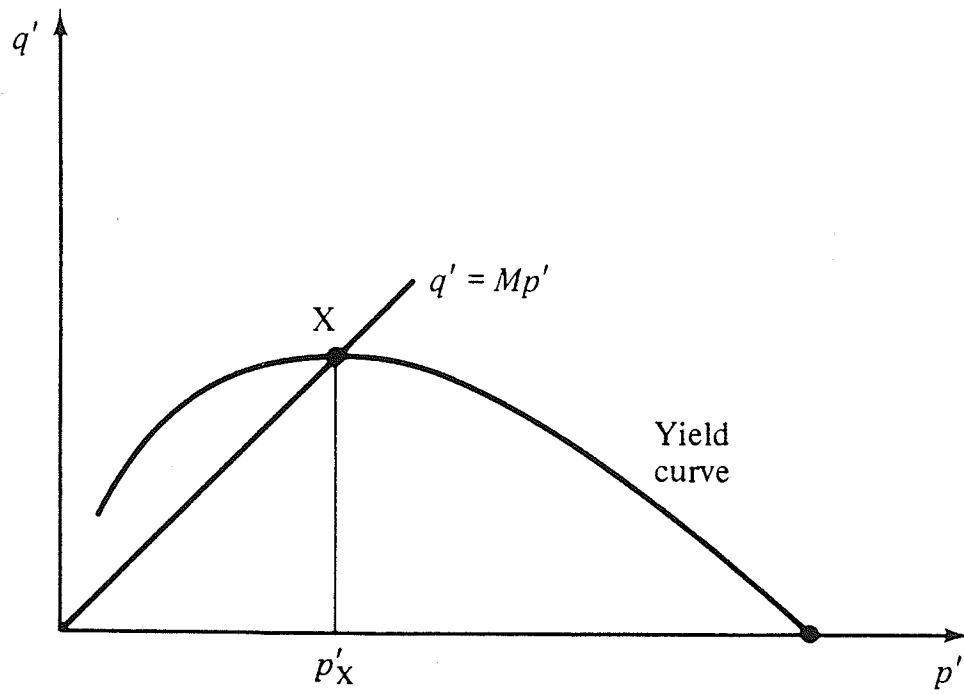


FIGURE 2.7 Yield function predicted by Cam-clay constitutive model.

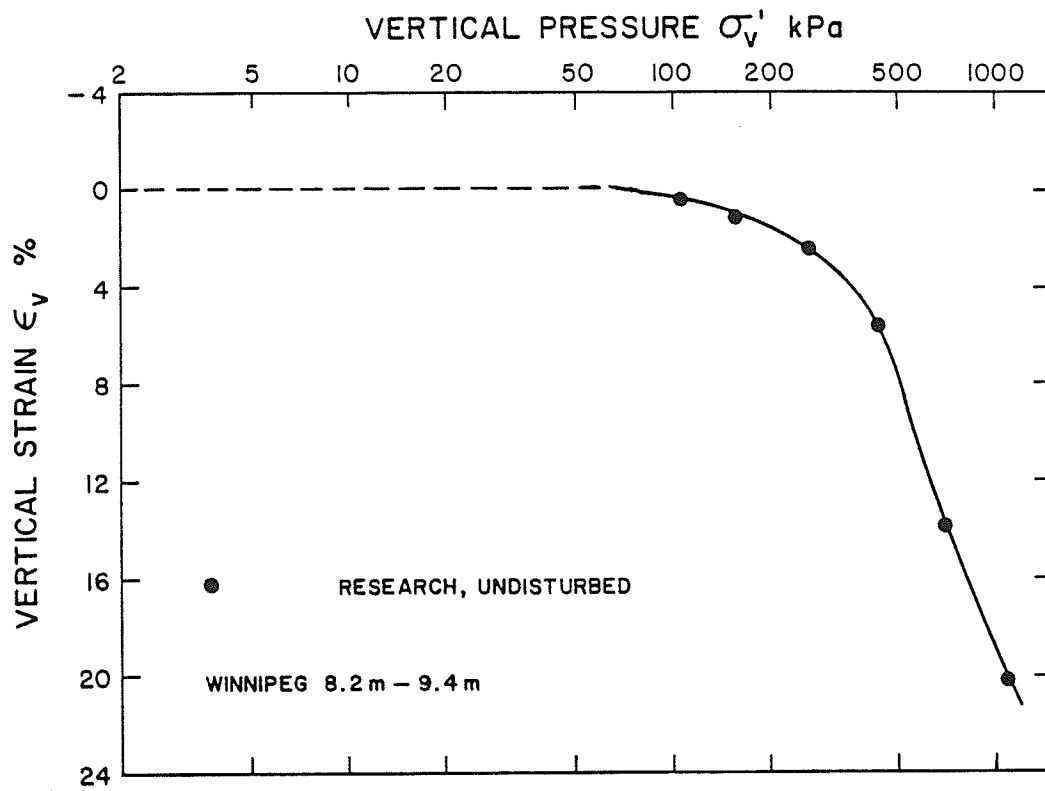


FIGURE 2.8 One dimensional consolidation of Winnipeg clay (from Graham and Au 1985).

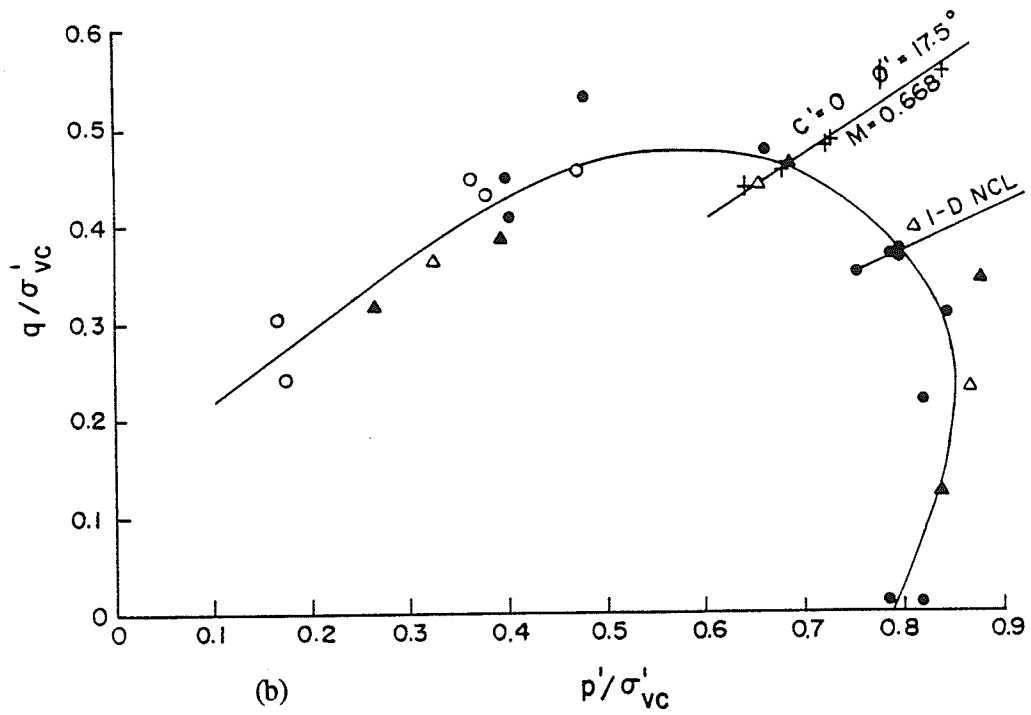
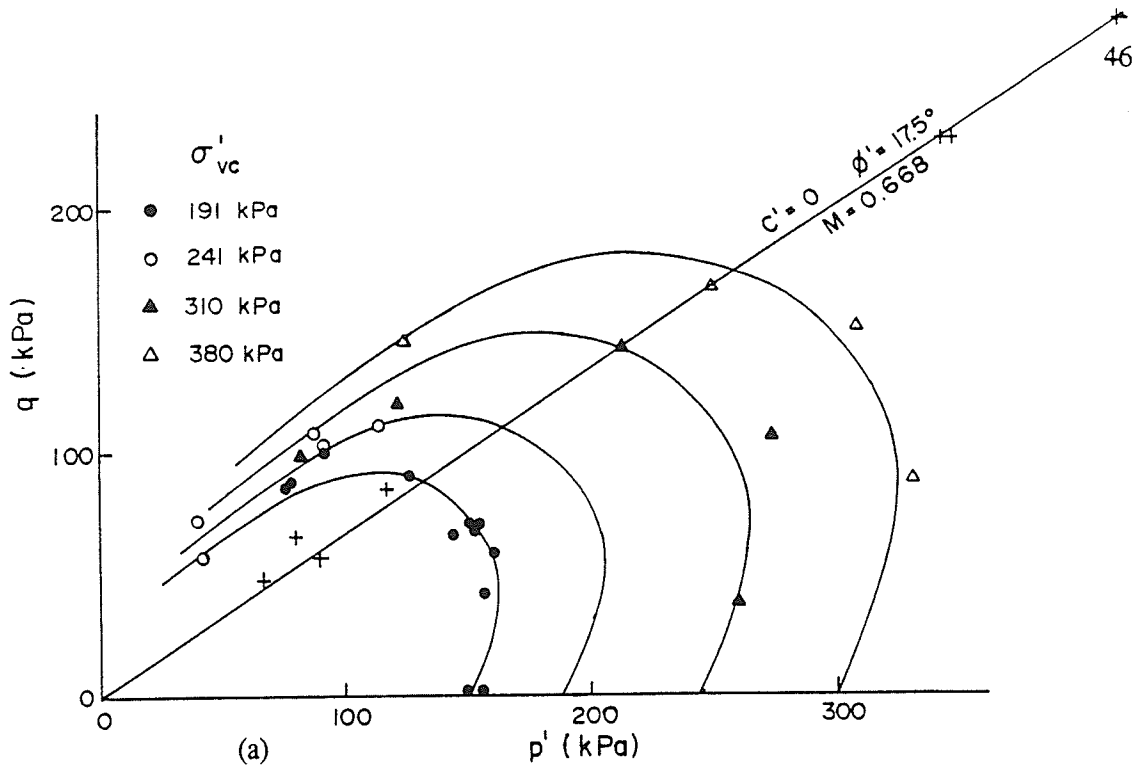


FIGURE 2.9 Yield data for Winnipeg clay (a) in q, p' -space and (b) in normalized q, p' -space (from Graham, Noonan and Lew 1983).

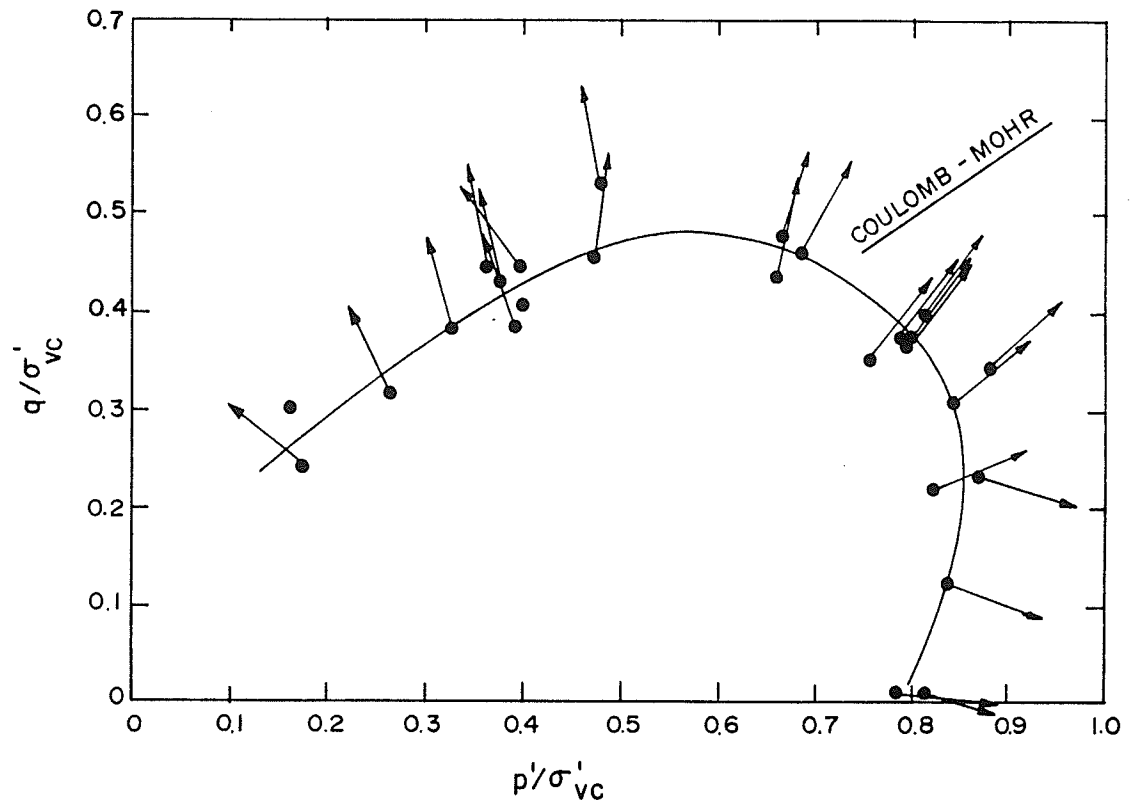


FIGURE 2.10 Normalized yield envelope and plastic strain increment vectors for Winnipeg clay (from Graham, Noonan, and Lew 1983).

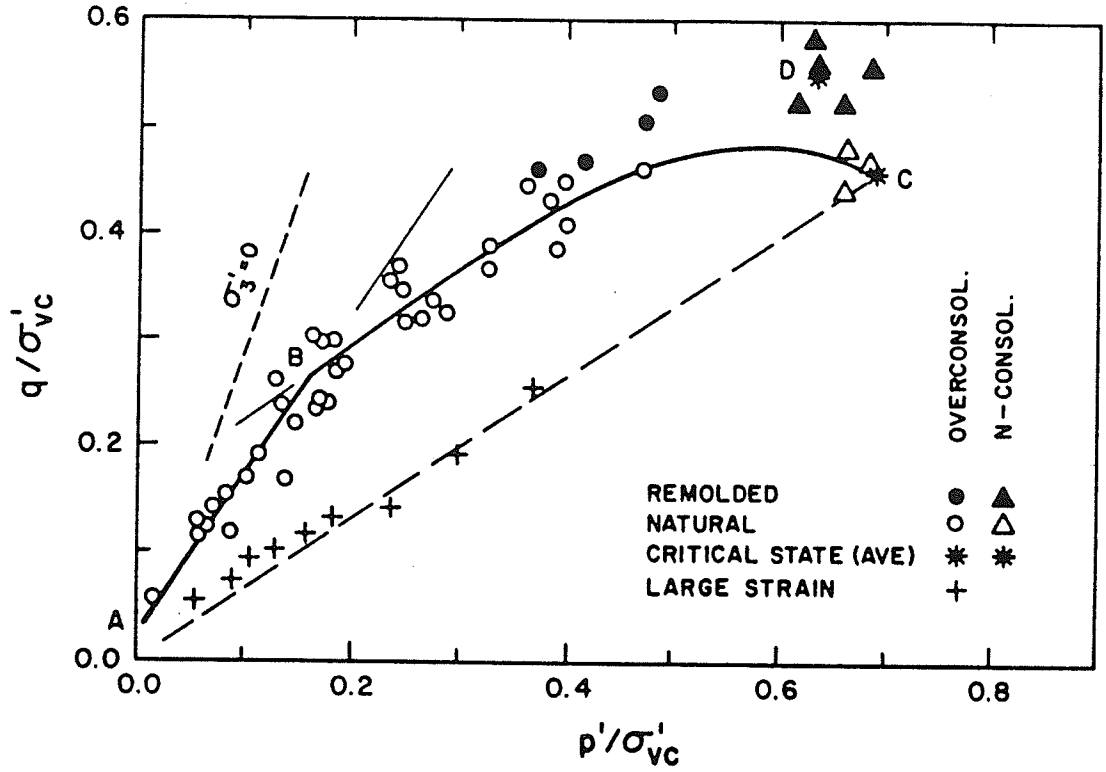
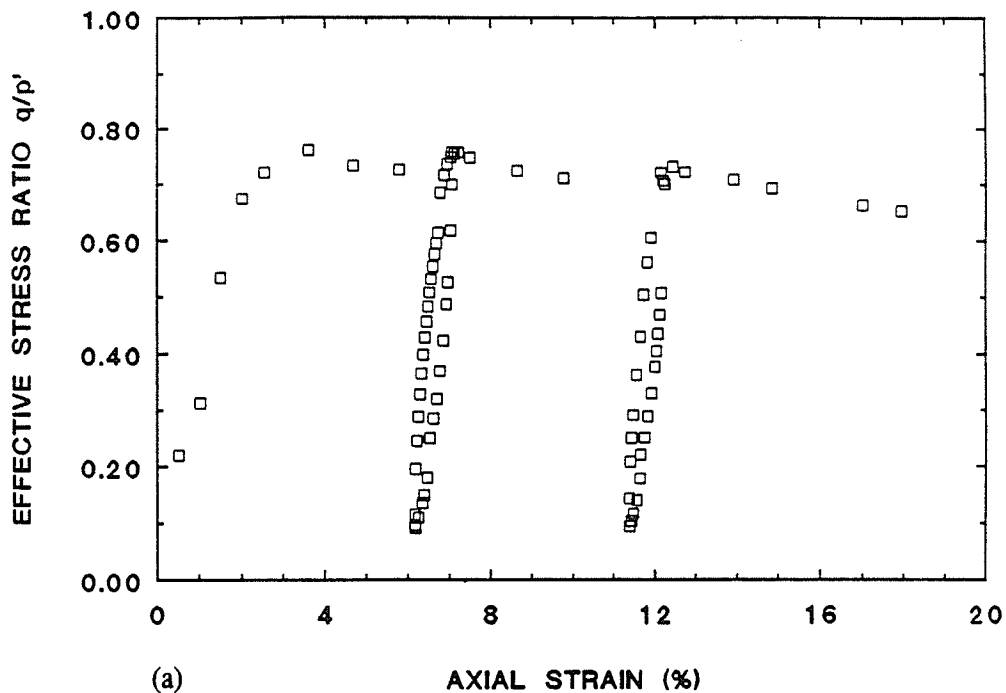


FIGURE 2.11 Normalized yield envelope for Winnipeg clay showing low stress strength, overconsolidation strength, and critical state strength (from Graham and Li 1985).

BUFFER SPECIMEN T927
DRY DENSITY = 1.66 Mg/m³



BUFFER SPECIMEN T931
DRY DENSITY = 1.66 Mg/m³

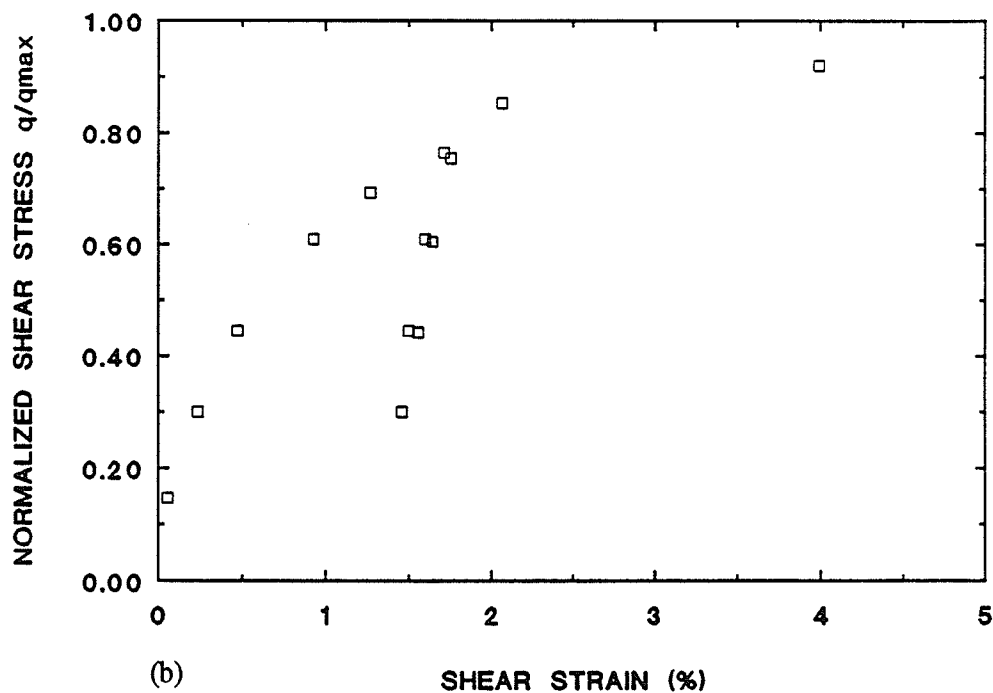


FIGURE 2.12 Normalized stress-strain data for buffer specimens. (a) T927 and (b) T931 (from Saadat 1989).

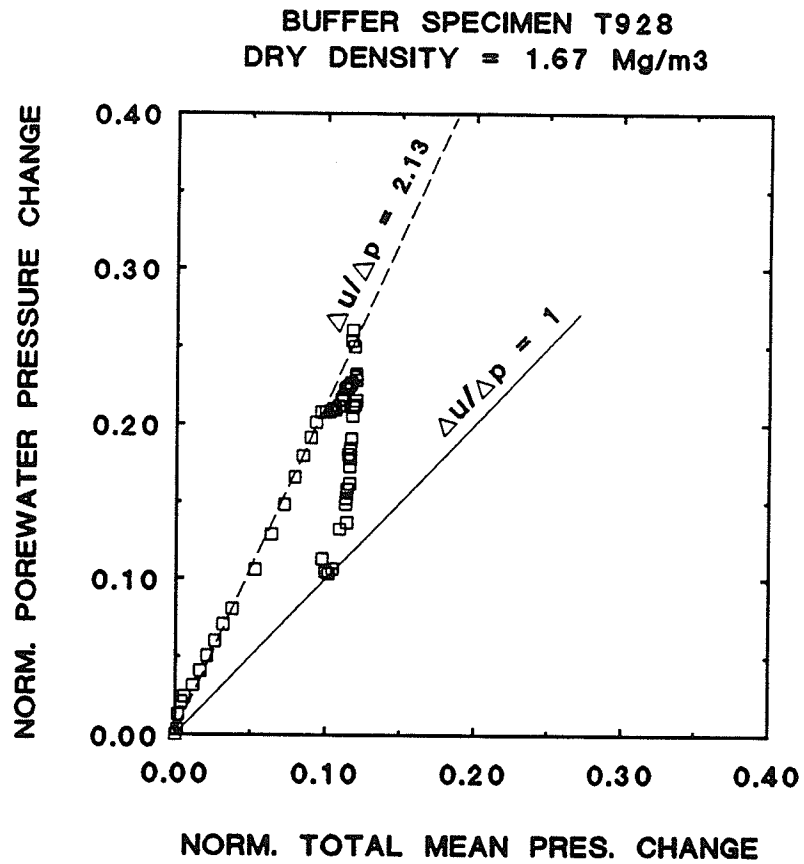


FIGURE 2.13 Normalized porewater pressure response *versus* normalized total mean pressure change (from Saadat 1989).

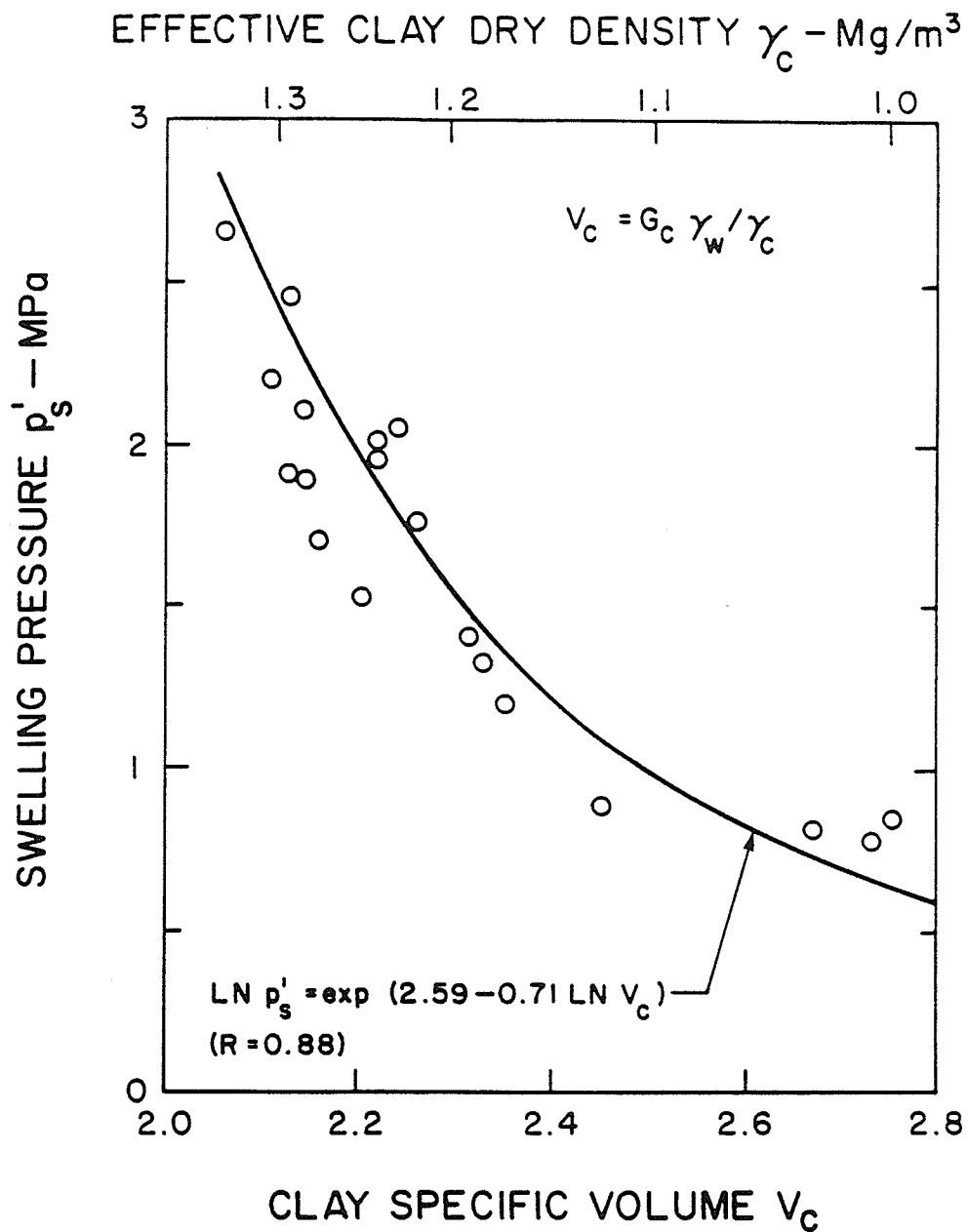


FIGURE 2.14 Swelling equilibrium pressure *versus* clay specific volume (Hardening Law) for buffer (from Graham *et al.* 1986).

CHAPTER 3 EXPERIMENTAL EQUIPMENT, TEST MATERIALS AND SPECIMEN PREPARATION/INSTALLATION/REMOVAL

3.1 Equipment - Triaxial Cells

The testing was done in triaxial cells. These involve a pressurized container that allows all-round pressure to be applied to specimens using water or other liquids as the cell fluid. Axial loading can be applied separately through a piston in the top of the cell. Connections for measuring volume changes or porewater pressure changes in the specimen are provided at the base of the cells. Details of the planning of the test program will be given in Chapters 4 and 5 where appropriate.

3.1.1 Standard Triaxial Cells

Two Brainard Kilman (B-K) triaxial cells and four Wykeham Farrance (W-F) triaxial cells (Fig. 3.1a) were used in this investigation. The B-K cells had aluminium cell walls, and operated to confining pressures of 3500 kPa. These cells had an internal diameter of 115 mm and a length of approximately 270 mm. Axial stresses were applied to specimens by a 12.7 mm stainless steel ram passing through the top of the cell. Linear bearings maintained ram alignment. The bearings were designed to reduce frictional resistance to the ram movement. A seal stopped cell fluid leakage through the linear bearings. Drainage or porewater pressures could be measured from both the top and base of the specimens.

Three of the W-F cells had a pressure capacity of 1700 kPa. The fourth cell, using a "home-built" steel sleeve had a pressure capacity of approximately 3500 kPa. The cells had an internal diameter of 150 mm and a length of about 285 mm. These triaxial cells were originally fitted with rotating bushing assemblies. The axial load ram passed through a brass sleeve into the cell. The sleeve connected to a worm screw driven by an electric motor. The sleeve, turned by the motor reduced friction between the axial ram and the cell housing. Although this system

performed adequately, cell fluid leakage was a persistent problem. The rotating bushings were later replaced by linear bearing assemblies, similar to those on the B-K cells. The diameter of the ram in the linear bearing assembly was 19 mm. The W-F cells, like the B-K cells, were capable of specimen drainage through both the top and the base of the specimen.

3.1.2 GDS Triaxial Testing System

The GDS triaxial system is a computer controlled apparatus, developed by Geotechnical Digital Systems Ltd. in England. (The principal equipment is shown in Fig. 3.1b) The main system comprises five components: an IBM - AT compatible computer, three hydraulic controllers operated using microprocessor controlled electric stepper motors, and a Bishop and Wesley (1975) "stress-path" triaxial cell (manufactured by Wykeham Farrance). Additional equipment added by the author permits measurement of porewater pressures at the base of the specimen and measurement of deviator stresses using an internal load cell.

The basic AT computer is augmented by a Hewlett Packard "Viper" card that had its own CPU and memory. The card is essentially a separate computer, and the "host" computer only provided the disk drives, power, and display. The Viper card communicates with the hydraulic controllers via a IEEE 488 plug.

The hydraulic controllers contain a microprocessor, stepper motor connected to a hydraulic cylinder, and a pressure transducer. The microprocessor can be programmed alone, or via the Viper card, using the IEEE 488 connection. The stepper motor in the controller receives signals from the microprocessor, and can seek a specified volume change (relative) or a pressure to a maximum of 2000 kPa. The pressure transducer measures fluid pressure in the hydraulic cylinder.

The GDS triaxial system used at the University of Manitoba used one controller for back pressure (or porewater pressure measurement during undrained tests), another controller for cell

pressure, and the third to provide axial stress.

The Bishop and Wesley ("stress-path") triaxial cell was capable of testing specimens of 50 mm to 100 mm diameter. The main difference between this cell and a conventional triaxial cell was that the deviator stress in the stress path cell was provided by a hydraulic ram in the base of the cell. The deviator stress was calculated as a difference between the top (cell) pressure and the lower (ram) pressure, multiplied by the ratio of the ram area to the specimen area.

A Users Manual was prepared to assist users in the start-up and operation of the GDS equipment in the University of Manitoba laboratories (Oswell 1990). Additional documentation was provided by GDS Ltd. The computer software that operated the GDS equipment was written in H.P. Basic 5.0. A complete series of testing routines was available.

Numerous modifications have been made to both the hardware and the software. These changes are documented in the Users Manual (Oswell 1990). One important change in the hardware was the addition of a pressure transducer to measure porewater pressures in the specimens, independently of the back pressure controller. A second change was the use of an internal load cell to measure axial loads directly. The porewater pressure data and load cell data were collected manually and later added to the data file during data reduction.

Software changes included the provision for continuous data storage, a routine to produce Lotus 123 readable data files, a change in read times during consolidation, and a provision for a constant rate of strain shearing test in any direction of q, p' -space (Oswell 1990).

Horsfield and Been (1987) and Sheahan *et al.* (1990) have discussed important shortcomings of the system and suggested numerous modifications and improvements.

3.1.3 High Pressure Isotropic Consolidation Cell

An isotropic stress cell was built for this research program. The cell consisted of heavy duty steel pipe (100 mm diameter), welded to a spherical cap at one end and a flange connection

at the other end. The cell top was bolted to an aluminium base plate. The cell has a working pressure of about 6.0 MPa, at room temperature. Top and base drainage is available to specimens.

3.2 Equipment: Peripherals

3.2.1 Axial Displacement Measurement (Non GDS Equipment)

Axial displacements were measured using linear variable differential transformers (LVDTs). The typical resolution of these instruments was in the order of 0.5% of full scale. In the case of 100 mm specimens and a 25 mm transducers, the accuracy was within about 0.12% strain. The instrument readings were made using a Hewlett Packard voltmeter and the computer data acquisition program, described in Section 3.2.5.

In some tests, manual dial gauges were used alone or to verify the LVDTs. The resolution of the dial gauges was typically to 0.005 mm.

3.2.2 Load Measurement

A submersible load cell measured the axial load on specimens in the GDS triaxial cell. The load cell was a Wykeham Farrance Model 4958. It had a capacity of 3000 N. The load cell was calibrated by adding dead weights to a hanger attached to the load cell. Axial loads were read on a HP voltmeter, separate from the GDS equipment.

In several tests using the conventional triaxial equipment external load cells were used to measure the axial load on the specimens. The load cells were used for the constant rate of strain tests and also whenever a lever arm assembly was used to apply the axial load during incremental stress controlled tests. These load cells had a capacity of either 2225 N (500 lbs) or 4450 N (1000 lbs). They were manufactured by Data Instruments Ltd. The resolution was better than 10 N. The load cells were read using the data acquisition system.

3.2.3 Pressure Measurement

All pressures were measured using diaphragm-type pressure transducers. The transducers were placed in brass housings attached directly to the triaxial cell base. Most of the pressure transducers were manufactured by Data Instruments Ltd. (Model AB). The design capacities of the transducers ranged from 100 psi (690 kPa) to 2000 psi (13500 kPa). The overload capacity without damage to the transducer was double the design capacity.

3.2.4 Volume Change Measurement (Non GDS Equipment)

Two types of automatic volume change devices were used in this study. One was an Imperial College Volume Change Transducer from Shape Instruments. Full details are provided by Saadat (1989). A photograph of this volume change is shown in Fig. 3.1a.

The other device was a Fisher differential pressure transducer (DPT). This instrument measured the change in the height of water in a burette attached to the triaxial cell. A schematic of the equipment arrangement is shown in Fig. 3.2. (See also Fig. 3.1a). The back pressure line was connected to the top of the porewater burette and the low pressure side of the DPT. The bottom of the burette was attached by a tee connection to the triaxial cell (and then to the top of the specimen) and to the high pressure side of the DPT. Since both sides of the DPT experienced the applied back pressure, the only pressure difference was the height of the column of water in the burette. The use of DPT's to measure volume change was reported by Lade (1988) and discussed by Oswell, Lingnau, Osiowy, and Graham (1989).

3.2.5 Data Acquisition System

The pressure, load and volume change data from most tests were collected using a computer operated data acquisition system (DAS). It had been developed earlier at the University of Manitoba based on a system reported by Indrawan (1986). Details were presented by Saadat

(1989) and Nordien and Saadat (1988). Data were collected in a format that could be imported into spreadsheet software and manipulated as required. In a few tests completely manual readings were made using self-contained read-out boxes.

The DAS used for the GDS system has been discussed briefly in Section 3.1.2 and in more detail by Oswell (1990).

3.3 Test Materials

The soil mixture used in this research program was a 50:50 mix by dry weight of quartz sand and bentonite. The sand was a blended mix with $D_{10} = 0.2$ mm and $D_{85} = 1.3$ mm. A sieve analysis of the blended sand is shown on Fig. 3.3. The specification of the sand was reported by Gray, Cheung and Dixon (1984).

The bentonite was sodium rich smectite commercially available from AvonLea Minerals Industries, Regina, Sask. Composition and mineralogy were reported by Dixon and Woodcock (1986) and Quigley (1984). The liquid limit was in the order of 225% to 250% with a plasticity index of about 200%.

Distilled, de-aired water was used in the preparation of all specimens.

3.4 Specimen Preparation and Installation Techniques

3.4.1 Specimen Preparation

Sun (1986), Wan (1987), Yarechewski (1988), and Saadat (1989) detailed the methods and equipment used to prepare the test specimens by "static" compaction in a rigid cylindrical mold. Thus specimen preparation will not be described here in detail. Only changes to earlier methods will be discussed.

Specimens were prepared according to the method developed by Yarechewski (1988). This technique produced specimens of uniform density along the height of the specimen by

compacting equal-mass lifts of the moist sand and bentonite mixture to carefully controlled thicknesses in the mold. Using Yarechewski's method the height of the specimen in the mold was 100 mm. However, during the preliminary phases of this study it was found that, after extrusion from the mold, the final height was in the order of 102 mm. Consequently, Yarechewski's method was improved so that each lift was overcompacted by approximately 0.4 mm. This produced specimens with a final height closer to the 100 mm specification.

In the yielding study specimens of two dry densities were prepared. The target dry density was either 1.50 Mg/m³ (low density) or 1.67 Mg/m³ (high density). These dry densities correspond to Modified Proctor Dry Densities of approximately 85% and 95% respectively. The statistical data for these specimens are presented in Table 3.1. Details of individual tests are given in Table A.1 (Appendix A, at the end of this thesis).

TABLE 3.1 Statistical Data on Specimen Preparation of "Yielding" Specimens

Target γ_d Mg/m ³	Number of Specimens	Aver. γ_d Mg/m ³	Std. Dev.	Aver. w %	Std. Dev.	Aver. Sat. %	Std. Dev.
1.50	25	1.485	0.01	29.4	0.33	96.9	0.78
1.67	15	1.668	0.01	21.9	0.34	95.4	0.93

Note: Aver. = average
Std. Dev. = standard deviation
w = moisture content
Sat. = saturation

3.4.2 Side Drain Permeability Study

Filter paper end-disks and side drains were used to aid drainage of most specimens. The filter paper used by previous researchers at the University of Manitoba was Whatman No. 1 grade, described by the manufacturer as "medium fast, qualitative". Both Bishop and Henkel (1962) and Head (1986) recommend using Whatman No. 54 grade, described as "fast, hardened". The hardened grades of filter paper do not soften when soaked in water. Tests on filter materials were conducted to determine the influence of confining pressure and time on their flow

properties. Based on the results it was decided to use two layers of No. 54 filter paper strips on specimens when the confining pressure was less than about 1000 kPa. At higher confining pressures a layer of No. 54 filter paper and a layer of Mirafi 140NS geotextile was used for the side filter strips. All side filter drainage strips were placed in a spiral arrangement to reduce the influence on the specimen stiffness (Gens 1982). Full details of the study are given in a paper by Oswell *et al.* (1991). This paper is given in Appendix B.

3.4.3 Specimen Installation

The methods and techniques for specimen installation described by Saadat (1989) were closely followed in this study. As in the previous sections, only changes to the earlier methods will be discussed.

Wan (1987) and Saadat (1989) applied a back pressure to the base of the specimens to improve their saturation. They made no provision for independent measurement of porewater pressures. In this testing program, the back pressure was applied to the top of the specimen and the porewater pressure was measured independently at the base. A filter stone, approximately 37 mm in diameter, in a brass sleeve (outer diameter of 51.7 mm) transmitted porewater pressure in the central part of the specimen to the pressure transducer. The side drainage strips extended from the top of the specimen to about 10 mm above the base. The brass ring, and limiting the length of the side drainage strips was designed to reduce the direct interaction between the applied back pressure and the porewater pressure.

Two thin (0.55 to 0.75 mm) latex-rubber membranes and five rubber O-rings were used to seal the specimen from the cell fluid. The membranes were soaked for several hours in de-aired water before being used. This reduced water absorption by the membranes (Leroueil *et al.* 1988).

3.5 Overconsolidation Procedure for Yielding Specimens

In this study it was necessary to create conditions in some specimens where yielding could be observed. This was done by building the specimens into the cell and then applying an effective cell pressure equal to the swelling equilibrium pressure (SEP). The SEP is the effective mean pressure for a given dry density of buffer at which there would be no volume change in a drained condition. Saadat (1989) and Wan (1987) developed the relationship between dry density (or moisture content) and the SEP. Figure 3.4 shows the relationship between effective mean swelling pressure and moisture content for the buffer. For the low density specimens the SEP was taken to be 550 kPa. Using a back pressure of 200 kPa, the total cell pressure applied was 750 kPa. For the high density specimens, six tests were performed using a SEP of 2100 kPa. After a review of these data, a SEP of 1700 kPa was used for the remaining high density specimens. Each specimen was left at this pressure for 10 days.

The cell pressure was then reduced to give the specimen a target overconsolidation ratio (OCR) of 1.75 (or 57% of the SEP). This value of the OCR was chosen after considering several factors. One factor was that yielding in natural soils has been most noticeable at OCRs of about 1 to 3. These soils would be termed lightly overconsolidated. Another consideration was that because the buffer had a high swelling potential, it would begin to swell as soon as the confining pressure dropped below the swelling equilibrium pressure. As the specimen swelled it would approach a new equilibrium moisture content/density relative to the new pressure. Hence the OCR would actually decrease during the swelling process. If the reduction in the confining pressure was too small then the specimen would swell towards an equilibrium moisture content before any yielding behaviour was observed.

Due to swelling and porewater pressure changes during the swelling period, the actual OCR was less than the targeted 1.75. For the low density specimens the average OCR was 1.54, and for the high density specimens the average OCR was 1.62. In addition, three low density

specimens were tested at higher OCRs of 2.66, 2.90, and 4.15.

3.6 Post-Test Procedures

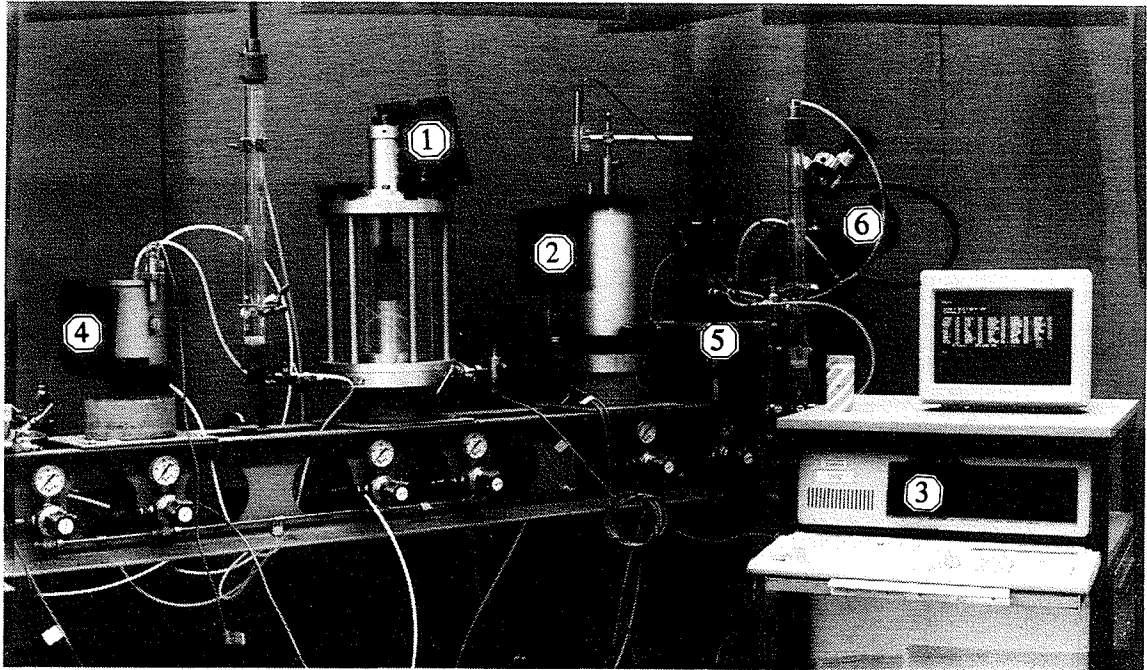
When each test was finished, valves to the top and base of the specimen were closed. This reduced the inflow of water to the specimen on the release of the confining pressure. The loading ram was locked in place. The cell was drained and the cell top, drainage leads, and membranes removed as quickly as possible. (This typically took about 15 minutes.)

Graham, Saadat, Lingnau, Yin, Oswell, and Azizi (1989) stated that water content distribution within the specimens may not be uniform. To check this, specimens in this study were split into five sections lengthwise. Each section was then cored with a 31.5 mm diameter tube. The moisture content of each core and shell portion were determined. This technique contrasted with earlier studies where specimens were cut into five sections and the moisture content of each whole section was determined.

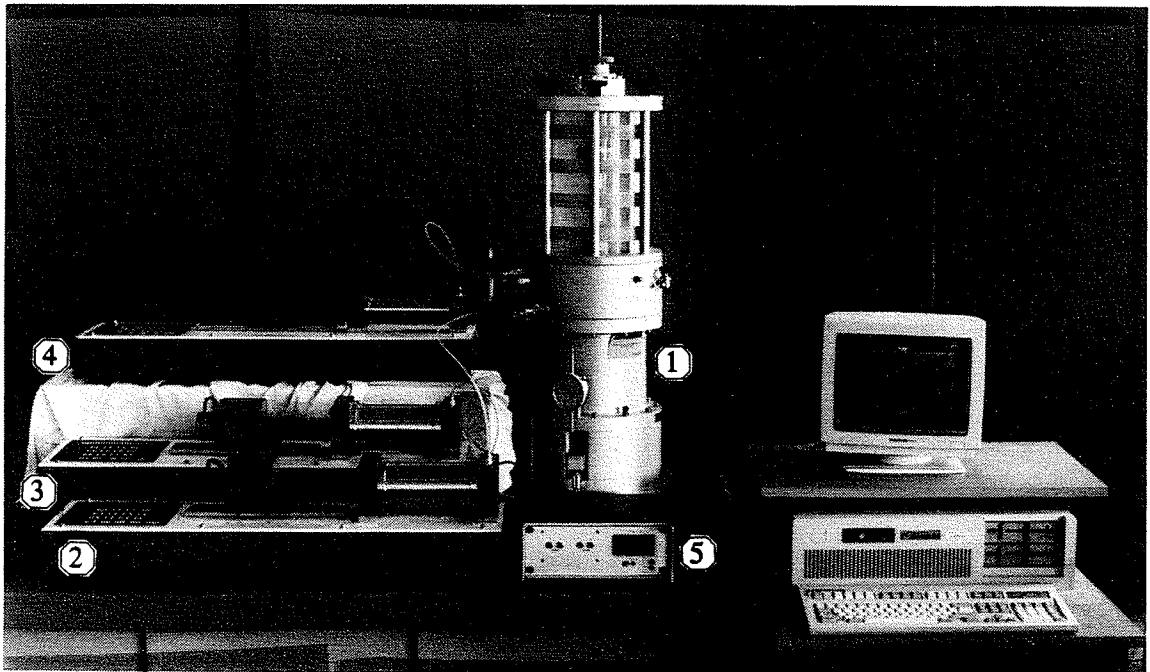
The average measured core and shell moisture content for the specimens in this study are listed in Table A.2 (Appendix A). The difference between the shell and core average moisture content, and the differences between the top and base moisture contents for the core and shell sections are also given. The (shell - core) difference reflects moisture equilibrium across the specimen. The data in Table A.2 shows that the difference between the average shell and core moisture content was only 0.4%. This suggests that the concern raised by Graham *et al.* (1989c) was unfounded. Atkinson, Evans and Ho (1985) examined the moisture content change across specimens of kaolin subjected to one-step consolidation. They found that for specimens with bottom drainage only, the moisture content from the centre to the edge of the specimen varied by less than 0.5%. For specimens with radial drainage, the moisture content from the centre to the edge of the specimen varied by about 1.7%. The variation in radial moisture content of the buffer was therefore less than that reported by Atkinson *et al.* (1985).

The average difference between the top and base of the core portions was 0.8%; the average difference between the top and base of the shell portions was 1.6%. The (top - base) difference reflects moisture equilibrium along the specimen. Since drainage was connected to the top of the specimen it would be expected that the top of the specimen may have a slightly higher moisture content than the base.

The measured end-of-test water content (by drying) is compared with the calculated end-of-test water content (by volume change) in Table A.1 (Appendix A). The difference between the end-of-test water contents from each method is quite small, averaging 0.58%. Larger discrepancies in some tests between the measured and calculated final water content may be due to leakage, excessive water flushed into the filter stones and filter strips during the building-in process, or lack of full saturation of the specimens and/or filter stones.



1. Wykeham Farrance triaxial cell, 2. Brainard Kilman triaxial cell, 3. Data acquisition system
4. Imperial College volume change device, 5. Differential pressure transducer, 6. Nitrogen tank for confining pressure.



1. Bishop-Wesley stress path triaxial cell, 2. Cell pressure controller, 3. Lower chamber (axial) controller, 4. Back pressure controller, 5. Base porewater pressure read-out display

FIGURE 3.1 Photograph of Triaxial equipment. (a) Wykeham Farrance and Brainard Kilman equipment, (b) GDS stress path cell and controllers.

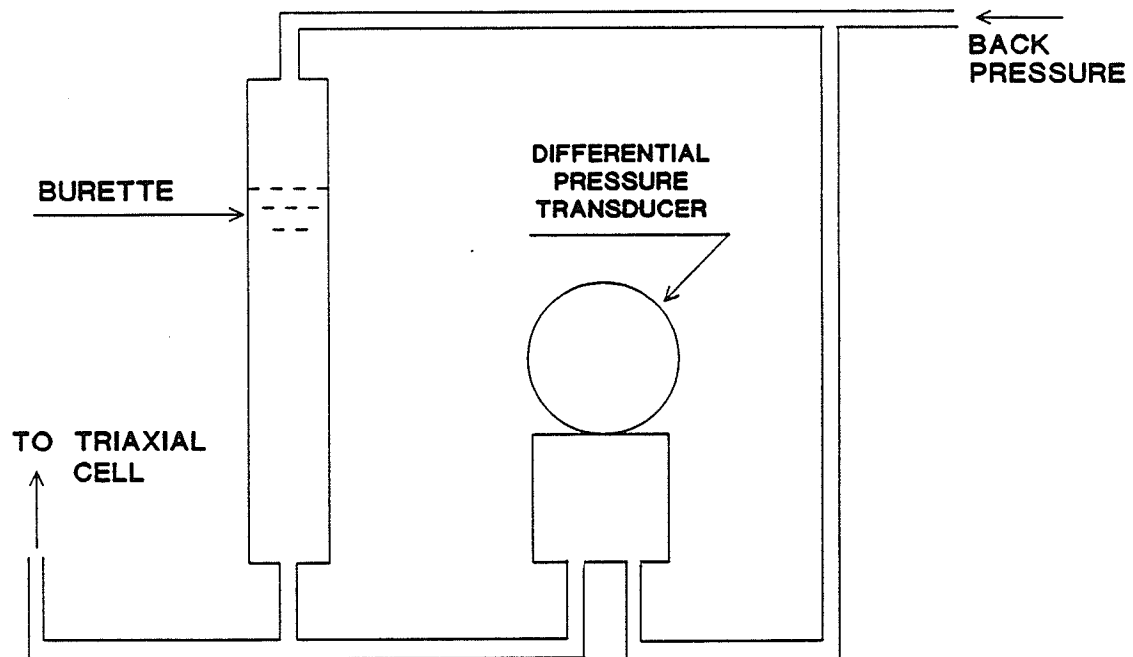


FIGURE 3.2

Schematic diagram illustrating the use of a differential pressure transducer as a volume change device.

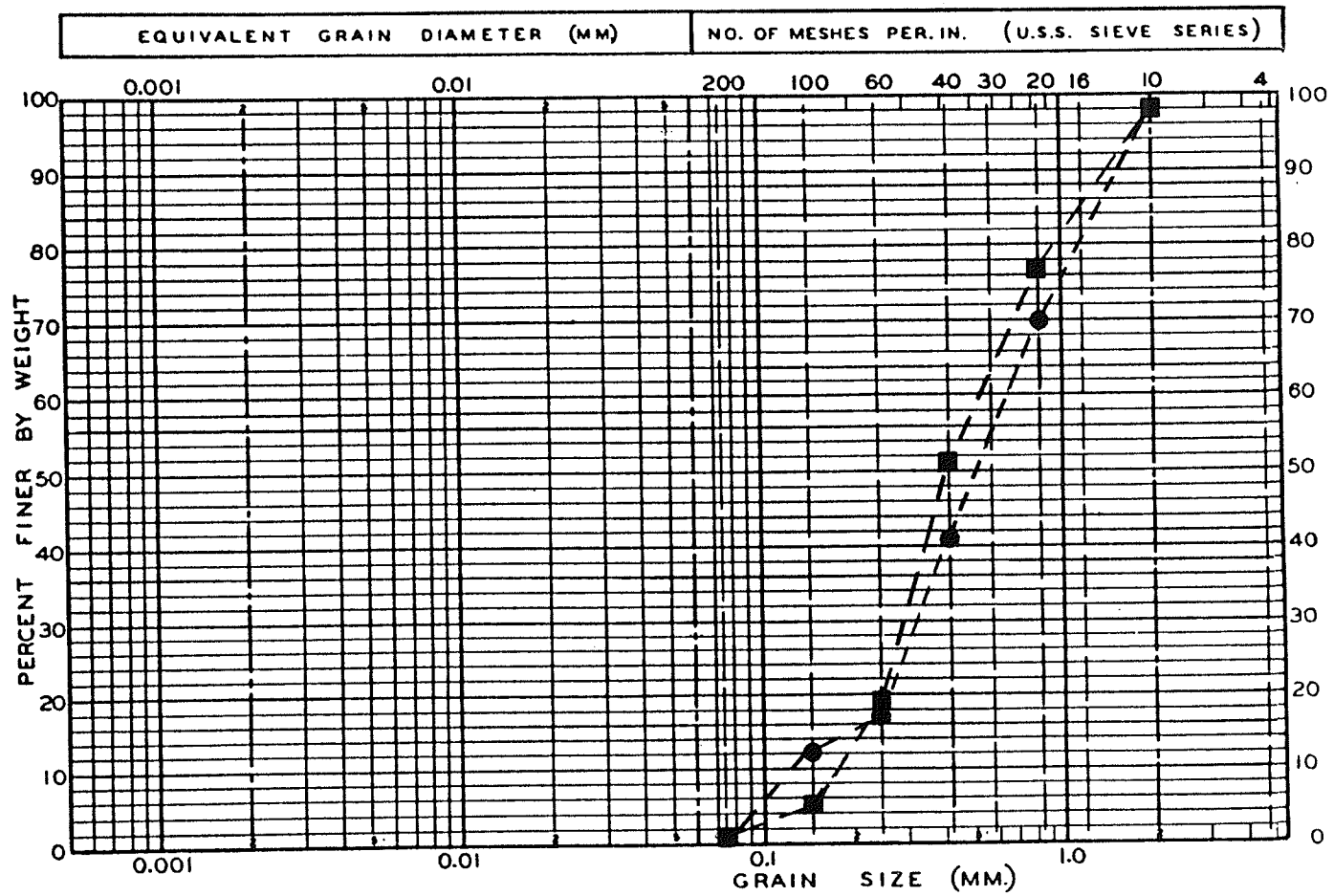


FIGURE 3.3 Sieve analysis of blended sand used in buffer specimens.

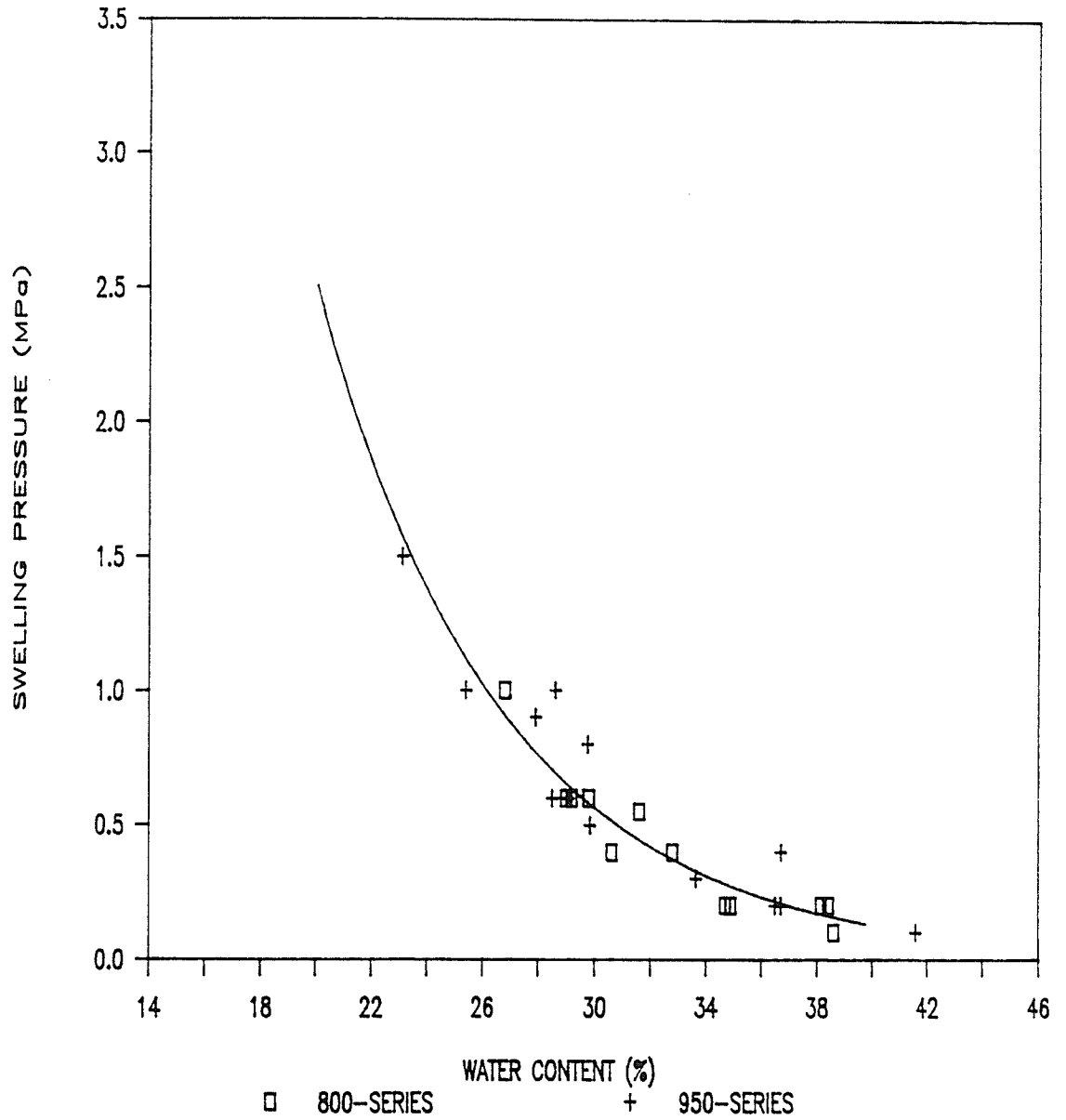


FIGURE 3.4

Swelling equilibrium pressure *versus* moisture content of buffer (from Wan 1987).

CHAPTER 4 EFFECTIVE STRESSES IN THE BUFFER

4.1 Introduction

Chapter 2 discussed the classical theory of effective stress and some modifications that have been proposed to deal with active clays. To review briefly, the modifications such as proposed by Balasubramonian (1972) included the net repulsive force ($R - A$) in the interlayer water, between the clay platelets. He then defined "apparent" and "true" effective stresses:

$$[2.7 \text{ bis}] \quad \sigma' = \sigma^* + (R - A)$$

where σ' is the apparent effective stress and σ^* is the true effective stress. Lambe (1960) correctly pointed out that only the total pressure (σ) and a porewater pressure (u) external to the specimen can be measured in the laboratory, and thus the difference between them is a measure of the (apparent) effective stress.

Equation [2.7] can then be rewritten collecting knowns and unknowns on opposite sides of the equation:

$$[4.1] \quad \sigma - u = \sigma^* + (R - A) = \sigma'$$

Equation [4.1] is Terzaghi's effective stress equation. The equation has been repeatedly demonstrated to be applicable, within engineering accuracy, for granular soils and well-behaved fine grained soils. However as discussed in Chapter 2 (Section 2.3) a considerable amount of literature has been presented that suggests that Terzaghi's equation does not apply directly to active clays. In the extreme, some researchers testing bentonites (for example Börgesson, Hökmark, and Karnland Undated; Börgesson, Brock and Plas 1990) have reported test data using total stresses only, implicitly denying the applicability of effective stresses. At a conference in Sweden in 1988, R. Pusch and R.N. Yong both argued that porewater pressures could not be measured in buffer, and therefore, that effective stresses could not be used to describe its

behaviour (J. Graham, personal communication 1991).

The effective stress principle can not be proven directly. It can only be examined by testing its corollaries, which if shown to be valid, would support the applicability of the principle. In this chapter, two corollaries will be examined directly through two novel sets of tests. It will be assumed that equilibrium conditions exist with respect to physico-chemical, environmental, and stress conditions. Other types of test have been performed by other researchers at the University of Manitoba, for example Wan (1987), and Saadat (1989) (Chapter 2).

4.2 Experimental Evidence in Support of the Effective Stress Concept

Two new test series were designed and performed to confirm the effective stress behaviour in the buffer. This section will present data from this testing program and from other researchers that supports the use of [4.1] for active clays.

4.2.1 Undrained Stress-Change Tests

A corollary of the effective stress principle states that if the volume of a specimen is held constant then the effective stress is constant. That is, $\Delta\sigma = \Delta u$ (Equation [4.1]). It could be argued by proponents of the modified effective stress concepts, that changes in total pressure could induce changes in the (R - A) balance, thus contradicting the effective stress principle, $\Delta\sigma \neq \Delta u$. This provides a test for the applicability of the principle.

Three tests were conducted in which total stresses were changed on undrained, constant volume specimens and the porewater responses observed. In these so-called "undrained stress-change tests" an initially high confining pressure was applied to an undrained (constant volume) specimen. The porewater pressures were measured at the top and bottom of the specimen during a period lasting typically 5 to 7 days. The confining pressure was then reduced and the porewater pressure response observed again. This procedure of reducing the total confining

pressure was continued until the measured porewater pressure reached zero or atmospheric pressure. As a final stage the confining pressure was raised to the original value. When the test was completed, the specimen was removed from the cell and the moisture content determined. No drainage was permitted during the test so the initial and final moisture contents were to be the same. Two low density specimens (T1131 and T1142), and one high density specimen (1127) were tested in this series. The initial dry density and moisture content of these specimens is given in Table 4.1. Final moisture contents are given in Table A.2 (Appendix A).

Figs. 4.1, 4.2, and 4.3 show the pressure *versus* time graphs. The figures show how the total (cell) pressure was changed in a stepwise manner. The tests lasted up to 1600 hours (67 days). Porewater pressures were measured at the top and bottom of the specimen. (Side drainage strips connected to the top porous stone and pressure transducers, while at the bottom, porewater pressures were measured from a porous stone inside a brass ring). There is excellent correlation between the two porewater transducers. The spikes in the pressure data prior to each decrement are due to a B-test that was conducted to confirm specimen saturation.

The difference between the cell pressure and the observed porewater pressure response represents the effective stress. Figs. 4.4, to 4.6 show the cell pressure and effective stress for the three specimens. These data raise two points. First, they show that in the buffer specimens, a portion of the total applied stress is carried by the soil skeleton and that this is independent of changes in total stress. More precisely, the test shows that in a closed system of active clay $\Delta\sigma = \Delta u$. (An assumption is made here that any deviation from $\Delta\sigma = \Delta u$ in the specimen would not be caused by factors such as loss of saturation, but would be physico-chemical in origin.) As mentioned earlier this is a test that the classical effective stress concept is valid for active clays.

Second, a drop in effective stress was observed when the porewater pressures decreased to, or slightly below zero (atmospheric) pressure. Below a threshold total pressure less than the

swelling equilibrium pressure (SEP), the specimen would have a tendency to suck in water and swell. If this happened in a closed system, the pressure on the diaphragm of the pressure transducer would reduce as water in the drainage leads is drawn into the specimen and cavitation would occur in the cell base passages. The ability of the pressure transducers to measure the porewater pressure at confining pressures below the SEP depends on several factors. One is that the transducers should be mechanically capable of reading negative (tensile) pressures. Perhaps more importantly, the pressure measuring system of transducers, drainage leads and filter stones should be able to resist cavitation of the water. The drop in porewater pressure and apparent effective stress at the threshold total pressure is therefore more "apparent" than real. It is simply that the closed system can not adequately maintain negative pressures. It does not negate the effective stress principle.

TABLE 4.1 Effective Stress Tests: Undrained

Test	Initial Conditions			Remarks
	γ_d (Mg/m ³)	w (%)	w _c (%)	
T1127	1.65	22.3	46.6	Undrained stress-change
T1131	1.49	29.4	58.6	Undrained stress-change
T1142	1.50	29.0	58.0	Undrained stress-change

4.2.2 Drained-Isotropic Tests

A second corollary of the classical effective stress principle with direct implications to active clays states that a specimen subjected to an isotropic stress condition will reach an equilibrium specific volume directly related to the effective stress. In the case of the buffer, it has been previously established that the properties are dominated by the bentonite. Thus it should be expected that the effective stress-specific volume relationship is the same for the buffer (which is a 50:50 mix of sand and bentonite) as for pure bentonite. The relationship should be

independent of initial moisture content. Furthermore, the same pressure-specific volume relationship should be obtained from different test types.

In the so-called "drained-isotropic tests", seven specimens were consolidated from high moisture contents under isotropic pressures. Drainage was permitted from the top of the specimen with independent porewater measurement at the base. Total confining pressures ranged from 1.7 MPa to over 5.5 MPa. The initial test conditions are given in Table 4.2. Final moisture contents are given in Table A.2 (Appendix A). Four soils were tested in this series. Two specimens were of buffer (although they were prepared at different moisture contents and different mixing procedures). Two specimens were illite. One of these was cut from a block consolidated one-dimensionally from a slurry by Jamieson (1989). The second was prepared at the specified moisture content by directly mixing oven dried soil and water. One specimen was of pure Avonseal bentonite. This was the bentonite used in the buffer. Two specimens were of a Wyoming bentonite (Volclay Waterstoppage: liquid limit \approx 600%.)

TABLE 4.2 Effective Stress Tests: Drained

Test	Initial Conditions			Remarks
	γ_d (Mg/m ³)	w (%)	w _c (%)	
T1126	0.89	73.3	146.6	Drained-isotropic test
T1199a	0.60	110.2	220.4	Re-constituted buffer Drained-isotropic test
T1199b	1.02	61.3	61.3	Illite: Drained-isotropic test
T1199c	0.38	212	212	Pure bentonite: Drained-isotropic test
T1199d	1.16	50.1	50.1	Illite: Drained-isotropic test
T1199e	0.16	572	572	Wyoming bentonite: Drained-isotropic test
T1199f	0.12	661	661	Wyoming bentonite: Drained-isotropic test

A high confining pressure was applied to an initially undrained specimen and the

porewater pressures allowed to stabilize. After stabilization the top drain was opened with a back pressure of 200 kPa (500 kPa in one case). The specimen was permitted to consolidate until the average moisture content reduced appreciably. Drainage was then closed, and the porewater pressures allowed to stabilize. This procedure was repeated until the specimen would not consolidate any more at the applied cell pressure. At the end of the test, the specimens were divided into five sections and the moisture content of each section determined. The variation in moisture content along the length of the specimen would provide an indication of fabric non-uniformities as a result of high pressure gradients experienced by the specimen during the consolidation phases. Examination of the stress-specific volume relationship would provide an indication of the applicability of the effective stress principle.

Fig. 4.7 shows pressures *versus* time data for specimen T1199a. The graph was typical of all specimens; hence pressure-time data from all tests have not been repeated here. At the start of the test the porewater pressures were very close to the total pressure, within several kPa. As drainage occurred the porewater pressure responded by decreasing while the total pressure was kept constant. At the end of each consolidation stage the top porewater pressure (which was used for drainage) was allowed to stabilize. The pressure in the top transducer rose from the applied back pressure to meet the base porewater pressure. (The small difference between the two porewater pressures is probably due to a small difference in water content inside the specimen.)

The effective stresses in each test can be easily measured, and there is little uncertainty in their values. Figs. 4.8 to 4.10 present the apparent effective stresses as a function of clay specific volume for buffer, illite and Wyoming bentonite specimens respectively. The effective stress is taken as the difference between the cell pressure and the base porewater pressure.

Three tests are shown on Fig. 4.8. These are for the buffer and Avonseal bentonite specimens. Also shown is a regression curve for the swelling equilibrium line (SEL) reported by Dixon, Gray, Baumgartner, and Rigby (1986b) for confined swell tests on buffer. These data

show that the effective stress response is apparently independent of both initial water content and confining pressure.

The fact that the effective stress behaviour of the specimen of pure Avonseal bentonite is the same as those of the buffer shows that the bentonite controls the buffer behaviour and that the sand acts, to a large degree, only as a filler. This was previously suggested by Dixon *et al.* (1986b).

The "violent" nature of the test where in the specimen is subjected to alternating very high and very low effective stresses could potentially lead to permanent changes in fabric within the specimen, between the top (drained) and the base (undrained). To check this, at the end of the test the specimen was cut into multiple sections and the moisture content of each section was determined. No significant non-homogeneities in soil structure or fabric would be inferred if the longitudinal variation in moisture content of the specimen was small. Remember that the bentonite is a strongly-swelling clay mineral.

There were three buffer/bentonite specimens tested (T1126, T1199a, and T1199b). The variation in moisture content ranged from 0.6% to -2.5% with an average of -0.7%. This difference approaches the error generally accepted for moisture content determination. For comparison, quality control tests by Saadat (1989) showed longitudinal variations in moisture content of as much as 1% in so-called homogeneous specimens. For the two illite specimens (T1199b and T1199d) the variation in moisture content was from 0.1% to -0.1%, with an average of 0%. The Wyoming bentonite specimens were not sectioned due to the small final weight (less than 50 grams).

Thus there is only a small variation in moisture content at the end of each test, which on average is less than experimental error. This confirms that although the specimens experienced very large effective stress gradients across their length during the drained stages, the soil fabric of the swelling bentonite re-adjusted itself during the equalization stages.

Fig. 4.10 shows data from two specimens of Wyoming bentonite. The initial moisture contents were 572% and 661%, and the final moisture contents were 73% and 47% respectively. Both specimens experienced small leakage or moisture loss during the test. The differences in final moisture contents estimated separately by volume change and drying were 23% and -29% respectively. (Table A.1, Appendix A) The data in Fig. 4.10 have been corrected for the leakage by assuming the moisture content discrepancy (and specific volume) to be a linear function of the effective stress. The difference in corrected specific volume of the specimens is about 1. The shape and form of the graphs are the same and consistent with those presented in Figs. 4.8 and 4.9.

Figs. 4.8 to 4.10 show that the general relationship between apparent effective stress and specific volume is valid over a wide range of soil types. Fig. 4.8 shows data for four buffer specimens prepared in very different ways, Fig. 4.9 shows data for the two illite specimens, and Fig. 4.10 shows data for two Wyoming bentonite specimens. The consistency of the results supports the applicability of the effective stress principle. These figures suggest that an intrinsic property of the soil is being measured. The development of effective stresses within the specimens is generally independent of specimen preparation. That is, it is only a function of clay mineralogy (and of course pore fluid chemistry).

As a separate issue, if the data in Figs. 4.8 to 4.10 are plotted in $V, \ln p'$ -space, consolidation curves are obtained. (It is important to note however, that these tests differ significantly in kind and methodology from a 1-D or isotropic consolidation test.) The material property being measured is the slope of the normal consolidation line. The slope of the straight line portion is denoted λ . Other research has shown that the positions (but not the slope) of the normal consolidation line (NCL) and critical state line (CSL) in $V, \ln p'$ -space may vary as a function of soil fabric. For example Graham and Li (1985) showed that for Winnipeg clay, the NCL and CSL for undisturbed and remolded specimens were parallel but shifted vertically from

each other. Thus λ is constant and is independent of the soil fabric. This conclusion can also be reached by examining the conditions of normal consolidation and critical state. The critical state is reached by shearing to a large strain so that soil particles re-orientation occurs at a constant rate. Thus the soil fabric at critical state may represent a type of "remolded" fabric. A similar process may occur during consolidation since large plastic volume strains are taking place, resulting in a re-orientation of soil particles.

4.2.3 Other Experimental Evidence

A third corollary of the effective stress principle states that specimens should exhibit the same shear-strain and volume change behaviour when consolidated at the same effective stress, regardless of the total stress conditions. Saadat (1989) conducted tests on two similar specimens at the same apparent effective stress but with different total and back pressures. The specimens had the same initial moisture content and dry density. Both were consolidated at effective pressures of 1.5 MPa, but with back pressures of 1.8 MPa and 4.0 MPa. Fig. 4.11 shows the stress-strain response in undrained triaxial compression. The curves are very similar.

Saadat (1989) also performed tests where he changed the total stresses during consolidation while maintaining the same effective stress. The result was no change in the volume strain (or volume strain rate where some volume straining was still continuing). Results of some of these tests were reported by Graham *et al.* (1989a)

One of the most important aspects of understanding different laboratory test data is the concept of normalization. This is a method of rationalizing strength data at different pressures for similar specimens. Normalization means dividing the strength data by a common variable. The effective preconsolidation pressure or the equivalent effective pressure are possible normalizing factors (Atkinson and Bransby, 1978). However, normalization of data is possible only on "effective" stress data; total stress data do not normalize. Wan (1987) and Saadat (1989)

presented normalized strength data for the buffer that were consistent with each other, and reasonable within the context of the reported values. More normalized stress path data are presented in Chapter 5 of this thesis.

4.3 Discussion

The introduction to this Chapter listed several restricting conditions which may need to be met in order to apply [4.1]. The conditions required equilibrium with respect to volume, environment (for example temperature) and chemistry. However, the conditions may be too restrictive, and may not necessarily need to apply at all times.

As an example, consider the case of the drained-isotropic tests (Section 4.3.2). Some researchers (for example Barbour and Fredlund 1989) maintains that active clays behave as semi-permeable membranes. Thus the solvent (ie: water) may pass, but the solute (ie: dissolved salts) do not pass. In these tests, where significant volumes of water were expelled from the specimens, there can be little question that the porewater chemistry is changing. It is well documented that $(R - A)$ is affected by changes in porewater chemistry. However, if in [4.1] we observe only the gross sum of skeletal (σ^*) and physico-chemical $(R - A)$ components then it may be argued that it does not matter which of the individual component changes. Thus in the drained-isotropic tests the increase in the effective stress may be due to changes in $(R - A)$. This reasoning strengthens the case for the use of an equation such as [4.1].

Although a condition of constant volume was suggested for applicability of the principle, tests such as the drained-isotropic tests, and the normalization of drained shear data often exhibit significant volume changes. The use of [4.1] nevertheless remains valid.

Preceding sections presented evidence to support the effective stress principle. In no instance was consideration given to the actual physico-chemical forces acting at the microscopic level. It may seem to some that this examination is a "trivial pursuit". To observers outside the

immediate research field [4.1] may seem intuitively reasonable, even for active clays. Yet as was documented earlier, many respected researchers argue in favour of quantifying the physico-chemical forces within an active clay. To those researchers in this field the debate is real, justifiable, and persistent. Experimental evidence from this research program reinforces data previously collected in support of the effective stress concept.

Analyses of data in subsequent chapters of this thesis will accept the validity of [4.1]. A discussion of this concept and the associated evidence for it is presented in a paper currently in preparation for publication (Graham, Oswell and Gray 1991).

BUFFER SPECIMEN T1127
DRY DENSITY = 1.65 Mg/m³

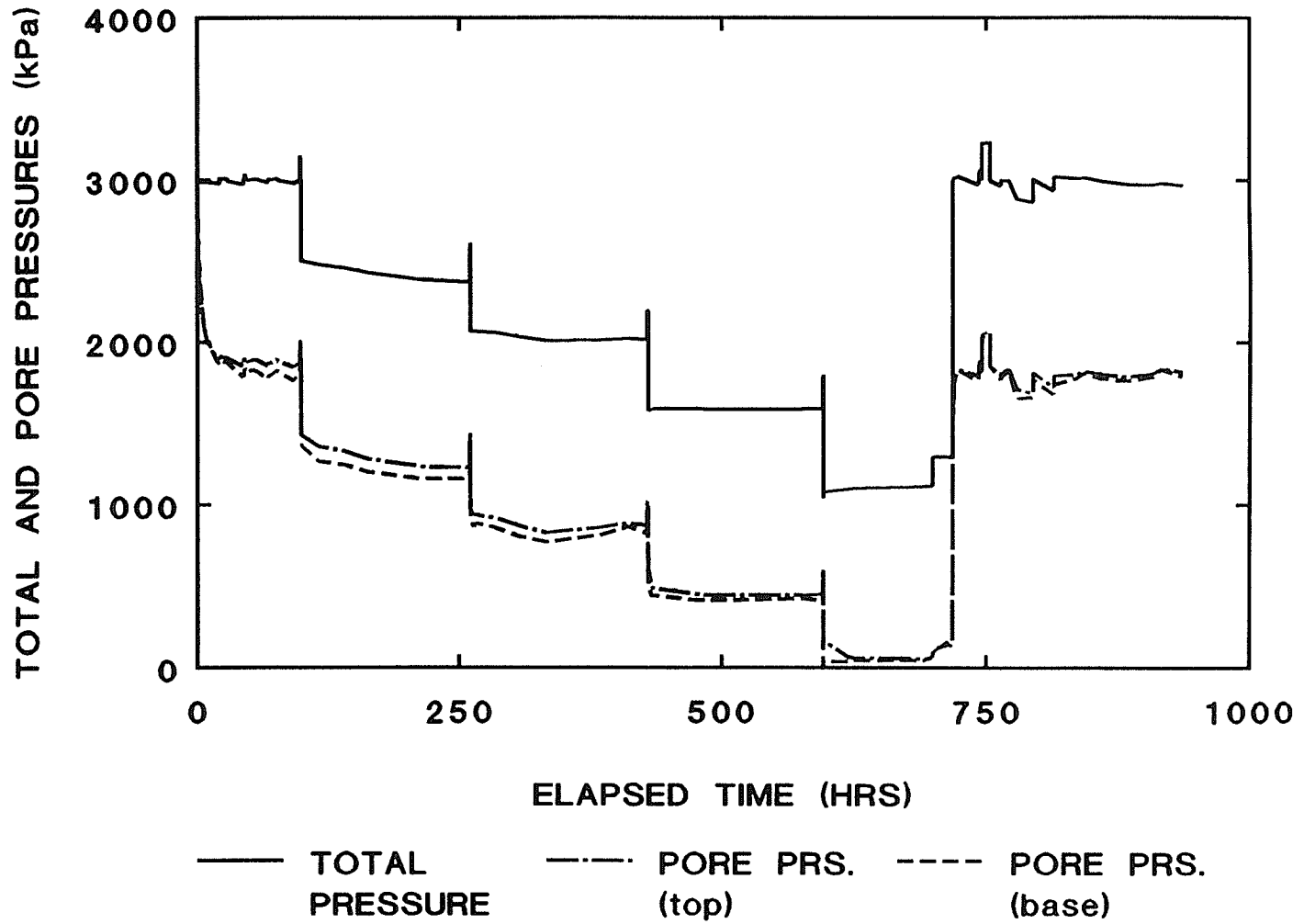


FIGURE 4.1 Total (cell) and porewater pressures *versus* time under undrained conditions. Buffer specimen T1127.

BUFFER SPECIMEN T1131
DRY DENSITY = 1.49 Mg/m³

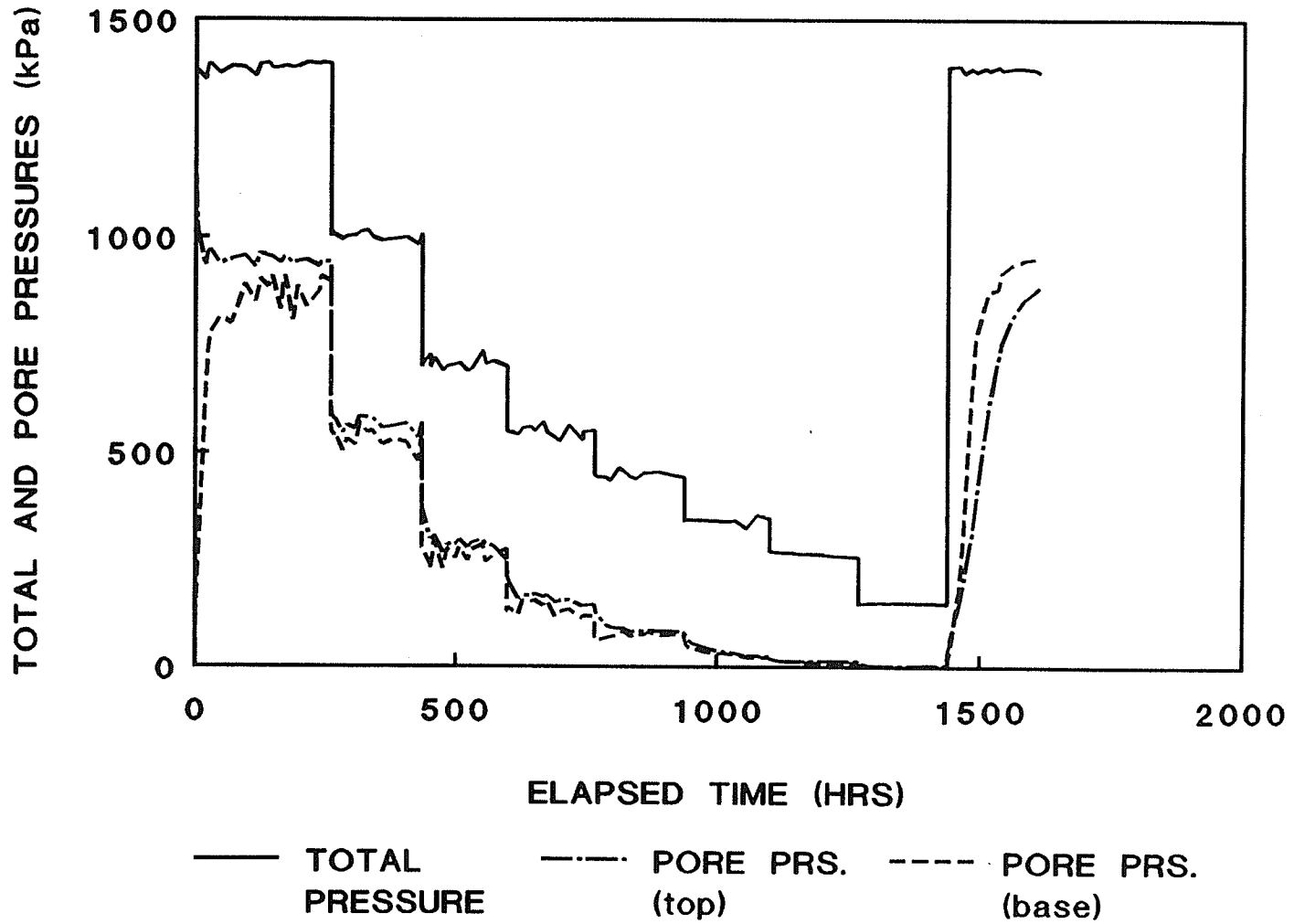


FIGURE 4.2 Total (cell) and porewater pressures *versus* time under undrained conditions. Buffer specimen T1131.

BUFFER SPECIMEN T1142
DRY DENSITY = 1.50 Mg/m³

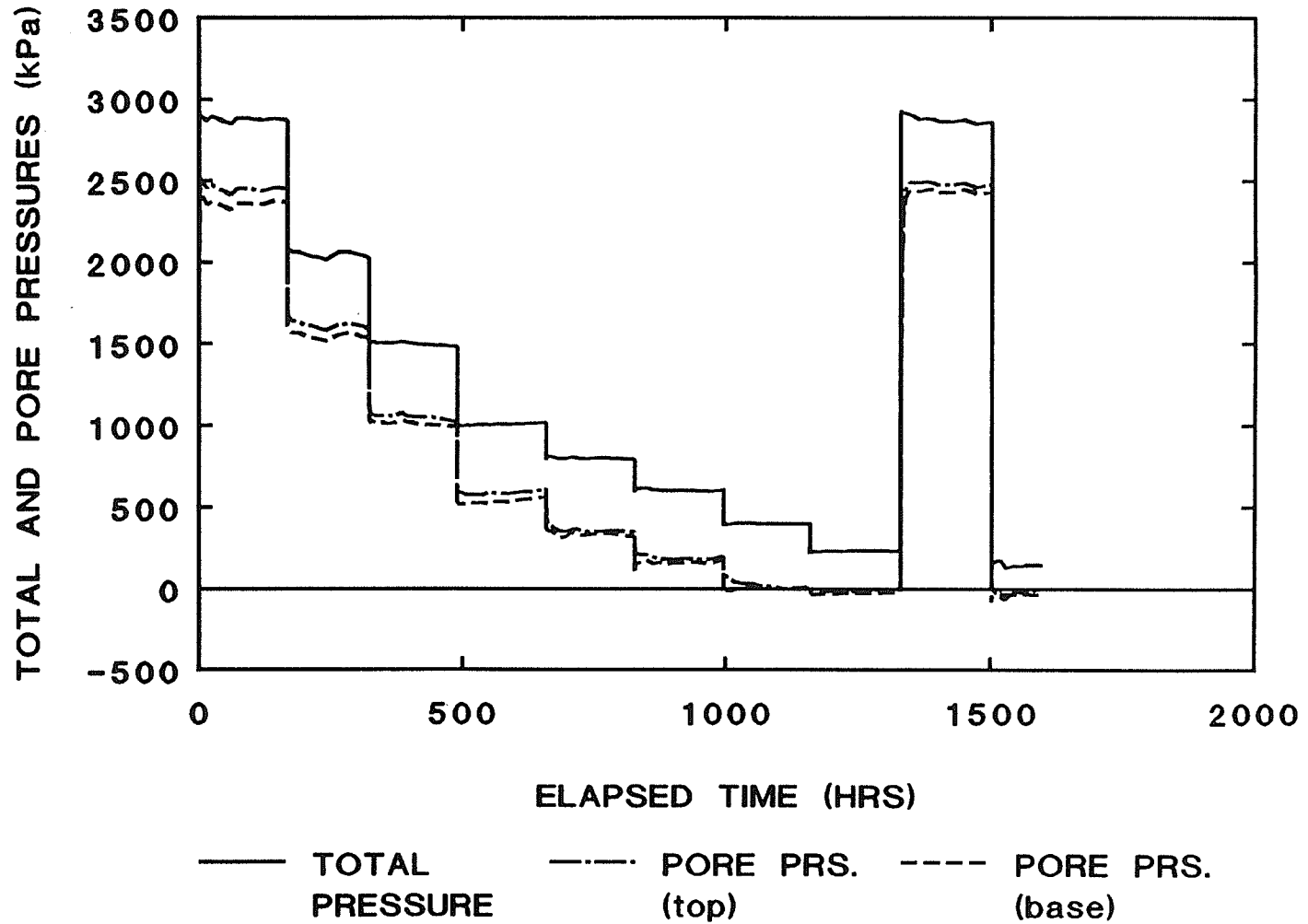


FIGURE 4.3

Total (cell) and porewater pressures *versus* time under undrained conditions. Buffer specimen T1142.

BUFFER SPECIMEN T1127
DRY DENSITY = 1.65 Mg/m³

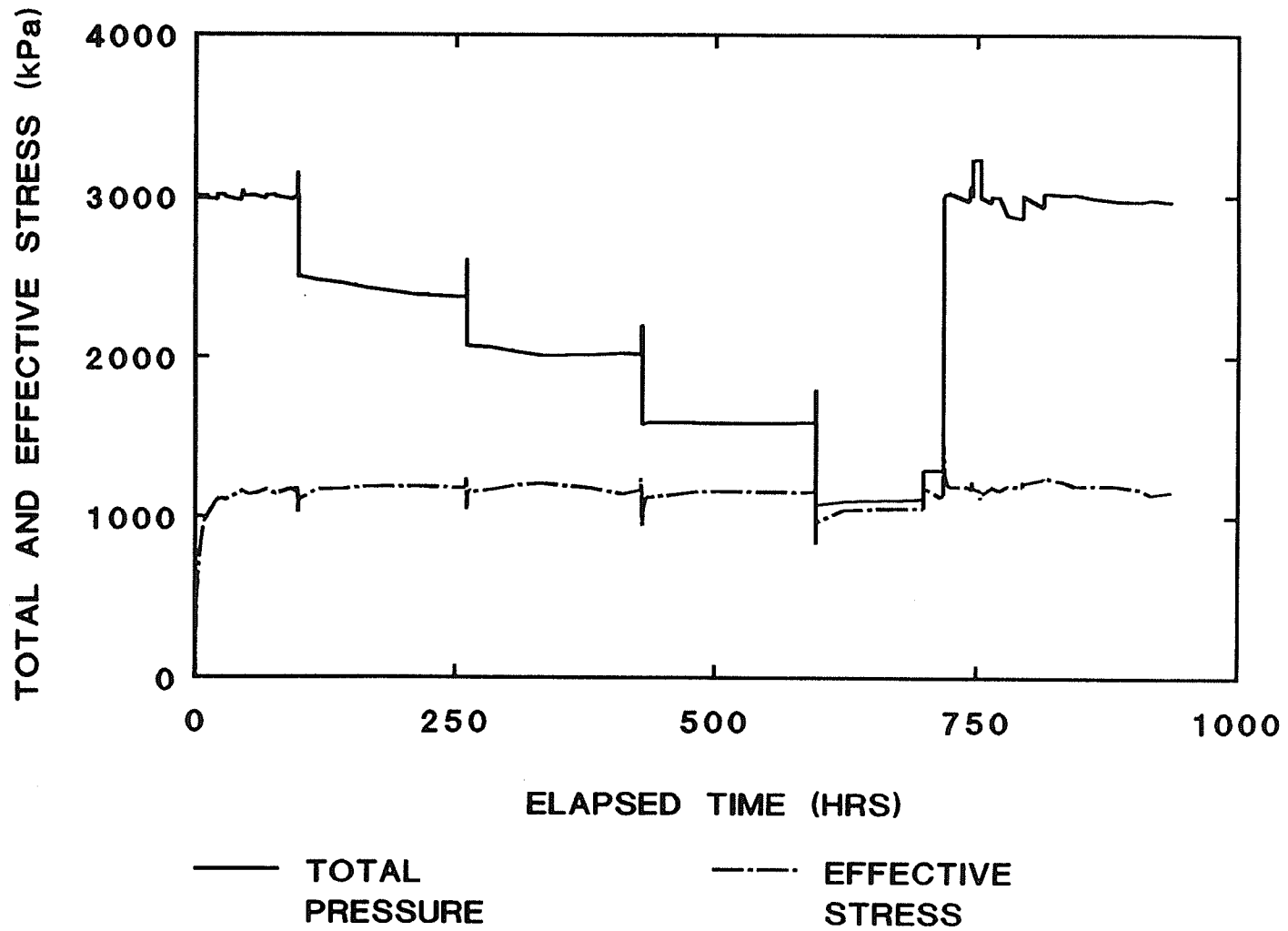


FIGURE 4.4 Total pressure and apparent effective stress *versus* time under undrained conditions. Buffer specimen T1127.

BUFFER SPECIMEN T1131
DRY DENSITY = 1.49 Mg/m³

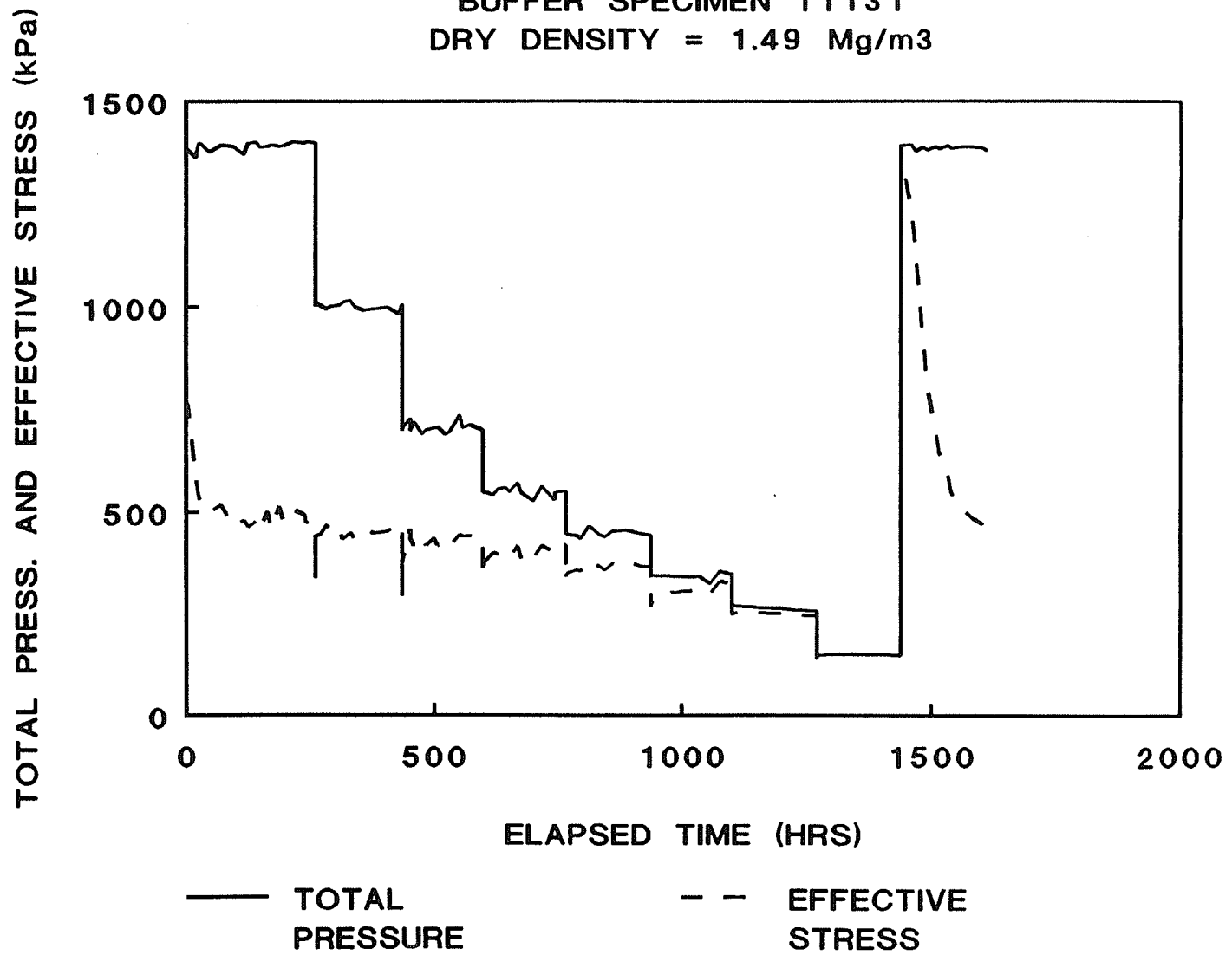


FIGURE 4.5 Total pressure and apparent effective stress *versus* time under undrained conditions. Buffer specimen T1131.

BUFFER SPECIMEN T1142
DRY DENSITY = 1.50 Mg/m³

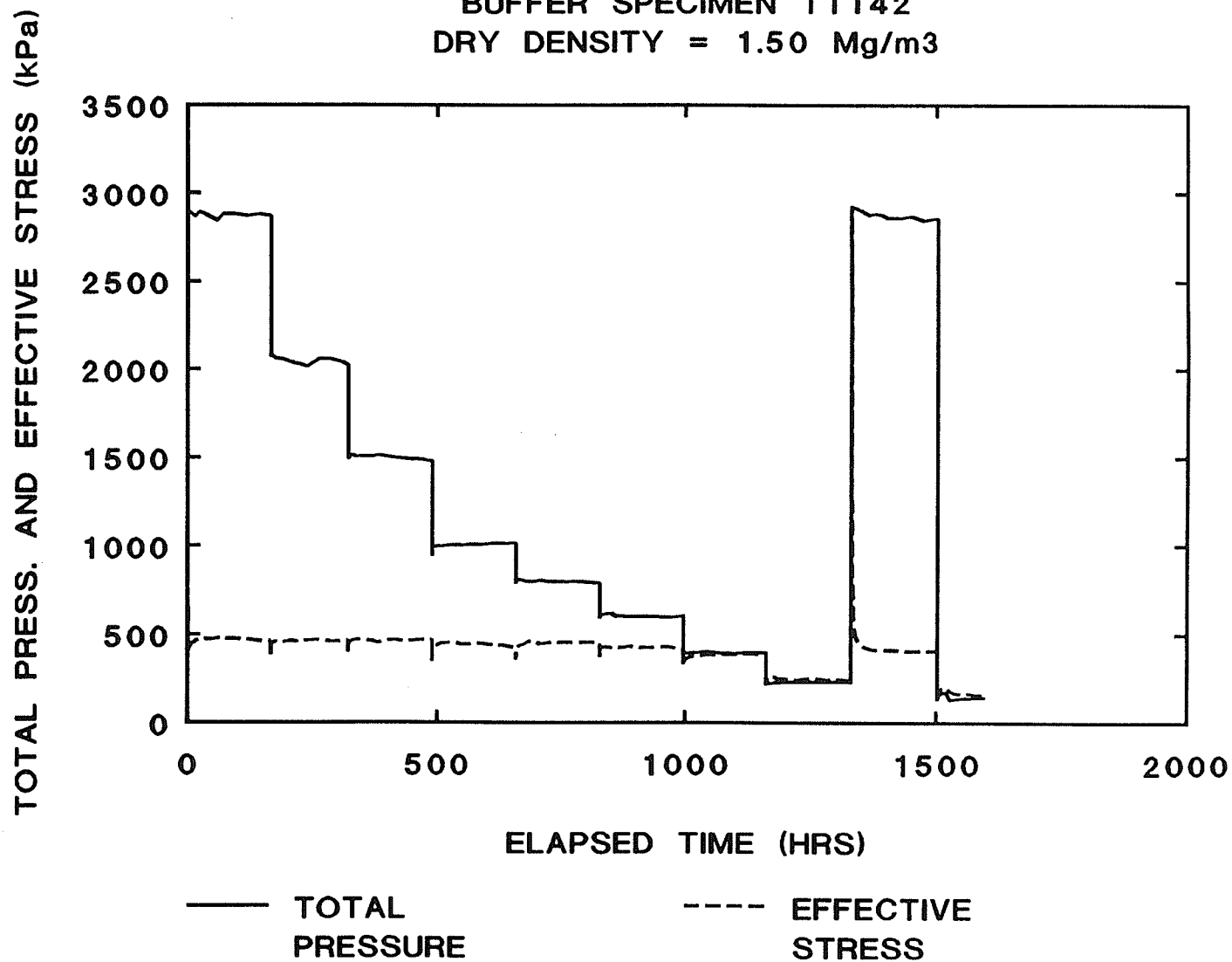


FIGURE 4.6

Total pressure and apparent effective stress *versus* time under undrained conditions. Buffer specimen T1142

BUFFER SPECIMEN T1199a
 DRY DENSITY = 0.6 Mg/m³

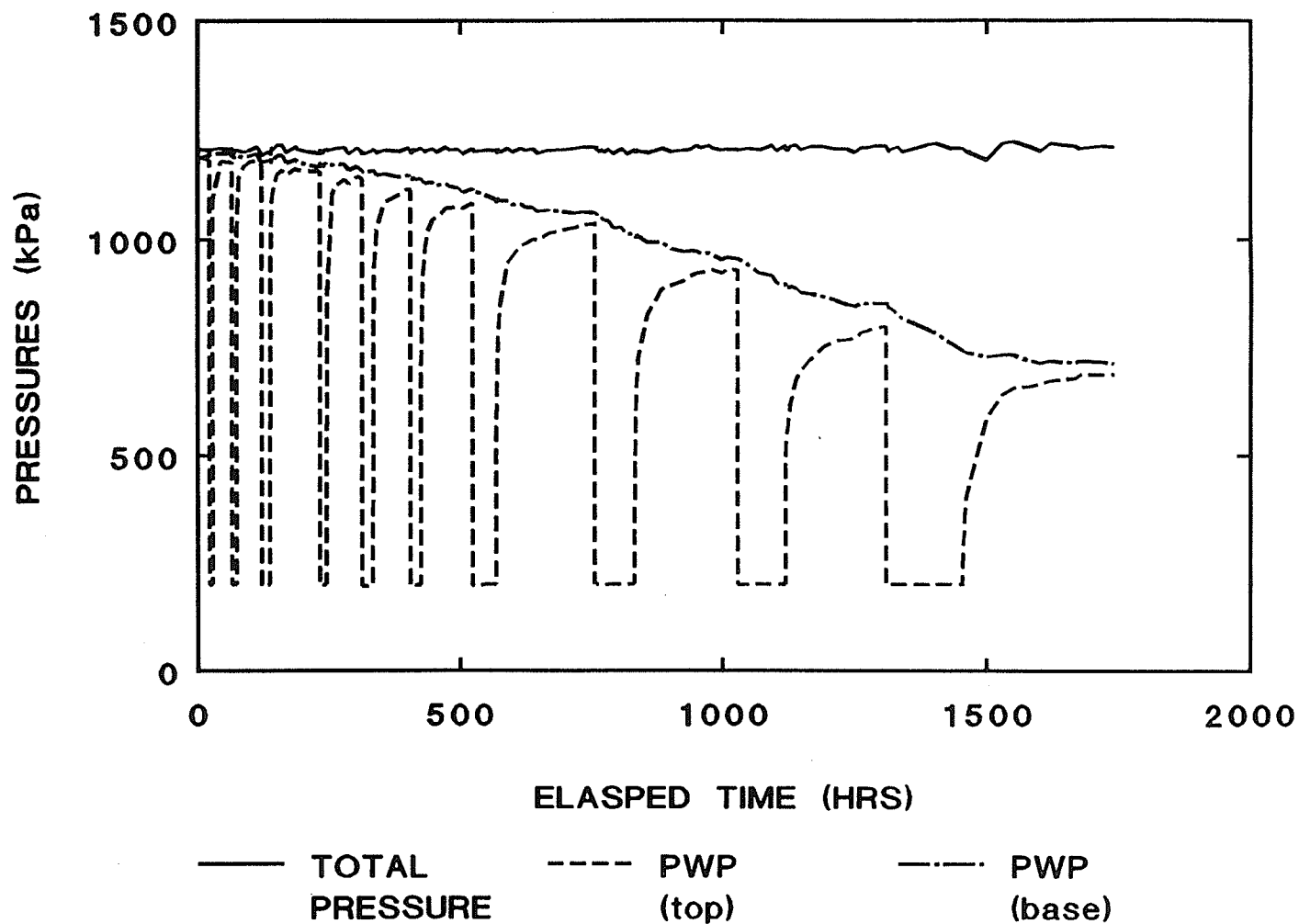


FIGURE 4.7 Total (cell) and porewater pressure *versus* time during consolidation and undrained conditions. back pressure (top) during consolidation was 200 kPa. Buffer specimen T1199a.

BUFFER SPECIMENS
1100 SERIES

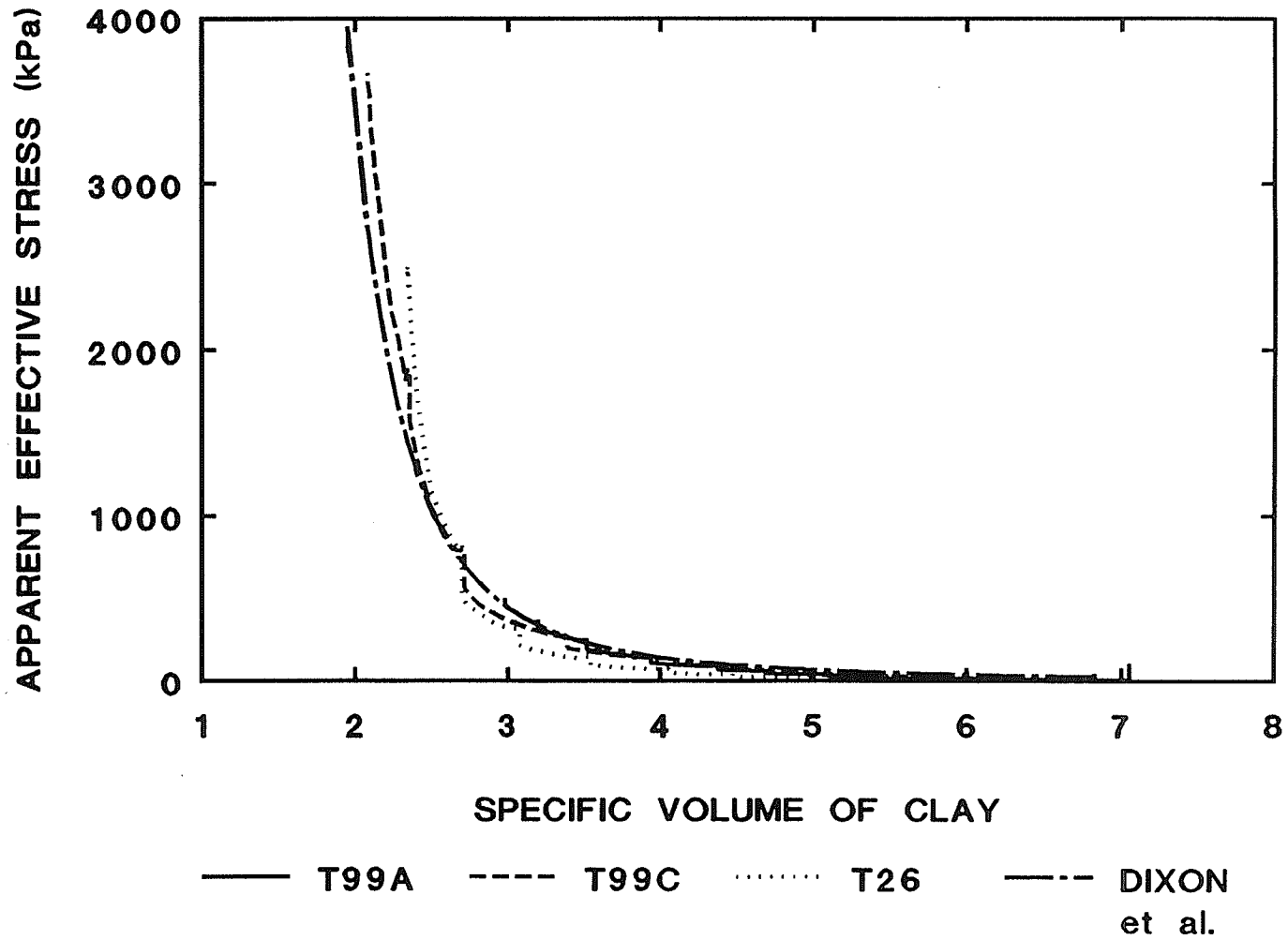


FIGURE 4.8 Apparent effective stress *versus* specific volume of clay: buffer specimens (1100 series).

ILLITE

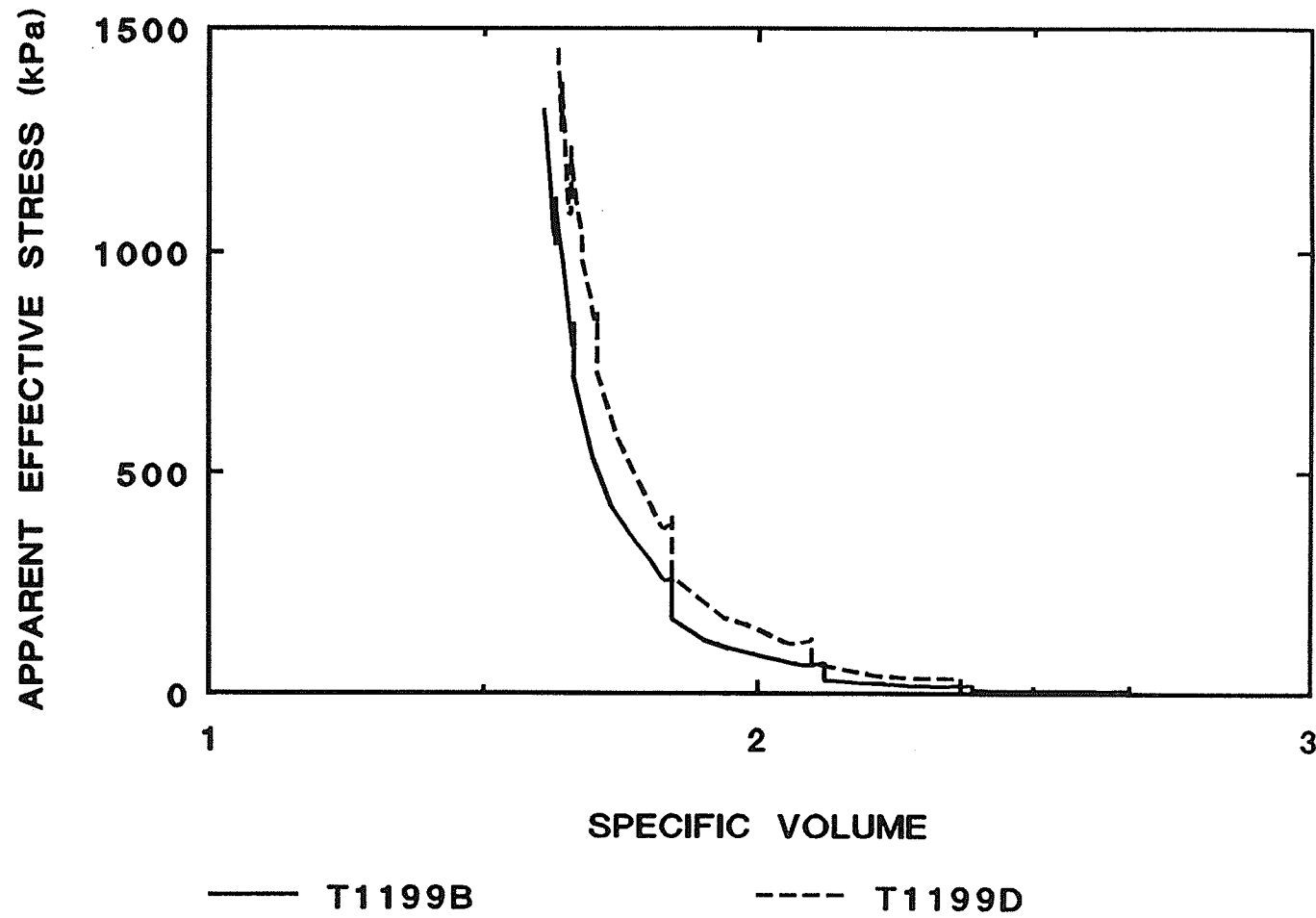


FIGURE 4.9

Apparent effective stress *versus* specific volume of clay: illite specimens.

WYOMING BENTONITE
WATERSTOP CLAY

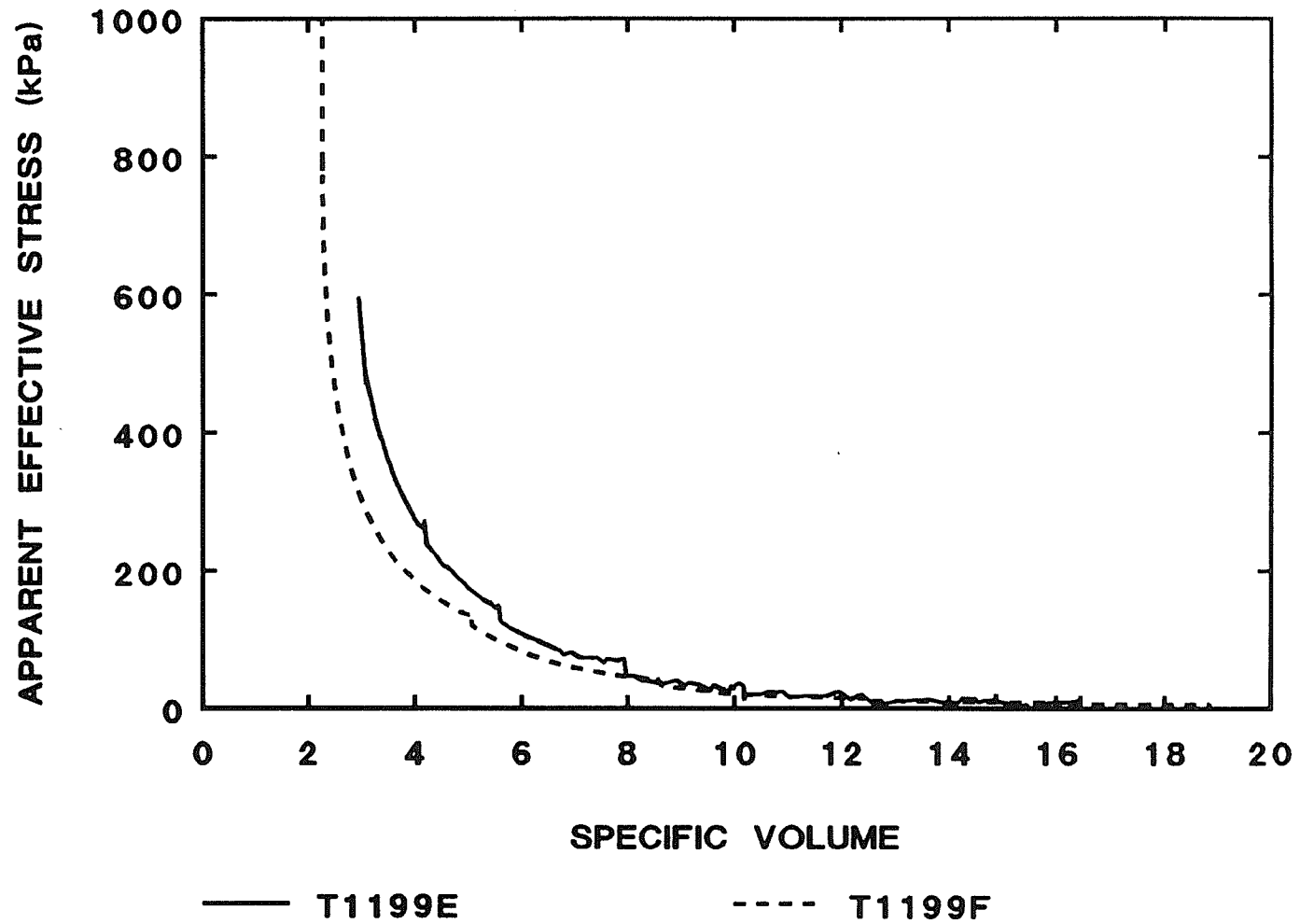


FIGURE 4.10 Apparent effective stress *versus* specific volume of clay: Wyoming bentonite specimens.

BUFFER SPECIMENS T927 & T932
DRY DENSITY = 1.66 Mg/m³

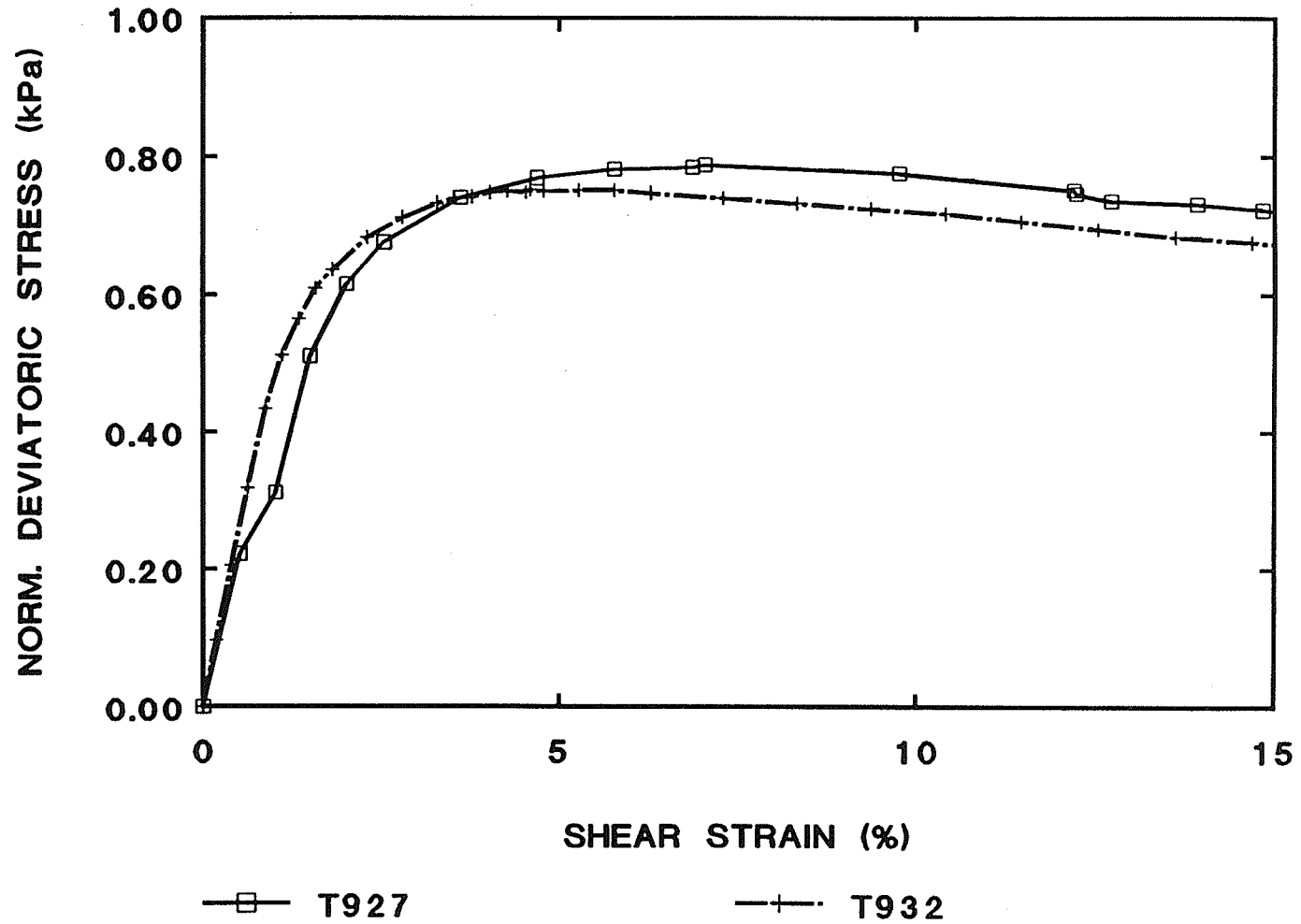


FIGURE 4.11

Normalized stress-strain data for undrained triaxial compression test.
T927 and T932. (from Saadat 1989).

CHAPTER 5 PRESENTATION OF YIELD AND END-OF-TEST DATA

5.1 Introduction

This chapter presents details of the testing program to examine the elastic plastic behaviour of the buffer. One of the first tasks in developing an elastic plastic model is to determine the yield locus. The flow rule and plastic potential are then usually determined after the yield behaviour has been established. The yield locus in q, p' -space is determined from stress probe tests. A group of such probes or paths is shown schematically illustrated in Fig. 5.1. Also shown in the figure is an elliptical yield locus and failure envelope of slope M . This figure represents the classical elastic plastic soil model, known as modified Cam Clay (the flow rule is assumed to be "associated"). The stress probes shown in the figure fall into three categories. Stress path #1 is such that yielding will be observed, but the specimen will not fail. The stress path does not intersect the failure envelope. A specimen following a stress path such as #2 will yield and then, with further stressing, move to failure. For these stress paths, post-yield stressing will involve plastic straining. The normal to the local yield locus involves compressive plastic volume straining ($\epsilon_v^p > 0$). Associated with these compressive strains, the region of elastic behaviour expands so that the current stress state remains on the State Boundary Surface. The reduced water content and expanded elastic region produce a stiffer, stronger specimen.

A specimen that follows a stress path such as #3 will yield and then, because the yield surface lies above the failure envelope, will "strain soften" to failure. Strain softening involves negative (expansive) plastic volume straining and a contracting region of elastic behaviour. The resulting higher water content and decreased elastic region produce a less stiff, weaker specimen.

To achieve a particular stress path ($dq/dp' = \text{constant}$) the cell pressure is changed in response to changes in deviator stress. Only for one stress path ($dq/dp' = 3$, in the so-called drained triaxial compression test) does the cell pressure remain constant.

Tests to identify the stresses at which yielding occurs are usually performed under drained conditions. In undrained tests, the effective stress paths are constant, regardless of the total stress path and only one yield stress could be obtained (from Graham and Houlsby 1983). The effective stress path determines the yielding and the plastic parameters for the material.

The triaxial tests used in this study were (1) incremental stress controlled tests, (2) constant rate of strain tests, and (3) constant rate of stress tests.

Tests using incremental stress control have been the tests traditionally used to examine yielding behaviour in clays (for example Mitchell 1970). Although strain softening behaviour cannot be examined in such tests, the yield points for any stress path can be found. In this research program, the axial stress was applied by adding dead weights to a hanger on the axial ram. The cell pressure was adjusted with each new dead weight increment to give the desired stress path. The duration of each load increments had to be such that excess porewater pressures would dissipate during the test. The size of the applied load increment was chosen so that four or five increments preceded yielding. In the case of strain hardening specimens, several more increments were added after yielding. In strain softening specimens, the load increment that caused yielding would also produce rupture of the specimen.

Constant rate of strain tests have the advantage over the other two types of tests in that strain softening behaviour will be observed if it occurs. The disadvantage is that the cell pressure must be adjusted frequently in order to maintain the desired stress path. Furthermore, the strain rate has to be slow enough so that excess porewater pressures do not build up during testing.

Constant rate of stress tests require a feed-back facility in the loading apparatus that allows the equipment to continually seek a higher deviator stress. The stress-path type cells (Bishop and Wesley 1976) described in Chapter 3 are well suited for this type of test when controlled by GDS equipment. The rate of stress must be slow enough to permit dissipation of any excess porewater pressures. Since the test always seeks a higher deviator stress, the strain rate is left uncontrolled.

As the specimen reaches peak strength, the test apparatus (if not controlled) rapidly increases the strain rate as it seeks higher deviator stresses. This test can not be used to examine strain softening behaviour.

In this research program, the majority of yielding tests were done using incremental stress controlled compression. This was done for several reasons. First, there was more laboratory equipment available for this type of test. Therefore research productivity would be higher. Second, the need to continually monitor the deviator stress and adjust the cell pressure to achieve the desired stress path was reduced substantially. Third, most previous research on yielding had been done using this type of test, and hence there was good review literature available on testing procedures and techniques.

As a subsidiary program, yielding of the buffer was also studied using the other two test methods. Four tests of each method were carried out on low density specimens.

In the next three sections, the procedures for each of the compression test methods for yielding will be given. Typical yielding data will be presented in following sections. Several different techniques are available for determining the yield stresses from the data. These include examination of stress-strain data or consideration of energy (work) absorbed by the specimens during shear. A yield locus will then be developed for the two buffer densities that have been tested. The yield data will be presented in different stress-strain spaces.

Only selected results from a limited number of tests will be presented in this chapter. Shear stress-shear strain plots from all the yielding tests are given in Appendix C. The volume of data collected from nearly 40 tests is too large to be presented here in its entirety. Data for tests completed to the end of May 1990 (T1147) have been presented in a report to AECL (Graham *et al.* 1990a). The remaining test data (T1148 to T1156) have been reported in a supplement to the 1990 AECL report (Graham and Oswell 1991).

5.2 Incremental Stress Controlled Tests

This series contained 27 drained (and three undrained) stress controlled triaxial tests. The tests were conducted in a similar manner to that described by Noonan (1980) and Lew (1981).

The specimens were prepared and built into the cells as described in Chapter 3. Both low and high density specimens were tested in this series. All specimens were held at a previously selected swelling equilibrium pressure (SEP) for 10 days. For the low density specimens (1.49 Mg/m^3), a total pressure of 750 kPa and back pressure of 200 kPa was used. For the high density specimens (1.67 Mg/m^3), six tests used an effective SEP of 2100 kPa. After preliminary examination of these data and an additional test at an effective SEP of 1400 kPa, it was decided to use an effective SEP of 1700 kPa for the remaining tests on high density specimens. After the stabilization period at the SEP, the cell pressure was reduced to give the specimen an OCR of 1.75, as described in Section 3.6. The specimen was allowed to swell under an isotropic cell pressure for 3 days.

A small dead load was maintained on the axial ram during the 3 day swell period. This load was only sufficient to overcome the upward force on the ram created by the internal pressure in the cell. The resulting axial stress was typically 5 to 10 kPa larger than the cell pressure. This load allowed the ram to remain in contact with the specimen so that axial deformations could be measured during swelling.

Shearing was carried out by adding dead weights to the axial ram and adjusting the cell pressure to achieve the desired stress path. The load was increased every three days. The three day loading increment was used as a compromise between allowing too much swelling and the time needed to dissipate excess porewater pressure. (Wan, (1987) used five day loading for a similar series of tests.) Whenever a new load was added, the axial deformation, volume change and the various pressures were recorded using an approximately geometrically increasing time sequence. There were ten readings in the first hour, and two in the next hour. The reading

frequency gradually decreased until there were two readings per day after two days.

The size of the load increments was such that yielding would occur around the fourth increment. In this way, there would be a sufficient number of increments to establish trends in behaviour. In some cases more than one test was conducted along a particular stress path to achieve the desired number of load increments before yielding.

At least one specimen at each density was loaded to yield under nominally isotropic (equal all-round) pressures. A small load was maintained on the axial ram at all times to counteract the cell pressure and maintain contact with the specimen. The resulting axial stress was typically 5 to 10 kPa larger than the cell pressure.

Table 5.1 lists the test conditions in the series of incremental stress controlled tests.

TABLE 5.1 Incremental Stress Controlled Tests

Low Density Tests (Target $\gamma_d = 1.49 \text{ Mg/m}^3$)			High Density Tests (Target $\gamma_d = 1.66 \text{ Mg/m}^3$)		
Test	p'_o kPa	dq/dp' (actual)	Test	p'_o kPa	dq/dp' (actual)
T1114	135	3.8	T1118	1267	4.1
T1123	356	6.2	T1122	1211	-3.5
T1124	362	5.3	T1130	1238	2.5
T1125	376	3.1	T1132	1250	3.3
T1128	362	2.9	T1137	1239	0.72
T1129	358	5	T1140	1200	2.9
T1134	369	1.4	T1141	830	2.8
T1135	361	-15	T1146	992	3.0
T1136	339	-2.7	T1147	1011	-2.0
T1138	368	0	T1148	980	20
T1139	340	0.4	T1149	1006	0.4
T1144	343	0.5	T1150	993	0
T1145	353	0.6	T1151	1020	1.01
			T1152	976	-0.6

5.3 Constant Rate of Strain Tests

In this series, four tests were conducted on low density specimens. The main purpose was to see in it was possible to maintain sufficient control of the cell pressure during the test to achieve the desired stress path, and also confirm if yielding behaviour could be observed. As stated above, strain control triaxial tests have usually not been used to study yielding. Information on each of the tests is listed in Table 5.2.

The specimens were prepared and installed in the triaxial cells according to the methods previously described. A total confining pressure of 750 kPa and a back pressure of 200 kPa was applied to the specimen for 10 days. The total (cell) pressure was then reduced to 515 kPa (back pressure was fixed at 200 kPa) for 3 days before shearing started.

TABLE 5.2 Strain Controlled Tests

Test	Strain Rate (%/day)	P'_o kPa	dq/dp' actual	Remarks
T1116	0.24	190	-133	Initial strain rate was 0.45 %/day
T1117	0.27	215	-1.8	
T1120	0.35	366	3.3	Unload/reload cycle
T1121	0.30	365	1.2	Unload/reload cycle

The strain rate selected was approximately 0.0002 mm/min. Based on a specimen height of 100 mm, the strain rate was about 0.3% per day. Saadat (1989) used strain rates of between 2.4%/day and 28.8%/day for his undrained shear tests. Shearing of these specimens lasted for periods from 30 to 55 days.

To maintain a stress path different from the standard ($dq/dp' = 3$) the cell pressure was manually changed in response to the axial stress. Adjustments were made in the morning, in the afternoon, and if necessary again in the late evening.

5.4 Constant Rate of Stress Tests

Four drained shear tests were performed on low density specimens. The GDS stress-path equipment was used for these tests. The method of installation was the same as for the other test methods. The total confining and applied back pressures were controlled by the computer.

The stress paths for each test are given in Table 5.3. During the shearing phase, a termination axial strain rate of 10 to 15 percent was imposed. Because the strain rate was uncontrolled, the axial strain would increase rapidly near failure. The target stress rate was 1 kPa/hr for tests T1153, T1154, and T1155, and 0.75 kPa/hr for test T1156. The actual rate, listed in Table 5.3 is approximately the same for the tests which had a positive stress path, but was 55 to 60 percent higher than the target rate for the tests with negative stress paths. The cause for this is not known, but probably lies in the GDS program algorithm for calculating the stress increment. The program was modified to permit any stress path, and the stress increment subroutine may not be able to calculate the stress increase if the confining pressure is continually decreasing. Refinements to the GDS programs may be necessary to correct this problem.

TABLE 5.3 Constant Rate of Stress Tests

Test	Stress Rate kPa/hr	p'_o kPa	dq/dp' (actual)
T1153	0.8	295	5.0
T1154	1.0	360	9.2
T1155	1.55	395	-8.6
T1156	1.2	394	-2.7

As a consequence of the applied stress rate, the time to yield was generally shorter in these tests than for the incremental stress controlled tests. Tests T1155 and T1156 yielded after about 6 days of shearing compared to about 10 to 12 days for the incremental stress controlled tests.

5.5 Yield States of the Buffer

5.5.1 Analysis of Yield Data

Twenty-one low density specimens and thirteen high density specimens were tested in triaxial compression. From these tests the yielding behaviour for each density could be examined.

The yield stress in each test can be found by considering appropriate stress-strain parameters (Graham *et al.* 1982). By examining more than one set of parameters the yield stress can be determined with more confidence. In this study, the following sets of parameters were used: q versus ϵ_s , σ_3' versus ϵ_3 , σ_1' versus ϵ_1 , and Work versus LSSV. In the last case, the work absorbed by the specimen during shear is (Graham *et al.* 1983c):

$$[5.1] \quad W = \sum (\bar{\sigma}_1 \delta \epsilon_1 + 2\bar{\sigma}_3 \delta \epsilon_3)$$

where $\bar{\sigma}$ is the average effective stress in a load increment and $\delta \epsilon$ is the strain during the increment. LSSV stands for the length of the stress vector, and means the straight line distance in p', q - space from the start of shearing to the current increment. That is:

$$[5.2] \quad LSSV = \sqrt{(p' - p_i')^2 + (q - q_i)^2}$$

where p_i and q_i are the initial values of the effective mean stress and deviator stress respectively.

Of the different parameters, work versus LSSV is the most versatile since it is independent of stress path. The q versus ϵ_s criterion is less useful where dq/dp' is small. Likewise, σ_3' versus ϵ_3 is not useful where $\Delta\sigma_3' = 0$ as in a standard drained triaxial test.

Figs 5.2 and 5.3 present data showing the plots of the different stress-strain parameters. Fig. 5.2 presents data for a low density test (T1134) and Fig. 5.3 presents data for a high density test (T1141). In each case bilinear behaviour was interpreted from the data. The bilinear behaviour of natural clays was discussed by Graham *et al.* (1983c). In many instances a transition section exists. Some judgement is necessary in interpreting the data where the stress-strain relations do not exhibit significant changes in pre- and post-yield behaviour. The use of more than

one criterion is useful in this respect.

Figs. 5.2 and 5.3 represent "good" typical behaviour of the buffer in drained triaxial compression. The yield stresses were relatively well defined. In some cases the interpretation of yielding was less clear, and the data could be subject to several interpretations. In these cases the interpretation that was most consistent with adjacent data was accepted. The q versus ϵ_s plots of all yield tests are presented in Appendix C. The pre- and post-yield sections have been included and the yield stress is taken as the intersection of the two linear sections.

The yield deviator stress was found for each set of parameters (for instance, q_y corresponding to σ_{3y}^* or $LSSV_y$), and then averaged. The shear strain at yield was scaled from the plots of q versus ϵ_s (ϵ_{sy} on Fig. 5.4).

There are alternative approaches to find p_y' corresponding to the value of q_y . One approach is done graphically from a stress path plot of q versus p' , or by interpolating between sets of tabulated data at the appropriate q_y . This approach is weak because it implies that yield stresses and strains occur at different times in the test. This is illustrated schematically in Fig. 5.4. Since q_y lies above the actual test data, the value of p_y' will correspond in the test to a shear strain ϵ_{sy}^* . The true shear strain at yield is marked ϵ_{sy} .

The other approach is to find p_y' corresponding to the shear strain at the yield deviator stress q_y . This can only be graphically. It involves a rationalization of the stress-strain data to avoid the transitions between elastic and elastic plastic behaviour that are always seen in testing. This approach is weak because p_y' can only be determined graphically. It requires plotting p' versus ϵ_s , and drawing either the pre- or post-yield line through the same data points as in the plot of q versus ϵ_s . The yield shear strain is fixed. The value of p_y' is scaled off at the intersection of the vertical ϵ_{sy} line and the pre- or post-yield line through the data. Fig. 5.5 shows plots of shows plots of p' versus ϵ_s for tests T1134 and T1141 (the same tests in Figs. 5.2 and 5.3).

In this thesis, p_y' was determined using the first approach. The volume strain and specific

volume at yield were determined based on the shear strain corresponding to q_y (that is, ϵ_{sy} in Fig. 5.4, not ϵ_{sy}^*). The errors associated with determining p_y' are small when the transition zone at yield is small.

The error between each approach is not random. For stress paths where $\Delta q/\Delta p'$ is positive, the first approach will give higher values of p_y' compared to the second approach. For stress paths where $\Delta q/\Delta p'$ is negative, the first approach will give lower values of p_y' compared to the second approach.

The value of p_y' for 12 tests was determined using both methods. The average difference in p_y' between the two approaches was -3 kPa, well within experimental error.

5.5.2 Yield Locus and End-of-Test Data in q, p' -Space

Table 5.4 presents the yield stresses for each specimen. The stresses were normalized with respect to the effective preconsolidation pressure at which the specimens were initially stressed during the 10 day equalization period. (The preconsolidation pressure should equal the swelling equilibrium pressure. However, the porewater pressure measured at the base of the specimen was usually different from the applied back pressure. This resulted in an average effective mean pressure slightly different from the targeted effective SEP. In this analysis, the use of the actual effective preconsolidation pressure is more appropriate than the targeted SEP).

Figs. 5.6 and 5.7 present the yielding data for the two densities. The yield stresses and end-of-test stresses are marked for each specimen. The Figures also show the stress paths for each test. (In a few cases a curved stress path was observed. This was due to some small variation in the base porewater pressure during the shearing. This suggests that truly drained conditions were not always met during these tests. Despite this, the yield data remain valid.)

TABLE 5.4 Yield Stresses for Buffer Specimen

Low Density Tests (Average $\gamma_d = 1.49 \text{ Mg/m}^3$)				High Density Tests (Average $\gamma_d = 1.67 \text{ Mg/m}^3$)			
Test	q_y kPa	P_y' kPa	P_c' kPa	Test	q_y kPa	P_y' kPa	P_c' kPa
T1114	139	170	561	T1118	648	1426	1876
T1116	93	198	595	T1122	678	1018	2076
T1117	87	166	572	T1130	682	1506	2038
T1120	183	421	611	T1132	678	1460	1944
T1121	181	511	548	T1137	658	2156	2076
T1123	234	402	598	T1140	670	1435	1914
T1124	238	407	549	T1141	574	1038	1332
T1125	228	450	542	T1146	590	1189	1546
T1128	247	448	534	T1147	429	792	1699
T1129	235	405	582	T1148	544	1007	1584
T1134	245	550	536	T1149	271	1663	1656
T1135	219	346	539	T1150	0	1480	1577
T1136	178	272	525	T1151	476	1490	1695
T1138	0	508	525	T1152	324	420	1647
T1139	84	555	564				
T1144	83	540	483				
T1145	89	533	530				
T1153	245	345	486				
T1154	225	385	605				
T1155	214	370	602				
T1156	193	300	621				

Peak strength and/or failure envelopes developed by previous researchers, are shown on the figures, for comparison. The failure envelope by Wan (1987) was derived from undrained, strain controlled tests, and drained, constant p' , incremental stress controlled tests at pressures less than 1500 kPa. The peak strength failure envelope by Saadat (1989) was derived mostly from

undrained strain controlled tests at pressures up to 3500 kPa.

End-of-test failure stresses for the low density tests lie very close to the strength envelope developed by Wan (1987) having Mohr-Coulomb strength parameters of $c' = 40$ kPa and $\phi' = 14^\circ$. For the high density specimens, the peak strength envelope developed by Saadat (1989) is very close to the end-of-test strengths from this study. Saadat used a power law to model the peak strengths ($q_p = 2.59 p'^{0.80}$). His failure envelope (critical state line) lies below the peak strength line. This is due to post-peak strain softening that was observed in many of Saadat's undrained strain controlled tests. The current high density data give end-of-test strength parameters of $M = 0.55$ ($\phi' = 14^\circ$) and a deviator stress intercept of 186 kPa (not shown in Fig. 5.7). This corresponds to a cohesion $c' = 88$ kPa. Thus the slope of the line is the same as Saadat (1989) but a small cohesion intercept has been introduced. (As will be discussed in Chapter 7, the end-of-test stresses in this study should be distinguished from the critical state stresses.)

The differences between the present end-of-test data and that obtained by previous researchers is quite small and could be attributed to differences in testing techniques. In particular, the use of a transducer to measure porewater pressures independent of the back pressure resulted in a better understanding of the true porewater pressure regime in the specimen. In light of this, the effective stresses experienced in this program were generally higher than would have been experienced if only the back pressure was considered.

Fig. 5.8 presents the normalized yielding data from all tests in a single diagram. For clarity the stress paths and end-of-test stresses have been omitted. Several comments can be made about Fig. 5.8.

1. A single yield criterion representing both buffer densities appears to be reasonable. Although there is no *a priori* reason for having a single locus, from a conceptual and modelling viewpoint it is much simpler than having different loci for each density.
2. The locus intersects the p'_y/p'_c axis at about 0.95. Intuitively one may expect the yield

locus to intersect the p'_y/p'_c axis at 1.0, which represents the preconsolidation pressure. A conceptual model, shown in Fig. 5.9, illustrates the discrepancy. When a specimen is off-loaded after the 10 day equalization period at the SEP (from Point A to B), it will immediately begin to swell. Some of the swelling is due to release of elastic strain energy stored in the specimen (so-called "consolidation swell") while the rest is due to physico-chemical processes. The consolidation swell causes volume change (to B') along the κ - line (unload-reload line) associated with A (the unload to B' is associated with the classical consolidation/swelling process of well-behaved soils). The physico-chemical processes cause additional volume change, raising the specific volume to B''. The physico-chemical swelling rate is both time and pressure dependent. This two-phase unloading sequence is an idealization, as the specimen would move from B to B'' with both mechanisms acting concurrently.

When the specimen is reloaded, it will move along the κ - line associated with B'', not B'. This κ - line intersects the normal consolidation line (NCL) at point A', slightly to the left of (and at a lower pressure than) point A. In general, the magnitudes of yield stresses depend on the stresses at A', not A. Thus if the stress states along B''-A' are normalized by the mean isotropic stress at A, they will be smaller than if normalized with respect to A'. A specimen that traverses to the κ -line B''-A', implies that some of the swelling (B'-B'') due to physico-chemical processes is visco-plastic (that is, time dependent and non-recoverable), and further that it occurs within the elastic region. Yin and Graham (1989) discussed elastic visco-plastic straining in one dimensional consolidation. However in that case, all volume strains were compressive, rather than expansive.

3. A yield locus can be drawn through the yield data points. A locus that intersects the p'/p'_c axis at right angles indicates isotropic elasticity, and a barrel-shape will signify a degree of elastic anisotropy (Graham *et al.* 1983b). Visual "best-fit" yield loci for both interpretations are shown on Fig. 5.8.

Saadat, Graham and Gray (1989) documented anisotropy in buffer specimens that were normally consolidated (above their SEP) and subjected to undrained triaxial compression. They stated that forming the specimens by static compression one-dimensionally in a rigid mold will produce a soil fabric that is stiffer horizontally than vertically. The shape of the yield locus shown in Fig. 5.8 suggests that the degree of anisotropy in the unloaded (overconsolidated) specimens in this study is likely to be small. The relative stiffnesses in vertical and horizontal planes can be determined by examining the pre-yield stress-strain behaviour. The elastic moduli will be developed and discussed in Chapter 6.

4. The yield locus is, at all places, below the failure envelope for these tests. This means that the specimens harden plastically in shear along all stress paths (even though they are expanding (softening) plastically in terms of volume change behaviour). The yield locus shown in Fig. 5.1 represents the classical elastic plastic model. Specimens plastic strain harden or soften (in stress space) depending on the stress path during shear. One implication of a purely strain hardening material such as that shown in Fig. 5.8 is that the flow rule should be non-associated. Other evidence of the plastic strain behaviour will be examined later in Sections 5.3 and 6.3.

The yield locus can also be normalized in terms of an equivalent pressure (p'_e), rather than the original preconsolidation pressure (p'_c). The equivalent pressure is the effective pressure on the swelling equilibrium line (here considered identical with the normal consolidation line) corresponding to the current specific volume of the specimen. If this normalization is performed, Graham *et al.* (1989b) showed that the shape of the yield locus will change to an ellipse, ideally originating at 1.0 on the p'/p'_e axis, with the apex of the ellipse at $0.5p'/p'_e$. This implies that while the yield locus appears asymmetric to the p' -axis, the state boundary surface is symmetric.

The equation of the SEL and NCL used to normalized the yield data, was determined by Saadat (1989). There are two relationships, one for each density:

$$[5.3] \quad p'_{sel} = \exp(20.708 - 5.848V_c)$$

for high density specimens, and

$$[5.4] \quad p'_{sel} = \exp(16.594 - 3.831V_c)$$

for low density specimens. (In [5.3] and [5.4], V_c is the specific volume of the clay fraction in the specimen.) The correlation coefficients (R^2) were 0.95 and 0.92 respectively. One reason these equations were used for normalizing the data was that the triaxial consolidation tests conducted in this program (T1138 and T1150) gave $V_c, \ln p'$ values very close to the lines predicted by [5.3] and [5.4].

Fig. 5.10 presents the data from Figs. 5.6 and 5.7, but normalized with respect to p'_e . Not all the data shown in Figs. 5.6 and 5.7 could be used in this figure. Since p'_e was a function of V_c , any test that experienced leakage problems could not be included (whereas they could be included in the development of Figs. 5.6 to 5.8). There is considerable scatter of the data in Fig. 5.10, however the low and high density data are intermixed, which supports the principle of normalization. An elliptical yield locus for both densities has been drawn through the data. It intersects the p'/p'_e axis near 1.0 and is symmetrical about $0.5 p'/p'_e$. The lack of fit for both sets of data can be attributed to the general scatter in the data from this testing program, and from that used to derive [5.3] and [5.4]. The ellipse is not an unreasonable choice for the shape of the normalized state boundary surface.

5.5.3 Yield Locus and End-of-Test Data in V, p' -Space

The yield and end-of-test data for most tests, plotted in V_c, p' -space, are shown in Figs. 5.11 and 5.12. Also shown in Fig. 5.11 for the low density data, are the critical state lines (CSL) from Saadat *et al.* (1989) and Wan *et al.* (1990). In Fig. 5.12, the critical state line from Saadat

et al. (1989) is shown. An interpretation of the peak strength line based on the current data is also shown as a light dashed line. Only data from well controlled drained tests (without leakage problems *etc.*) have been included in these figures.

The yield locus can also be plotted in $V_e, p'/p'_c$ -space. Fig. 5.13 presents these data. A yield locus has been drawn in for each density. These data are difficult to interpret in terms of anisotropy. A yield locus with a "hook" around the normal consolidation line should result if anisotropy is present. The low density data do not appear to fit a hook shaped yield locus. The high density data also appears to fit an anisotropic yield locus rather tenuously. As a first interpretation, a slightly curved yield locus, terminating at the normal consolidation line (to represent isotropic elasticity) has been shown for both sets of density data. Because the stress data has been normalized, the normal consolidation line plots in $V_e, p'/p'_c$ -space as a vertical line (In normalized q, p' -space, the NCL is a point on the p'/p'_c axis at 1.0).

In Fig. 5.13 there are 3 low density data points that appear to be at specific volumes much higher than the others. These points are for specimens that had OCRs ranging from 2.66 to 4.15, compared to the other low density specimens that had an average OCR of 1.54. Although their positions on the yield locus in normalized q, p' -space (Figs. 5.6 and Fig. 5.8) to not appear abnormal, their positions in Fig. 5.13 appear inconsistent with the other low density data. Their positions in $V_e, p'/p'_c$ -space can be explained using the conceptual model for swelling, shown in Fig. 5.9. When a specimen is unloaded from point A to B in a single stress decrement, the amount of physico-chemical swelling will depend on both the size of the stress decrement, and the time permitted for swelling. More importantly, the rate of swell will also be a function of the stress decrement and time. The swell rate, at any time, will be lower for small decrements, and high for large decrements.

All specimens represented by data in Fig. 5.13 were allowed to swell for 3 days prior to the start of triaxial compression. However, in the case of the 3 specimens with the higher OCRs,

the amount of physico-chemical swelling in the 3 day swell period was greater than for the specimens with OCRs of 1.54 because the swell rate was higher. Referring again to the conceptual model in Fig. 5.9, the data for the two OCRs (but at the same density) will lie on different κ -lines and therefore there will be different yield loci associated with each OCR. This concept is supported by the yield locus plotted in $q/p'_e, p'/p'_e$ -space (Fig. 5.10). In Fig. 5.6 the high OCR data lie far to the left of the other data, however in Fig. 5.10, these data points (marked with arrows), with the exception of one erratic point, lie among the other data, independent of OCR.

In Fig. 5.13, yield loci have been drawn through these high OCR data towards the vertical NCL.

The yield loci for each density in $V_c, p'/p'_e$ -space are separate, but generally similar in size and slope. This suggests that they could be normalized using a suitable specific volume parameter. Possible parameters include the initial specific volume, specific volume corresponding to the swelling equilibrium pressure, or some variation of the state parameter ψ (Been and Jefferies 1985).

Fig. 5.14 shows the yield data normalized in $V_c, p'/p'_e$ -space, using the specific volume of the normally consolidated specimen at yield as the normalizing parameter. The three low density specimens with high OCRs have been normalized using the specific volume corresponding to a hypothetical specimen on their yield loci at the NCL. The test data lies along a rather narrow band.

It could be argued that there are other, perhaps better normalizing factors than the one chosen here. Been and Jefferies (1985) demonstrated the usefulness of plotting the behaviour of sand in terms of its state parameter which is the difference in specific volume between the current state and the critical state. However the state parameter is not a normalizing factor in itself, since it measures only a difference in specific volume. Graham *et al.* (1989b) showed the advantage

of using the equivalent pressure as a normalizing factor. Extending this to V, p' -space, one could use the specific volume on the SEL (or NCL), at the current pressure (a so-called "equivalent specific volume") as a normalizing parameter. The disadvantage of using this parameter lies in the uncertainty regarding the true position of the SEL in V, p' -space of the buffer. The scatter of the yield data in $q/p'_e, p'/p'_e$ -space illustrates the weakness of this approach for the buffer.

5.6 Discussion and Summary

The differences in yield stresses as determined by the three tests deserves comment. Fig. 5.6 presented the yield and end-of-test data for the low density specimens. In general, the constant rate of strain tests gave yield stresses lower than the incremental stress controlled tests while the stresses from the two stress controlled tests were more comparable. The differences between the strain controlled and stress controlled tests is likely due to strain rate effects. Tavenas and Leroueil (1977), and Graham, Crooks, and Bell (1983a) showed that increasing the strain rate in a triaxial compression test increased both the yield stresses and the peak strength. For example, Graham *et al.* (1983a) found that increasing the strain rate by a factor of 10 caused a 10 to 20 percent increase in undrained strength.

In a customary stress (load) controlled compression test the strain rate is uncontrolled. Immediately after each load increment is applied, the strain rate is relatively high, and decreases with time. The high initial strain rates in an incremental stress controlled test are associated with higher stiffnesses and hence higher strengths, compared to a strain controlled test, even though the average strain rate in each type of test may be similar.

The failure envelope for high density specimens from Saadat (1989) was developed from strain controlled tests on specimens, many of which experienced post-peak strain softening. Since strain softening behaviour cannot be observed in the stress controlled tests in this program, Saadat's failure envelope could be expected to be lower than the end-of-test peak stresses observed

in this study. In the other case, shown in Fig. 5.6 for low density specimens, Wan (1987) used some drained stress controlled tests to determine the failure envelope. That envelope is more consistent with the current data.

Three different preconsolidation pressures were used for the high density buffer specimens (2100 kPa, 1700 kPa, and 1400 kPa). The shear data, once normalized with respect to the preconsolidation pressure, behave very similarly. This is to be expected, and supports the discussion on the use of the effective stress concept in Chapter 4.

The use of more than one set of stress-strain parameters for determining the yield stresses has proved very useful. Although some judgement was required in a few cases, bilinear behaviour prior to and after yield was evident for at least one set of parameters for most specimens. A few tests were poorly designed and produced only two or three increments before yielding. However, yield stresses were found from these tests that were consistent with yield stresses from comparable tests.

The normalized state boundary surface in triaxial compression is now complete. Figs. 5.8 and 5.14 describe the complete locus in normalized q, p', V_c -space. The buffer, in spite of its high volume change capacity appears to behave like many "ordinary" soils. From the shape and position of the yield locus it can be concluded that the buffer exhibits some limited elastic anisotropy, and that the flow rule may be non-associated. Both these behavioural characteristics will be studied in more detail in Chapter 6.

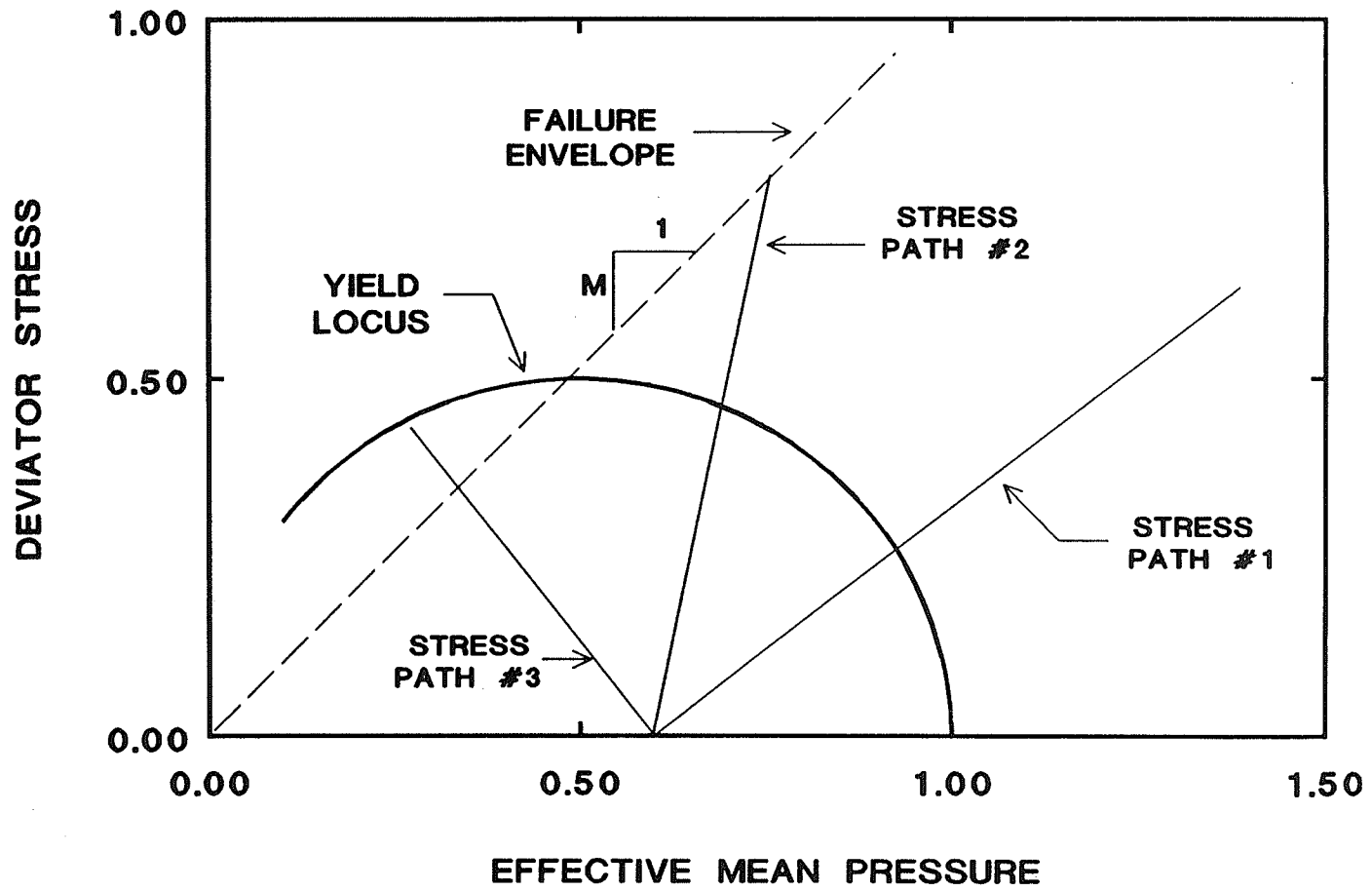


FIGURE 5.1

The classical elastic plastic soil model in q, p' -space.

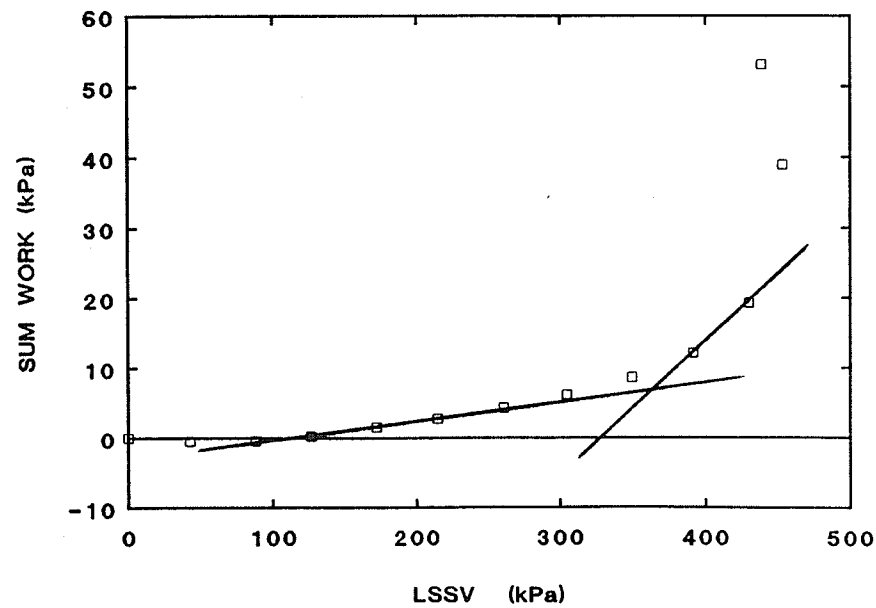
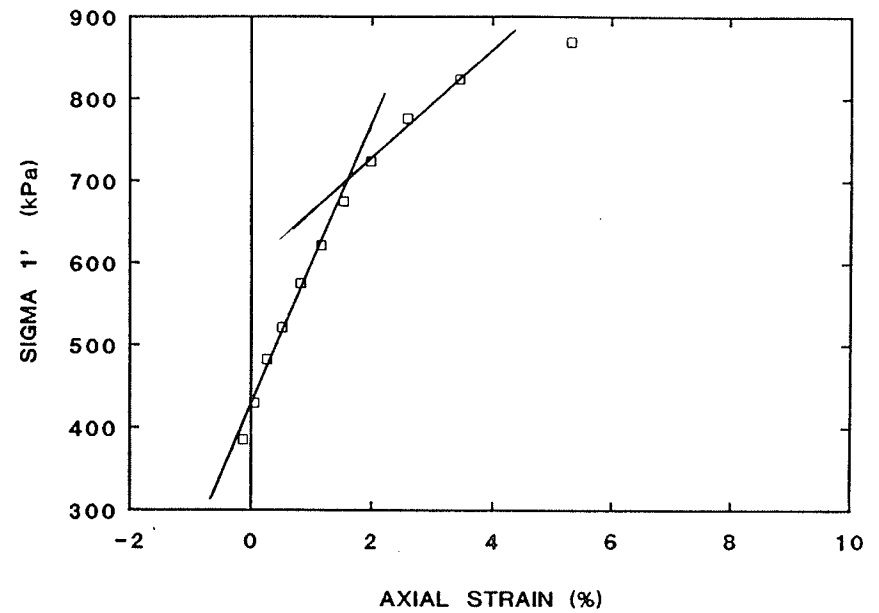
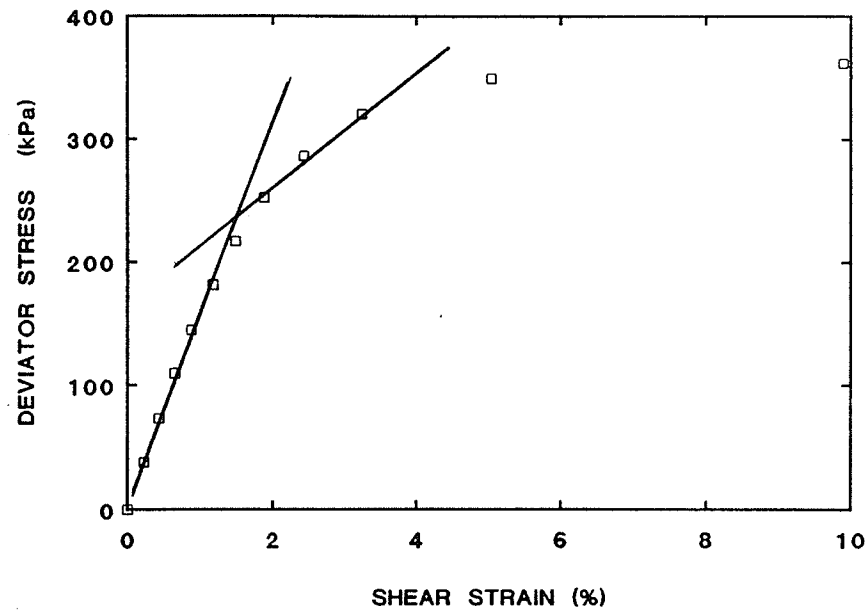


FIGURE 5.2

Stress-strain parameters showing yielding for low density specimen (T1134). (a) q versus ϵ_s (b) σ_1' versus ϵ_1 (c) Work versus LSSV.

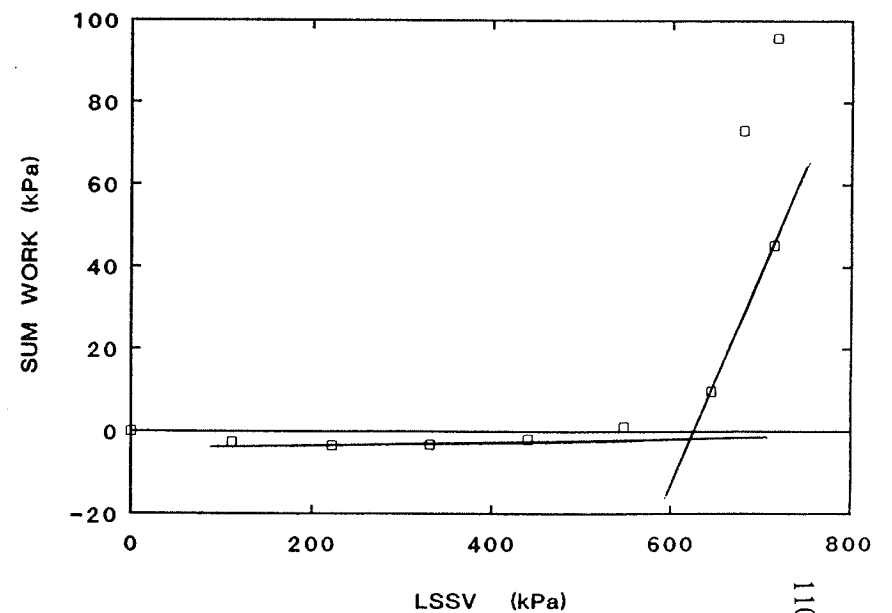
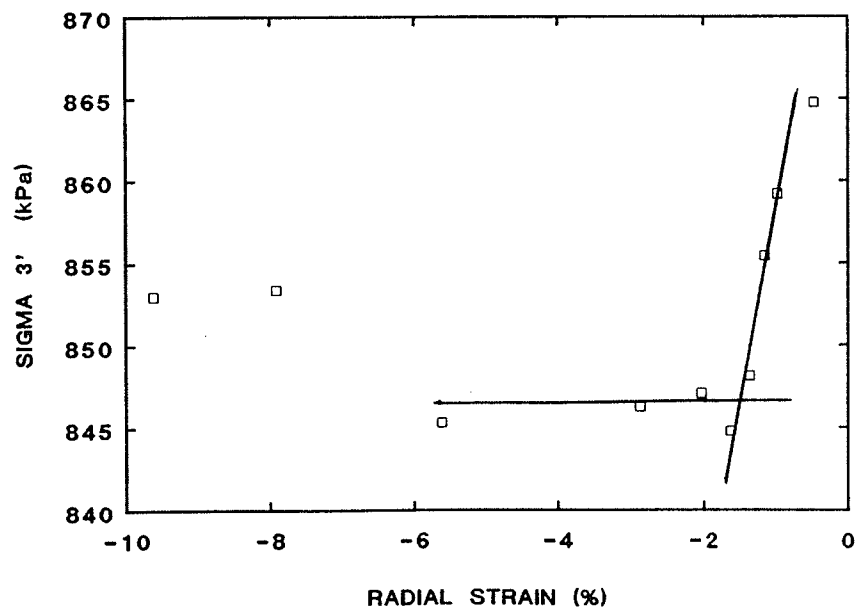
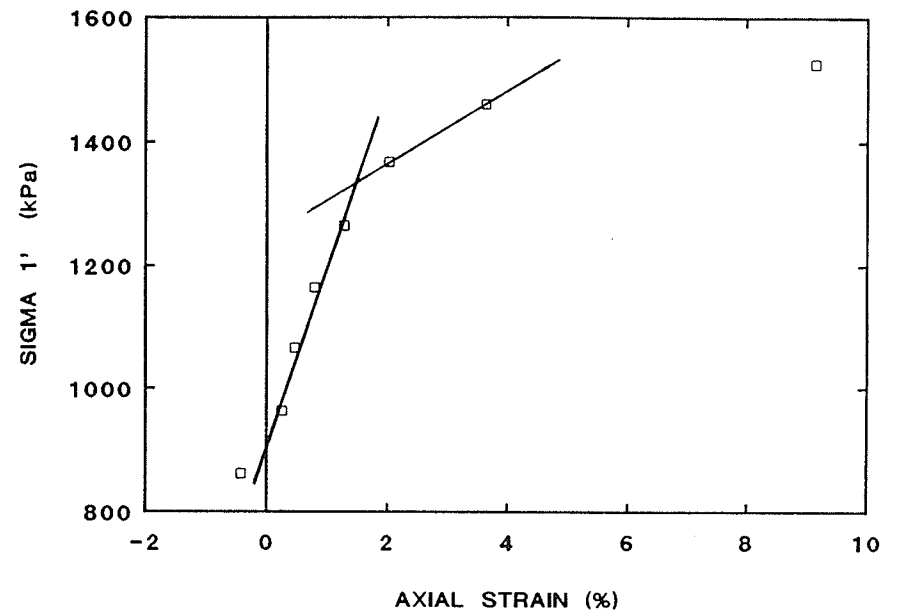
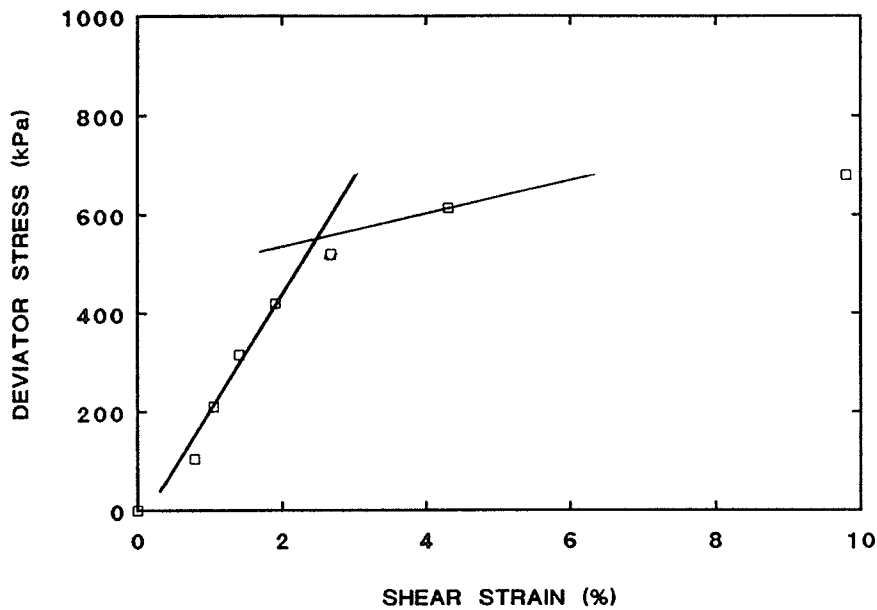


FIGURE 5.3 Stress-strain parameters showing yielding for high density specimen (T1141). (a) q versus ϵ_s (b) σ_3' versus ϵ_3 (c) σ_1' versus ϵ_1 (d) Work versus LSSV.

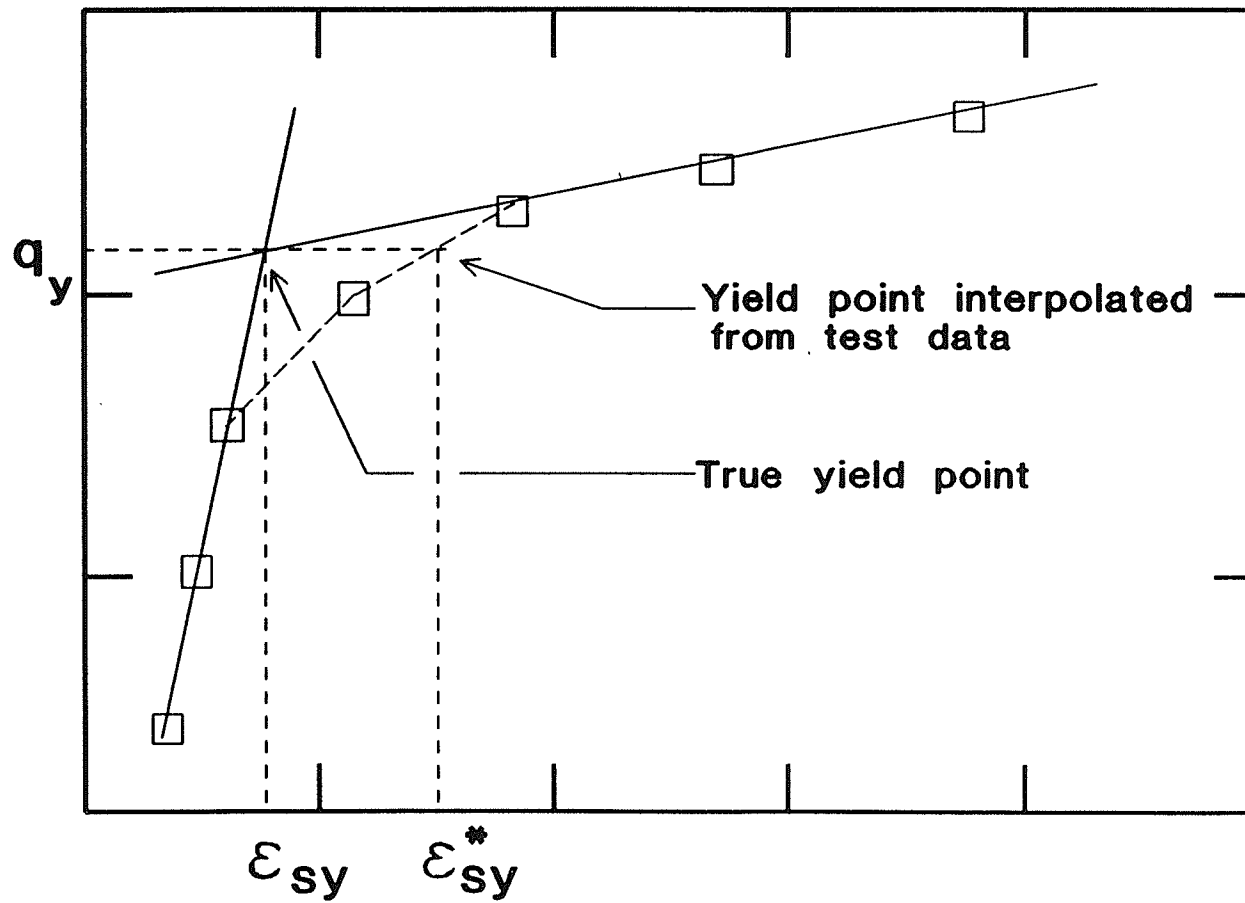


FIGURE 5.4

Schematic diagram illustrating potential errors in shear strain at yield associated with the yield deviator stress.

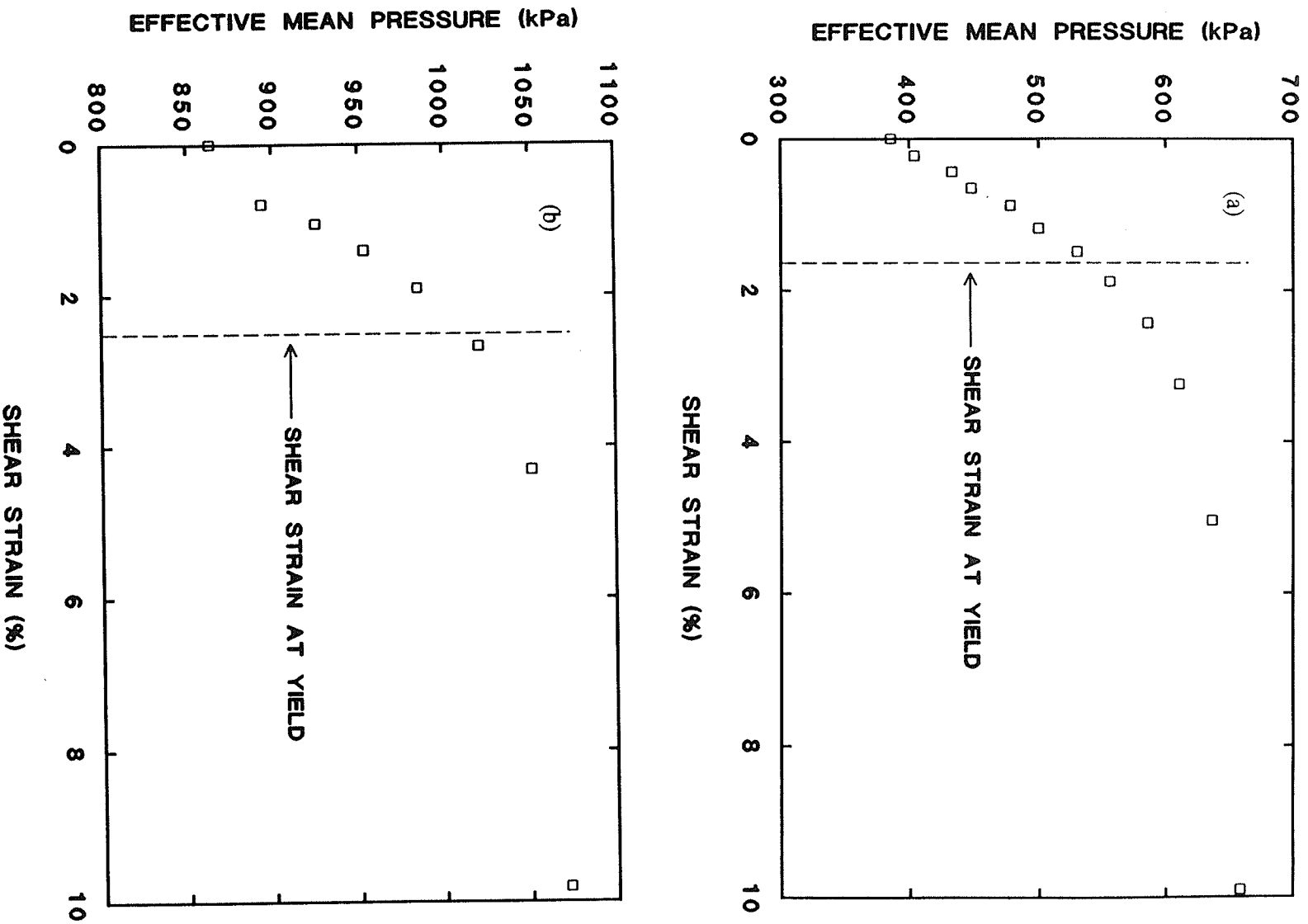


FIGURE 5.5

Graphical method to determine p_y' at a pre-determined value of shear strain. (a) low density specimen T1134 (b) high density specimen T1141.

LOW DENSITY BUFFER
 DRY DENSITY = 1.49 Mg/m^3

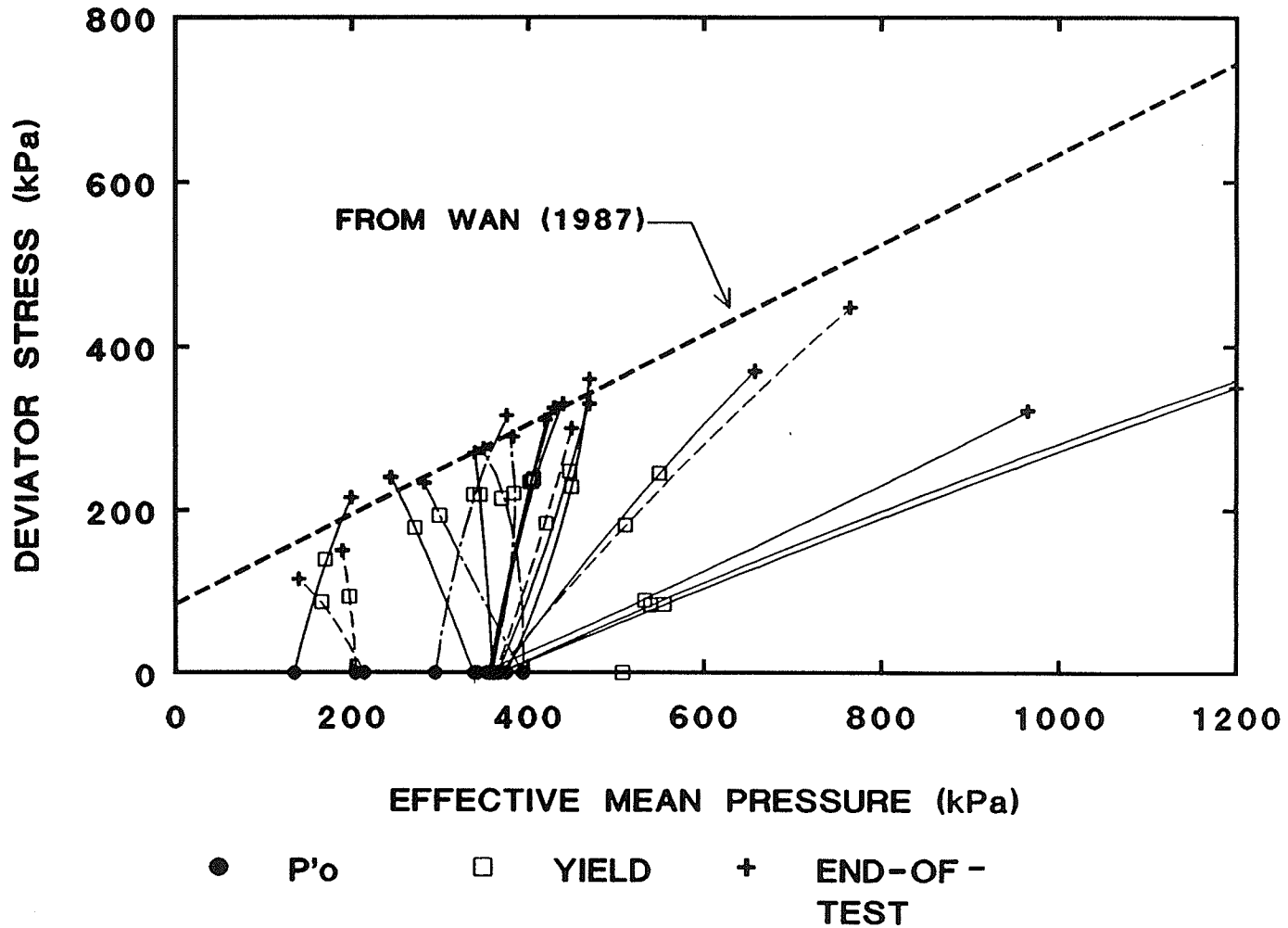


FIGURE 5.6

Yield and end-of-test data for low density specimens. Failure envelope from Wan (1987) is shown for comparison. The solid lines are incremental stress controlled tests, the dashed lines are strain controlled tests, and the dash-dot lines are constant rate of stress tests.

HIGH DENSITY BUFFER
 DRY DENSITY = 1.66 Mg/m³

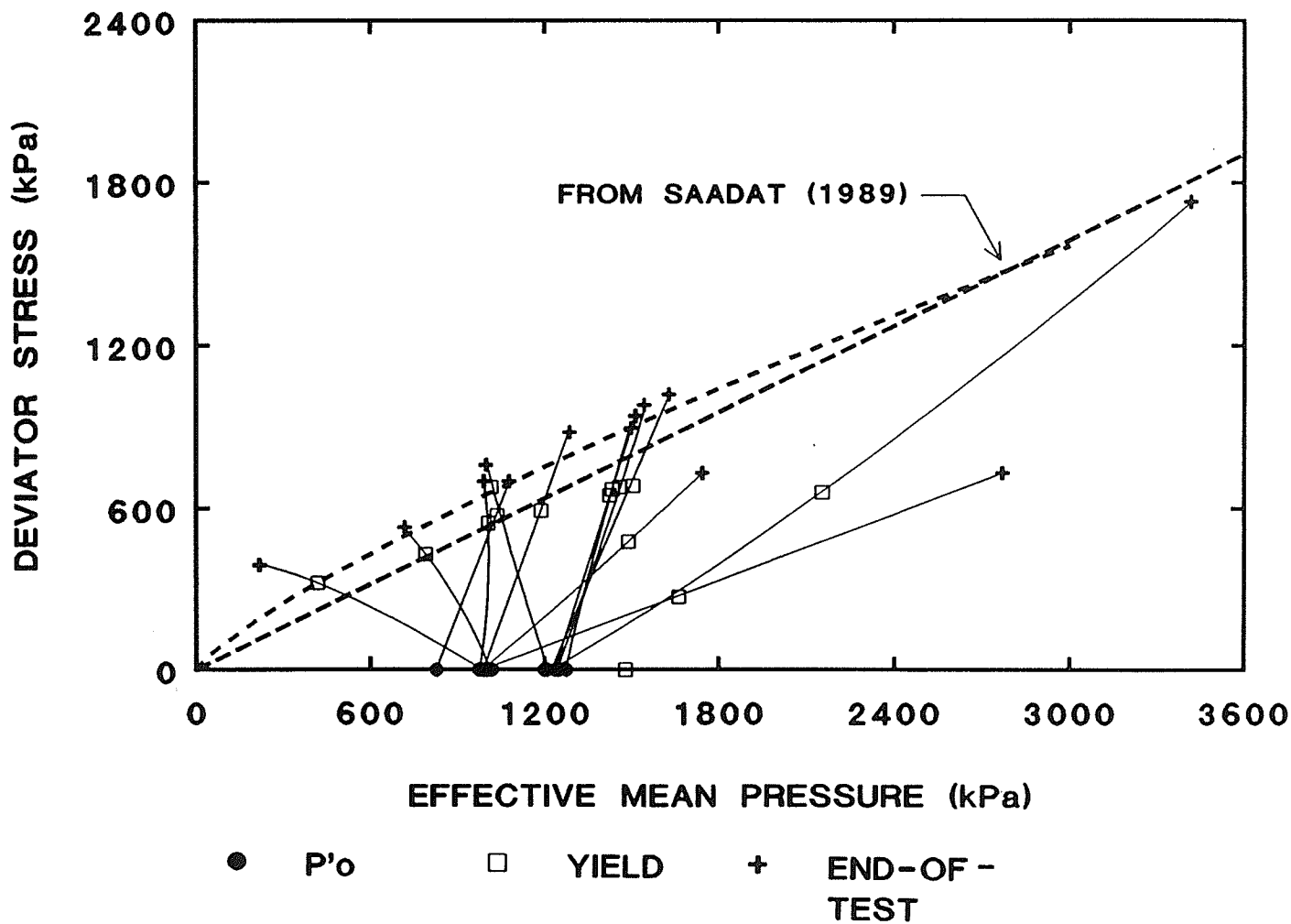


FIGURE 5.7 Yield and end-of-test data for high density specimens. Peak strength (short dashed line) and failure (long dashed line) envelopes from Saadat (1989) is shown for comparison.

BUFFER SPECIMENS
DRY DENSITY = 1.49 Mg/m³ and 1.67 Mg/m³

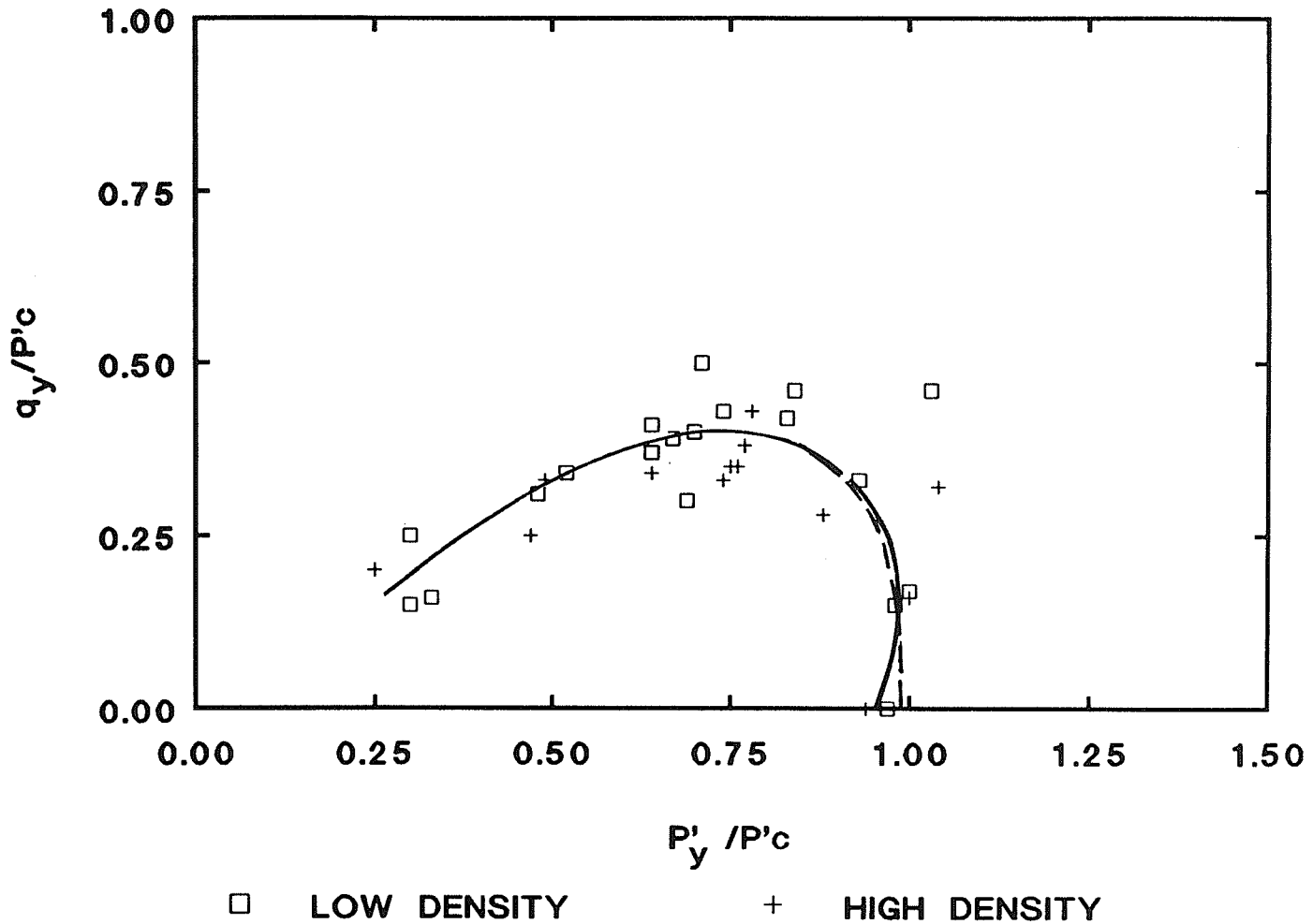


FIGURE 5.8

Normalized yield data for low and high density specimens with interpreted yield locus. The solid line is the yield locus assuming anisotropic elasticity. The dashed line is the yield locus assuming isotropic elasticity.

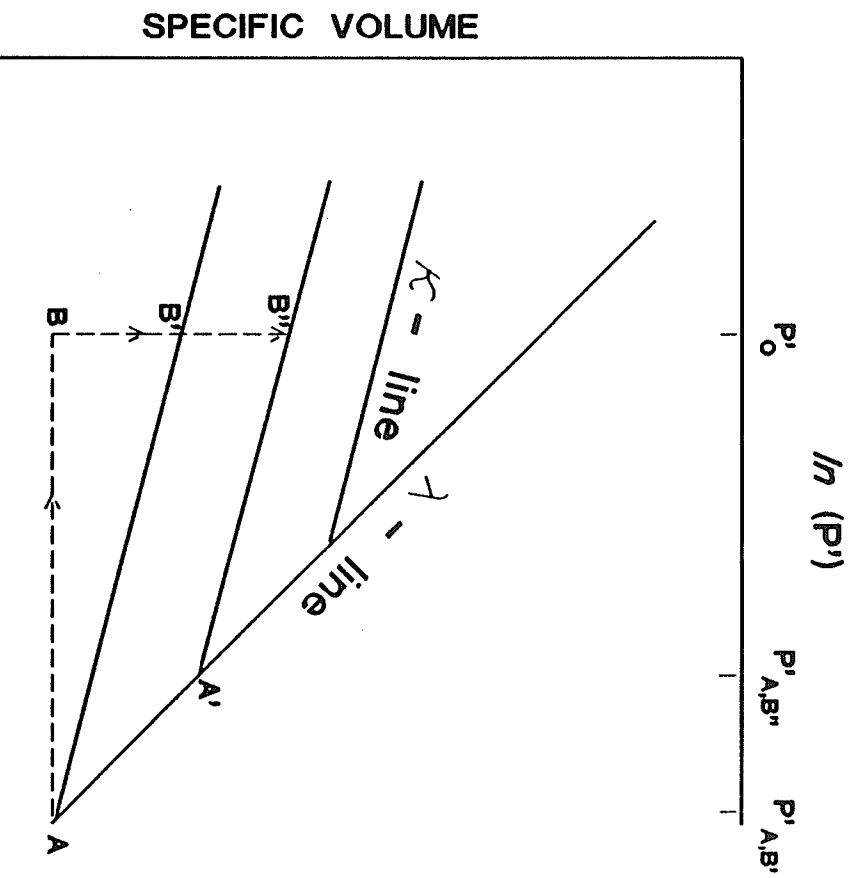


FIGURE 5.9

Conceptual model for swelling of buffer on effective mean stress release.

BUFFER SPECIMENS
DRY DENSITY = 1.49 Mg/m³ and 1.67 Mg/m³

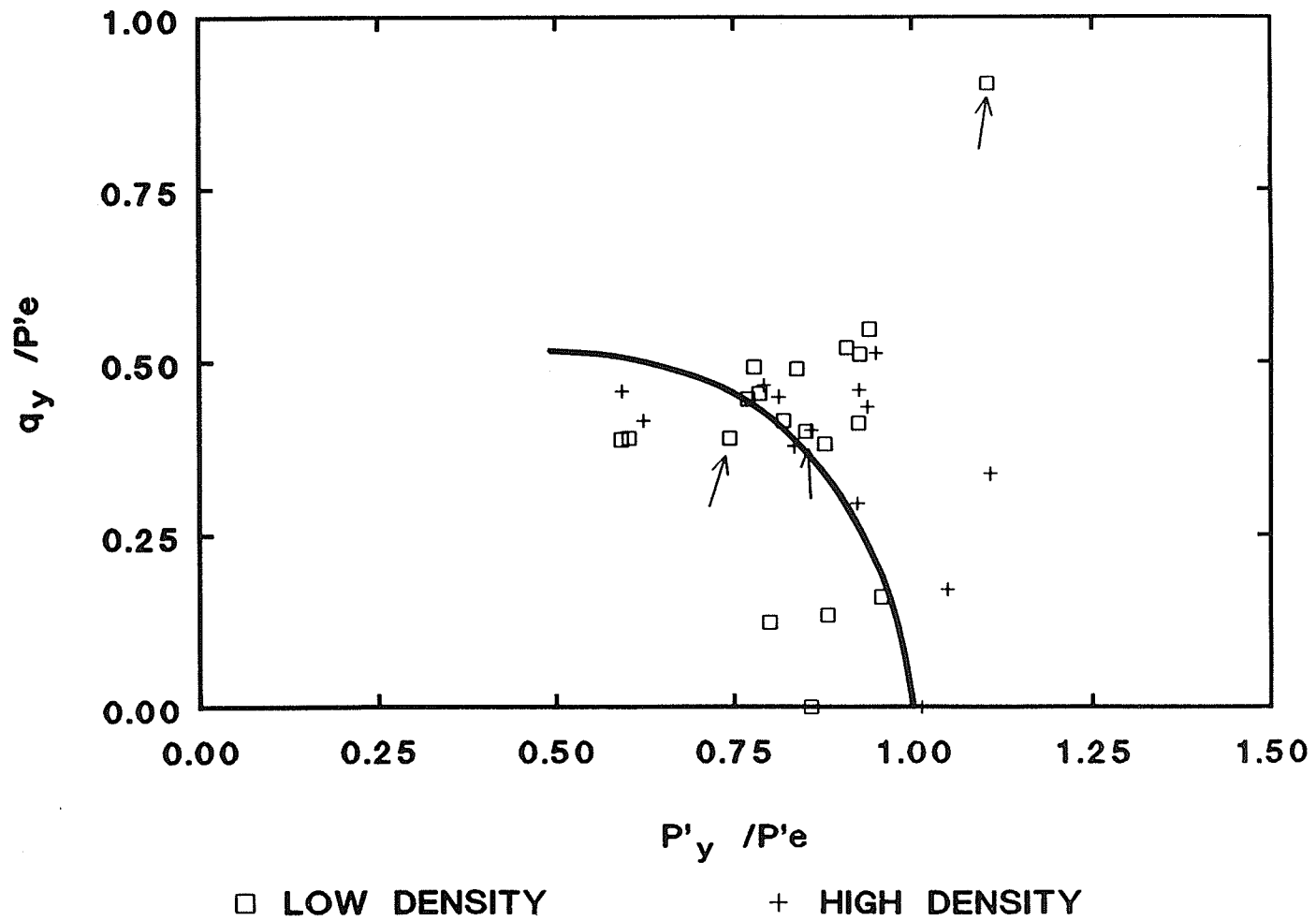


FIGURE 5.10 Yield locus for low and high density specimens in q, p' -space, normalized with respect to p'_e . An elliptical yield locus is shown.

LOW DENSITY SPECIMENS
 DRY DENSITY = 1.49 Mg/m³

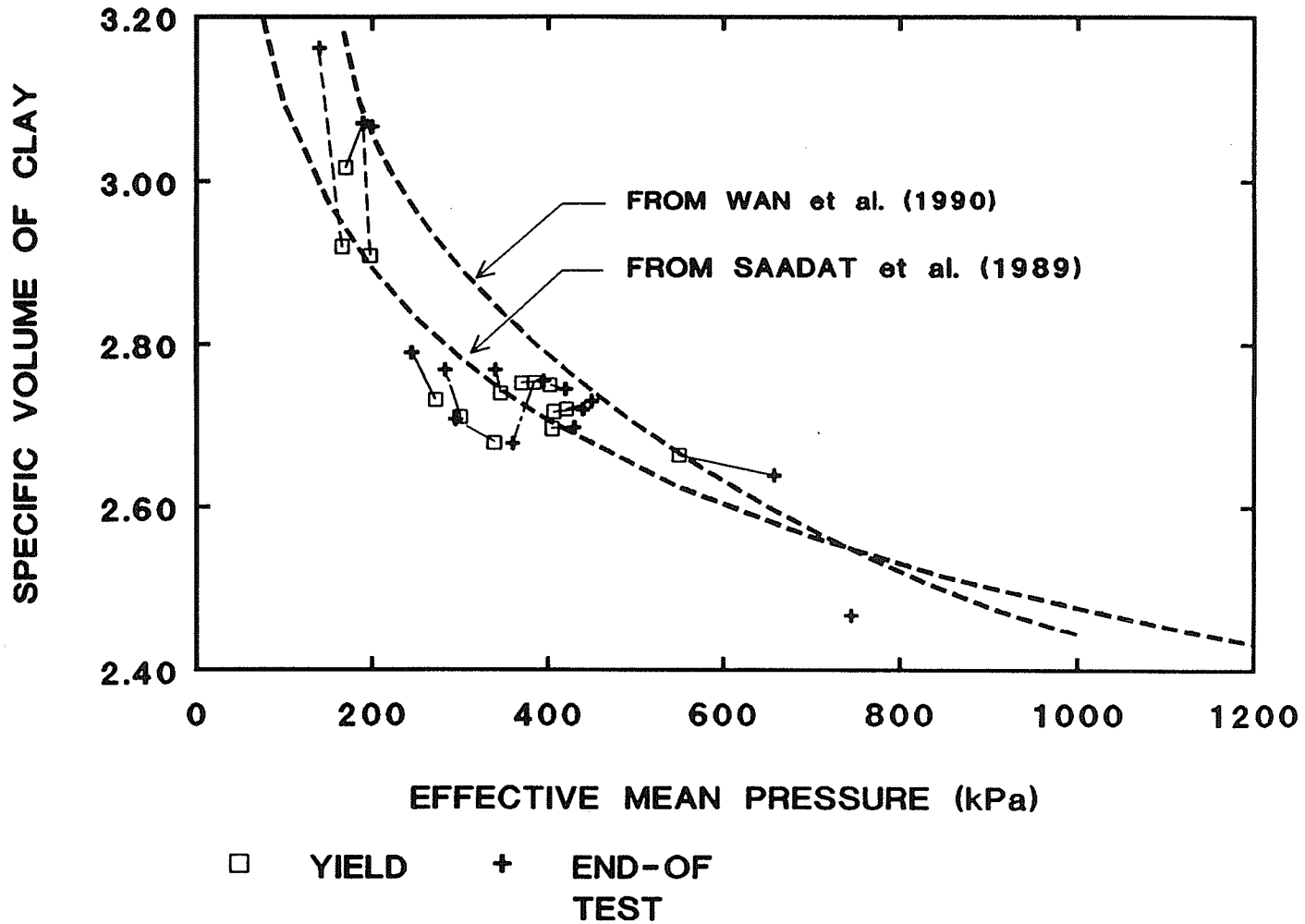


FIGURE 5.11

Yield and end-of-test data for low density specimens, plotted in V_c, p' -space. Critical state lines from Saadat *et al.* (1989) and Wan *et al.* (1990) are shown for comparison.

HIGH DENSITY SPECIMENS
 DRY DENSITY = 1.67 Mg/m^3

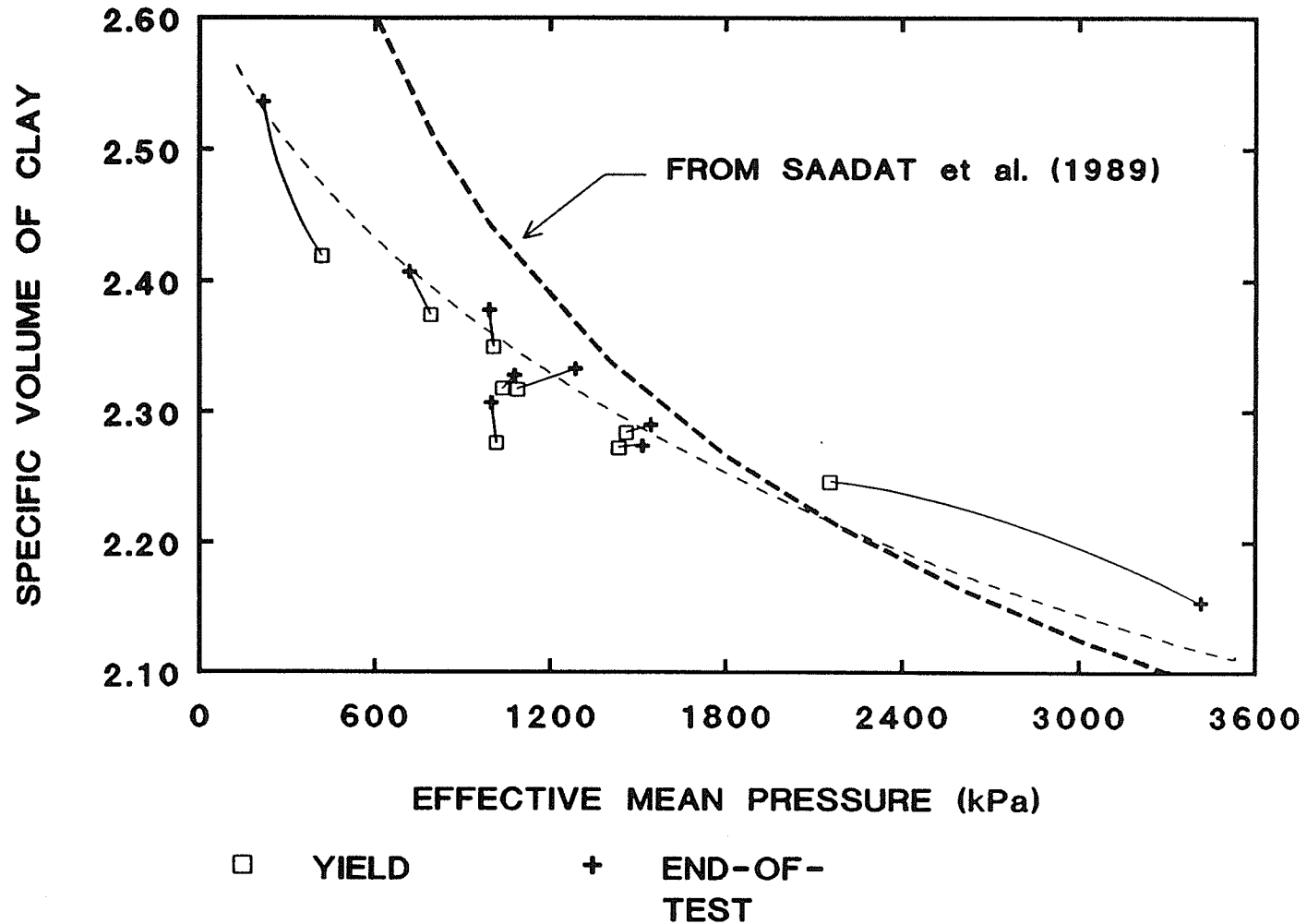


FIGURE 5.12

Yield and end-of-test data for high density specimens, plotted in V_c, p' -space. The critical state line from Saadat *et al.* (1989) is shown for comparison. The light dashed line represents the critical state line based on the data presented.

BUFFER SPECIMENS
DRY DENSITY = 1.49 Mg/m³ and 1.67 Mg/m³

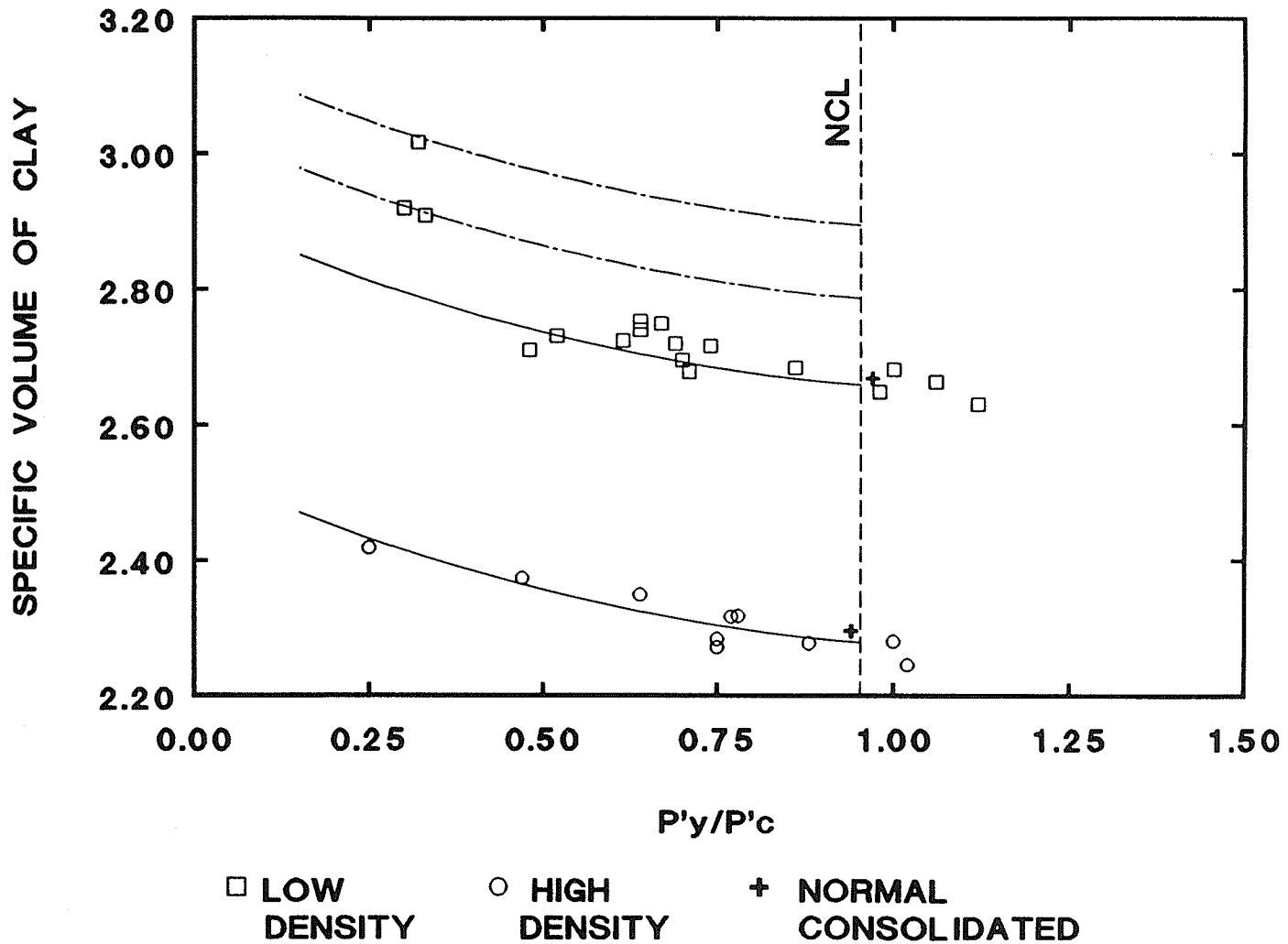


FIGURE 5.13

Yield locus for low density and high density specimens in $V_c, p'_y/p'_c$ -space. The slope lines represent the yield loci for the different densities. The dashed lines represent interpolated yield loci based on limited data.

BUFFER SPECIMENS
DRY DENSITY = 1.49 Mg/m³ and 1.67 Mg/m³

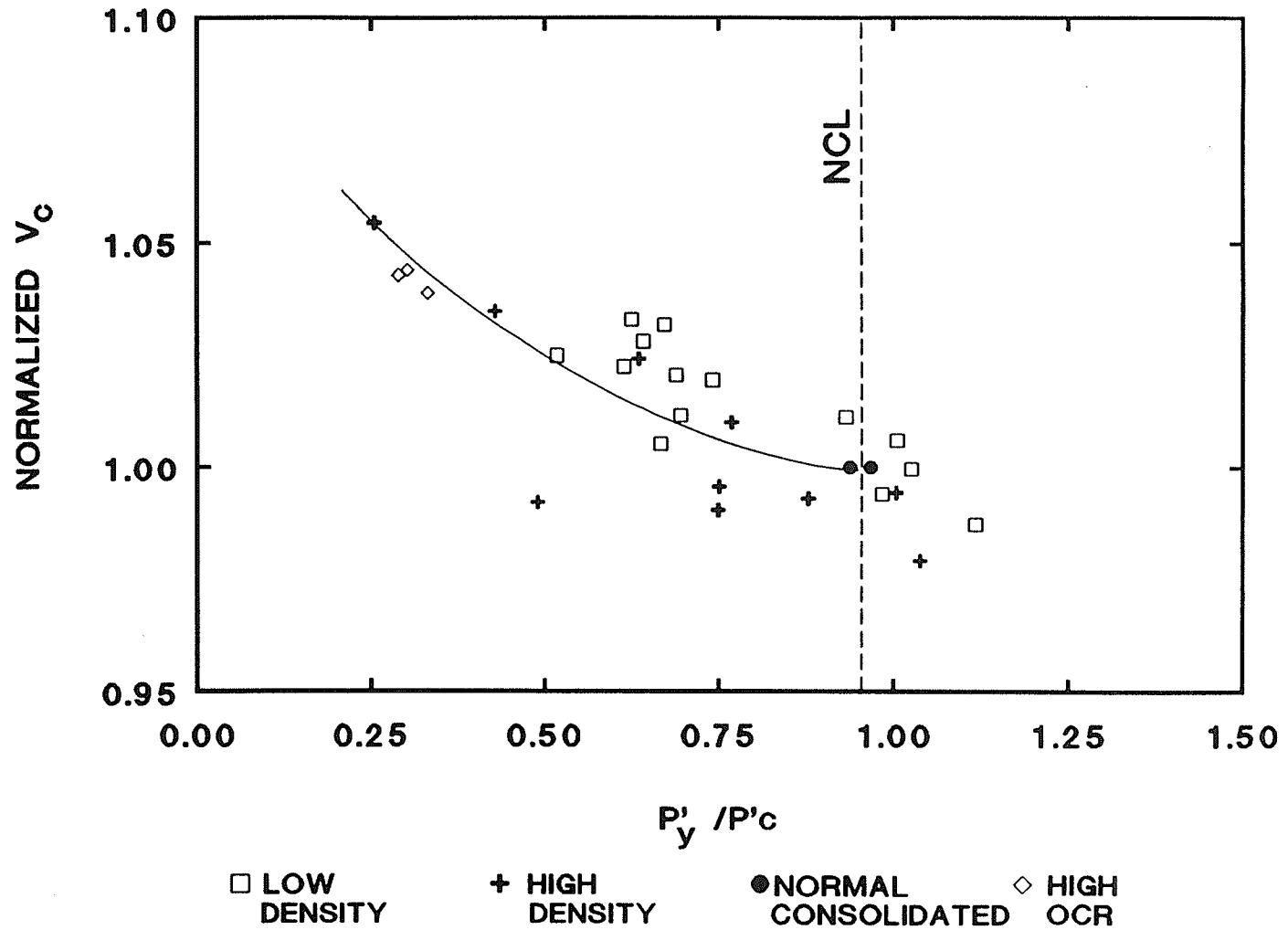


FIGURE 5.14

Normalized yield locus for high and low density specimens in $V_c \cdot p'_y / p'_c$ -space.

CHAPTER 6 EVALUATION OF ELASTIC PLASTIC PARAMETERS OF THE BUFFER

6.1 Introduction

The yield locus for the buffer was developed in Chapter 5. The remaining components of the elastic plastic model will be developed in this chapter. Elastic parameters will be determined using the techniques developed by Graham and Houlsby (1983). There is some evidence that the buffer may be anisotropic within the elastic range of stresses. An anisotropic elastic model comprises a minimum of the three material moduli that were introduced in Chapter 2. The flow rule and plastic potential will be evaluated by examining plastic strain increment vectors. This requires separation of the elastic and plastic strains. Evidence from Chapter 5 has suggested that the flow rule may be non-associated. Finally, the hardening law will be discussed. This has been determined from work by previous researchers (Wan 1987; Saadat 1989). However it will be re-evaluated in light of the current data.

6.2 Elastic Behaviour

6.2.1 Elasticity in Drained Shear

Graham and Houlsby (1983) developed a simple anisotropic elastic model based on 3 material constants. They are: an elastic bulk and shear modulus, K^* and G^* , and a coupling modulus, J :

$$[6.1] \quad \begin{bmatrix} \delta p' \\ \delta q \end{bmatrix} = \begin{bmatrix} K^* & J \\ J & 3G^* \end{bmatrix} \begin{bmatrix} \delta \epsilon_v^e \\ \delta \epsilon_s^e \end{bmatrix}$$

A single triaxial test is insufficient to solve [6.1] since there are two equations and three unknowns. Two triaxial tests give four equations with three unknowns and there is therefore a redundancy of equations. By using a least squares regression method it is possible to solve [6.1] for a number of tests and minimize the errors.

Data for the two densities of buffer were examined separately. The analyses were done on data normalized with respect to the preconsolidation pressure for each specimen. Nineteen low density tests and 13 high density tests were used in the elastic analysis.

The procedure for determining the moduli was as follows. The changes in p' , q , ϵ_v and ϵ_s between the first or second load increment and the yield stress were found for each test. The following least square coefficients were calculated: $\Sigma \Delta p'^2$, $\Sigma \Delta p' \Delta \epsilon_v$, $\Sigma \Delta q^2$, $\Sigma \Delta q \Delta \epsilon_s$, $\Sigma \Delta q \Delta p'$, $\Sigma \Delta p' \Delta \epsilon_s$, and $\Sigma \Delta q \Delta \epsilon_v$ (Graham and Houlsby 1983).

The isotropic elastic moduli can be calculated directly from [6.2]:

$$[6.2a] \quad K = \frac{\Sigma p'^2}{\Sigma \Delta p' \Delta \epsilon_v}$$

$$[6.2b] \quad 3G = \frac{\Sigma q^2}{\Sigma \Delta q \Delta \epsilon_s}$$

The anisotropic elastic moduli (K^* , $3G^*$, and J) are calculated by solving three simultaneous equations using the least square coefficients above:

$$[6.3a] \quad \begin{aligned} \Sigma 2(C_1 \delta p^2 + C_2 \delta q - \delta \epsilon_v) \delta p &= 0 \\ \Sigma 2(C_1 \delta p + C_2 \delta q - \delta \epsilon_v) \delta q + 2(C_2 \delta p + C_3 \delta q - \delta \epsilon_s) \delta p &= 0 \\ \Sigma 2(C_2 \delta p + C_3 \delta q - \delta \epsilon_s) \delta q &= 0 \end{aligned}$$

$$[6.3b] \quad \begin{aligned} K^* &= C_3 / (C_1 C_3 - C_2^2) \\ 3G^* &= C_1 / (C_1 C_3 - C_2^2) \\ J &= -C_2 / (C_1 C_3 - C_2^2) \end{aligned}$$

Moduli were determined using all the available tests. From these moduli, the predicted volume and shear strains were calculated and compared to the measured strains. Following comparison of the predicted and measured strain vectors, certain tests that had abnormally large errors were removed from the data base. New moduli were then re-calculated. This procedure was repeated until the error between the predicted and measured strain vectors was minimized.

Use of this procedure led to removing only one low density test and two high density tests from the data base.

The final elastic parameters determined for the buffer, and Winnipeg clay for comparison, are listed in Table 6.1.

TABLE 6.1 Elastic Parameters for the Buffer and Winnipeg Clay

Moduli	Low Density	High Density	Winnipeg Clay
K/p'_c	34.0	31.5	15.6
$3G/p'_c$	24.8	21.9	23.8
K^*/p'_c	27.3	27.2	18.2
$3G^*/p'_c$	29.4	23.4	32.1
J/p'_c	7.1	10.1	-6.9

Winnipeg clay is also an active clay, comprising mostly smectites. Note that the moduli for Winnipeg clay in Table 6.1 are different from those reported by Graham and Houlsby (1983), which were normalized with respect to σ'_{vc} (vertical preconsolidation pressure). The moduli in the table have been normalized with respect to p'_c . The relationship between p'_c and σ'_{vc} is: $p'_c = \sigma'_{vc}(1 + K_o)/3$. The data in Table 6.1 shows that the buffer is considerably stiffer than Winnipeg clay. Also, the coupling modulus of the buffer is positive, which implies a soil fabric that is stiffer vertically than horizontally. In contrast, the coupling modulus of the Winnipeg clay is negative, suggesting a soil fabric that is more stiff horizontally than vertically. Remember that these moduli for the buffer correspond to material that has been off loaded and allowed to swell.

Comparisons of the measured strain vectors and predicted strain vectors for the two densities of buffer are shown in Figs. 6.1 and 6.2. All available test data have been plotted in these figures. The figures show that several strain vectors for each density have been poorly predicted. The worst predictions occurred for tests with large negative (expansive) volume strains.

A measure of the error between the predicted and measured elastic strains can be calculated from the following equation:

$$[6.4] \quad R = \frac{\sum (\epsilon_p - \epsilon_m)^2}{\sum (\epsilon_m)^2}$$

where the subscripts p and m represent the predicted and measured total strain vectors respectively. The total strain vector is $\epsilon = (\epsilon_s^2 + \epsilon_v^2)^{0.5}$.

The error for each set of moduli was calculated for all tests and also for a reduced data set after removing tests with large apparent errors. (The tests removed have been labelled with arrows in Fig. 6.1 and 6.2.) Table 6.2 lists the error between the predicted and measured strain vectors for each set of moduli.

TABLE 6.2 Errors between Predicted and Measured Elastic Strain Vectors.

	Isotropic	Anisotropic
Low Density Specimens		
R (all tests)	0.34	0.38
R (reduced data set)	0.24	0.25
High Density Specimens		
R (all tests)	0.41	0.33
R (reduced data set)	0.23	0.19

Graham and Houlsby (1983) found that the errors in their predictions of the isotropic and anisotropic strain vectors were 0.28 and 0.19 respectively. The errors for the reduced data set in Table 6.2 compare very favourably to the errors experienced by Graham and Houlsby. It is seen in the table that the error is very sensitive to a few bad tests, and by removing those tests from the data set, the error is reduced substantially (the tests that were removed from the data set used to calculate the error were not the same tests that were removed when the moduli were calculated).

The errors associated with assuming isotropic or anisotropic elasticity are not very different. This reinforces the comments made in Chapter 5 (Section 5.5.2) that any anisotropy would likely be small.

An examination of the stress paths data for the tests revealed that, without exception, when the stress path was such that the cell pressure (σ_3) increased, the specimen compressed (positive volume strain), and when the cell pressure decreased, the specimen expanded (negative volume strain). In isotropic materials the change from positive to negative volume strains occurs at $\Delta p' = 0$. At this time it is a matter of conjecture whether the apparent control of volume strain during drained shear by the confining pressure (σ_3) is a coincidence, represents a special case of [6.1], or reflects a rheological phenomenon.

6.2.2 Elasticity in Undrained Shear

Saadat (1989) presented data from undrained triaxial compression tests that showed evidence of anisotropy. From his research, Wan (1988) concluded that the anisotropy may depend on the specimen state relative to the SEL. Wan found that specimens that had swelled prior to shearing exhibited isotropic behaviour during the initial stages of undrained strain controlled triaxial compression. Specimens that compressed prior to shearing exhibited anisotropic shear behaviour. Wan made his conclusions based on porewater pressure changes during undrained shear (Graham and Houlsby 1983, Wan *et al.* 1990). Graham *et al.* (1989a) stated that forming the specimens in a rigid mold one dimensionally produces an anisotropic soil fabric. The implication of Wan's work is that swelling will remove the anisotropy induced by compaction of the specimen.

In this testing program undrained tests were performed on 2 low density and 1 high density specimens. There are two differences in these particular undrained tests compared to those reported by Wan and Saadat. First, the tests in this program were stress controlled, rather

than the strain controlled shear procedures used by Wan and Saadat. Second, whereas Wan and Saadat used the back pressure transducer to monitor the porewater pressure response during undrained shear, in the present program a porewater transducer independent of the back pressure transducer was used to measure porewater pressure changes.

Fig 6.3 and 6.4 present plots of normalized porewater pressure change *versus* normalized total mean pressure change for the two low density tests. The response of both porewater transducers are shown. The base porewater change is immediately positive in response to the applied stress increment. The top porewater change (formerly the back pressure transducer) is initially different, and contrasts with the experience of Wan (1989) and Saadat (1989) in the use of back pressure transducers to measure porewater pressure changes during undrained shear.

Both Wan (1987) and Saadat (1989) recorded immediate positive changes in the porewater pressure transducers that were previously used to monitor the back pressure. The difference in behaviour between their response and the present behaviour can be explained in terms of the state of the specimen in relation to swelling equilibrium. In the case of Wan and Saadat, their specimens were either at swelling pressure equilibrium, or would likely be near an equilibrium condition prior to shear (because most of their specimens compressed prior to shear). Thus there would be little or no out-of-balance porewater pressure in the specimens. In the case of the present tests, significant expansive volume straining occurred in the specimens immediately prior to (undrained) shear, indicating the specimens were still some distance from equilibrium. For these specimens, the top (former back pressure) porewater pressure at the beginning of undrained shear would not be in a state of equilibrium. The buffer in the vicinity of the top porewater pressure transducer would attempt to equalize, and experience a cavitation process since it is unable to absorb water from the drainage burette. Thus the top porewater pressure transducer measurements would likely be unreliable. In contrast, the base porewater pressure had 13 days to reach equilibrium prior to shearing. As a result, the base porewater pressure transducer would

be more representative of the internal pressure conditions of the specimen than the transient conditions around the top porewater pressure transducer.

The slopes of the base porewater response for both low density tests are approximately, or somewhat less than 1.0. This suggests isotropic elasticity, or a small degree of anisotropy, and supports the conclusions of Wan *et al.* (1990) that swelling of the buffer reduces the anisotropy of the specimens induced by compaction. The anisotropy displayed in Figs. 6.3 and 6.4 indicates that the buffer is more stiff vertically than horizontally, which confirms that the coupling modulus previously determined in Section 6.2.1 should be positive.

Two high density specimens in undrained stress controlled shear are available for comparison. One specimen, from this study was tested in the same manner as the two low density specimens. The other specimen was an unreported test by Saadat (1989). It swelled for 12 days at an OCR of approximately 8.5 prior to undrained shear. The porewater response was measured only by the former back pressure transducer. The porewater response during undrained shear for these tests is shown in Figs. 6.5 and 6.6. The porewater pressure changes in the former back pressure transducer of both tests are very similar. There is an immediate decrease in porewater pressure, stabilizing at a pressure somewhat lower than the applied back pressure (this is observed as a negative porewater pressure change). As discussed above with reference to the low density specimens these responses are due to a non-equilibrium transient condition in the specimen, resulting in a cavitation phenomenon near the former back pressure transducer.

The behaviour of the base porewater pressure change in Fig. 6.5 is different from that observed for the low density specimens. In this test, little or no change in porewater pressure during undrained shear was recorded. The cause of this is related to the pre-shear porewater pressure conditions (including the applied back pressure of 200 kPa). These conditions are discussed in detail in Chapters 4 and 7.

6.2.3 Elasticity in Swell under Isotropic Stress Conditions

The nature of the elasticity of the buffer can also be determined from an examination of strains due to isotropic stress changes. All specimens in this testing program underwent 3 days of swelling prior to being sheared. During this swell period, a small weight was maintained on the axial ram to overcome the cell pressure and maintain contact with the specimen. Thus measurements of axial and volume strains are available during the swelling at the isotropic stress.

Fig. 6.7 presents shear strain *versus* volume strain data for 11 low density tests. Fig. 6.8 presents shear strain *versus* volume strain data for 10 high density tests. For isotropic elastic materials, no shear strain should occur as a result of changes in isotropic stress conditions. Thus a plot of shear strain *versus* volume strain should have a slope of zero. Examination of Figs 6.7 and 6.8 show that this is broadly the case for most of the tests. This lends further support to the previous discussion of isotropic elasticity.

In a few tests however, a negative slope ($\Delta\epsilon_s/\Delta\epsilon_v < 0$) is observed in the figures. This indicates a degree of anisotropy. Consider [6.1] and the case of an isotropic stress change ($\Delta p'$) without any deviator stress change. Therefore:

$$[6.5a] \quad \Delta q = 0 = J\Delta\epsilon_v + 3G^* \Delta\epsilon_s$$

$$[6.5b] \quad \frac{\Delta\epsilon_s}{\Delta\epsilon_v} = - \frac{J}{3G^*}$$

It can be reasonably assumed that $3G^*$ should be positive. Therefore, to get a negative slope as shown in Figs. 6.7 and 6.8, J must also be positive. The coupling moduli J given in Table 6.1 are positive for both densities.

Further, the ratio $J/3G^*$ in Table 6.1 for the low and high density specimens is 0.24 and 0.43 respectively. Lines of slopes $\Delta\epsilon_s/\Delta\epsilon_v = -0.24$ and -0.43 have been added to Figs. 6.7 and

6.8. It is seen that these lines are of approximately the same slope as the lines for the test data that exhibit anisotropic swell.

There are no clearly apparent causes why most tests would behave isotropically when swelling, yet a few tests for each density would behave anisotropically.

6.2.4 Elasticity during Unload/Reload in Shear

Three tests on low density specimens were unloaded after drained shear had progressed for some time. In addition, Saadat (1989) reported unload/reload data for two of his specimens tested in undrained shear. Estimates of the elastic shear and bulk moduli can be obtained from these data (The unload/reload portions of the tests in this study are shown in Appendix C. The unload/reload data from Saadat (1989) were discussed in Chapter 2. See Fig. 2.12.)

The isotropic elastic moduli, normalized with respect to preconsolidation pressure are listed in Table 6.3. Bulk moduli can not be obtained from undrained tests since there is no volume change. The data presented in Table 6.3 display considerable scatter. However, several comments can still be made regarding these moduli. The moduli appear to be at least 3 times as stiff on unload/reload compared to initial loading. In ideal elastic materials, the moduli are independent of the loading cycle. The difference in moduli values between first loading and subsequent unloading is probably due to visco-plastic (time dependent, non recoverable) straining during the initial loading stage. It is proposed that during the initial loading the specimens experience volume strains that result from (1) the physico-chemical imbalance within the specimen, and (2) a change in the effective mean pressure (p') during shearing. By the time the specimens were unloaded, much of the physico-chemical volume strain had subsided, leaving only the shearing induced volume change. It is interesting to compare the data for T927 (Saadat, 1989) shown in Fig. 2.12b with data from the present testing program. (See tests T1120, T1121, and T1139, Appendix C). Test T927 was consolidated near its swelling equilibrium pressure (ϵ_v

= -0.2% in 12 days) and then sheared in undrained triaxial compression. It had no opportunity for physico-chemical or consolidation swelling. As a result, the slope of the deviator stress *versus* shear strain plot during first-time shear is nearly the same as the slopes of the two unload/reload cycles. This behaviour contrasts with the present testing program where the slope of the initial loading was much lower than the unload/reload sections.

TABLE 6.3 Isotropic Elastic Moduli from Unload/Reload Data

Test	K/p'_c	$3G/p'_c$	Remarks
T1120	22	60	strain controlled $dq/dp' = 3.3$
T1121	91	148	strain controlled $dq/dp' = 1.2$
T1139	177	68	incr. stress cont. $dq/dp' = 0.4$
T927 1 st	-	59	undrained strain controlled
T927 2 nd	-	65	undrained strain controlled
T931	-	143	undrained strain controlled

6.3 Plastic Potential and Flow Rule

The flow rule describes the relationship between plastic shear strains and plastic volume strains. The flow rule also relates the shape of the yield locus to the plastic potential. The plastic potential is a function, such that the resultant plastic strain vectors are perpendicular to it. When this function is the same shape as the yield locus, the flow rule is termed associated. When the plastic potential is a different shape from the yield locus, the flow rule is termed non-associated.

In this program, plastic strains were separated from the elastic strains graphically. Figs. 6.9 and 6.10 show plots of q *versus* ϵ_s and p' *versus* ϵ_v for typical specimens of each density. The separation of the elastic and plastic strains is shown. A constant stress increment of magnitude $0.05 p'_c$ in the direction of the stress probe was used to determine the plastic strain components. Although it is not necessary to be consistent in the use of the stress increment

between tests, it is essential that the same increment be applied to the two stress-strain plots for any single test. The technique of determining the plastic strains is illustrated on the figures. The plastic strains were scaled off the graphs at the separation of the elastic and plastic segments in the stress-strain plots, for the applied stress increment.

The ratio of plastic strains for specimens that were tested under isotropic stress was determined in a manner different from described above. During these consolidation tests the volume strains and axial strains were measured with changes in isotropic pressure. Thus the shear strain could be calculated. The shear strain data was plotted as a function of volume strain. From the pressure data, the yield volume strain was known. Thus the plots could be separated into pre-yield elastic strains, and post-yield elastic plastic strains. From this the ratio of plastic shear strain to plastic volume strain was determined.

Not all tests were suitable for examining the plastic strains. Those tests that experienced leaks or undrained conditions were not used.

The ratio e_g^p/e_v^p defines the slope of a plastic strain vector that is normal to the plastic potential. By plotting the plastic strain vectors at the yield stress of each test the shape of the plastic potential, and association or non-association of the flow rule can be determined.

Plastic strain vectors have been plotted for each available test in Figs 6.11 and 6.12. The low and high density data have been separated. After an initial analysis of the data, individual tests were examined in light of adjacent tests. Tests with strain vectors that deviated significantly from adjacent vectors were re-examined. There is a risk however, that the re-examination will force the data into a pre-disposed regime, one expected by the analyzer, rather than by the soil itself. For this reason, re-examination of the data was minimized. The initial interpretation of the plastic strain vectors for those tests that were re-examined are shown in Figs. 6.11 and 6.12 as dashed arrows.

As with the yield locus examined in Chapter 5, it would be convenient if the plastic

potential for each density was the same. Thus data from both densities have been combined in Fig. 6.13 with the strain vectors for each density marked with different arrows.

The isotropic yield locus from Fig. 5.8 is also shown in Fig. 6.13. The association of the flow rule is determined by comparing the direction of the strain vectors to the normals of the yield locus. Examination of the data reveals that the strain vectors deviate from a normality condition quite substantially on some parts of the yield locus. The deviation is not however, random. Careful inspection of Fig. 6.13 reveals that the strain vectors near the "front" of the yield locus (near the intersection of the yield locus with the p'/p'_c axis) deflect counter clockwise from the normal to the yield locus, while near the "tail", the vectors deflect clockwise from the normal. (Yield points that did not lie directly on the yield locus were projected to the locus along a line with a slope equal to their stress path angle ($\arctan(\Delta q/\Delta p')$).) The deviation of the strain vectors from normality are plotted against the stress path angle in Fig. 6.14 for both densities. There is a systematic variation in the strain vector deviation with stress path. The maximum deviation, (up to about 30° if "random" scatter is excluded), occurs for stress states near the beginning and end of the yield locus.

The change from clockwise to counter clockwise deflections occurs at a stress path angle of 60° to 90° and may be associated with the earlier finding (Section 6.2.1) that swelling and compressive volume strains are separated by the stress path direction $\Delta q/\Delta p' = 3$. The conventional drained triaxial test ($\Delta\sigma_3 = 0$) has a stress path angle of 71.5° .

From this data it can be concluded that the plastic potential and yield locus are not coincident. However, the yield locus shown in Figs. 5.8 and 6.13 may not clearly represent the real shape of the state boundary surface (Graham *et al.* 1989b). A better representation of the state boundary surface comes from the yield locus plotted with respect to the equivalent pressure (p'_e), as discussed in Chapter 5 (see Fig. 5.10). Thus it may be proposed that association of the flow rule is more correctly compared to the yield locus normalized with respect to p'_e , rather than

the preconsolidation pressure (p'_c).

Figs. 6.15 and 6.16 present the strain vector data for each density plotted with yield data normalized with respect to p'_c . The yield locus interpreted from Fig. 5.10 is also shown in the figures. Following the same procedure as before, the deviation of the strain vectors from the normal to the yield locus have been measured, and are shown on Figs. 6.17a and b. These figures show that the deviation from normality is less systematic, but of generally greater magnitude compared to the data normalized with respect to p'_c . The deviation for both densities is consistently negative (counter clockwise). In this particular case, the comparison of strain vectors to the yield locus normalized with respect to p'_c did not show an improvement in the association of the flow rule. This may be due more to uncertainties in the equilibrium pressures (p'_c) at yield, than to problems in theory. Comparisons of the strain vectors to the SBS for soils have not been published before.

Fig. 6.18 presents an interpretation of the plastic potential for the buffer. The shape is similar to that of the yield locus, but somewhat flatter over the top of the curve.

6.4 Hardening Law

The hardening law controls how the yield locus changes in position and size with plastic straining. During plastic strain hardening, the yield locus expands, with the current stress state lying along the state boundary surface. During strain softening the yield locus contracts, with the current stress state lying on the shrinking locus.

For soils, it is common to use the isotropic consolidation line, plotted in $V, \ln(p)$ -space (see Fig. 2.14) to represent the hardening line. The line, of slope λ represents total volume strain. The unload/reload line, of slope κ represents pure elastic volume strain.

Data from Wan (1987) and Saadat (1989) were correlated with data from this testing program. Only specimens from Wan and Saadat that were in the range of pressures of 100 to

3000 kPa were considered. Further, several tests were excluded after they were shown to be highly inconsistent with adjacent tests. Nine tests were used from Wan, 20 tests were used from Saadat, and 34 tests were used from this study (taken at the end of the 10 day stabilization period). The specific volume and effective mean pressure data at the end of consolidation for 63 specimens are shown in Fig. 6.19. The tests from each investigator have been given different symbols. A linear regression analysis was performed on these data resulting in the following equation:

$$[6.6] \quad V_c = 4.651 - 0.3142 \ln p'$$

The coefficient of correlation is 0.94 indicating good correlation, and consistent with similar equations presented by Saadat (1989).

One advantageous of this relationship over others proposed by Saadat (1989) is that a single relationship describes consolidation behaviour over the range of densities considered in this study. Thus a single hardening law can be used in the numerical modelling of the buffer.

The slope λ of the hardening line is -0.3142. This value is given in terms of V_c . In terms of V (specific volume of the whole mix) $\lambda = -0.154$. This latter value compares to -0.128 and -0.084, for low and high density specimens respectively reported by Saadat *et al.* (1989).

6.5 Summary

The elastic moduli for the buffer were presented in Section 6.2. Both isotropic and anisotropic moduli were developed. The errors associated with each are of the same order as encountered by other researchers on other, less active clays. Based on the results calculated for the anisotropic moduli and a comparison of the errors for isotropic and anisotropic moduli the degree of anisotropic in the buffer is likely to be small.

The anisotropic coupling moduli was found to be positive, but small. This indicates a soil fabric that is somewhat more stiff vertically than horizontally. The measurement of shear

and volume strains in the specimens during the 3 day swelling period, and porewater pressure changes during undrained shear both indicate a soil fabric that is slightly stiffer vertically. Although these results contradict conclusions of others (for example Saadat 1989, and Graham *et al.* 1989a), Wan *et al.* (1990) suggested that swelling may remove the strong anisotropy induced by specimen compaction.

The flow rule and plastic potential were examined in Section 6.3. The flow rule appears to be non-associated with the yield locus normalized with respect to p'_c . This was inferred from data presented in Chapter 5. A systematic variation in total strain vector direction was shown to exist. The association of the flow rule with respect to the state boundary surface was also examined. A comparison of the strain vector directions relative to the yield locus normalized with respect to p'_e did not indicate any greater association. This latter comparison however, deserves more attention, particularly for well behaved soils, since a yield locus normalized with respect to p'_c does not represent the shape of the state boundary surface in the same way that a yield locus normalized with respect to p'_e does.

A tentative plastic potential was developed for the buffer. The potential has a shape generally similar to the yield locus, but is flatter over the top of the curve.

Finally, the hardening law, describing the expansion (or contraction) of the yield locus was determined. A single functional relationship based in data at the end-of-consolidation of 63 tests was developed. The slope of the line in $V_c, \ln p'$ -space was similar to that determined by other researchers.

LOW DENSITY BUFFER
STRAIN VECTORS

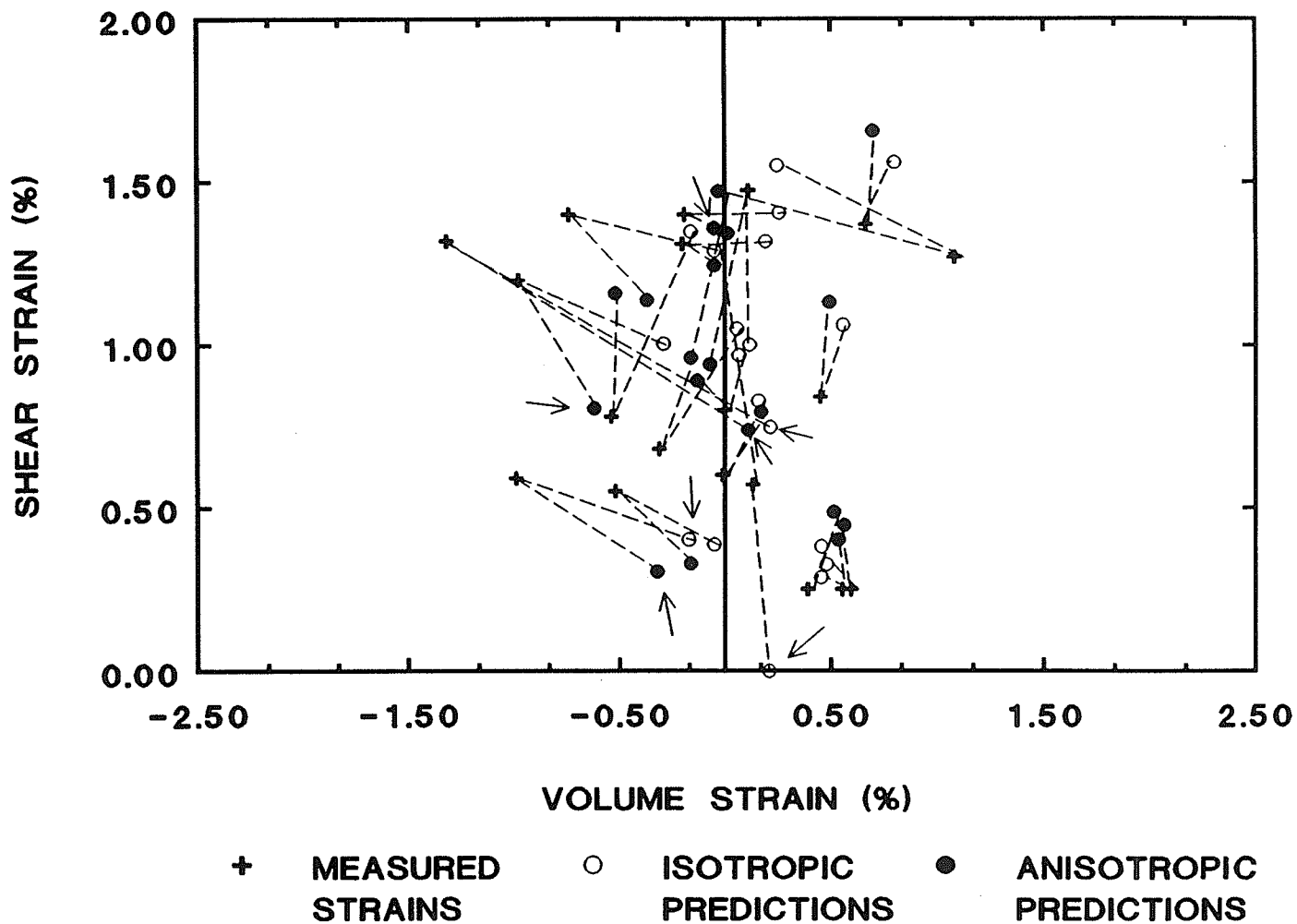


FIGURE 6.1

Predicted and measured elastic strain vectors for low density buffer. The predicted stains marked with arrows were removed from the error estimates in Table 6.2.

HIGH DENSITY BUFFER STRAIN VECTORS

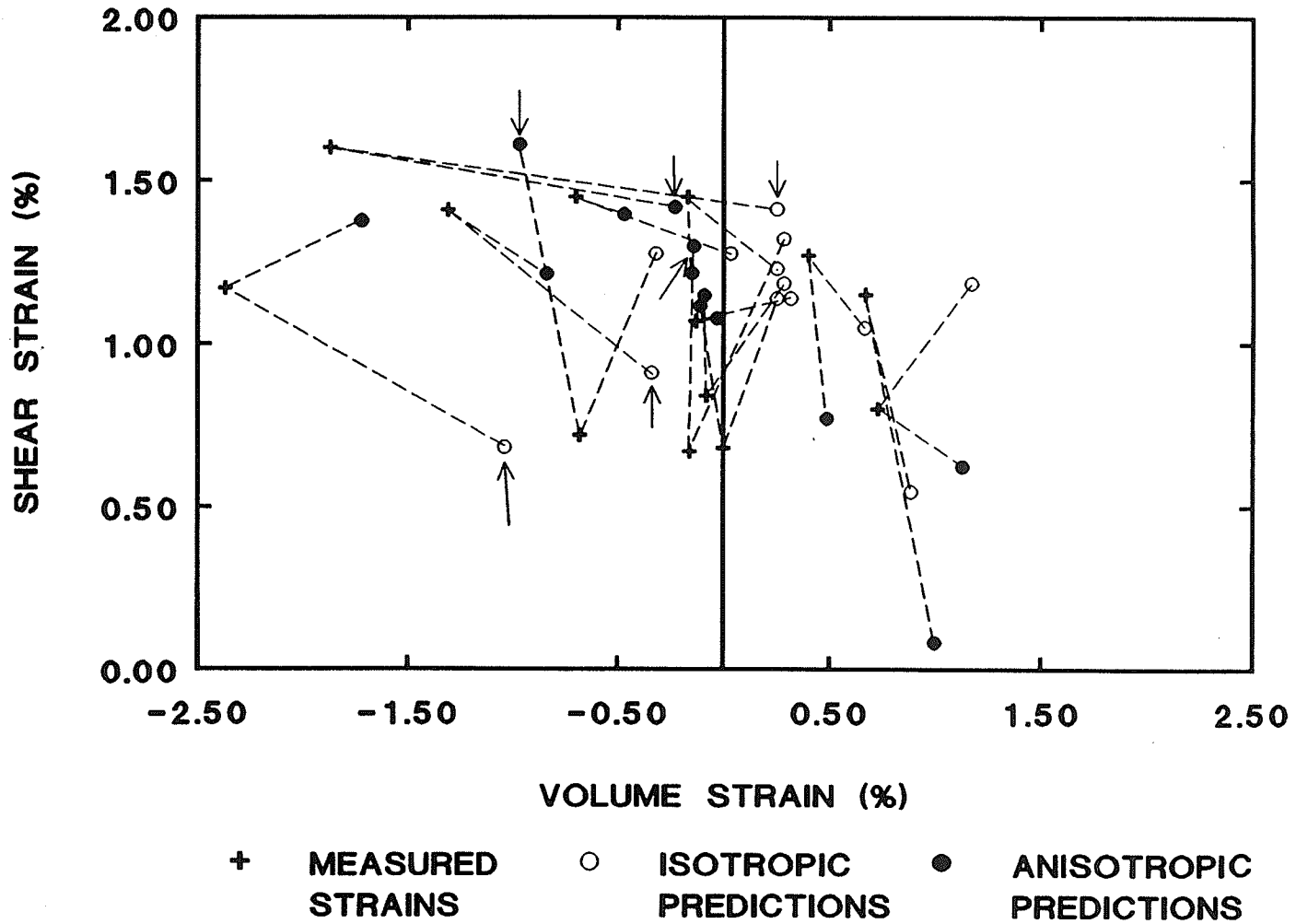


FIGURE 6.2

Predicted and measured elastic strain vectors for high density buffer. The predicted stains marked with arrows were removed from the error estimates in Table 6.2.

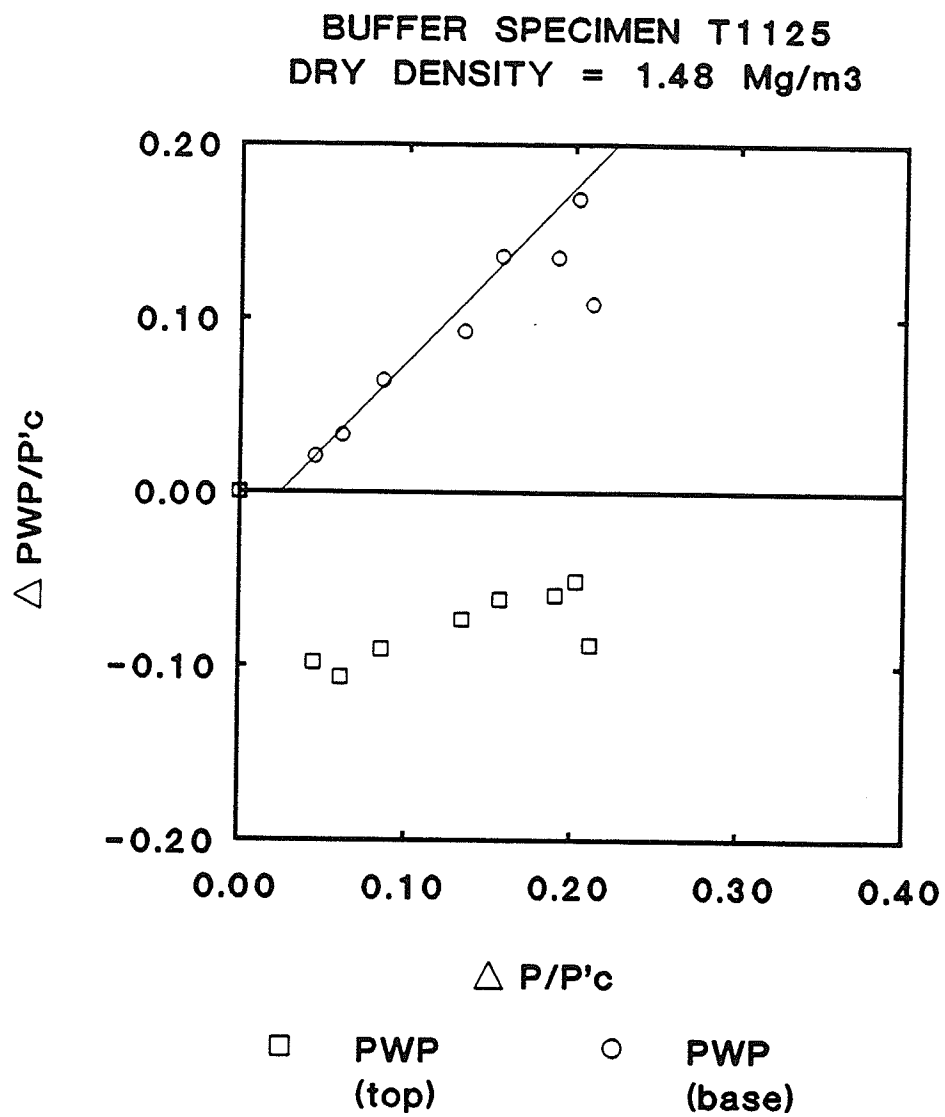


FIGURE 6.3

Normalized porewater response *versus* normalized total mean pressure change during undrained stress controlled shear. Buffer specimen T1125.

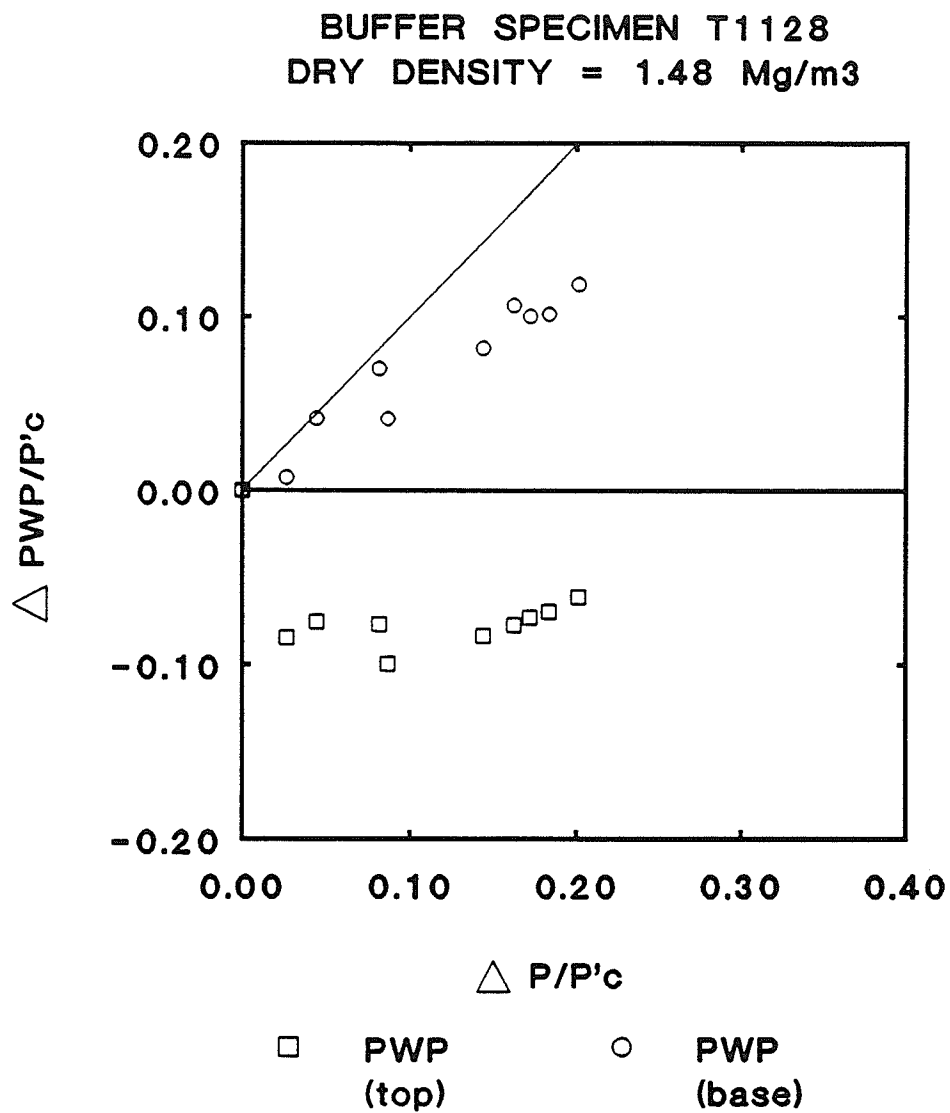


FIGURE 6.4

Normalized porewater response *versus* normalized total mean pressure change during undrained stress controlled shear. Buffer specimen T1128.

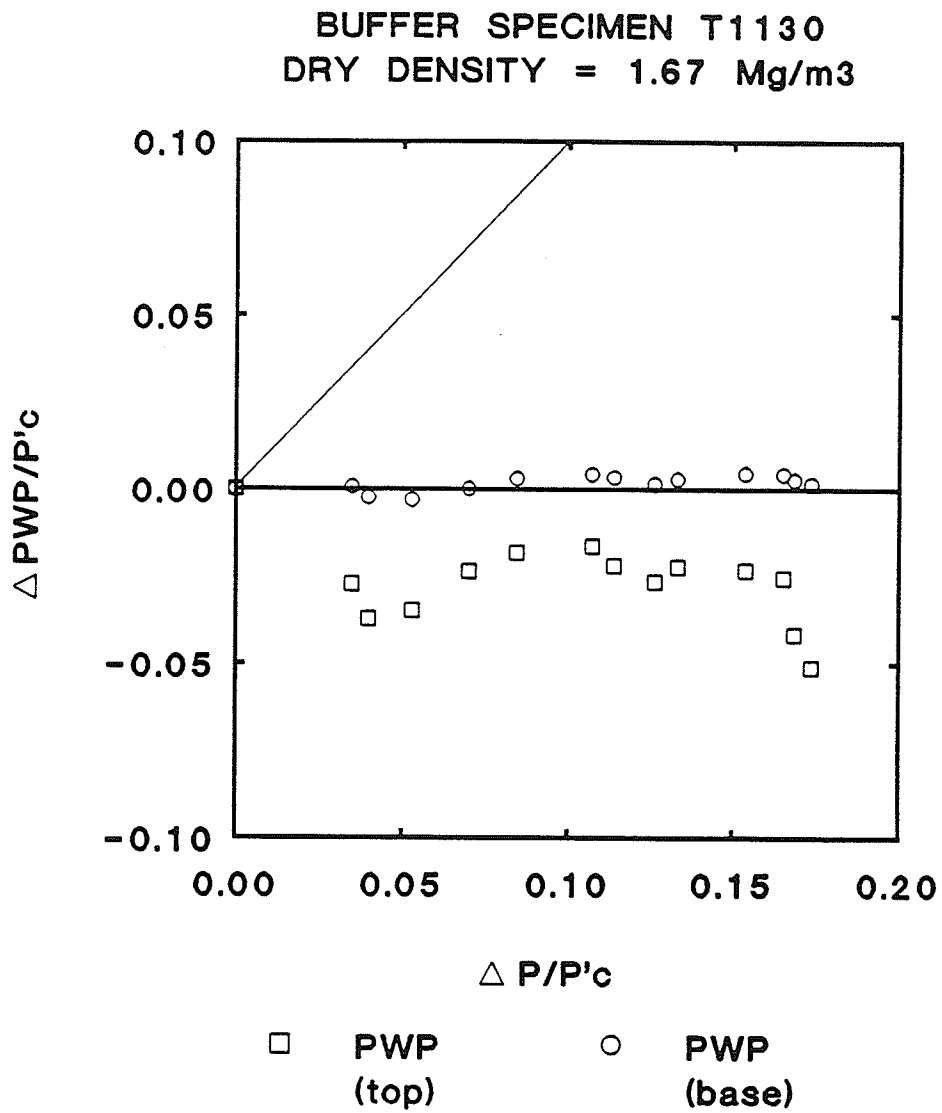


FIGURE 6.5

Normalized porewater response *versus* normalized total mean pressure change during undrained stress controlled shear. Buffer specimen T1130.

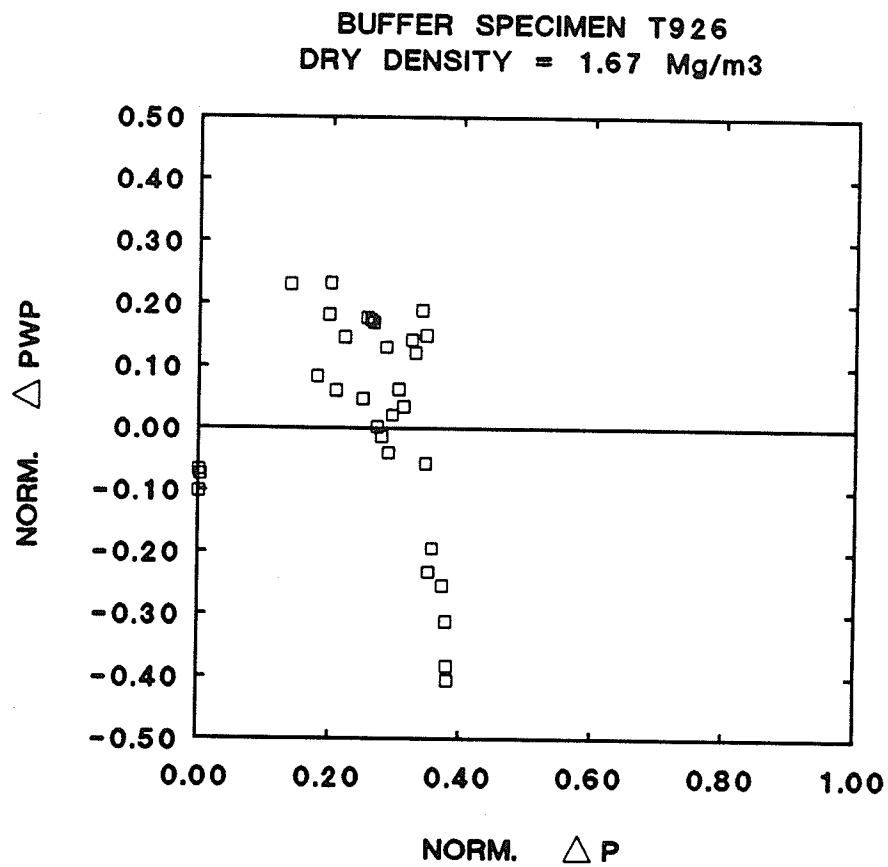


FIGURE 6.6

Normalized porewater response *versus* normalized total mean pressure change during undrained stress controlled shear. Buffer specimen T926 (unreported data from Saadat (1989)).

**BUFFER SPECIMENS
 DRY DENSITY = 1.49 Mg/m³**

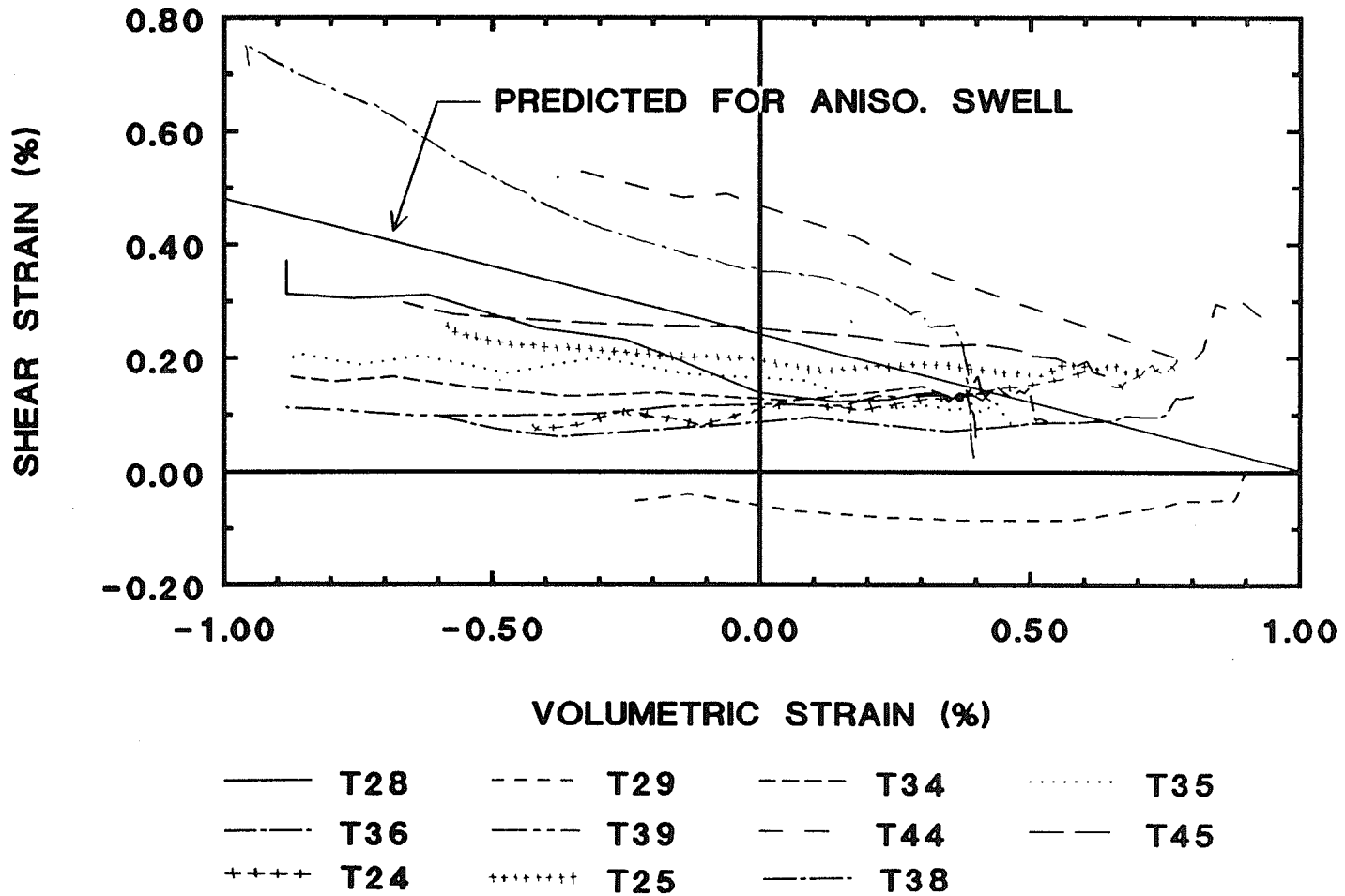


FIGURE 6.7 Shear strain *versus* volume strain during 3 day swelling under isotropic stress. Low density specimens (1100 series).

**HIGH DENSITY BUFFER
 DRY DENSITY = 1.66 Mg/m³**

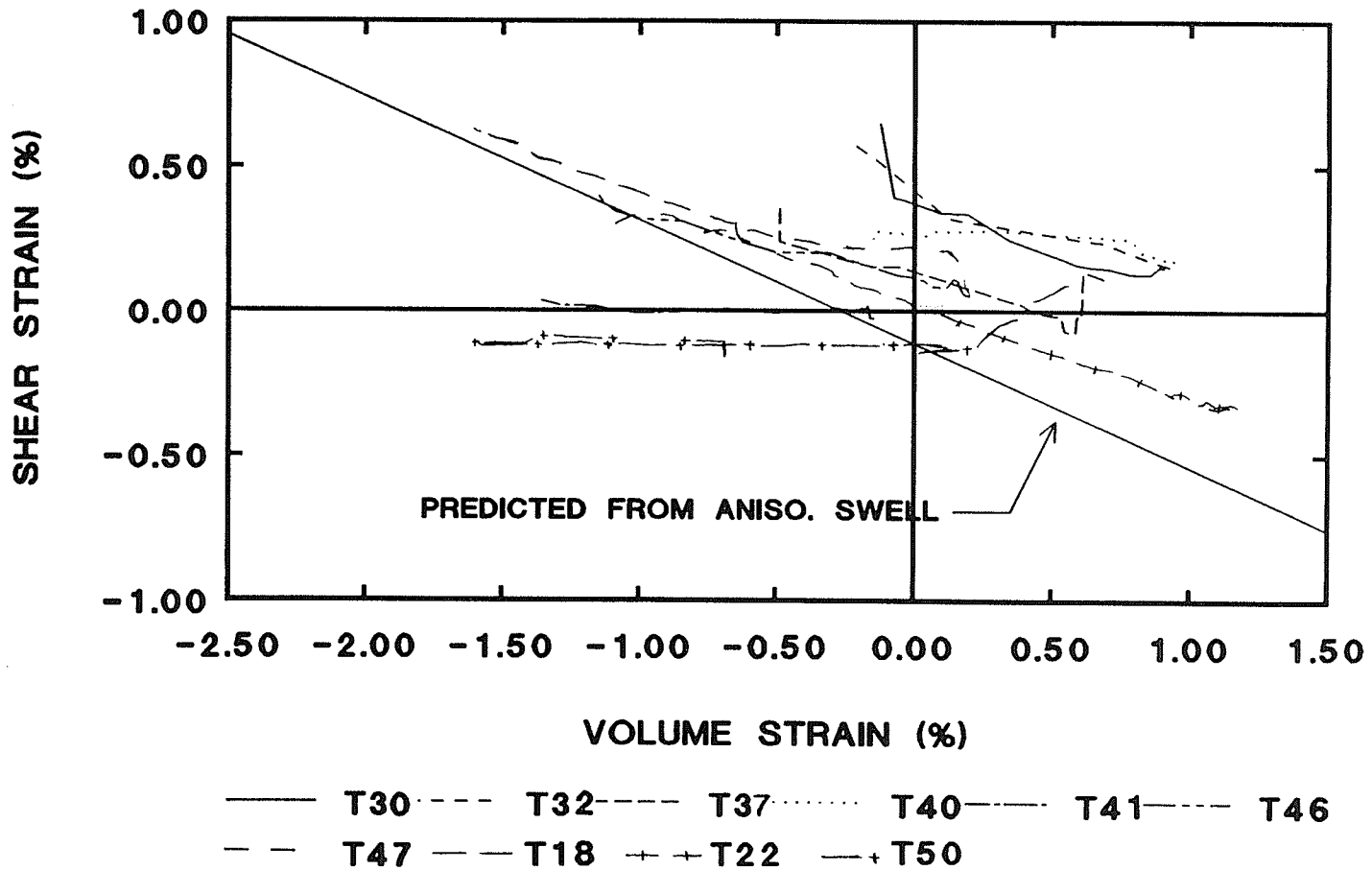


FIGURE 6.8 Shear strain *versus* volume strain during 3 day swelling under isotropic stress. High density specimens (1100 series).

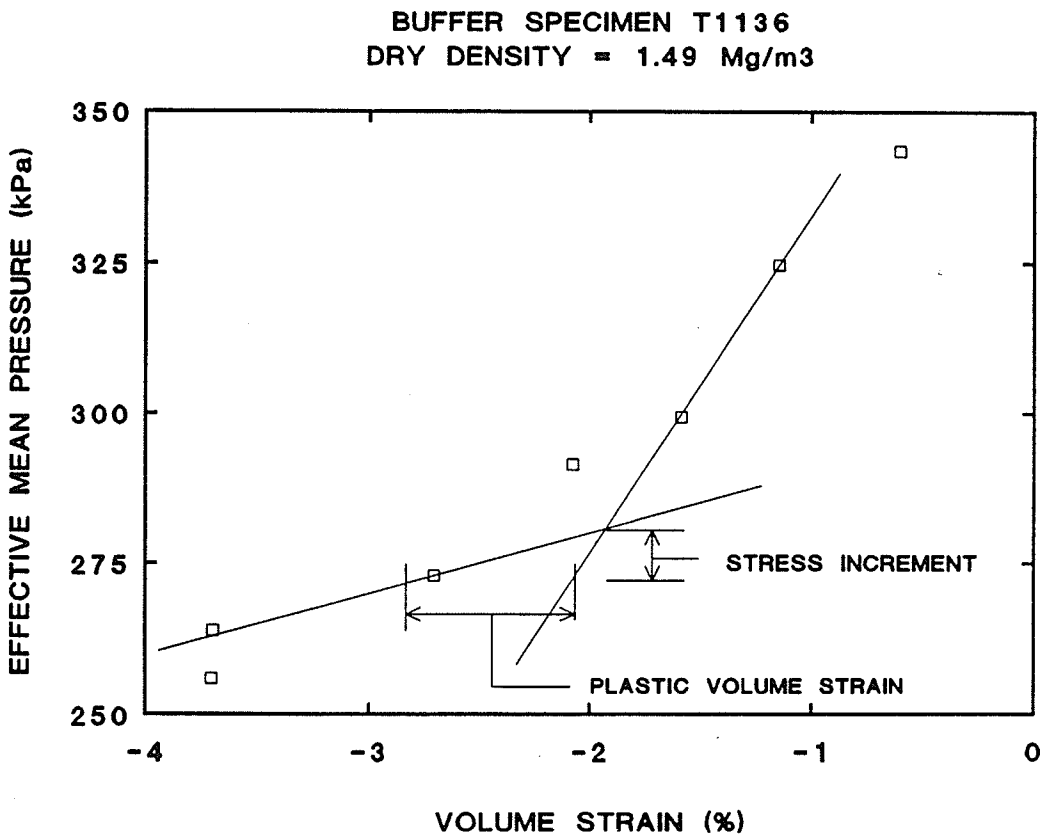
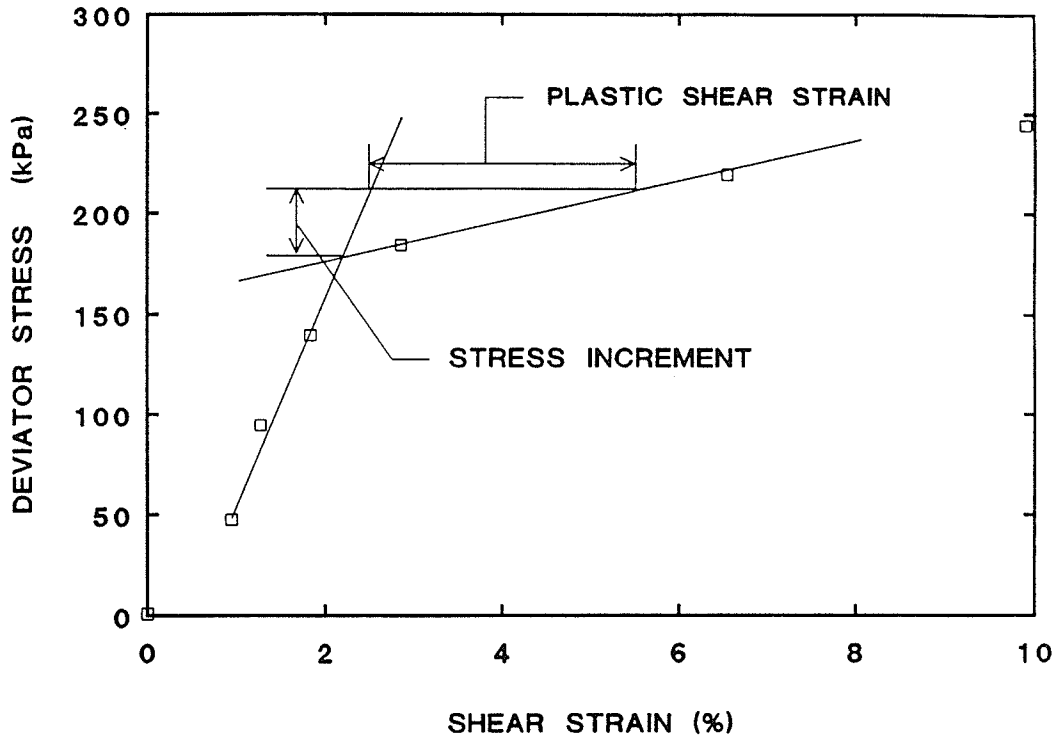


FIGURE 6.9 Graphical method to determine plastic strains by separation of elastic strains (a) deviator stress versus shear strain, (b) effective mean pressure versus volume strain. Buffer specimen T1136.

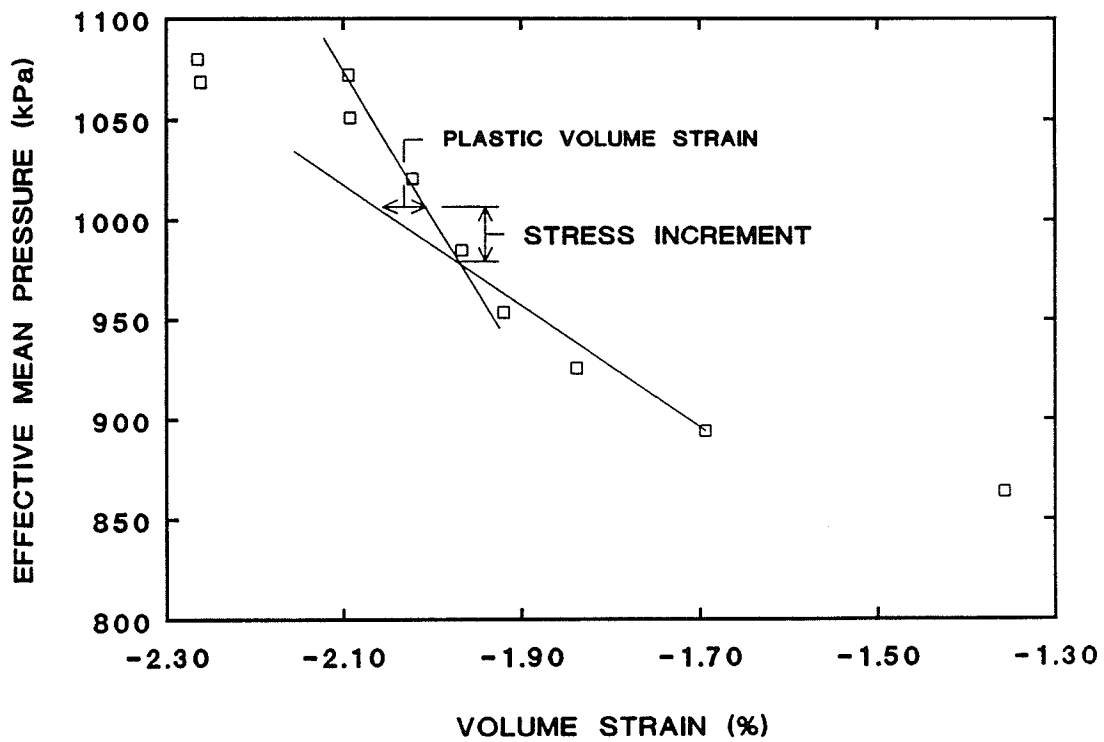
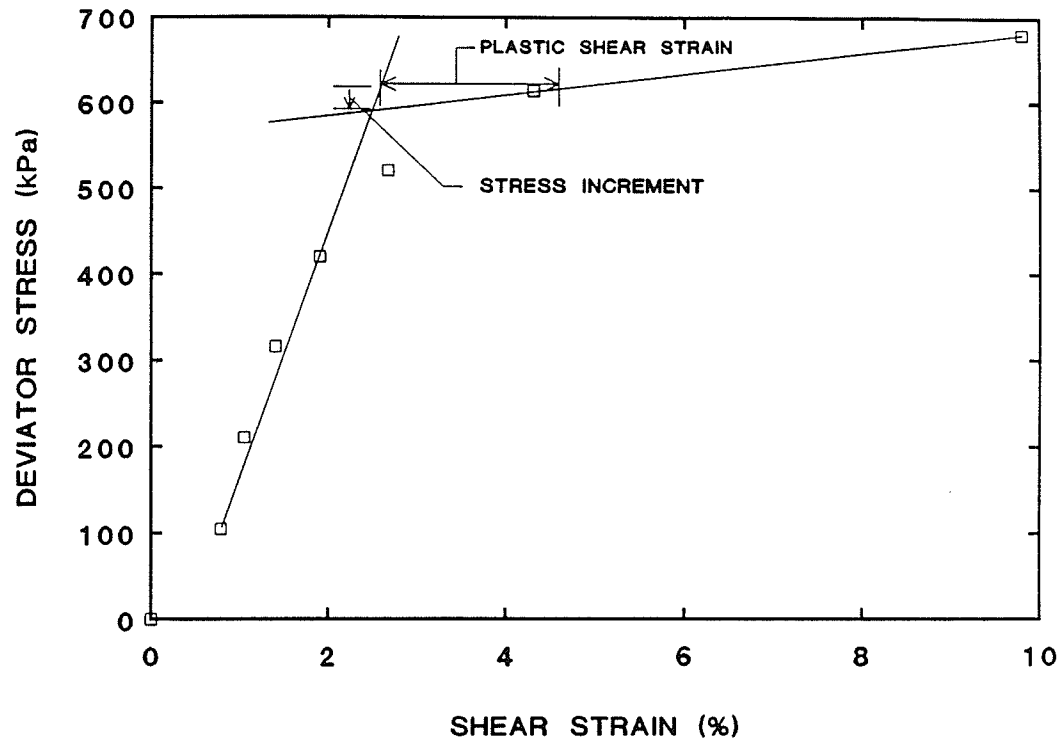


FIGURE 6.10 Graphical method to determine plastic strains by separation of elastic strains (a) deviator stress *versus* shear strain, (b) effective mean pressure *versus* volume strain. Buffer specimen T1141.

LOW DENSITY BUFFER
 DRY DENSITY = 1.49 Mg/m^3

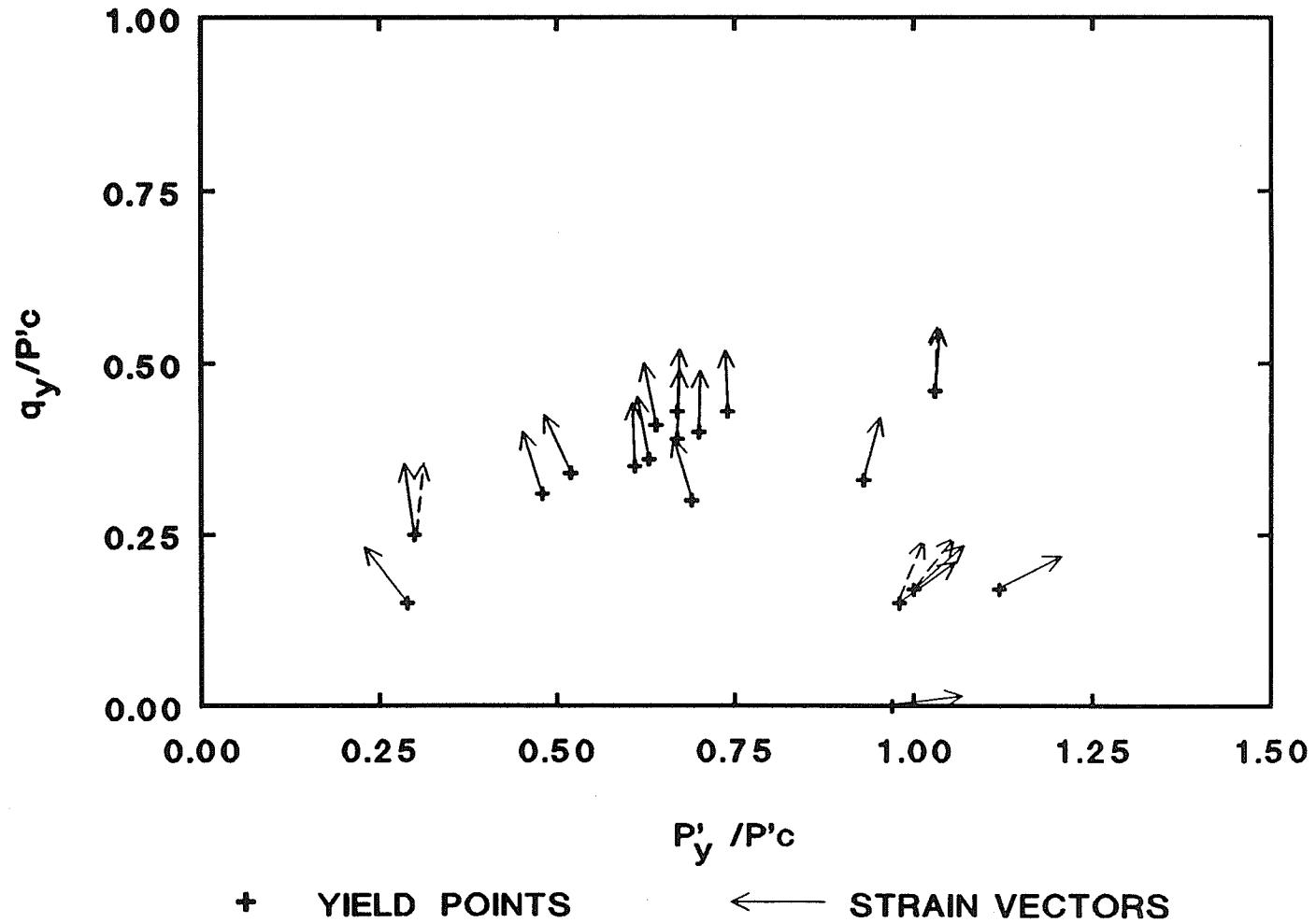


FIGURE 6.11 Plastic strain increment vectors originating from yield stresses. Low density specimens, normalized with respect to p'_c . The dashed arrows denote initial interpretation of strain vectors for that test.

HIGH DENSITY BUFFER
DRY DENSITY = 1.67 Mg/m³

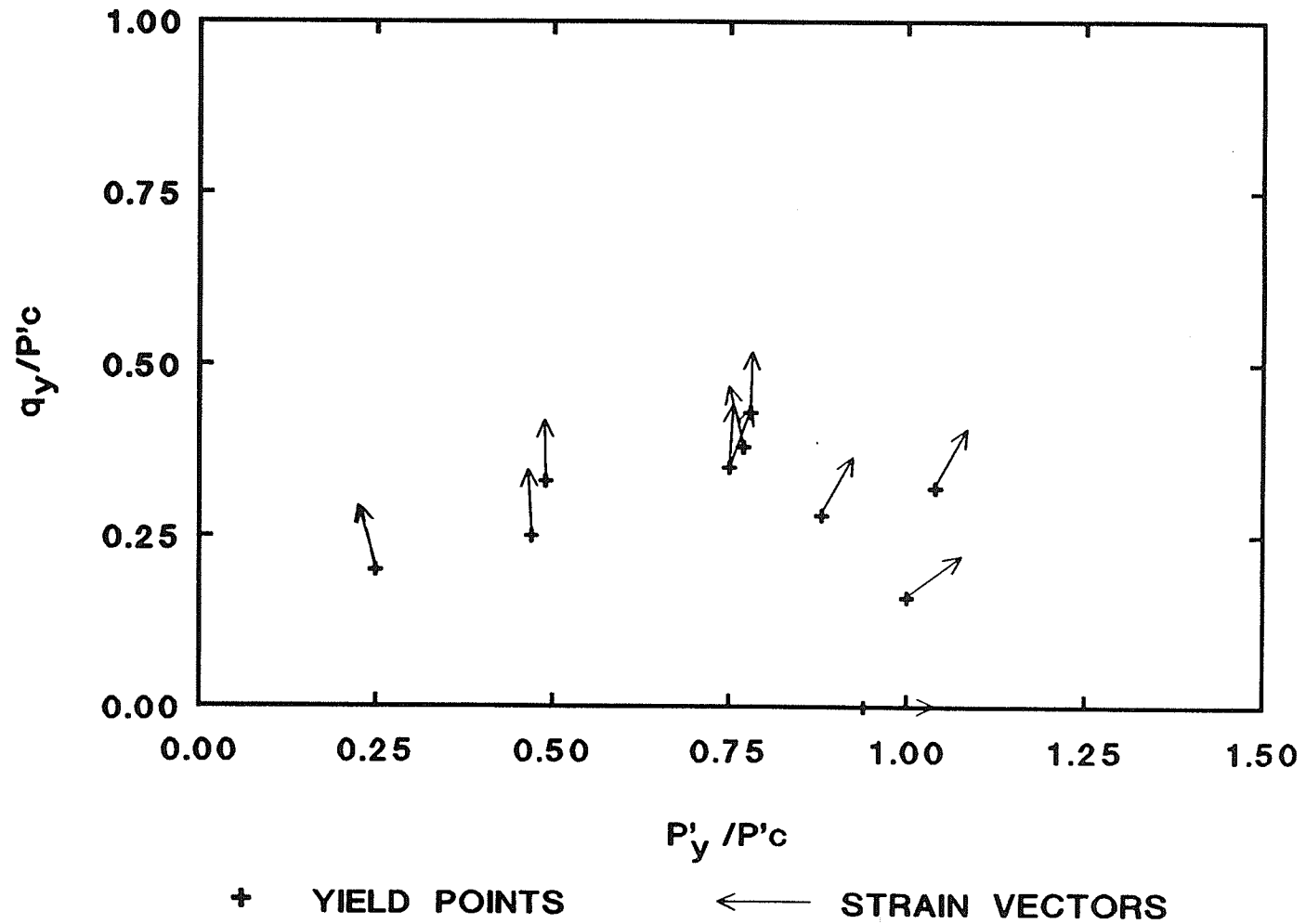


FIGURE 6.12 Plastic strain increment vectors originating from yield stresses. High density specimens, normalized with respect to p'_c . The dashed arrows denote initial interpretation of strain vectors for that test.

BUFFER SPECIMENS
DRY DENSITY = 1.49 Mg/m³ and 1.67 Mg/m³

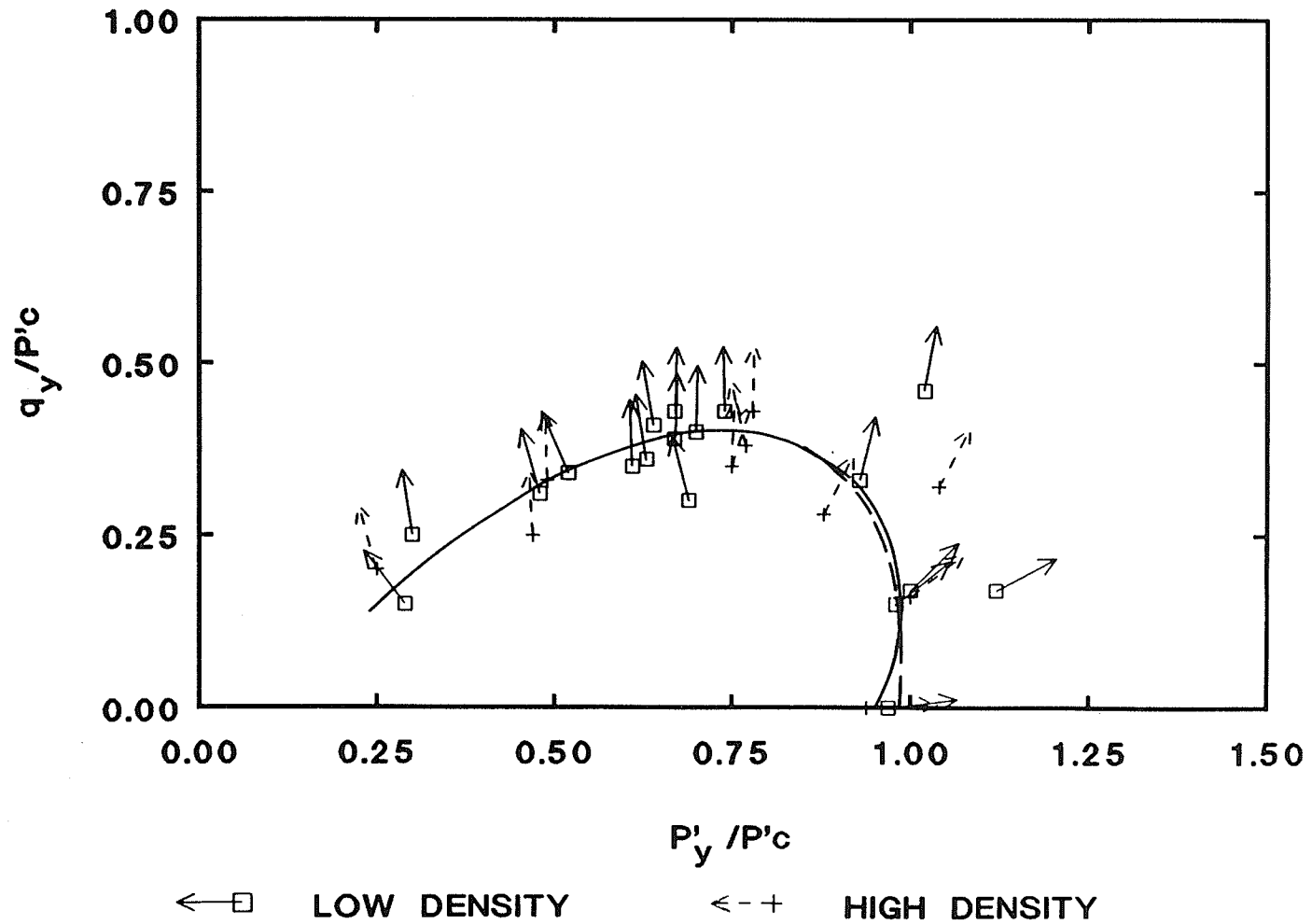


FIGURE 6.13 Plastic strain increment vectors for low and high density specimens.

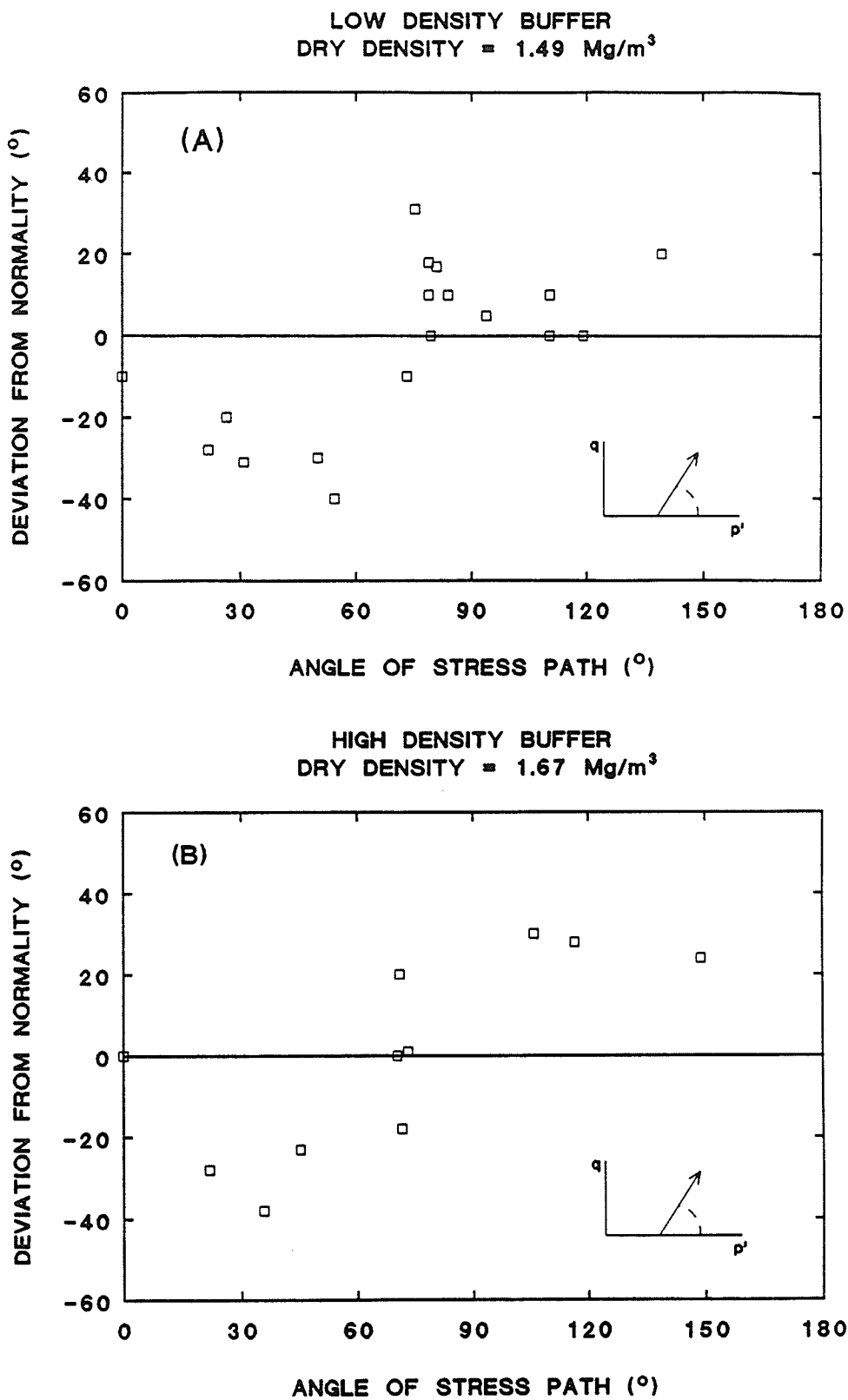


FIGURE 6.14

Deviation of strain vectors from normality on the yield locus (normalized with respect to p'_c), as a function of stress path angle. (a) for low density specimens, (b) for high density specimens.

LOW DENSITY BUFFER
DRY DENSITY = 1.49 Mg/m³

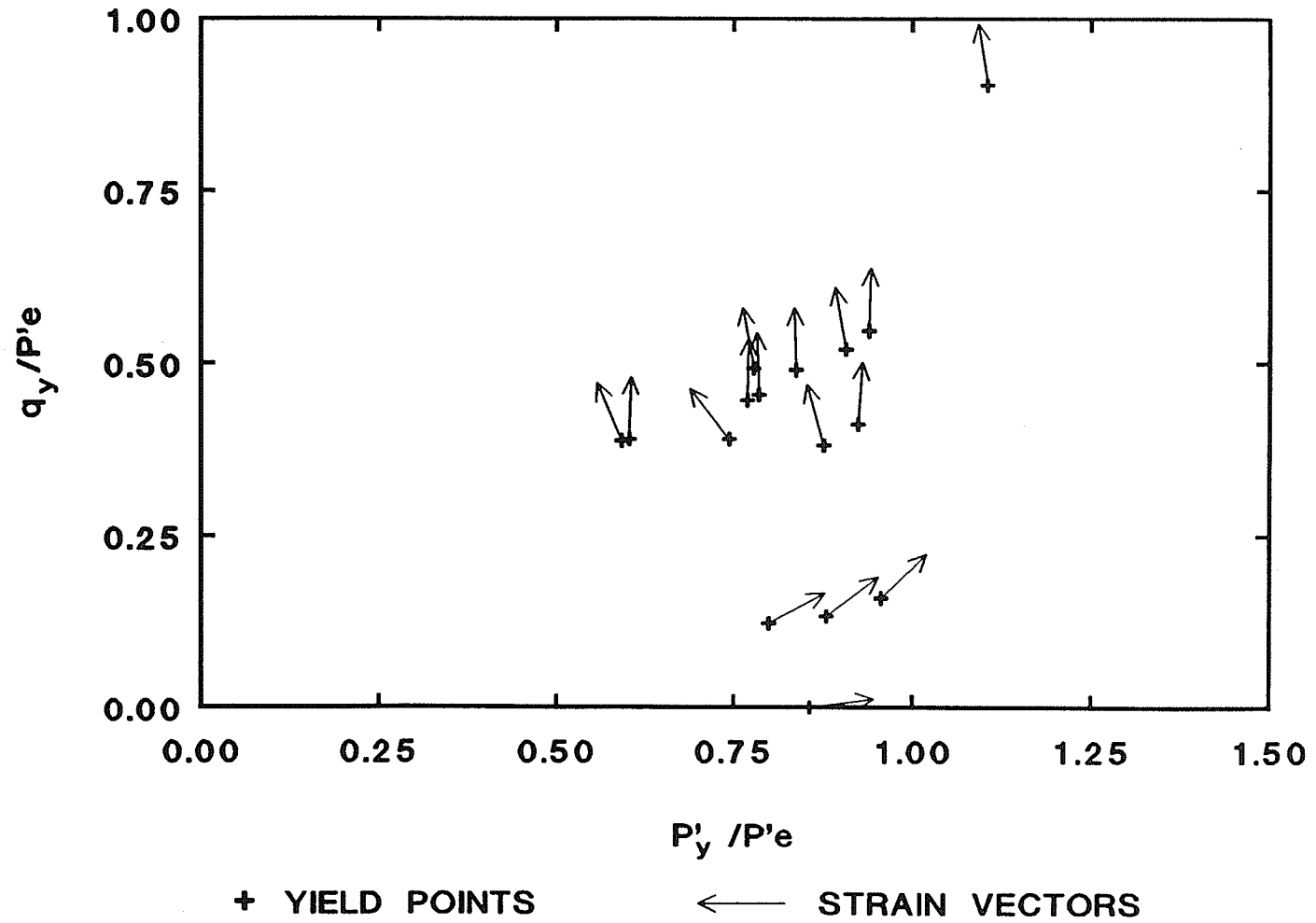


FIGURE 6.15

Plastic strain increment vectors originating from yield stresses. Low density specimens, normalized with respect to p_e^* .

HIGH DENSITY BUFFER
DRY DENSITY = 1.67 Mg/m³

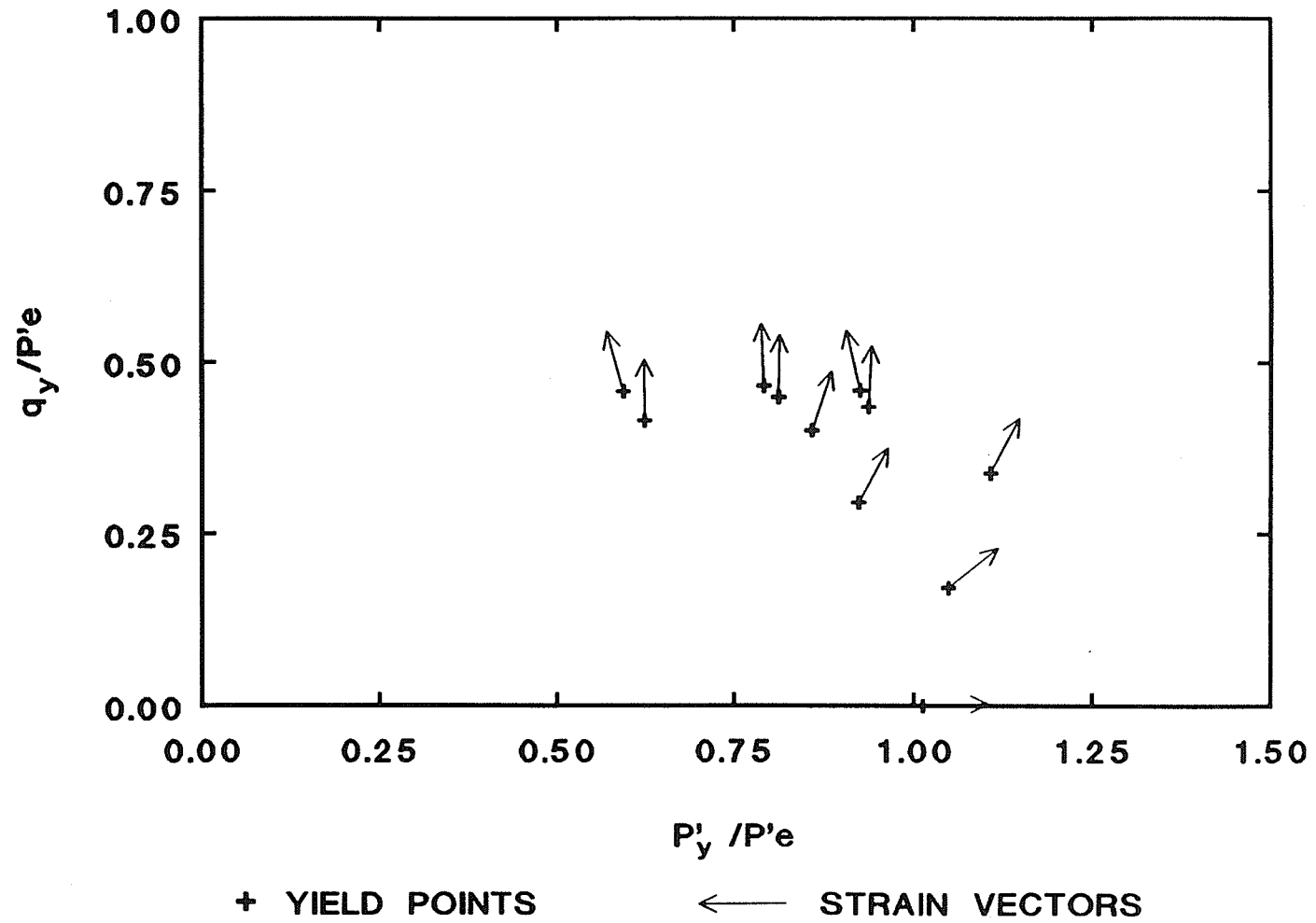


FIGURE 6.16 Plastic strain increment vectors originating from yield stresses. High density specimens, normalized with respect to p'_e .

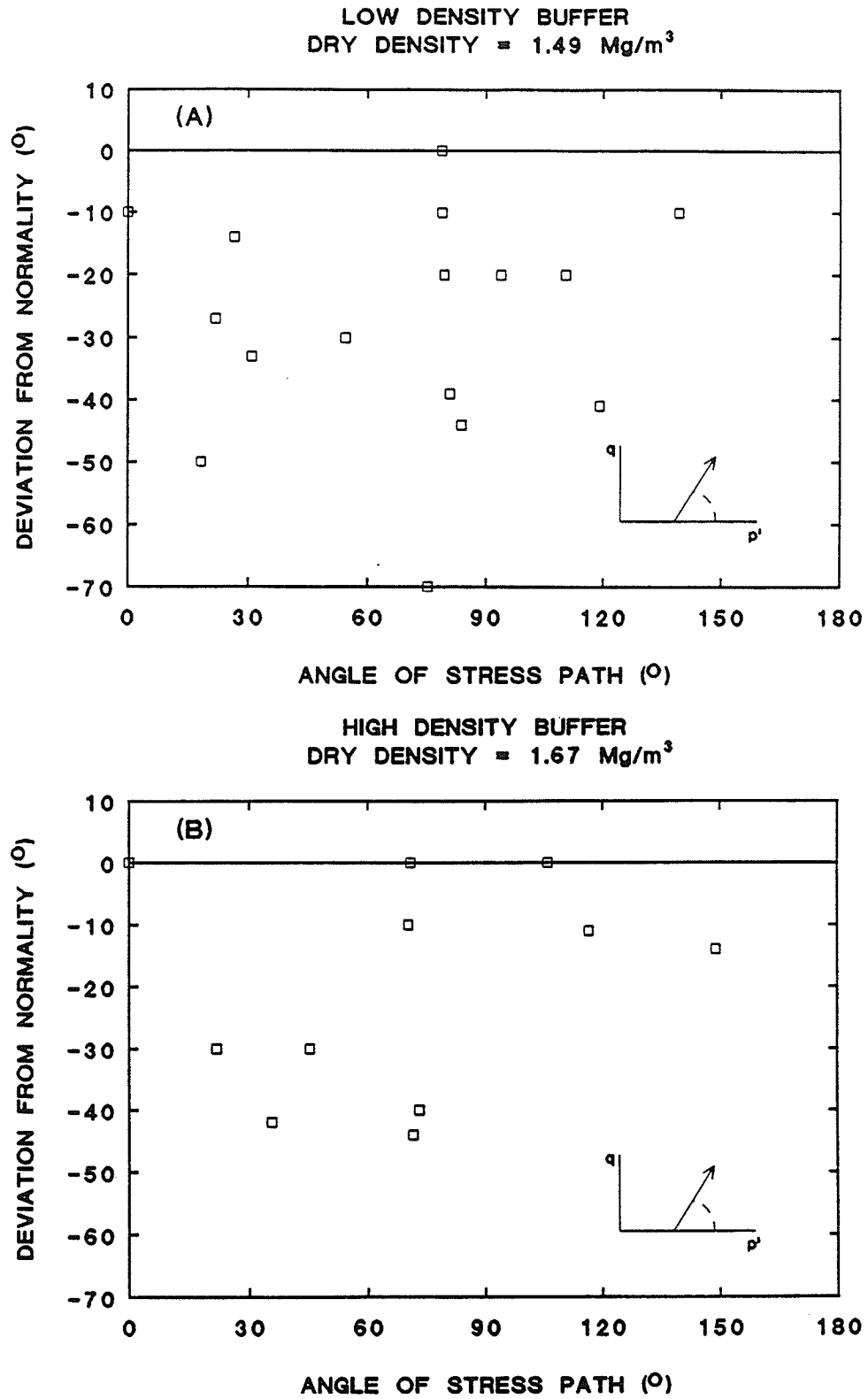


FIGURE 6.17 Deviation of strain vectors from normality on the yield locus (normalized with respect to p'_e , as a function of stress path angle. (a) for low density specimens, (b) for high density specimens.

BUFFER SPECIMENS
DRY DENSITY = 1.49 Mg/m³ and 1.67 Mg/m³

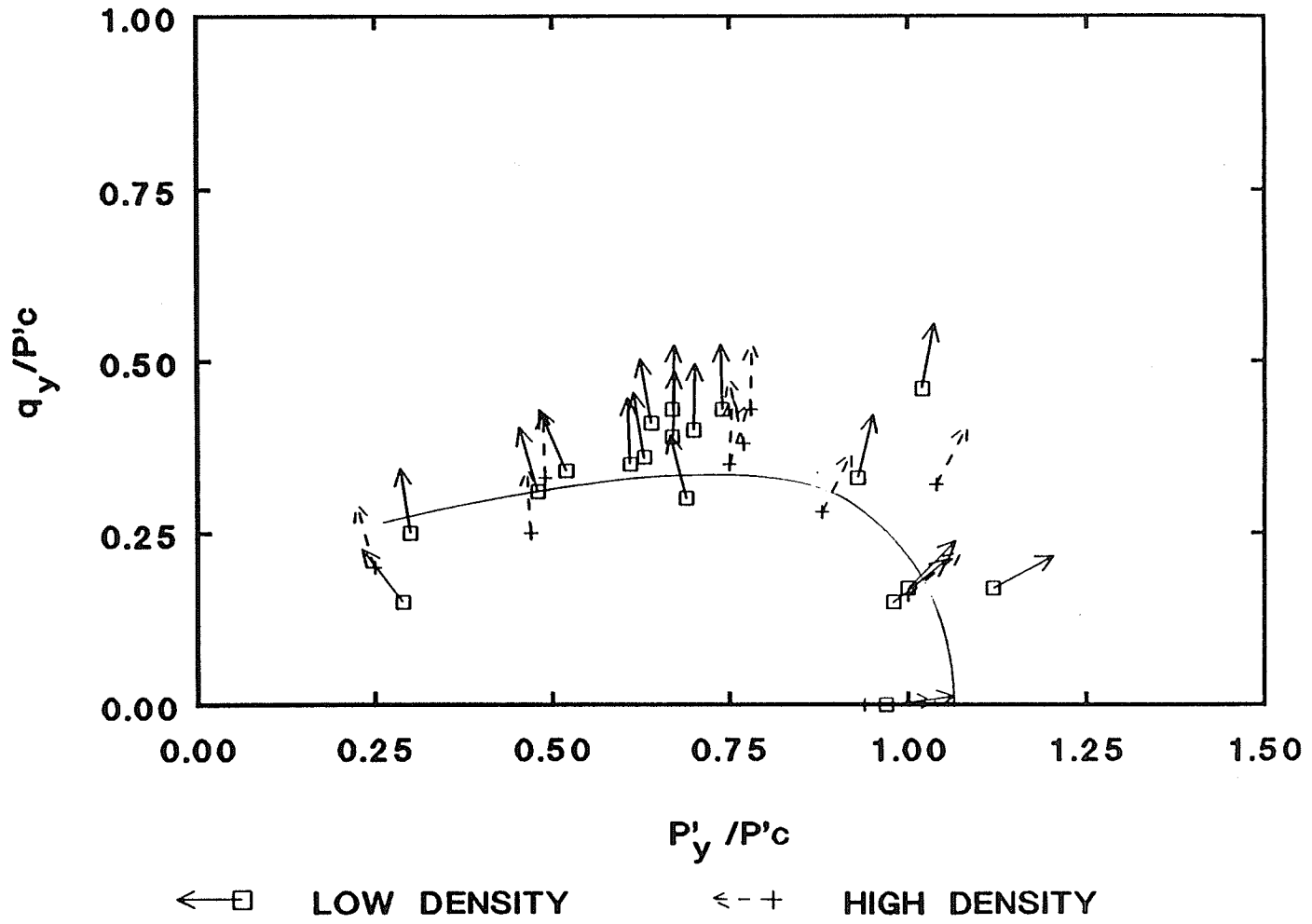


FIGURE 6.18 Proposed plastic potential for buffer data, normalized with respect to p'_c .

BUFFER SPECIMENS

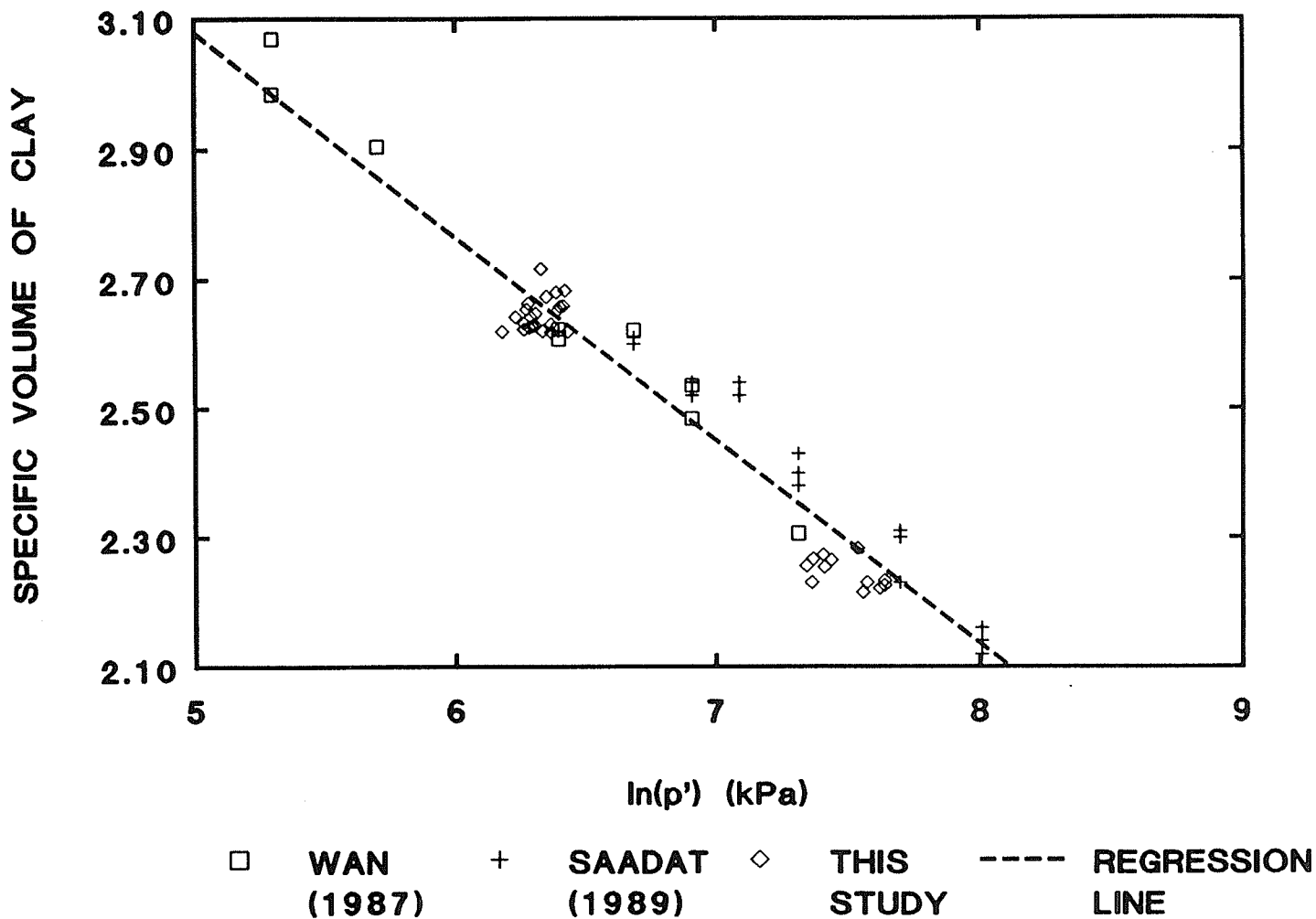


FIGURE 6.19 Hardening function for the buffer. Specific volume of clay fraction *versus* effective mean pressure (natural log scale). Additional data from Wan (1987) and Saadat (1989).

CHAPTER 7 REVIEW AND MODIFICATIONS TO THE ELASTIC PLASTIC MODEL

7.1 Introduction

This chapter will briefly review the analysis of data presented in Chapters 5 and 6 in order to bring the elastic plastic model together as a whole. Section 7.2 will discuss each of the elastic plastic components, and highlight the important findings of the analysis.

Chapter 5 and 6 raised several important issues that require further attention in this chapter. First, Chapter 6 noted that the porewater pressure response during undrained shear was different between the top and base pressure transducers. Also, the high density specimens behaviour was inconsistent with the undrained low density specimens. (Remember that the top transducer had earlier been used to monitor the applied back pressure, and the bottom transducer used to monitor the porewater response at the base of the specimen.) Section 7.3 will describe the porewater pressure behaviour of the buffer, with particular attention being given to the behaviour during shear.

It was found in Chapter 5 that the yield locus did not intersect the failure envelope. This implies that all specimens experienced post-yield strain "hardening" in shear. In contrast, examination of $V_{c,p}'$ data suggested that many specimens underwent post-yield strain softening in terms of volume change. This conflicting behaviour is incompatible with the assumption of the classical elastic plastic model, originally proposed in Chapter 1. Section 7.4 introduces modifications to the yield criterion that explain these inconsistencies in the shear-volume behaviour.

The behaviour of some low density specimens having higher-than-average OCRs was explained in Chapter 5 using a visco-plastic swelling model. In Section 7.5, this model will be re-introduced and expanded. Some data is available to show the effects of OCR, and time on the swelling behaviour of the buffer. The model will then be used to examine swelling behaviour during shear.

The discussion presented in Sections 7.4 and 7.5 is rather speculative at this stage, being based on limited data. The primary goal of this discussion is to provide directions to which future research should follow.

7.2 Review of the Original Model

7.2.1 Elasticity

Elasticity was examined in detail in Section 6.2, which developed appropriate values for isotropic and anisotropic elastic moduli for the buffer. For the specimens tested in this program, the analysis indicates that any anisotropy is weak, that is overconsolidated buffer can be adequately modelled by isotropic parameters. Moreover, the anisotropy that was found, indicated a soil fabric that was stiffer vertically than horizontally at the end of the 3 day swell period. This conclusion is based on analyses of data from three independent test stages - swelling at isotropic pressures, drained shearing, and undrained shearing. Thus confidence in the conclusions is high. These data also support comments by Wan *et al.* (1990) that swelling reduces anisotropy induced by specimen compaction. Saadat (1989) found that specimens which compressed before shearing displayed anisotropic elastic behaviour that was stiffer horizontally than vertically. He attributed this anisotropy to compaction of the specimen in a rigid mold. The stress history of his specimens was different from the history of the specimens in the present study. Consequently it is not unreasonable to expect different undrained porewater pressure responses.

These differences in behaviour have implications for numerical modelling of container-buffer-rock interaction. Different soil properties must be considered depending on the stress-strain conditions the buffer is subjected to prior to shear. The anisotropy of the soil fabric may also need to be considered in the case of relaxation conditions (zero total strain change, release of stress.) In this case clay platelet re-arrangement may occur at no net volume change.

7.2.2 Yielding

Considerable work was done to quantify the yielding behaviour of the buffer. Chapter 5 showed that a single yield locus could be used to describe yielding of low and high density specimens. This has considerable advantages for numerical modelling work.

Fig. 5.8 presented two yield loci, one assuming isotropic elasticity and the other assuming anisotropic elasticity. The difference between the two loci is small, which reinforces the analysis of elastic moduli in Chapter 6 referred to in the previous section.

The shapes of the yield loci in $V_c, p'/p'_c$ -space (Fig. 5.13) are similar for each density. A single yield locus results (Fig. 5.14) if the specific volume is normalized by the specific volume of a specimen (on the same κ -line) at the preconsolidation pressure. There is some scatter of the data, but the range of error in specific volume is about 5%.

The shape of the yield locus depends on the normalizing parameter used. Graham *et al.* (1989b) suggest that plotting yield loci (in q, p' -space) normalized with respect to p'_e will result in an elliptical yield locus. This ellipse represents the shape of the state boundary surface at constant volume. In this work, normalization of yield data with respect to p'_e was not particularly useful (Fig. 5.10). One problem encountered for the buffer was that separate V_c - p' relationships were used for each density.

7.2.3 Flow Rule and Plastic Potential

Examination of the plastic strain vectors indicated that the flow rule is non associated. When the strain vectors were compared to the yield locus normalized with respect to p'_e (Fig. 6.13), the deviation from normality was systematic, depending on the stress path direction dq/dp' . Similar observations were made for Winnipeg clay by Graham *et al.* (1983c). The deviation from normality was counter clockwise for stress paths where $\Delta\sigma_3 > 0$, and was clockwise for stress paths where $\Delta\sigma_3 < 0$.

The flow rule also appeared to be non-associated when the strain vectors were compared to the yield locus normalized with respect to p'_e (Fig. 6.16). In this case the plastic potential was being compared to the state boundary surface at constant volume. The deviation of the strain vectors from normality was greater in magnitude compared with Fig. 6.13, but more random in orientation. This comparison has not been reported before in the literature, and deserves further attention, perhaps by testing the concept on well behaved soils, such as anisotropically consolidated specimens kaolin and illite.

The plastic potential (Fig. 6.17) was found by examining the plastic strain vectors. The shape is generally similar to the yield locus, but flatter over the top of the curve. The shape of the potential indicates that negative plastic volume strain (strain softening in volume) would occur for some stress paths. This is consistent with the volume change data, but conflicts with the yield locus, which implies plastic strain hardening in post-yield shear. This conflict is discussed further in Section 7.4.

7.2.4 Hardening Law

The hardening law was presented in Chapter 6 (Fig. 6.19). It was determined from consolidation data from Wan (1987), Saadat (1989), and this program. The equation for the hardening law is given in [6.6]. The advantage of this relationship over others proposed by Wan (1987), Saadat (1989), and others is that [6.6] covers the range of buffer densities considered in this study. The other researchers gave separate relationships for low and high density buffer specimens. The single equation given in [6.6] has a higher degree of correlation (0.94) than for many of the equations provided by the other researchers.

The slope of the hardening (consolidation) line given in [6.6] was -0.3142. In critical state soil mechanics this slope is termed λ . Its value from this study is consistent with that of other clays. The slope of the unload/reload lines, on which elastic volume strains are measured

was not determined from this study. (Values of κ were not determined from data in this study because of the significant visco-plastic swelling associated with off-loading. Thus the values of κ would be time-dependent, and not reflect pure elastic consolidation/swell.) Values of κ reported for low and high density specimens is -0.0448 (Saadat 1989). (Note that the values of λ and κ in this thesis are reported in terms of V_c , not V . The conversion is: $V_c = 2.037V$).

7.2.5 Failure Criteria

Most of the specimens in this program were sheared to failure. The end-of-test data from this study, and failure envelopes developed by others are shown in Figs. 5.6 and 5.7. The low density data from this program fit the failure envelope derived by Wan (1987). The effective Mohr-Coulomb failure parameters are $c' = 40$ kPa and $\phi' = 14^\circ$. The high density end-of-test data fit a power law rupture envelope developed by Saadat (1989) for his peak strength values. The end-of-test data were somewhat higher than the critical state line (CSL) developed by Saadat (1989). The end-of-test envelope from this study gives $c' = 88$ kPa and $\phi' = 14^\circ$. The slope of the high density failure envelope is the same as Saadat's CSL, but a small cohesion intercept is introduced. The difference in the position of the end-of-test line and Saadat's CSL is due to strain softening of Saadat's specimens to a strength less than the peak strength. Note that "end-of-test" in these stress controlled tests correspond with "peak" conditions in Saadat's strain controlled tests (Fig. 5.7)

7.3 Porewater Behaviour in the Buffer

This section discusses the observed porewater pressure of the buffer specimens in this study. The discussion will be separated into pre-shear and shear stages of the test. Most specimens had two pressure transducers attached. The top transducer monitored the back pressure applied during consolidation. This was kept at 200 kPa for nearly all the tests.

During shear, the back pressure lead was closed and the top pressure transducer measured porewater pressures at the top and sides of the specimen. The base transducer, connected to a small porous stone in the centre part of the base of the specimen measured the internal porewater pressure during both consolidation and shear. When side drainage was used, the drainage strips extended from the top porous stone to approximately 10 mm above the bottom of the specimen. It was expected that this arrangement would exclude a direct hydraulic link between the pressure transducers, and therefore the base transducer would experience a degree of independence from the top, back pressure transducer.

7.3.1 Porewater Behaviour with Isotropic Stress Application

When consolidation was started, the top porewater pressure was set at the applied back pressure. The base porewater pressure often rose very rapidly to a value much higher than the applied back pressure. The peak was usually reached within the first hour of the test. Fig. 7.1 shows the pressure changes with time for two specimens (T1134 and T1141). This behaviour is probably due to some residual excess water in and around the base filter stone from the installation process. This water was then pressurized by the total confining pressure. The porewater pressures at the base dissipated over time (as the excess water was either expelled from the specimen, or absorbed into the clay), and reached equilibrium at the end of the 10 day stabilization period. The porewater pressures measured at the base of the specimens were typically 150 kPa to 175 kPa for the low density specimens and about 200 kPa for the high density specimens. These pressures compare closely to the back pressure of 200 kPa, suggesting an internal pressure equilibrium condition. The total confining pressures were 750 kPa (low density), and 1600 to 2300 kPa (high density).

Following off-loading for the 3 day swell period, the base porewater pressures in all specimens dropped (Fig. 7.1). A new equilibrium base porewater pressure of about 100 kPa was

observed in both low and high density specimens. The relatively small drop in base porewater pressure was probably due to the rapid dissipation of negative porewater pressure by the inflow of water from the drainage burette. (The coefficient of consolidation c_v is usually much higher in the overconsolidation range than in the first-loading range of stresses.)

7.3.2 Porewater Pressure Behaviour During Shear

The base porewater pressure during shear was only moderately influenced by changes in total pressure. Fig. 7.2 shows four tests (two low density, and two high density specimens) with different stress paths, and the pressure changes observed with time. In two tests (T1145 and T1137) the total (cell) pressure increased, and in the other two tests (T1136 and T1147) the total (cell) pressure decreased.

In the tests that experienced increasing total pressures, the base porewater pressure tended to increase also. However, as observed in Fig. 7.2a and c, the increase was not as great as the total pressure change, and furthermore, dissipation of some excess porewater pressure occurred during the 3 day loading period. The lack of complete excess porewater dissipation is attributed to the low permeability of the buffer.

In the tests that experienced decreasing total pressures, the base porewater pressure response is very muted. In Fig. 7.2b and d, the base porewater pressure declined only slightly with little observed variation in porewater pressure during each 3 day loading period. The possible cause is that the transducer is unable to accurately measure porewater pressure response at these total pressure conditions due to a cavitation process in the specimen drainage leads. In the case of the high density specimen (Fig. 7.2d) the situation is similar to that discussed in Chapter 4. Referring to Figs. 4.1 and 4.4, it was shown that a change in apparent effective stress of the high density specimen (Fig. 4.4) occurred at porewater pressure above zero (atmospheric) pressure. From Fig. 4.1 it is seen that the porewater pressures were about, or slightly less than

100 kPa when the apparent effective stress response dropped in Fig. 4.4. Thus in the case of T1147 (Fig. 7.2d), rather than being a real measure of the soil behaviour, the lack of response is probably due to a poor, albeit innocent, choice of total and back pressures. That is, if the total pressure was 3900 kPa with a back pressure of 2200 kPa (both increased by 2000 kPa from the values that were actually used) then the base porewater pressure would have a larger positive pressure range over which to respond with negative changes. At these higher pressures, a change in total pressure would be accompanied by a similar response from the base porewater pressure transducer. The same mechanisms are also likely to be acting on the low density specimens, but perhaps to a lesser degree.

The porewater behaviour during undrained shear was discussed in Chapter 6 (Section 6.2.2). The undrained response of the high density specimen (T1130) was very small. The lack of response is attributed to the choice of total and back pressures during shear, as discussed above. The response of the low density specimen was more typical of undrained shear behaviour. The pressure behaviour can also be seen by comparing the pressure changes with time of T1128 (low density) and T1130 (high density), shown in Fig. 7.3.

It is also seen that during drained shear, the base porewater pressure did not actively attempt to equalize with the top back pressure of 200 kPa - the specimen appeared to be content to maintain a pressure gradient between the top and base. This behaviour is not normally seen in well behaved soils, and requires further study. The behaviour may be linked to the concept of a critical gradient, which allows a pressure gradient to build up in drained specimens before the excess pressure is relieved. An example of this behaviour (but for isotropic stress conditions) is shown in Fig. 7.4. Test T1119 was a low density specimen that was prepared and off-loaded to an OCR of about 1.54 in the usual manner. The specimen remained at this OCR without shearing for nearly 1000 hours. The top drain to the specimen was open. It is seen in the figure that after 1000 hours a stable pressure difference of about 50 kPa exists between the top and base

transducers. This represents a gradient of about 50 m/m ($\approx 50 \text{ kPa} \div 9.81 \text{ kN/m}^3 \div 0.1 \text{ m}$). Recent research has suggested that the gradient required to initiate flow through a bentonite specimen with an equivalent buffer dry density of 1.66 Mg/m^3 may be in the order of 60 m/m (D.A. Dixon, personal communication, 1991).

7.4 An Alternative Yielding Concept

7.4.1 Introduction

Previous discussion suggested that the observed behaviour in some specimens of post-yield strain hardening in shear, and strain softening in volume behaviour is incompatible with classical elastic plastic theory that incorporated a single yield surface. Fig 7.5 shows the yield locus and plastic potential superimposed on the same Figure. The region of behavioural incompatibility is shown as the dashed region of the yield locus on which negative plastic volume strains occur. The tests in this study that are in question are: T1114, T1116, T1117, T1136 (low density), and T1122, T1147 T1152 (high density).

In this section, the concept of early yielding will be discussed as a means of rationalizing the inconsistent shear-volume behaviour. The early yield concept suggests that specimens can undergo different states of elasticity, while remaining essentially non-plastic. It will be shown that the behaviour of some buffer specimens in this study (for which inconsistencies in behaviour exist) is the same as for specimens where early yield behaviour has been established. Thus, for the purposes of this discussion, it will be assumed that early yielding occurred in those buffer specimens which were used to develop the dashed region of the yield locus in Fig. 7.5.

As part of this analysis, other modified yield criteria were examined and rejected as being not applicable to this problem. Specifically, bounding surface plasticity and multiple yield loci theories were considered (for example Al-Tabaa and Wood 1989). Both require adherence to the same "rule" as the classical theory that strain softening or hardening must be consistent in stress-

and volume-space. The discussion will be qualitative, but it will be shown that the concept of early yielding explains a number of inconsistencies in the buffer behaviour.

It is important to re-affirm the validity of the data and analysis given in Chapters 5 and 6. The use of the early yield concept to rationalize the behaviour of some specimens does not invalidate the yield locus developed in Chapter 5, nor the elasticity, plastic potential, and hardening law developed in Chapter 6. Further detailed experimental work will be required.

7.4.2 The Concept of Early Yielding

Au (1982) observed shear behaviour in Winnipeg clay that he described as early yielding. This was characterized as relatively stiff behaviour giving way to less stiff but still elastic (linear) behaviour prior to rupture. Graham and Au (1985) were unable to provide a definitive explanation of the behaviour. Vaughan (1988) discussed early yielding in residual soils in terms of a cemented or bonded soil structure and fabric.

For the present study, the data of Au (1982) on early yielding of Winnipeg clay have been re-examined in detail. He compared the strengths of Winnipeg clay under three conditions at low strength: undisturbed (re-consolidated directly to the *in situ* stresses), "fully-softened" (undisturbed specimens that were allowed to swell under low anisotropic stresses for about 10 days), and "freeze-thawed" (specimens subjected to 5 cycles of freezing and thawing lasting up to 4 days).

Early yielding was observed in 7 specimens (out of a total of 22) during drained triaxial compression. Two specimens were undisturbed, three specimens were "fully-softened", and two specimens were "freeze-thawed". The effective stress paths for 5 of the specimens were constant p' ($\Delta q/\Delta p' = \infty$) and for the remaining specimens the stress paths were $\Delta q/\Delta p' = -1$ and -2 . These tests were done in the stress range (p'/p'_c) of about 0.1 to 0.45.

There are a number of important similarities between the behaviour observed by Au and

the behaviour of the buffer in this study. First, five of his seven specimens experienced swelling or fabric changes prior to shear. The buffer specimens in this study also swelled prior to shear.

Second, the stress paths ($\Delta q/\Delta p'$) of the early yield specimens by Au were generally similar to those in this study that showed early yield. All the buffer specimens had stress paths where $\Delta q/\Delta p'$ was negative or very steep. No specimens in either study where the total pressure increased displayed early yielding.

Third, the stress states of the specimen in both studies were very low, typically less than $0.5 p'_c$.

The similarities in behaviour of the specimens in these studies suggests that the cause of early yielding is the same in both studies. The question of cause will be addressed later in this section.

There are several implications to the early yield concept, as it applies to the buffer data. If the yield stresses for the specimens in question are indeed early yield points, then an examination of the data indicates that the second yield corresponds with rupture of the specimen. This means that the last load stress corresponds to yield and that there could be no post-yield strain hardening. This leaves open the opportunity for post-yield strain softening. However in stress controlled tests it is impossible to observe strain softening.

It is observed in Fig. 5.7 that the peak strength of these tests in question correspond very closely to the peak strength found by Saadat (1989), but is higher than his critical state line. The critical state line was developed predominantly from undrained, strain controlled tests, sheared to high strains. Strain softening behaviour was observed in many of Saadat's tests. Thus the peak strengths reported in Fig. 5.7 may not be critical state stresses. This explains why the Mohr Coulomb strength parameters reported by Saadat (1989) were of the same slope ($\phi' = 14^\circ$), but did not have a cohesion intercept.

Fig. 7.6 shows the yield data from Fig. 5.8, with the end-of-test stresses for the tests in

question added as open circles. The sections of the early yield and rupture yield loci are shown. Note that the rupture locus terminates at the CSL ($\phi' = 14^\circ$, $M = 0.53$) and corresponds with the Hvorslev surface for overconsolidated specimens.

The rupture yield locus in this figure and the plastic potential in Fig. 6.17 and 7.5 have similar shapes, suggesting that the association of the flow rule would increase if based on the rupture yield locus.

The elasticity moduli developed in Chapter 6 are valid for only the original (inner) yield locus. (It should be stressed that the early yield locus remains valid, but simply signifies the onset of a different "elasticity".) The moduli for the second "elastic" section would have to be developed from a suite of tests specifically designed for that purpose. No tests have yet been done to determine reversibility in the second "elastic" region.

It is necessary to examine the cause of early yielding. Based on the behaviour of all specimens, in this study and Au's (1982), the early yield is likely associated with fabric changes due to expansive volume strains prior to, or during shear. Re-orientation of clay platelets may produce a quasi-stable soil structure that is initially relatively stiff, but gives way to a less stiff, but still elastic soil structure. Further research of this question is required.

7.5 Visco-Plastic Swelling of the Buffer

7.5.1 Introduction

This section will introduce a visco-plastic model that helps to explain some of the observed behaviour of the buffer. Parts of the model were used in Chapter 5 to explain the isotropic consolidation data. The model is mainly based on experimental data from swelling tests as a result of a single large stress decrement. The model is able to rationalize the behaviour of the buffer in different situations, and this is supported by experimental data. However, it is still conceptual in nature at this stage and requires further research.

7.5.2 Conceptual Model of Visco-Plastic Swelling

The behaviour of the buffer following stress release was described conceptually in Fig. 5.9, and is re-introduced as Fig. 7.7. This model was introduced to explain why, as a result of stress release and swelling, the yield stress of specimens reloaded isotropically was less than the original preconsolidation pressure. To review briefly, the model proposed that on stress release (A-B), two types of swelling occurred. One type was elastic consolidation swelling (B-B'), which is recoverable and non time dependent. This swelling occurs in all soils. The second type was visco-plastic swelling (B'-B''), which is time dependent and non recoverable. During swelling, a buffer specimen will experience both types of swelling simultaneously. The effect of the first type (elastic) swelling is to move the specimen's stress-volume state to an equilibrium position (B') of the κ -line associated with its original preconsolidation pressure. The effect of the second type (visco-plastic) swelling is to move the stress-volume state vertically to other κ -lines (for example to B''). On reloading, the specimen will traverse the κ -line (B''-A') associated with its current stress-volume state (A') which, as a result of plastic swelling, is different from the original (A). The model was also useful in rationalizing the low density $V_{o,p'}$ data of specimens with high OCRs.

This model can be extended to more completely describe the time, rate, and OCR effects of stress release. There is at present, limited data to support this model, and it will require laboratory verification. However, it can be developed in a general way as follows.

Since most specimens in this program were allowed to swell for 3 days, there is a large amount of data for this swell duration. Most specimens had OCR's of about 1.5, although as discussed in previous chapters, three specimens had significantly higher OCRs. In addition, one low density specimen was allowed to swell for over 50 days at an OCR of about 1.7. Finally, Saadat (1989) performed one test on a high density specimen that swelled for over 20 days with an OCR of about 8.5. These time and volume strain data have been correlated and plotted in

Fig. 7.8 as a function of OCR. Volume strain data was used instead of specific volume of clay in order to avoid accounting for factors such as initial saturation and specimen density. In the figure, negative volume change is expansive, and an OCR of 1 represents a specimen on the normal consolidation line or swelling equilibrium line (OCRs less than 1 are impossible). The data at OCR = 8.5 is different from the others in two respects. First, the specimen from Saadat (1989) is a high density specimen. Second, all specimens in this program were left for 10 days at their swelling equilibrium pressure (SEP) before being off-loaded; the specimen from Saadat was stressed directly to a pressure lower than its SEP, corresponding to an OCR of about 8.5.

Time lines, representing swell durations have been shown in Fig. 7.8 for 1,2,3,10, and 20 days. These lines represent the amount of total swell a specimen would experience for any OCR. Although it is impossible to separate the total volume strain into the elastic and viscoplastic components the figure illustrates several important features of the model:

1. The time lines spread in a series of curves from a common origin of an OCR equal to 1.0. The separation between the time lines decreases with increasing time. This indicates a decreasing swell rate with time.
2. The time lines are curved, being steep near the origin and flattening off with increasing OCR. This behaviour should be expected, and the time lines should, at very high OCRs, reach a constant low slope. The curved shape is due to limiting hydrodynamics. That is, although the swell potential may increase with increasing OCR, the specimen, due to a finite permeability, can absorb water only up to a limiting rate. The maximum swell rate is limited by the permeability of the specimen, and the drainage arrangement (that is, single or double drainage, and the presence of side drainage). Thus, the rate of increase of swell rate will decrease with increasing OCR.
3. The lower limit of the slope of the time lines must be equal to κ , which represents non-viscous, purely elastic swelling.

7.5.3 Implications for the Elastic Plastic Model

The model was shown, in previous sections to be useful in explaining buffer behaviour as a result of a single large stress release action. In this section, other scenarios will be considered, together with available experimental evidence.

It was asserted in Section 7.5.2 that a "fan" of time lines is associated with the current preconsolidation pressure. Thus the fan would be similar to the yield locus and would be carried along the NCL during consolidation under isotropic stresses, just as the yield locus would expand during similar consolidation.

One question this raises is the effect of visco-plastic swelling during shear. If a buffer specimen is subjected to drained shear from an overconsolidated state, then it is likely that visco-plastic swelling would occur during the shearing process. On the other hand, if a specimen is sheared undrained, then the volume is fixed and no visco-plastic swelling can occur (Normal plastic volume straining will of course occur). The effect of expansive visco-plastic straining during drained shear should be to increase the shear strain compared to undrained specimens, causing drained specimens to appear less stiff, and perhaps have lower peak strength. Thus comparison of undrained and drained shear-strain plots should show differences in shape.

Two high density specimens, one undrained and the other drained can be compared. The undrained specimen, T1130, had an effective stress path ($\Delta q/\Delta p'$) of 2.5. The drained specimen, T1140 had an effective stress path of 2.9. Both specimens had a dry density of 1.67 Mg/m^3 and a consolidation pressure of about 1220 kPa. Deviator stress *versus* shear strain data for both tests is shown in Fig. 7.9. It is evident that the two specimens have approximately the same stiffness in the early part of shearing. The undrained peak strength is about 10% higher than the drained peak strength.

It should be noted that the drained specimen with a stress path ($\Delta q/\Delta p'$) of 2.9, was in a condition where $\Delta\sigma_3 \approx 0$. Previous discussions in Chapter 6 alluded to the effect of cell

pressure on the volume change response of the specimens. It was found that if the cell pressure decreased then volume strains during shear were negative (expansive), and if the cell pressure increased during shear the volume strains were positive (compressive). In this particular test, volume strains during shear were essentially zero. Further testing is necessary before the visco-plastic behaviour can be completely understood.

The effects of unload/reload on visco-plastic swelling can also be examined. If the visco-plastic fan is carried on the yield locus, then post-yield unloading should re-initiate visco-plastic swelling. It was discussed in Section 6.2.4 that the unload/reload response of buffer specimens was much stiffer (approximately 3 times stiffer in shear) compared to first time loading. The conclusion made in Chapter 6 was that the initial less stiff response was the result of visco-plastic swelling, and that during subsequent unloading the visco-plastic swelling was either reduced or inhibited. The swelling of the buffer depends primarily on its mineralogy. Thus, it is unlikely that fabric changes that occur during shear could fundamentally affect the swelling characteristics of the buffer, particularly, as here, where the overconsolidated material has been shown to be isotropic. Phenomena other than those directly associated with the shearing process should also be considered. One of these is the possible existence of a minimum threshold value of hydraulic gradient below which there is no moisture flow through the buffer (Section 7.3.2). It has been speculated that such a mechanism may be involved in many other processes in the buffer (M.N. Gray, personal communication, 1989). In the present case, each stress decrement during unloading was quite small (0.05 to $0.1 p'_c$), and therefore the gradient necessary to initiate visco-plastic swelling may not be present. (The stress decrement during the 3 day swell period was about $0.4 p'_c$.)

The same behaviour occurred during compression or swell at isotropic stresses. Specimens subjected to small isotropic stress decrements also show reduced swelling, compared to the swell following the initial large stress decrement. As in the case of shearing, further

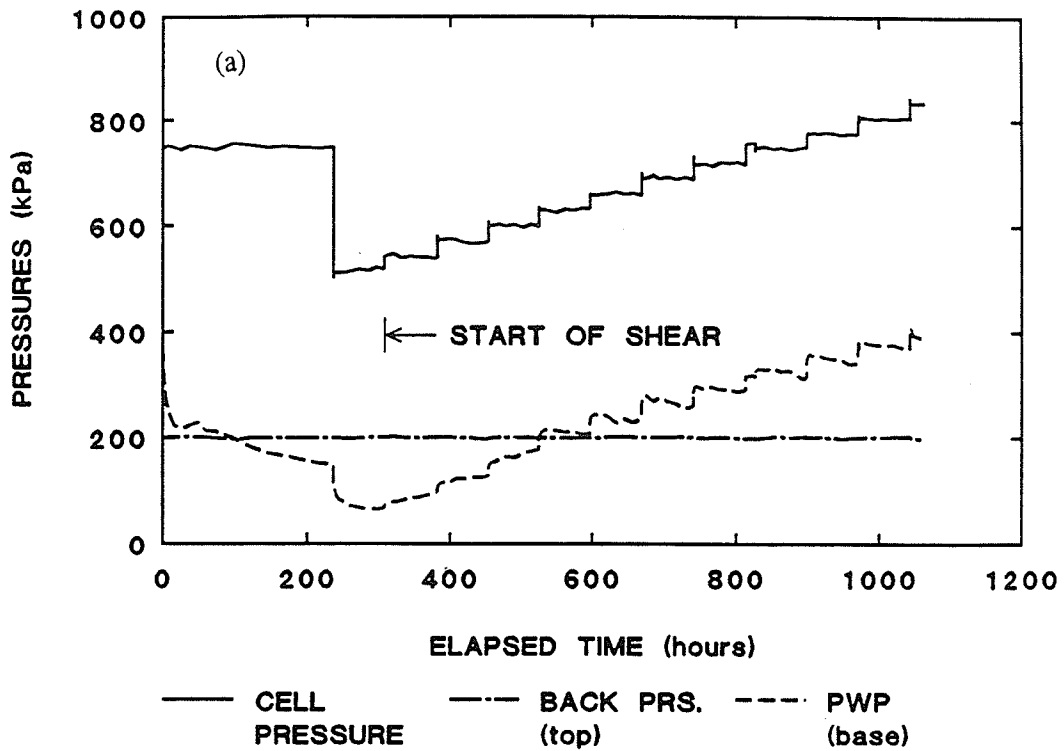
testing is necessary.

7.6 Concluding Remarks

Patterns of behaviour introduced in Chapter 5 and 6 have been rationalized using simple modifications to the classical theory, or by alternative simple qualitative models. The ideas developed in this chapter do not invalidate the interpretations made in the previous chapters but rather complement the previous work.

It is accepted that many of the ideas in this Chapter are speculative and only tentatively supported by the test program. Note however that the ideas only arose during final analysis of the data, after the testing was completed. The testing program was not designed specifically to examine early yielding, or visco-plastic swelling. The fact that some applicable data was available from the program should be accepted as a welcome, if unexpected contribution.

BUFFER SPECIMEN T1134
 DRY DENSITY = 1.49 Mg/m³



BUFFER SPECIMEN T1141
 DRY DENSITY = 1.67 Mg/m³

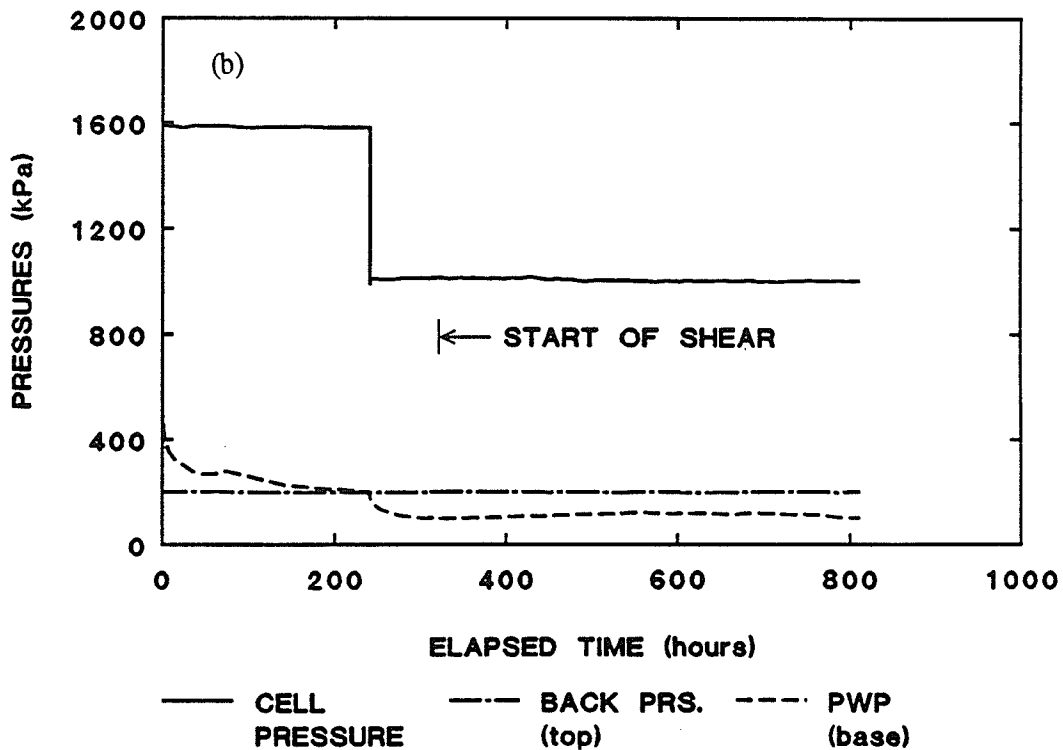


FIGURE 7.1 Pressure versus time data for (a) T1134, low density, and (b) T1141 high density specimens.

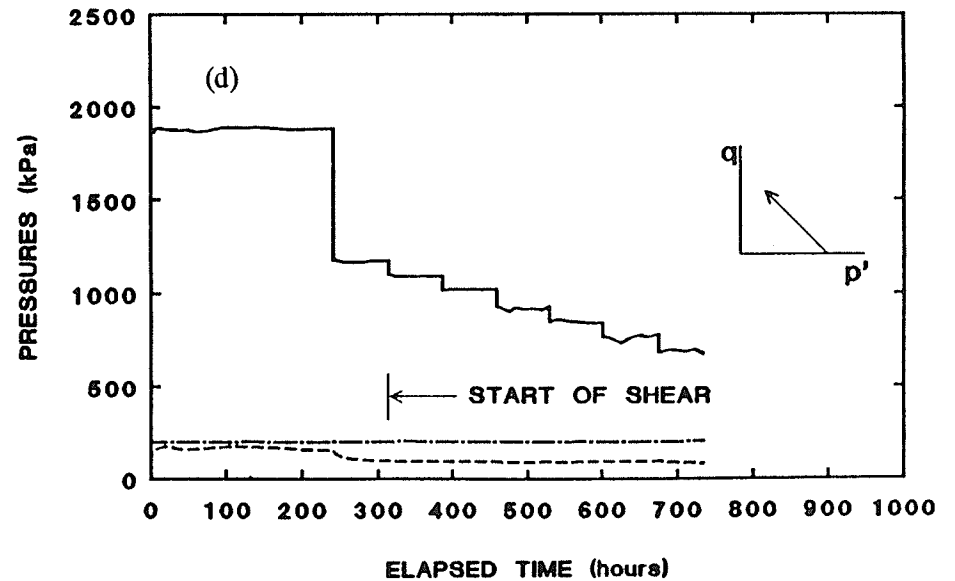
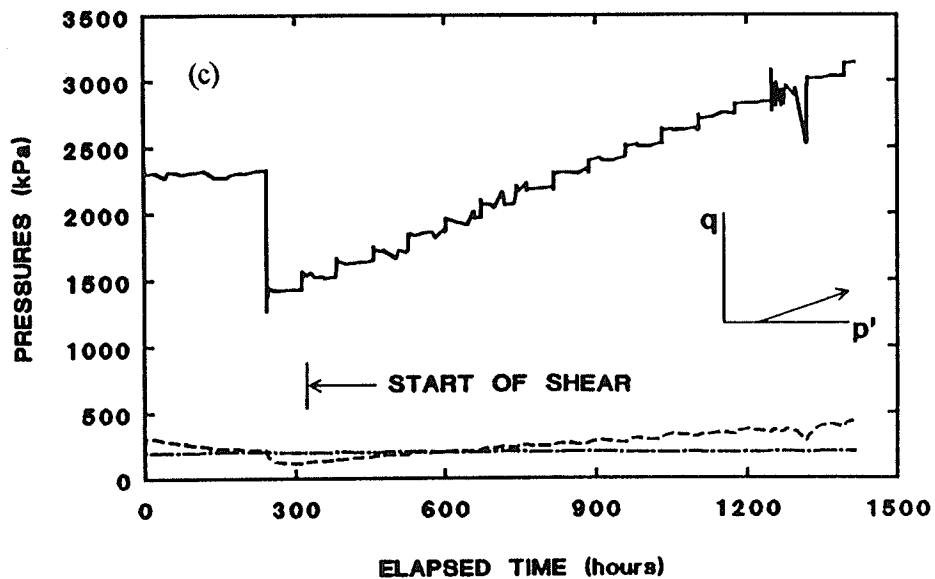
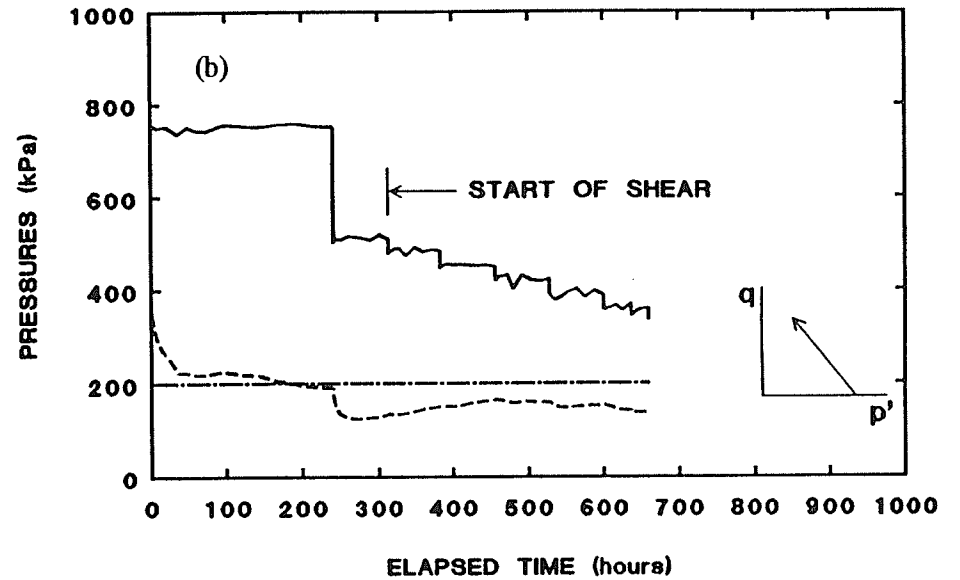
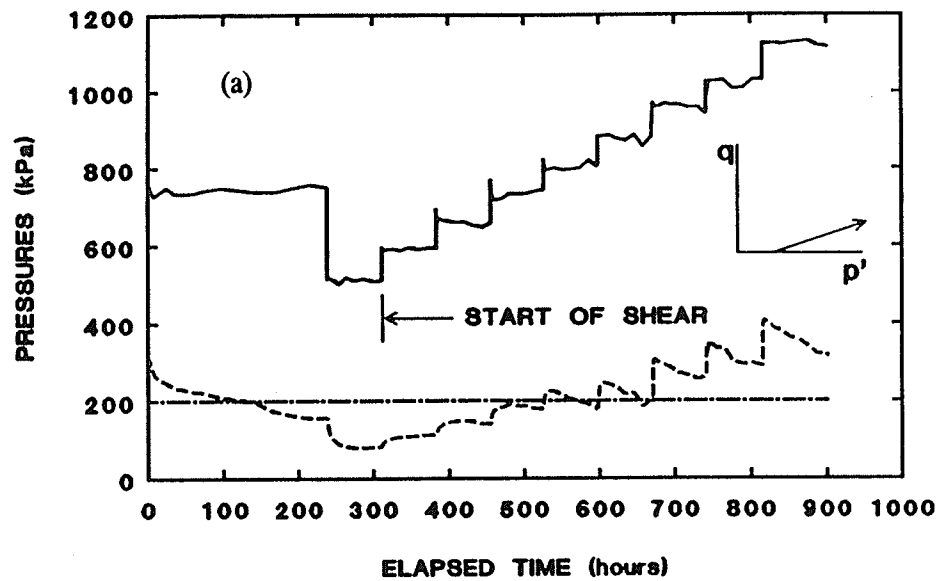
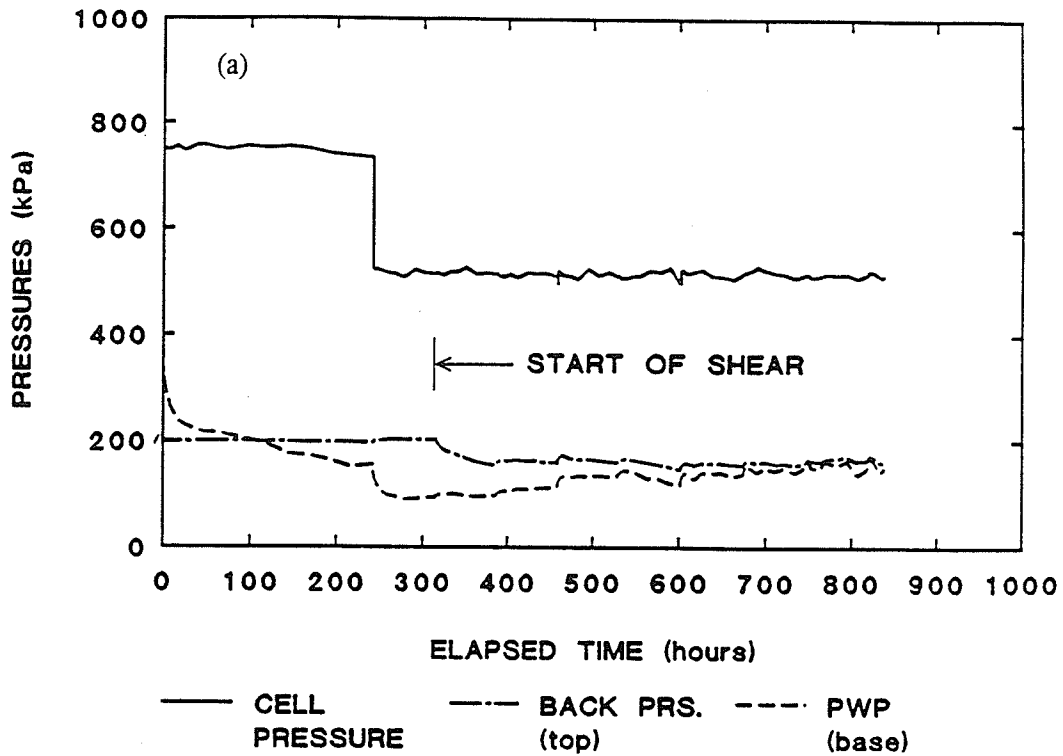


FIGURE 7.2

Pressure versus time data for low and high density specimens. (a) T1145 and (b) T1136, low density, and (c) T1137 and (d) T1147, high density. The inset q, p' plots show the approximate stress path of each specimen during shear. Legend: cell pressure ———, back pressure (top) ———, porewater pressure (base) - - - - .

BUFFER SPECIMEN T1128
 DRY DENSITY = 1.48 Mg/m³



BUFFER SPECIMEN T1130
 DRY DENSITY = 1.67 Mg/m³

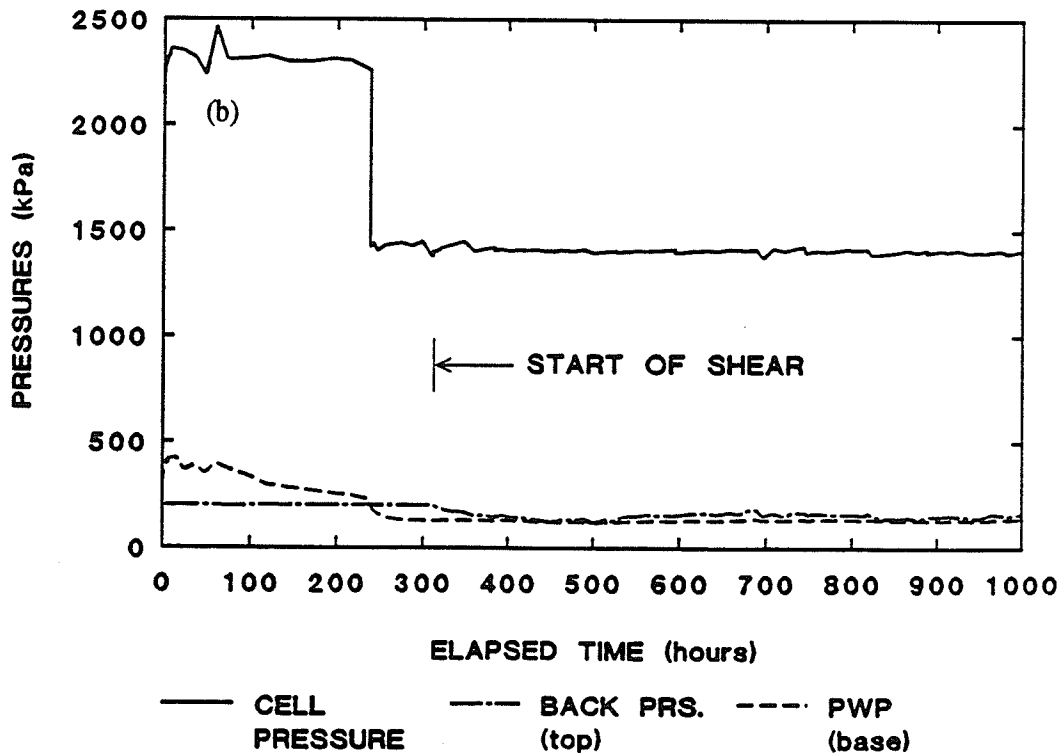


FIGURE 7.3

Pressure versus time data for low and high density specimens during undrained shear. (a) T1128, low density, and (b) T1130, high density.

BUFFER SPECIMEN T1119
DRY DENSITY = 1.48 Mg/m³

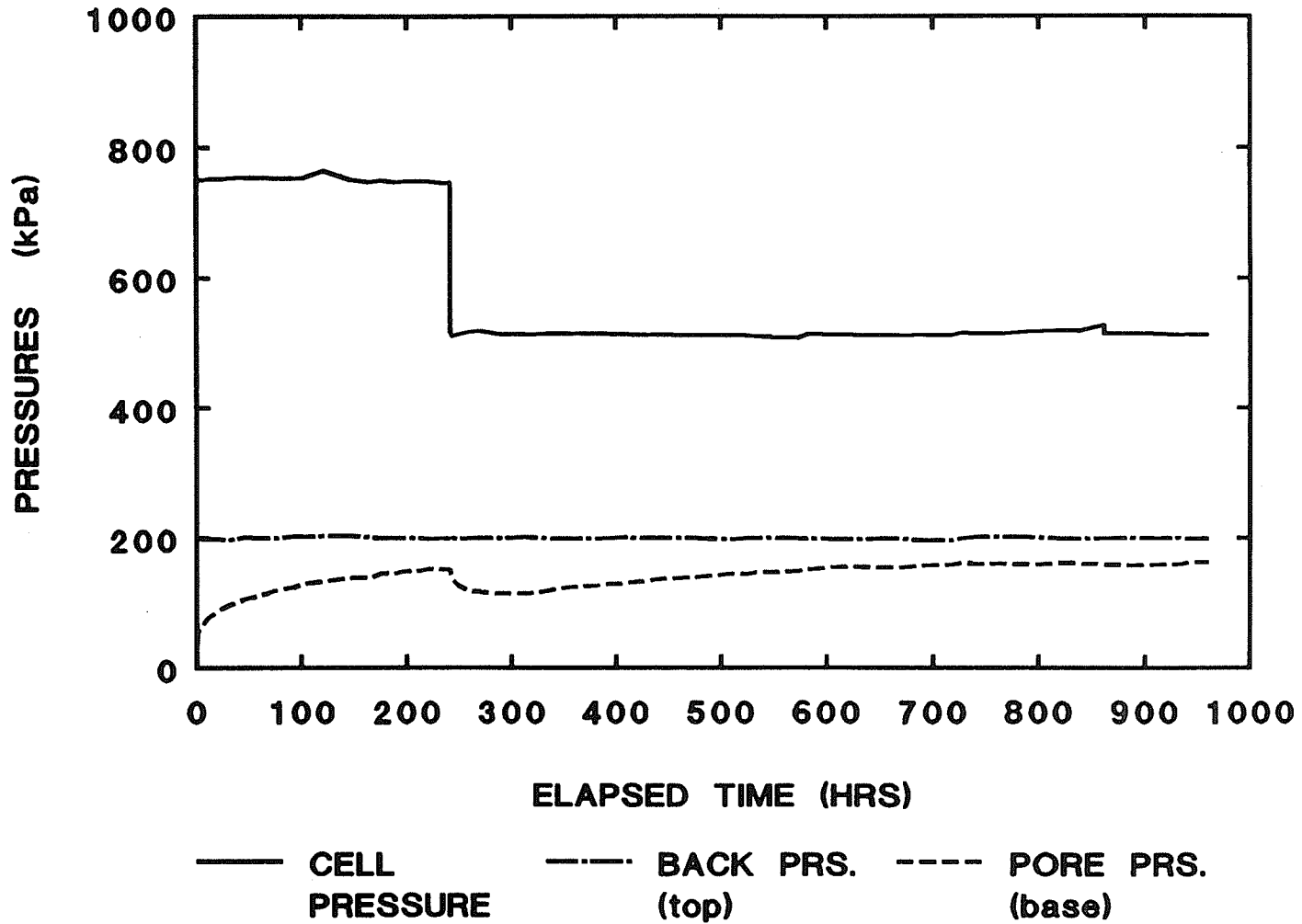


FIGURE 7.4

Pressure versus time data for T1119, low density specimen.

BUFFER SPECIMENS
DRY DENSITY = 1.49 Mg/m³ and 1.67 Mg/m³

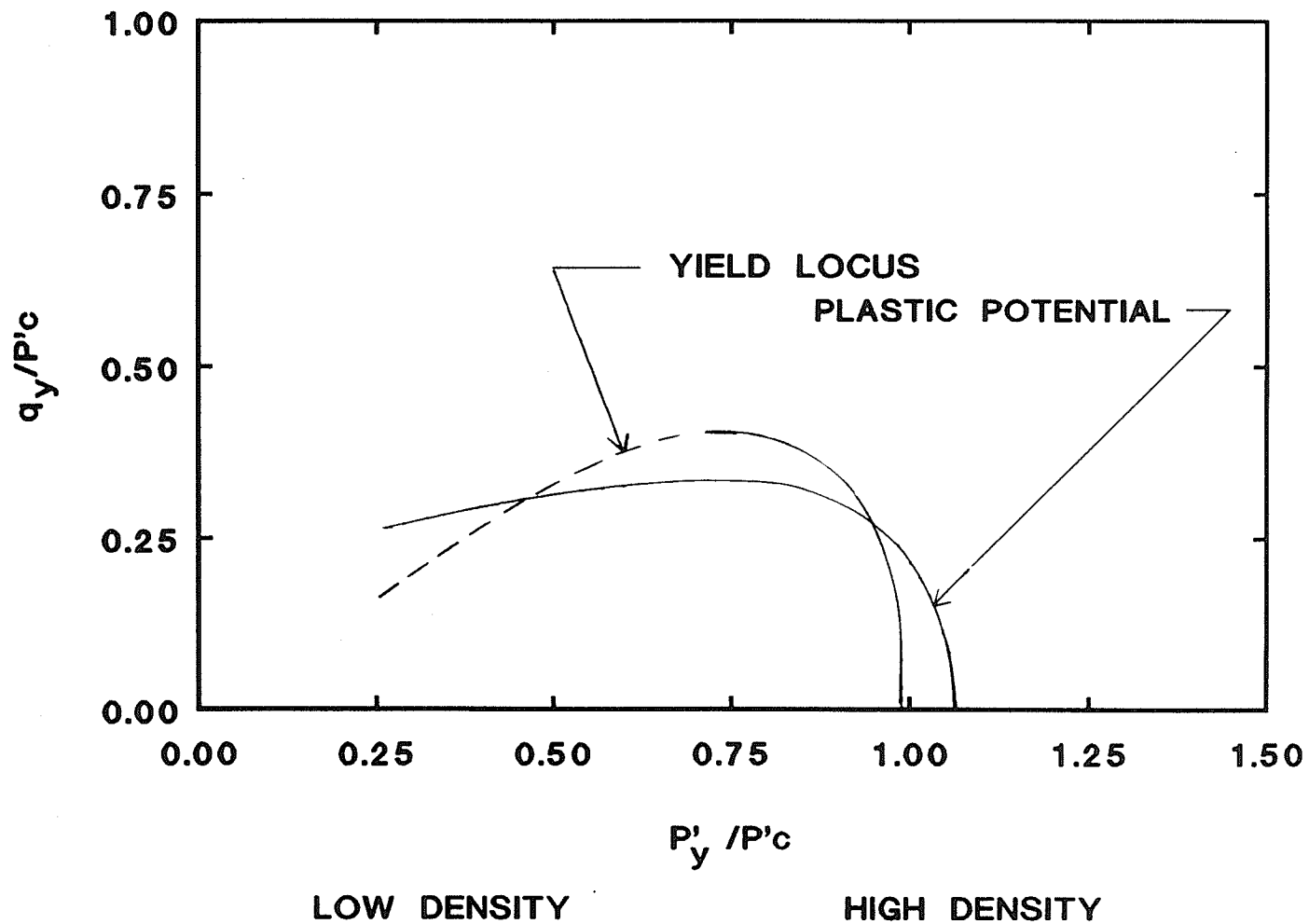


FIGURE 7.5

Yield locus and plastic potential for the buffer based on analysis from Chapters 5 and 6. The region subject to early yielding is denoted by the dashed section of the yield locus.

BUFFER SPECIMENS
DRY DENSITY = 1.49 Mg/m³ and 1.67 Mg/m³

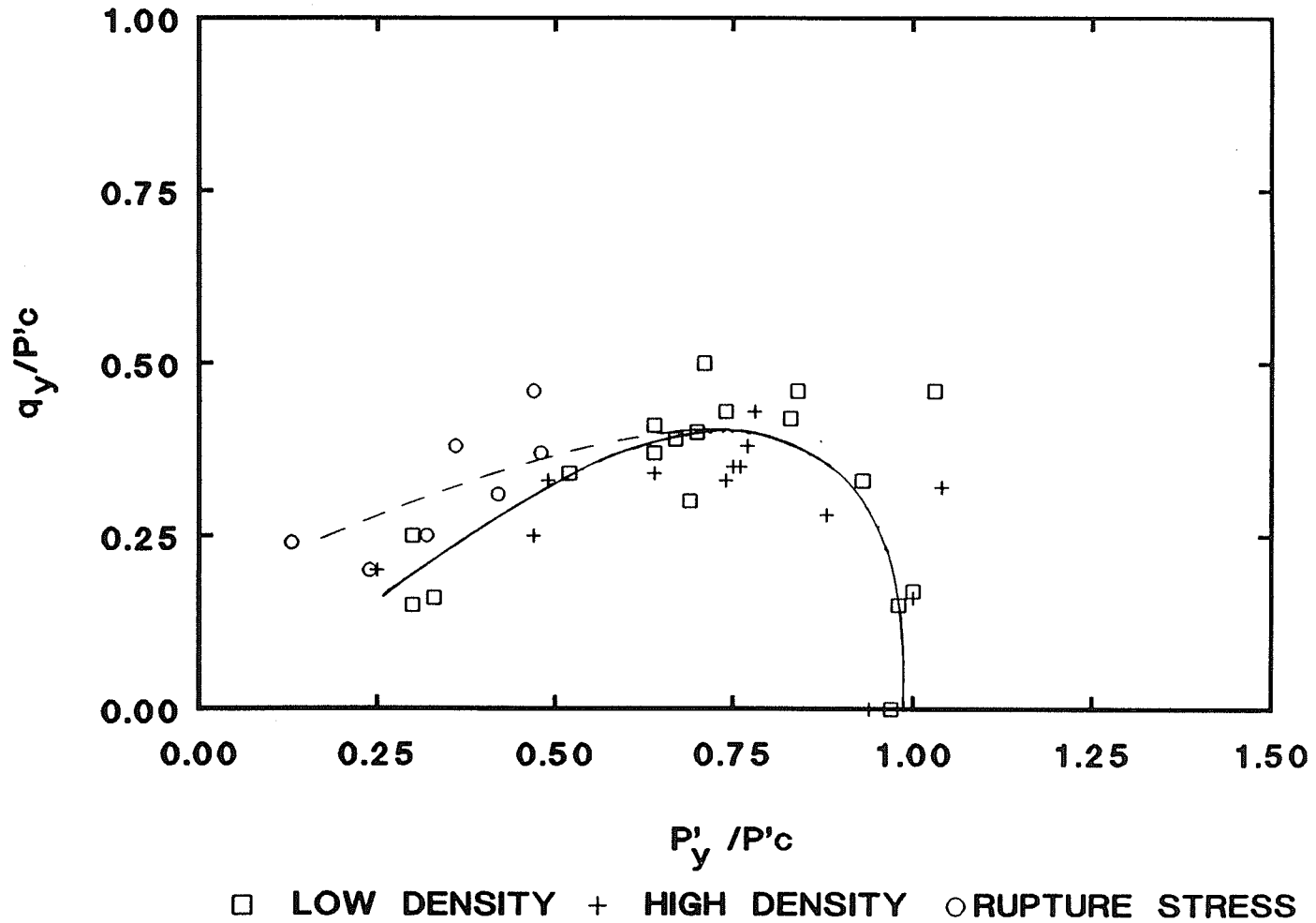


FIGURE 7.6

Yield data (early) and rupture data in q, p' -space. The solid yield locus is the original "first" early locus developed in Chapter 5. The dashed yield locus is the "second" rupture locus.

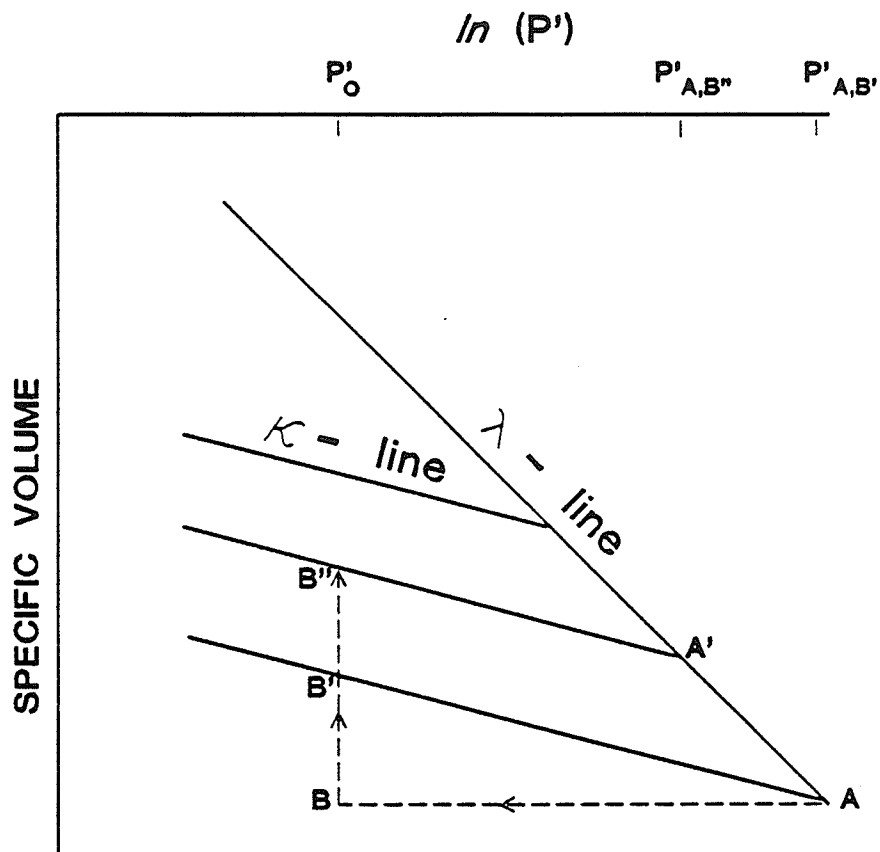


FIGURE 7.7

Conceptual model for visco-plastic swelling of the buffer due to large increment isotropic stress release. (same as Fig. 5.9)

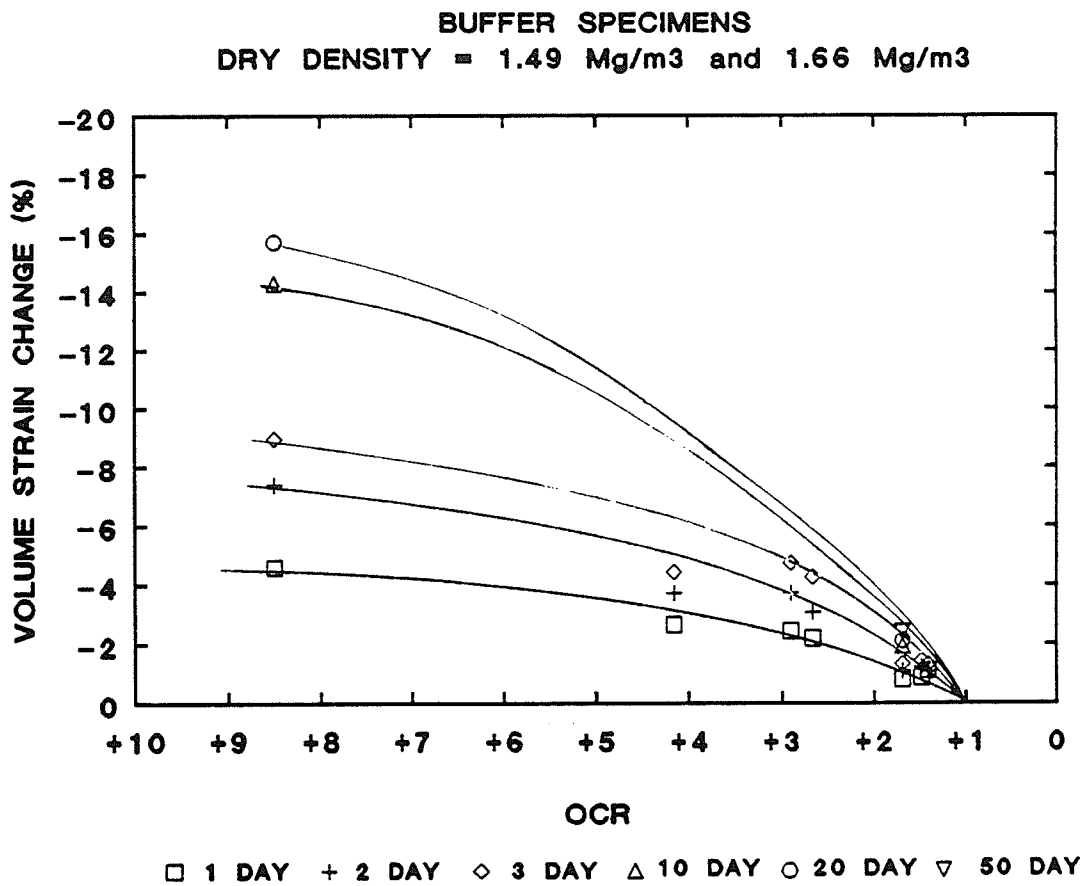


FIGURE 7.8

Volume strain *versus* overconsolidation ratio of the buffer, showing the effect of swell time.

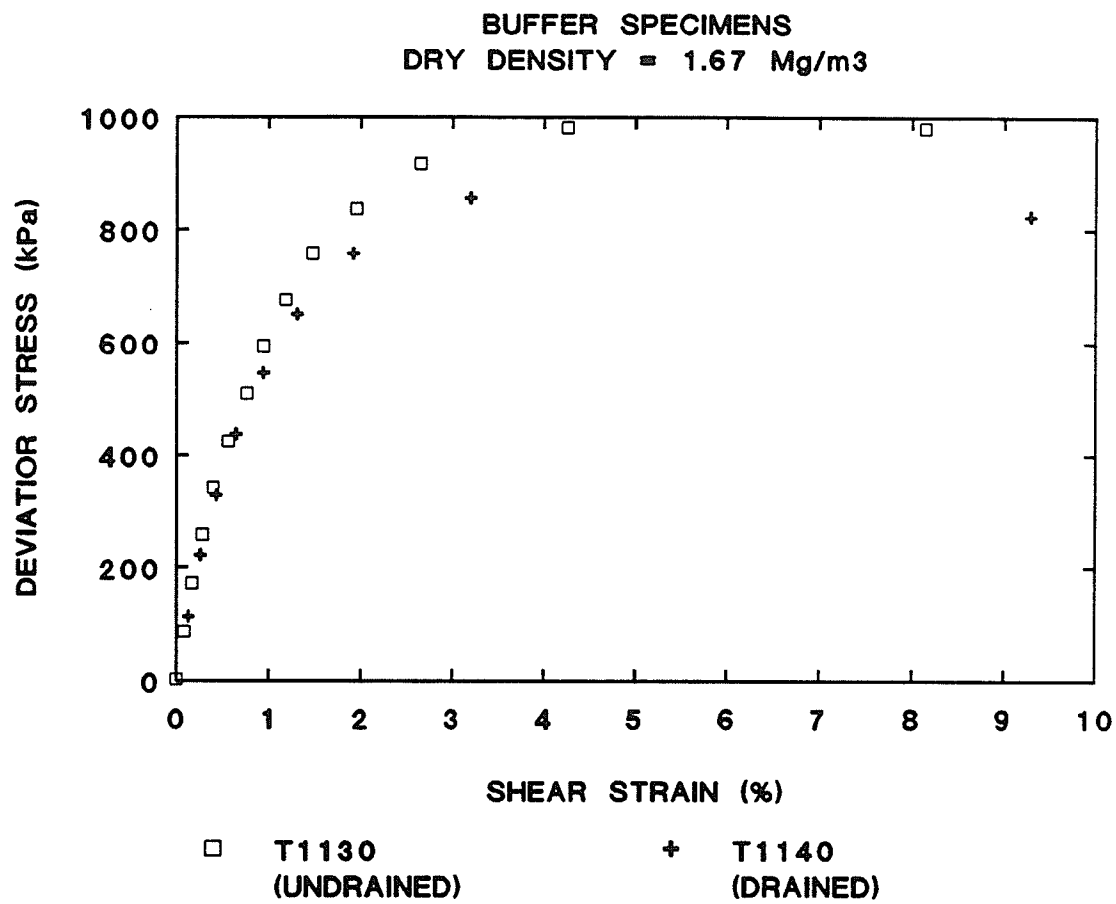


FIGURE 7.9 Deviator stress *versus* shear strain for high density specimens - T1130 undrained, and T1140 drained.

CHAPTER 8 CONCLUSIONS AND SUGGESTIONS FOR FUTURE RESEARCH

8.1 Conclusions

The principal conclusions from the research presented in this thesis are:

1. Subject to the qualifying restrictions (listed in Chapter 4) the effective stress principle is applicable to the sand-bentonite buffer and hence to other active clays in general. Knowledge of the true effective stress (σ^*) and the physico-chemical repulsive/attractive forces ($R - A$) acting in the soil is not necessary. These stress components can be taken together as the apparent effective stress (Section 4.1).
2. The buffer can be characterized as an elastic plastic material and can be modelled using classical elastic plastic theory. Specific to the model, the following was found:
 - 2a. The yield locus is the same for the low and high density buffer in normalized q, p' -space, and can be normalized in V, p' -space (Sections 5.5.2 and 5.5.3).
 - 2b. The buffer, as tested in this study exhibits limited anisotropic elasticity in shear. The weak anisotropy that is present suggests a soil fabric that is stiffer vertically than horizontally (Section 6.2).
 - 2c. The flow rule is non-associated (Section 6.3).
 - 2d. The plastic potential is the same for both buffer densities (Section 6.3).
 - 2e. A hardening law, describing the size of the yield locus was developed from consolidation data from this and other research programs (Section 6.4).
 - 2f. The low density end-of-test data from this study produces the same Mohr-Coulomb strength parameters determined by Wan (1987). The high density end-of-test data from this study produces the same peak strength power law developed by Saadat (1989) (Section 5.5.2).
3. The porewater pressure behaviour of some specimens depends on the applied total and

back pressures, although it is thought that this relates to features on the measurement system rather than to the buffer itself. Evidence was found that the buffer can maintain a hydraulic potential across the specimens. This may be linked to critical gradients (Section 7.3).

4. Inconsistencies in shear-volume behaviour during shear of some specimens was explained by introducing the concept of early yielding. As a result, two yield loci were developed, a first early yield, and second, rupture yield that coincide with Hvorslev (overconsolidated) strength (Section 7.4).
5. The buffer displays a significant degree of potential visco-plastic swelling. A conceptual visco-swelling model introduced in this thesis was used to explain different aspects of buffer behaviour, particularly as a result of large decrement stress release (Section 7.5).

8.2 Suggestions for Future Research

The discussion in Chapter 7 raised several issues that warrant further research:

1. It should be confirmed that the porewater pressure behaviour under conditions of swelling depends on the total and back pressure levels. This can be easily accomplished by performing undrained tests on similar specimens that are in a swelling condition ($p'_c < \text{SEP}$), but with different sets of total and back pressure (at constant apparent effective stress).
2. The shape of the yield locus with respect to the shape of the state boundary surface deserves continued study. It was proposed (Section 6.3) that association of the flow rule should be considered with respect to the state boundary surface, not the yield locus *per se*.
3. The concept of early yielding requires further study. Although two cases of early yielding are now documented, it is important to determine if it is a real rheological

phenomenon, or if it is an artifact of the testing techniques and equipment.

4. The visco-plastic swelling behaviour of the buffer needs to be studied in detail. (This research has concentrated on specimens with only a limited range of OCRs and only one time duration during which they were allowed to swell.) The role of visco-plastic swelling during shear requires further research. Related to this are the possibilities of stable and critical porewater pressure gradients within the specimens.
5. It would be useful to explore the role of temperature on the applicability of the effective stress concept to the buffer.

REFERENCES

- Al-Tabba, A. and Wood, D.M. 1989. An experimentally based "bubble" model for clay. Proceedings, 3rd International Symposium on Numerical Methods in Geomechanics (NUMOG III). Elsevier Applied Sciences, London, U.K.: 91 - 99.
- Atkinson, J.H. and Bransby, P.L. 1978. The mechanics of soils: an introduction to critical state soil mechanics. McGraw Hill, London, U.K. 375 pp.
- Atkinson, J.H., Evans, J.S., and Ho, E.W.L. 1985. Non-uniformity of triaxial samples due to consolidation with radial drainage. *Geotechnique*, 35(3): 353 - 355.
- Au, V.C.S. 1982. Rate affects and low stress strength of Winnipeg Clay. M.Sc. Thesis. Department of Civil Engineering, University of Manitoba. Winnipeg, Canada.
- Bailey, W.A. 1965. The effects of salt on the consolidation behaviour of saturated remolded clays. Contract Report No. 3-101. Sponsored by U.S. Army Material Command Project No. 1-V-0-14501-B-52A-01. Conducted for U.S. Army Engineer Waterways Experiment Station, Vicksburg, Miss.
- Balasubramaniam, A.S. 1969. Some factors influencing the stress strain behaviour of clay. Ph.D. Thesis, University of Cambridge, Cambridge, U.K. (from Atkinson and Bransby, 1978)
- Balasubramanian, B.I. 1972. Swelling of compaction shale. Ph.D. Thesis, Department of Civil Engineering, University of Alberta, Edmonton, Canada.
- Barbour, S.L. 1987. Osmotic flow and volume change in clay soils. Ph.D. Thesis, Department of Civil Engineering, University of Saskatchewan, Saskatoon, Sask. (from Barbour and Fredlund 1989).
- Barbour, S.L. and Fredlund, D.G. 1989. Mechanisms of osmotic flow and volume change in clay soils. *Canadian Geotechnical Journal*, 26(4): 551 - 562.
- Barden, L. 1963. Stresses and displacements in a cross-anisotropic soil. *Geotechnique*, 13(3): 198 - 210.
- Bechai, M. Mansson, N.C. and Rao, P.K.M. 1986. Disposal concepts for radioactive wastes in clay or till deposits. Proceedings, 2nd International Conference on Radioactive Waste Management, Winnipeg. pp. 87 - 92.
- Been, K., and Jefferies, M.G. 1985. A state parameter for sands. *Geotechnique*, 35(2): 99 - 112.
- Bird, G.W. and Cameron, D.J. 1982. Vault sealing research for The Canadian Nuclear Fuel Waste Management Program. Atomic Energy of Canada Ltd. Technical Report TR-145.

- Bishop, A.W. and Henkel, D.J. 1962. The measurement of soil properties in the triaxial test (2nd edition). Edward Arnold, London, U.K. 227 pp.
- Bishop, A.W., Webb, D.L. and Skinner, A.E. 1965. Triaxial tests on soil at elevated cell pressures. Proceedings, 6th International Conference on Soil Mechanics and Foundation Engineering. Montreal, 1: 170 - 174. (from Head, 1986)
- Bishop, A.W. and Wesley, L.D. 1975. A hydraulic triaxial apparatus for controlled stress path testing. *Geotechnique*, 25(4): 657 - 670.
- Börgesson, L., Hökmark, H., and Karnland, O. No Date. Rheological properties of sodium smectite clay. Unpublished internal report. Clay Technology Ltd., Lund, Sweden.
- Börgesson, L., Brock, D., and Plas, F. 1990. Mechanical properties of dense Ca-smectite clay. *Engineering Geology*, 28 (3,4): 419 - 430.
- Chapman, D.C. 1913. A contribution to the theory of electrocapillarity. *Philosophical Magazine*, 25(6): 475 - 481. (from Mitchell 1976)
- Chattopadhyay, P.K. 1972. Residual shear strength of some pure clay minerals. Ph.D. Thesis, Department of Civil Engineering, University of Alberta, Edmonton, Canada.
- Chen, W.F. and Baladi, G.Y. 1985. Soil plasticity theory and implementation. Elsevier, Amsterdam, The Netherlands. 231 pp.
- Cheung, S., Gray, M.N. and Dixon, D.A. 1985. Hydraulic and ionic diffusion properties of bentonite-sand buffer materials. Proceedings, International Symposium on Coupled Processes Affecting the Performance of a Nuclear Waste Repository. Lawrence Berkley Laboratories, Berkeley, USA.
- Dafalias, Y.F. and Herrmann, L.R. 1980. A boundary surface soil plasticity model. Proceedings, International Symposium on Soils under Cyclic and Transient Loading. Swansea, U.K.: 335 - 345.
- Dixon, D.A. and Gray, M.N. 1985. The engineering properties of buffer material - research at Whiteshell Nuclear Research Establishment. Atomic Energy of Canada. Technical Report TR-350, V 3: 513 - 530.
- Dixon, D.A. and Woodcock, D.R. 1986a. Physical and engineering properties of candidate buffer materials. Atomic Energy of Canada Ltd. Technical Report TR-352.
- Dixon, D.A., Gray, M.N., Baumgartner, P., and Rigby, G. 1986b. Pressures acting on waste containers in bentonite-based materials. Proceedings, 2nd International Conference on Radioactive Waste Management, Winnipeg, Canada. pp. 221 - 227.
- Drucker, D.C. and Prager, W. 1952. Soil mechanics and plastic analysis or limit design. *Quarterly of Applied Mathematics*, 10(2): 157 - 165. (from Scott 1985).
- Drucker, D.C., Gibson, R.E., and Henkel, D.J., 1955. Soil mechanics and work hardening

- theories of plasticity. Proceedings, ASCE, 81: 1 - 14. (from Scott 1985).
- Gens, A. 1982. Stress-strain and strength characteristics of a low plastic clay. Ph.D. Thesis, Department of Civil Engineering, Imperial College of Science and Technology, University of London, London, U.K. (from Head, 1986)
- Gillott, J.E. 1987. Clay in engineering geology. Elsevier, Amsterdam, The Netherlands. 468 pp.
- Gouy, G. 1919. Sur la constitution de la charge électrique à la surface d'un électrolyte. *Année Physique (Paris)*, Série 4(9): 457 - 468.
- Graham, J., Pinkney, R.B., Lew, K.V., and Trainor, P.V., 1982. Curve-fitting and laboratory data, *Canadian Geotechnical Journal*, 19(2): 201 - 205.
- Graham, J., Crooks, J.H.A. and Bell, A.L. 1983a. Time effects on the stress-strain behaviour of natural soft clays. *Geotechnique*, 33(3): 327 - 340.
- Graham, J. and Houlsby, G.T. 1983b. Anisotropic elasticity of a natural clay. *Geotechnique*, 33(2): 165 - 180.
- Graham, J., Noonan, M.L. and Lew, K.V. 1983c. Yield states and stress strain relationships in a natural plastic clay. *Canadian Geotechnical Journal*, 20(3): 502 - 516.
- Graham, J. and Au, V.C.S. 1985. Effects of freeze-thaw and softening on a natural clay at low stresses. *Canadian Geotechnical Journal*, 22(1): 69 - 78.
- Graham, J. and Li, E.C.C. 1985. Comparison of natural and remolded plastic clay. *Journal of Geotechnical Engineering, ASCE*, 111(GT7): 865 - 881.
- Graham, J., Gray, M.N., Sun, B. C.-C. and Dixon, D.A. 1986. Strength and volume change characteristics of a sand-bentonite buffer. Proceedings, 2nd International Conference on Radioactive Waste Management. Winnipeg, Manitoba. pp. 188 -194.
- Graham, J., Saddat, F., Gray, M.N., Dixon, D.A., and Zhang, Q.-Y. 1989a. Strength and volume change characteristics of a sand-bentonite mixture. *Canadian Geotechnical Journal*, 26(2): 292 - 305.
- Graham, J., Wood, D.M., Yin, J.-H., and Azizi, F. 1989b. Prediction of triaxial stress-strain behaviour of Winnipeg clay using an anisotropic elastic plastic model. Proceedings, 42nd Canadian Geotechnical Conference. Winnipeg, Canada. pp. 155 - 162.
- Graham, J., Saadat, F., Lingnau, B.E., Yin, J.-H., Oswell, J.M., and Azizi, F. 1989c. Constitutive modelling of sand-bentonite buffer (RBM). Progress Report of Atomic Energy of Canada (WNRE). Contract WS-27J-62961. Department of Civil Engineering, University of Manitoba.
- Graham, J., Yin, J.-H., Oswell, J.M., and Lingnau, B.E. 1990. Constitutive modelling of sand-bentonite buffer (RBM). Final Report to Atomic Energy of Canada (WNRE). Contract

- WS-27J-62961. Department of Civil Engineering, University of Manitoba.
- Graham, J. and Oswell, J.M. 1991. Constitutive modelling of sand-bentonite buffer (RBM) - supplement to the 1990 Final Report to Atomic Energy of Canada (WNRE). Contract WS-27J-62961. Department of Civil Engineering, University of Manitoba.
- Graham, J., Oswell, J.M. and Gray, M.N. 1991. The effective stress concept in saturated active clay. Workshop on Stress Partitioning in Engineered Clay Barriers. Duke University, Durham, North Carolina.
- Gray, M.N., Cheung, S. and Dixon, D.A. 1984. The influences of sand content on swelling developed by statically compacted Na-bentonite. Atomic Energy of Canada Ltd. Report. AECL - 7825.
- Head, K.H. 1986. Manual of soil laboratory testing, Vol. 3. Pentech Press Ltd., London, U.K. 743 - 1238 pp.
- Horsfield, D. and Been, K. 1987. Computer controlled triaxial testing. Proceedings, 1st Canadian Symposium on Microcomputer Applications to Geotechnique. Canadian Geotechnical Society, pp. 55 - 62.
- Indrawan, Z. 1986. Stress-strain and strength characteristics of an Auckland soil. Ph.D. Thesis, Department of Civil Engineering, University of Auckland, New Zealand.
- Iwan, W.D. 1967. On a class of models for the yielding behaviour of continuous and composite systems. Journal of Applied Mechanics, ASME, 34(3): 612 - 617.
- Iwan, W.D. and Chelvakumar, K. 1988. Strain space constitutive model for clay soils. Journal of Engineering Mechanics, ASCE, 114(EM9): 1454 - 1472.
- Jamieson, M.R. 1989. Effects of moderate stress-release disturbance on the shear behaviour of lightly overconsolidated simulated marine clays. M.Sc. Thesis. Department of Civil Engineering, University of Manitoba, Winnipeg, Canada.
- Ko, H.Y. and Sture, S. 1981. State of the art data reduction and application for analytical modelling. Laboratory Shear Strength of Soils. ASTM STP 740. American Society for Testing and Materials, Philadelphia, PA.: 329 - 386.
- Kjartanson, B.H. and Gray, M.N. 1987. Buffer/container experiments in the underground research laboratory. Proceedings, 40th Canadian Geotechnical Conference, Regina, Canada. pp. 275 - 283.
- Lade, P.V. 1988. Automatic volume change and pressure measurement devices for triaxial testing of soils. ASTM Geotechnical Testing Journal, 11(4): 263 - 268.
- Lade, P.V. and Kim, M.K. 1988. Single hardening constitutive model for frictional materials, II. Yield criterion and plastic work contours. Computers and Geotechnics, 6(1): 13 - 29.

- Lade, P.V. 1990. Single hardening model with application to N.C. clay. *Journal of Geotechnical Engineering, ASCE*, 116(3): 394 - 414.
- Lambe, T.W. 1958. The engineering behaviour of compacted clay. *Journal of the Soil Mechanics and Foundation Division, ASCE*, 84(SM2), paper 1655: 1 - 35.
- Lambe, T.W. and Whitman, R.V. 1959. The role of effective stress in the behaviour of expansive soils. *Quarterly of the Colorado School of Mines*: 34 - 65.
- Lambe, T.W. 1960. A mechanistic picture of shear strength in clay. *ASCE Research Conference on Shear Strength of Cohesive Soils*. Boulder, Colorado. pp. 555 - 580.
- Lambe, T.W. 1973. Predictions in soil engineering (13th Rankine Lecture), *Geotechnique*, 23(2): 149 - 201.
- Leonards, G.A. and Andersland, O.B. 1960. The clay-water system and the shearing resistance of clays. *Proceedings, ASCE Research Conference on the Shear Strength of Cohesive Soils*, Boulder Colorado: 793 - 818.
- Leroueil, S., Tavenas, F., La Rochelle, P., and Tremblay, M. 1988. Influence of filter paper and leakage on triaxial testing. *Advanced Triaxial Testing of Soil and Rock*. ASTM STP 977 (edited by R.T. Donaghe, R.C. Chancey, and M.L. Silver). American Society for Testing and Materials: 189 - 201.
- Lew, K.V. 1981. Yielding criteria and limit state in a Winnipeg clay. M.Sc. Thesis, Department of Civil Engineering, University of Manitoba, Winnipeg, Manitoba.
- Lopez, R.S. 1985. Review of vault sealing research. *Atomic Energy of Canada Technical Report TR-350, V.3*: 499 - 506.
- Loudon, P.A. 1967. Some deformation characteristics of kaolin. Ph.D. Thesis, Department of Civil Engineering, University of Cambridge, Cambridge, U.K. (from Atkinson and Bransby 1978)
- Mendelson, A. 1968. *Plasticity: theory and application*. The MacMillan Company, New York, U.S.A. 353 pp.
- Mitchell, J.K. 1976. *Fundamentals of soil behaviour*. John Wiley and Sons Inc. New York, USA. 422 pp.
- Mitchell, R.J. 1970. On the yielding and mechanical strength of Leda clays. *Canadian Geotechnical Journal*, 7(3): 297 - 325.
- Noonan, M.L. 1980. Limit state studies in Winnipeg clays. M.Sc. Thesis, Department of Civil Engineering, University of Manitoba, Winnipeg, Manitoba.
- Nordien, J. and Saadat, F. 1988. PC/Hewlett Packard PC Instruments data acquisition system for geotechnical engineering. Internal, unpublished report. Department of Civil Engineering, University of Manitoba, Winnipeg, Canada.

- Olson, R.E. and Mesri, G. 1970. Mechanisms controlling compressibilities of clays. *Journal of the Soil Mechanics and Foundation Division, ASCE*, 96(SM6): 1863 - 1878.
- Oswell, J.M., Lingnau, B.E., Osiowy, K.B.P., and Graham, J. 1989. Discussion on: Automatic volume change and pressure measurement devices for triaxial testing of soils (by: Lade, P.V.). *ASTM Geotechnical Testing Journal*, 12(4): 325 - 325.
- Oswell, J.M. 1990. User manual for the GDS triaxial equipment at the University of Manitoba. Internal, unpublished report. Department of Civil Engineering, University of Manitoba, Winnipeg, Canada.
- Oswell, J.M., Graham, J., Lingnau, B.E., King, M.L. 1991. Use of side drains in triaxial testing at moderate to high pressures. Submitted to *ASTM Geotechnical Testing Journal* for review and possible publication as a Technical Note.
- Prager, W. 1959. *Introduction to plasticity*. Addison-Wesley, Reading, Mass. 148 pp.
- Prevost, J.H. 1978. Anisotropic undrained stress strain behaviour of clays. *Journal of the Geotechnical Engineering Division, ASCE*, 104(GT8): 1075 - 1090.
- Quigley, R.M. 1984. Quantitative mineralogy and preliminary porewater chemistry of candidate buffer and backfill materials for a nuclear fuel waste disposal vault. Atomic Energy of Canada Ltd. Report. AECL - 7827.
- Roscoe, K.H., Schofield, A.N., and Wroth, C.P. 1958. On the yielding of soils. *Geotechnique*, 9(1): 22 - 53.
- Roscoe, K.H. and Burland, J.B. 1968. On the generalized stress-strain behaviour of 'wet' clay. In: *Engineering Plasticity*, Cambridge University Press, London, U.K.: 535 - 609.
- Saadat, F. 1989. Constitutive modelling of the behaviour of a sand-bentonite mixture. Ph.D. Thesis, Department of Civil Engineering, University of Manitoba, Winnipeg, Canada.
- Saadat, F., Graham, J., and Gray, M.N. 1989. High pressure behavior of sand-bentonite buffer of nuclear fuel waste containment. 42nd Canadian Geotechnical Conference, Winnipeg, Canada. pp. 280 - 288.
- Salençon, J. 1977. *Applications of the theory of plasticity in soil mechanics*. (translated from French by R.W. Lewis and H. Virlogeux) John Wiley & Sons, Toronto. 158 pp.
- Salvadurai, A.P.S. and Au, M.C. 1988. Coupled heat and moisture flow in buffer materials used in a nuclear waste disposal vault. Atomic Energy of Canada Ltd. Technical Report TR-443.
- Schofield, A.N. and Wroth, C.P. 1968. *Critical state soil mechanics*. McGraw Hill, London, U.K. 310 pp.
- Scott, R.F. 1985. Plasticity and constitutive relations in soil mechanics. *Journal of Geotechnical Engineering, ASCE*, 111(GT5): 563 - 605.

- Sheahan, T.C., Germaine, J.T., and Ladd, C.C. 1990. Automatic triaxial testing of soft clays: an upgraded commercial system. *ASTM Geotechnical Testing Journal*, 13(3): 153 - 163.
- Skempton, A.W. 1960a. Terzaghi's discovery of effective stress. In: *From theory to practice in soil mechanics*. Terzaghi, K. John Wiley and Sons Inc. New York, USA: 42 - 53.
- Skempton, A.W. 1960b. Effective stresses in soils, concrete, and rocks. *Proceedings, Conference on Pore Pressures and Suction in Soils*. Butterworths, London, U.K.: 4 - 16.
- Spencer, G.C. 1968. *Introduction to plasticity*. Chapman and Hall Ltd., London, U.K. 118 pp.
- Sridharan, A. and Venkatappa Rao, G. 1973. Mechanisms controlling volume change in saturated clays and the role of the effective stress concept. *Geotechnique*, 23(3): 359 - 382.
- Sridharan, A., Rao, A.S., and Swapullaiah, P.V. 1986. Swelling pressure of clays. *ASTM Geotechnical Testing Journal*, 9(1): 24 - 33.
- Sun, B.C.-C. 1986. Stress-strain properties in sand-clay buffer materials. M.Sc. Thesis, Department of Civil Engineering, University of Manitoba, Winnipeg, Canada.
- Tavenas, F. and Leroueil, S. 1977. The effects of stresses and time on yielding of clays. *Proceedings, 9th International Conference on Soil Mechanics and Foundation Engineering*. Vol. 1. pp. 319 - 326.
- Terzaghi, K. 1936. The shearing resistance of saturated soils and the angle between the planes of shear. *Proceedings, 1st International Conference on Soil Mechanics and Foundation Engineering*. Vol. 1. pp. 54 - 56.
- Tresca, H. 1868. *Memoire sur l'ecoulement des corps solides soumis a de fortes pressions*. *Memoires Presentees par Divers Savants*, 18: 733 - 799. (from Scott 1985)
- Valliappan, S. 1981. *Continuum mechanics fundamentals*. AA Balkema, Rotterdam. 228 pp.
- Vaughan, P.R. 1988. Characterising the mechanical properties of *in situ* residual soils: Keynote Paper. *Proceedings, 2nd International Conference on Geomechanics in Tropical Soils*. Singapore. pp. 469 - 487.
- von Mises, R. 1913. *Mechanik der festen korper im plastisch-deformablen zustand*. *Nachrichten der Koniglicher Gesellschaft der Wissenschaft, Gottingen, Mathematik-Physik Klasse*: 582 - 592. (from Scott 1985).
- Wan, A. W.-L. 1987. Compaction and strength characteristics of sand-clay buffer material formed at swelling pressure-water content equilibrium. M.Sc. Thesis, Department of Civil Engineering, University of Manitoba, Winnipeg, Canada.
- Wan, A. W.-L., Graham, J., and Gray, M.N. 1990. Influence of soil structure on the stress-strain behaviour of sand-bentonite mixtures. *ASTM Geotechnical Testing Journal*, 13(3): 179 - 187.

- Wood, D.M. 1990. Soil behaviour and critical state mechanics. University of Cambridge Press, Cambridge, U.K.
- Yarechewski, D. 1988. Quality control tests for making sand-bentonite specimens for nuclear waste containment studies. B.Sc. Thesis, Department of Civil Engineering, University of Manitoba, Winnipeg, Canada.
- Yin, J.-H. and Graham, J. 1989. Viscous-elastic-plastic modelling of one-dimensional time-dependent behaviour of clays. *Canadian Geotechnical Journal*, 26(2): 199 - 209.
- Yin, J.-H. 1990. Constitutive modelling of time-dependent stress-strain behaviour of soils. Ph.D. Thesis, Department of Civil Engineering, University of Manitoba, Winnipeg, Canada.
- Yoder, P.J. and Iwan, W.D. 1981. On the formulation of strain space plasticity with multiple loading surfaces. *Journal of Applied Mechanics*, 48(4): 773 - 778.
- Yong, R.N. and Warkentin, B.P. 1975. Soil Properties and behaviour. Elsevier, Amsterdam, The Netherlands. 449 pp.

APPENDIX A

TABLE A.1 Specimen Preparation and Moisture Control Data

Notes: 1. The numbering of tests is not consecutive. Missing test numbers denote tests that were preliminary, quality control, or in which leaks etc. developed. These tests will not be included in the analysis of data.

2. Saturation (Sat.) was calculated based on initial specimen moisture content and dry density.

3. V_c denotes specific volume of the clay fraction.

TEST	Initial Conditions				Final Moisture Content		
	γ_d No.	w (%)	Sat. (%)	V_c	w (%) (vol chg)	w (%) (drying)	Diff.
T1113	1.47	29.6	95.9	2.696	29.8	N.A.	
T1114	1.48	29.4	96.0	2.684	36.3	35.1	1.2
T1116	1.49	29.0	96.0	2.661	36.9	35.4	1.5
T1117	1.48	29.3	96.0	2.679	38.2	37.6	0.6
T1118	1.67	21.9	95.0	2.268	25.1	22.3	2.8
T1119	1.48	29.9	97.2	2.692	31.2	30.3	0.9
T1120	1.47	30.3	97.7	2.706	31.2	30.2	1.0
T1121	1.50	29.0	97.8	2.631	31.0	27.2	3.2
T1122	1.67	21.7	94.5	2.263	23.0	23.9	-0.9
T1123	1.48	29.6	96.8	2.682	30.8	30.2	0.6
T1124	1.48	29.3	96.1	2.677	30.3	30.2	0.1
T1125	1.49	29.5	97.4	2.666	N.A.	29.6	
T1126	0.89	73.3	97.5	5.135	24.3	23.7	0.6
T1127	1.65	22.3	94.4	2.299	22.3	22.8	-0.5
T1128	1.48	29.9	97.6	2.685	30.5	29.6	0.9
T1129	1.49	29.4	97.0	2.667	30.0	30.0	0.0
T1130	1.67	21.5	94.3	2.254	21.6	22.2	-0.6
T1131	1.49	29.4	97.2	2.664	29.4	28.7	0.7
T1132	1.66	21.5	93.4	2.266	22.0	22.3	-0.3
T1134	1.49	29.1	96.9	2.652	28.8	28.6	0.2
T1135	1.49	29.1	96.0	2.667	31.0	30.6	0.4

TEST	Initial Conditions				Final Moisture Content		
	γ_d	w	Sat.	V_c	w (%)	w (%)	Diff.
No.	Mg/m ³	(%)	(%)		(vol chg)	(drying)	
T1136	1.49	29.4	97.8	2.653	31.9	31.7	0.2
T1137	1.67	21.9	96.0	2.255	20.1	19.6	0.5
T1138	1.49	29.3	97.6	2.651	N.A.	N.A.	
T1139	1.49	29.3	97.7	2.649	27.1	26.3	0.8
T1140	1.67	21.8	95.6	2.254	22.2	22.5	-0.3
T1141	1.67 design	N.A.	N.A.	N.A.	N.A.	23.7	
T1142	1.50	29.0	97.0	2.644	29.0	30.2	-1.2
T1143	1.67	21.9	95.5	2.261	21.8	22.0	-0.2
T1144	1.49	29.0	96.2	2.658	25.6	26.0	-0.4
T1145	1.48	29.6	97.0	2.678	27.5	27.2	0.3
T1146	1.67	22.4	97.2	2.267	23.6	23.3	0.3
T1147	1.66	22.3	96.1	2.276	25.4	24.9	0.5
T1148	1.67	21.9	95.7	2.259	24.1	23.6	0.5
T1149	1.67	21.9	95.6	2.260	21.0	21.0	0.0
T1150	1.68	21.7	96.5	2.237	22.8	21.8	1.0
T1151	1.69	21.3	96.0	2.220	22.0	21.6	0.4
T1152	1.65	22.4	95.3	2.293	26.9	26.5	0.4
T1153	1.47	29.8	96.9	2.691	30.2	30.1	0.1
T1154	1.47	29.6	95.5	2.705	30.7	30.2	0.5
T1155	1.48	29.3	96.0	2.679	31.1	30.0	1.1
T1156	1.50	29.1	98.3	2.625	31.5	31.0	0.5
T1199a	0.6	110	0.85	8.13	35.6	37.0	-1.4
T1199b	1.02	61.3	1.00	2.64	22.3	23.2	-0.9
T1199c	0.38	212	0.93	7.27	39.0	41.7	-2.7
T1199d	1.16	50.1	1.00	2.34	23.4	25.7	-2.3
T1199e	0.16	572	0.97	16.92	97.0	73.7	23.3
T1199f	0.12	661	0.83	22.5	17.9	47	-29.1

TABLE A.2 Comparison of Core and Shell Moisture Contents

Notes: 1. Not all specimens were cored to determine the interior moisture contents. Only those specimens that were cored are reported in this table.

2. The average moisture content is of the 5 core or shell portions cut along the length of the specimens.

Test No.	Average	Average	Differences		
	Core w(%)	Shell w(%)	Shell-Core w(%)	Core (top-base) w(%)	Shell (top-base) w(%)
T1109	22.9	23.1	0.2	0.4	-0.2
T1111	25.8	25.8	0	-0.3	0.1
T1112	22.5	22.1	-0.4	0.7	1.3
T1114	34.7	35.5	0.8	1.0	3.0
T1116	34.6	36.2	1.6	2.4	3.1
T1117	36.7	38.5	1.8	3.9	4.9
T1119	30.4	30.1	-0.3	0.7	1.1
T1120	30.2	30.1	-0.1	1.7	2.1
T1121	27.4	27.1	-0.3	1.0	0.9
T1122	23.6	24.2	0.6	0.8	3.4
T1123	30.1	30.2	0.1	0.5	1.1
T1124	30.1	30.2	0.1	0.5	1.1
T1125	29.6	29.5	-0.1	0.6	1.5
T1126	N.A.	23.7	N.A.	N.A.	0.6
T1127	22.8	22.8	0	0.6	1.1
T1128	29.7	29.6	-0.1	0.5	1.2
T1129	29.9	30.0	0.1	1.0	1.3
T1130	22.2	22.2	0	0	1.5
T1131	28.9	28.5	-0.4	0	0.4
T1132	22.4	22.3	-0.1	0	0.8
T1134	28.7	28.5	-0.2	-1.2	-1.1
T1135	30.6	30.7	0.1	1.2	4.1
T1136	31.3	32.1	0.8	1.1	2.4
T1137	19.7	19.6	-0.1	0	1.0

Test No.	Average	Average	Differences		
	Core w(%)	Shell w(%)	Shell-Core w(%)	Core (top-base) w(%)	Shell (top-base) w(%)
T1139	26.6	25.9	-0.7	-0.2	0.5
T1140	22.4	22.7	0.3	0.6	1.3
T1141	23.6	23.7	0.1	0.4	1.8
T1142	30.4	30.0	-0.4	0.9	2.1
T1143	22.1	21.8	-0.3	0.5	1.2
T1144	26.3	25.8	-0.5	-1.0	0
T1145	27.3	27.2	-0.1	-0.4	0.3
T1146	23.2	23.3	0.1	0.9	1.8
T1147	24.6	25.3	0.7	1.2	3.0
T1148	23.4	23.9	0.5	0.4	2.3
T1149	20.9	20.8	-0.1	0.1	0.7
T1150	22.0	21.7	-0.3	0.3	0.7
T1151	21.5	21.6	0.1	0.2	0.6
T1152	26.0	26.9	0.9	2.3	4.3
T1153	30.2	29.9	-0.3	-0.4	-0.1
T1154	30.2	30.1	-0.1	0.6	1.4
T1155	29.9	30.1	.02	0.8	1.0
T1156	30.7	31.3	0.6	0.8	2.2

APPENDIX B

Use of Side Drains in Triaxial Testing at Moderate to High Pressures

by

James M. Oswell,¹ James Graham,¹ Brian E. Lingnau,¹ and Martin W. King²

Submitted to the ASTM Geotechnical Testing Journal

for review and possible publication as a Technical Note

November, 1990

¹ Department of Civil Engineering, University of Manitoba, Winnipeg, Canada, R3T 2N2.

² Department of Clothing and Textiles, University of Manitoba, Winnipeg, Canada, R3T 2N2.

ABSTRACT: Side drains are used in triaxial tests to increase the rate of consolidation and equalize porewater pressures within the specimen. However, the efficiency of the side drains has been shown to be a function of time and effective confining pressure.

This paper presents the results of (1) a mail survey on side drain practice which indicates many laboratory use side drains that are not recommended by standard references, and (2) an experimental program to assess the effects of time and moderate to high effective confining pressure on the flow properties of four side drain materials.

The four side drain materials used in the testing program were (1) a single layer of Whatman No. 1 filter paper, (2) a single layer of Whatman No. 54 filter paper, (3) a double layer of Whatman No. 54 filter paper, and (4) a single layer of geotextile. The lengthwise flow of these materials was examined as a function of effective confining pressure up to 6000 kPa, and also of time at a fixed effective confining pressure of 750 kPa.

Tests were also conducted on specimens of natural clay to compare consolidation rates using different drain materials.

KEY WORDS: side drains, high pressure, filter paper, laboratory testing, triaxial, consolidation

Introduction

Side drains are used in triaxial tests to increase the rate of consolidation in fine grained specimens, and also to equalize porewater pressures within the specimen. When compared against double-end drainage without side drains, Bishop and Henkel [1] stated that side drains will reduce by 90% the time to reach 95% consolidation. Leroueil *et al.* [2] studied the effect of side drains on consolidation of Champlain sea clay and found that for normally consolidated specimens, the use of side drains reduced the consolidation time by a factor of only 2.5.

An extensive testing program at the University of Manitoba is examining the stress-strain behaviour of sand-bentonite mixtures at effective confining pressures of 500 kPa to 7000 kPa. These pressures are higher than are normally used in routine testing. Side drains are used in this program to reduce the lengthy consolidation times in the specimens. During the test program, some questions arose about how effective the drains were at these high confining pressures. These questions stimulated the work described in this paper.

In practice, little attention appears to be given to the selection of side drains for triaxial testing. It seems to be assumed, that they perform adequately under all circumstances regardless of the drainage material used, the confining and back pressures applied, the specimen size, and the duration of the test.

Standard references on triaxial testing (for example, Bishop and Henkel [1] and Head [3]) recommend the use of Whatman No. 54 filter paper for side drains. Bishop and Henkel noted that the permeability of filter paper will vary with pressure, and so will the paper thickness. Leroueil *et al.* [2] found significant reductions in the effectiveness of several filter papers used for side drainage due to increases in confining pressures in the range of 40 to 500 kPa. They also found that estimates of the coefficient of consolidation may be influenced by the effectiveness

of the side drain.

In The University of Manitoba laboratory, Whatman No. 1 filter paper, not Whatman No. 54, had been used for side drainage strips for some years without careful evaluation. This raised two basic questions. One, if we were not using the preferred filter paper, were others doing the same? Two, what is the effect of confining pressures and lengthy test durations on the flow characteristics of side drains?

Current Practice in the Use of Side Drains

A mail-survey was sent to seventy-nine laboratories of consulting engineering companies, universities, and government agencies in the United States and Canada. The survey asked whether side drains were used in triaxial testing, and the type and arrangement of the drains.

Table 1 summarizes the responses.

TABLE 1 Responses of Mail-in Survey on Side Drain Practice

1.	Responses	43%
2.	Usage of Side Drains	82%
3.	Type of Side Drain Material (as percentage of 2.)	
	Whatman No. 1 Filter Paper	23%
	Whatman Nos. 54 or 541 Filter Paper	46%
	Other (Blotting paper, Paper towelling, Whatman No. 4, #5, Geotextile)	31%
4.	Arrangement of Side Drains (as percentage of 2.)	
	Vertical Strips	68%
	Spiral Strips	15%
	Full encasement - with vertical cuts	17%

Whatman No.1 is a general purpose filter paper, with a medium fast filtration rate. Whatman Nos. 1,4, and 5 have low strength when soaked in water. Whatman Nos. 54 and 541 are hardened, high wet strength filter papers with fast filtration rates.

The survey showed that current practice differs from conventionally recommended

practice. Less than one-half of the respondents use Whatman No. 54 (or No. 541) filter paper. The majority of respondents use drain materials that have low filtration rates and/or low strength in water.

The survey also found that the arrangement of filter strips was usually vertical. This contrasts with recommended practice [3,4] of placing the strips spirally on the specimen. This arrangement eliminates the need to make corrections in the specimen strength for the side drain stiffness.

Side Drain Testing Program

Tests were performed to determine the effects of confining pressure and time on the lengthwise flow of water in the different side drain materials listed in Table 2.

TABLE 2 Side drain materials tested.

Side drain material	Type	Number of Layers	Initial Thickness (mm)
Whatman No. 1	Filter paper	1	0.18
Whatman No. 54	Filter paper	1	0.19
Whatman No. 54	Filter paper	2	0.38
Mirafi 140NS	Non-woven geotextile	1	0.40

Fig. 1 shows a schematic of the testing arrangements. A brass dummy specimen (100.4 mm high by 50.7 mm diameter) was fully encased in the drain material, which therefore had a surface area of 15990 mm². Filter stones were positioned on the base pedestal and between the specimen and the top cap. A single latex rubber membrane sealed with four O-rings was placed over the specimen and drainage material.

A first test series examined the effect of confining pressure on water flow along the drains. Specimens with the subject drainage material were assembled and left overnight (about 17 hours) prior to testing. (Leroueil *et al.* [2] showed that membranes absorb water when they

are initially wetted.) The drainage leads at the top and the base of the specimen were attached to burettes filled with distilled water. The confining pressure on the specimen during the overnight period was low (resulting only from a hydrostatic pressure of several centimetres of water, and the small constriction applied by the membrane). The next morning the drainage valves were closed, the inlet burette filled with distilled water, and the outlet burette drained. Total confining pressures ranged from 2000 kPa to nearly 6000 kPa, depending on the drainage material being tested. The first confining pressure was applied together with an inlet pressure of 100, 250, or 500 kPa. The inlet pressure was always less than the confining pressure, and remained constant throughout each test. The outlet was kept at atmospheric pressure. The inlet and outlet drainage valves were opened, and the flow between the two burettes measured with time. After several measurement periods (each ranging from 5 to 30 minutes) the confining pressure was increased and another set of flow readings taken. The confining pressures were increased until the flow rates were small, less than 0.1 ml/min.

A second test series examined the effect of time on the lengthwise flow properties of the drain materials. The specimens were assembled as before. In these tests, a constant confining pressure of 1000 kPa and inlet pressure of 250 kPa was applied immediately after the tests were assembled. Flow rates were measured for periods from 200 hours to over 600 hours (25 days).

Results

Flow *versus* Pressure Tests

Figs. 2a-d show the effect of effective confining pressure on flow rate for the four drainage materials tested. Note that there is an order of magnitude difference in flow rate between Whatman No. 1 and the Whatman No. 54 tests. There are nearly two orders of magnitude difference in flow rate between the Whatman No. 54 and the geotextile. For any given confining pressure, increasing the applied inlet pressure from 100 kPa to 250 kPa to 500

kPa increased the flow rate.

It is common to express the lengthwise flow of fluid through a permeable material in terms of its transmissivity. Transmissivity is the lengthwise permeability multiplied by the thickness of the material. From Giroud [5] the transmissivity is:

$$T = k_p h = \frac{Q/B}{\Delta p / (\rho_w g L)}$$

where k_p = coefficient of lengthwise permeability in the plane of the drain material (m/s) (Note:

not the transverse permeability, k_t)

h = thickness of the drain (m)

Q = flow rate (m^3/s)

B = width (here, the circumference) of the drain (m)

Δp = hydraulic head loss = inlet pressure - outlet (atmospheric) pressure (N/m^2)

ρ_w = mass per unit volume of liquid (kg/m^3)

g = gravity ($9.81 \text{ m}/\text{s}^2$)

L = length of the flow path (m)

Figs. 3a-d show the flow rate data from Fig. 2 normalized using transmissivity. The data have now been plotted against an average effective confining pressure ($\sigma_{\text{conf}} - \Delta p/2$). The normalization of the data is good. Data from Leroueil *et al.* [2] are plotted on Figs. 3a and 3b for comparison. The two groups of data compare favourably.

In the case of the geotextile drain, normalization is less successful. Two causes may be responsible for this. One, because the flow rates were high, the test had to be frequently interrupted to refill the inlet burette. Thus transient conditions were present. Two, the use of transmissivity assumes Darcy's Law is valid and hence laminar flow. At the flow rates experienced with the geotextile it is possible that laminar flow was not always present, particularly at the lower confining pressures.

Flow versus Time Tests

Figs. 4a-d show the effect of time on the flow rates and transmissivity of the drain materials. The specimen dimensions, and the confining, inlet, and outlet pressures were kept constant. Thus the conversion of flow data to transmissivity data is direct. The filter papers experienced significant reductions in flow rate with increasing time. Whatman No. 1 exhibited the greatest reduction while the geotextile exhibited the smallest reduction. Most of the flow reduction occurred in the first 100 hours. Steady state flow was usually reached after 300 to 400 hours (12 to 17 days). The ratio of the steady flow rate to the initial flow rate is given in Table 3 for each material.

TABLE 3 Steady state flow relative to initial flow for the drainage materials tested.

Material	Steady Flow Rate
	Initial Flow Rate
Single layer Whatman No. 1	14%
Single layer Whatman No. 54	17%
Double layer Whatman No. 54	22%
Mirafi 140NS	50%

Tests on a Natural Clay

The effects of confining pressure and time on the lengthwise flow of side drains are clearly apparent in the data reported above. If, as the survey suggests, many laboratories are using filter paper other than Whatman No. 54 then assumptions concerning radial drainage may be inappropriately applied [2].

Triaxial consolidation tests were performed by adding a single large pressure increment to specimens of Winnipeg clay, a glaciolacustrine deposit covering large areas of southern Manitoba [6]. Specimen dimensions were nominally 50 mm diameter and 100 mm height with natural water content ranging from 58 to 61 percent. The vertical preconsolidation pressure was

200 kPa.

Specimens were tested with (1) no side drains, (2) Whatman No. 1 filter paper, (3) a single layer of Whatman No. 54 filter paper, and (4) Mirafi 140NS. The specimens with side drains were tested with 5 side drainage strips arranged spirally on the specimen, as described by Head [3]. Drainage was through the base of the specimen. The total confining pressure was 1000 kPa, with an applied back pressure of 250 kPa.

Volume strain *versus* time data for the four tests are shown in Fig. 5. The initial volume strain rates (that is, the rates of consolidation) were the highest for the geotextile, followed by Whatman No. 54, Whatman No. 1 and last, the specimen with no side drains. The specimen with geotextile drains reached equilibrium in about 25 hours. The Whatman No. 54 and Whatman No. 1 drains delayed equilibrium until about 40 hours and 150 hours respectively. Over 500 hours were required to reach equilibrium in the specimen with no drains.

Discussion and Conclusions

This testing program was conducted to examine the performance of side drains at moderate to high confining pressures in triaxial testing. Tests on a dummy specimen and natural clay confirm that flow rates depend on the drain material. As the effective confining pressure increases, the efficiency of the side drain material becomes more important. This reaffirms the findings of Bishop and Henkel [1] and Leroueil *et al.* [2]. At effective confining pressures greater than about 1000 kPa, or where long-term consolidation is expected, it is important that the side drain material retains its ability to transmit water along its length. Further, as the size of the specimen gets larger the time required to reach 95% consolidation increases. Longer consolidation periods will permit more time for the side drains to compress due to the confining pressure, thus reducing their effectiveness. In such circumstances, the use of a geotextile may be advantageous.

In "routine" triaxial tests at lower confining pressures, the use of drainage materials other than the recommended Whatman No. 54 may have only a small effect on consolidation rates or porewater pressure equalization. Leroueil *et al.* [2] suggested that in some weaker, lean clays, the use of a lower quality drain material may be advantageous. The effect of side drain stiffness on the specimen strength would be reduced if less stiff drain material was used (for example, Whatman No. 1).

The survey results suggest in a general way, that improvements may still be required in testing equipment, methodologies, and techniques.

Acknowledgements

The donation of the geotextile tested in this study by Mirafi (Canada) Inc. is gratefully acknowledged. Technical assistance was provided by N. Piamsalee and P. Mitra of the University of Manitoba, and P. Kennedy and D. Moore of Mirafi (Canada) Inc.

References

- [1] Bishop, A.W., and Henkel, D.J., "The Measurement of Soil Properties in the Triaxial Test," 2nd ed., Edward Arnold Ltd. London, U.K. 228 pp.
- [2] Leroueil, S., Tavenas, F., La Rochelle, P., and Tremblay, M., "Influence of Filter Paper and Leakage on Triaxial Testing," Advanced Triaxial Testing of Soil and Rock, ASTM STP 977, R.T. Donaghe, R.C. Chancey, and M.L. Silver, Eds., American Society for Testing and Materials, Philadelphia, 1988, pp. 189 - 201.
- [3] Head, K.H., "Manual of Soil Laboratory Testing Volume 3: Effective Stress Tests," Pentech Press. London, U.K., 1986, pp.
- [4] Gens, A., "Stress-Strain and Strength Characteristics of a Low Plasticity Clay," Ph.D. Thesis, Department of Civil Engineering, Imperial College of Science and Technology, University of London. London, U.K., 1982.
- [5] Giroud, J.P., "Introduction to Geotextiles and Their Applications," Proceedings, 1st Canadian Symposium on Geotextiles, Calgary, Alta., 1980.
- [6] Graham, J., and Shields, D.H., "Influence of Geology and Geological Processes on the Geotechnical Properties of a Plastic Clay," Engineering Geology, Vol. 22, 1985, pp. 109 - 126.

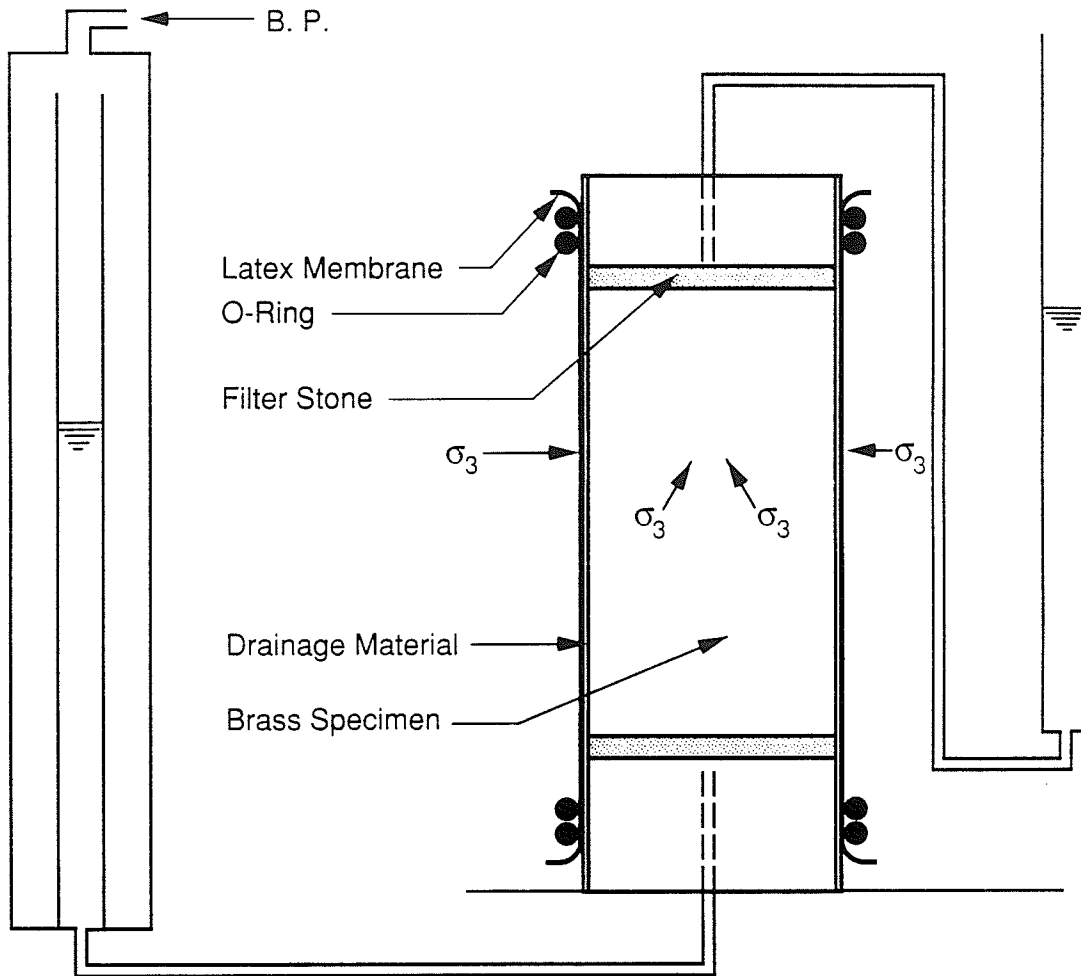


FIGURE 1 Schematic of testing set-up.

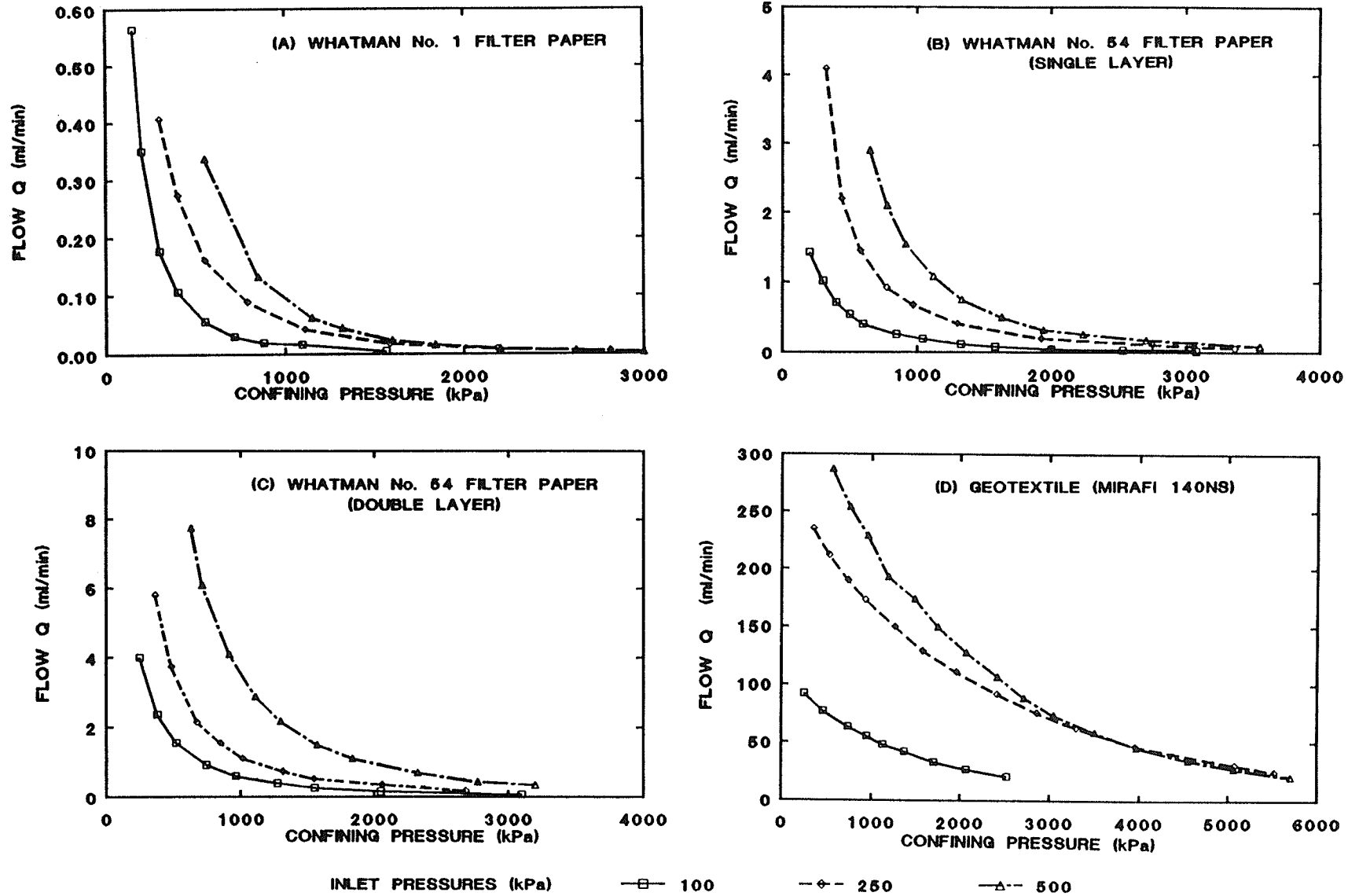


FIGURE 2 Flow versus total confining pressure for side drain materials on a brass specimen.

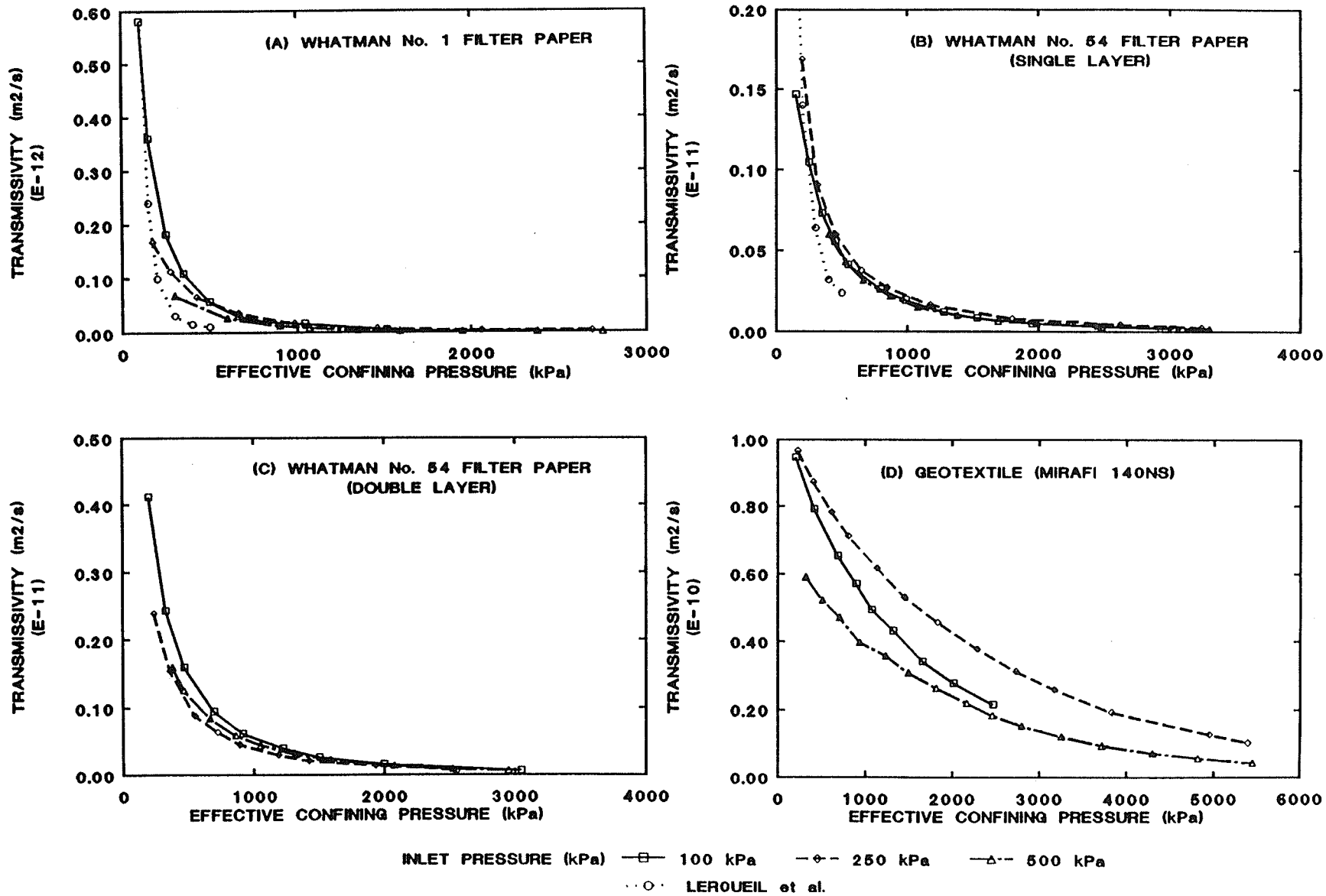


FIGURE 3 Transmissivity versus effective confining pressure for side drain materials on a brass specimen.

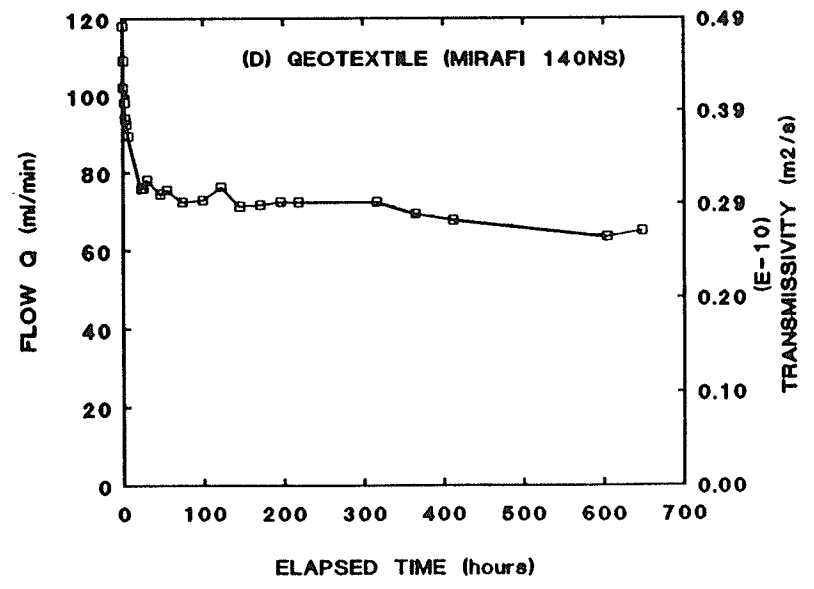
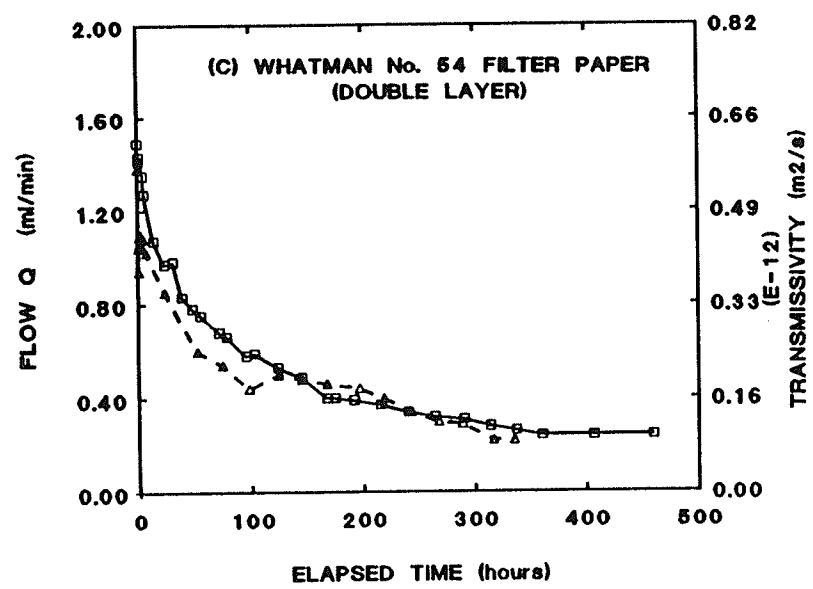
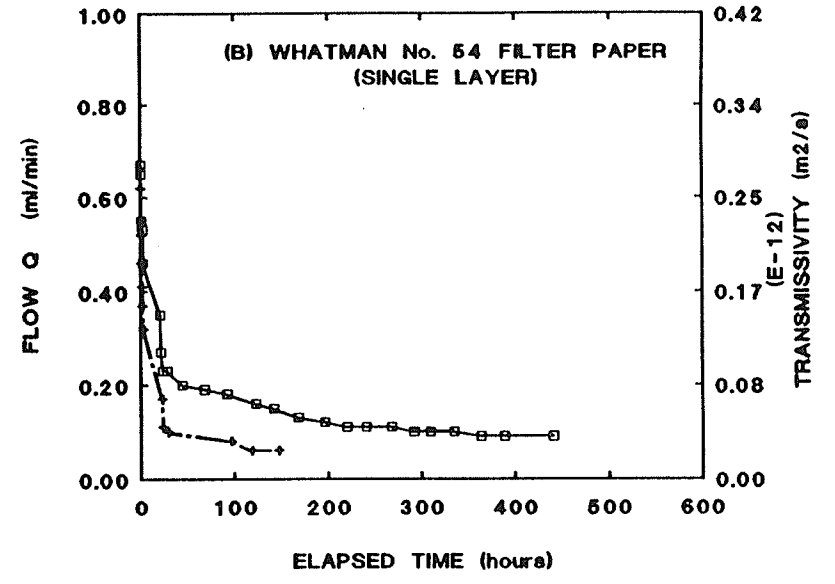
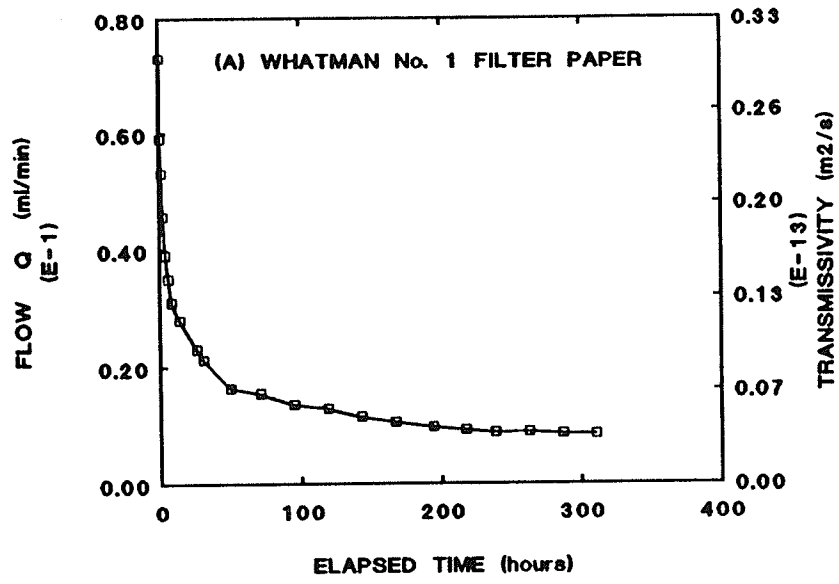


FIGURE 4 Flow and Transmissivity *versus* time for side drain materials on a brass specimen.

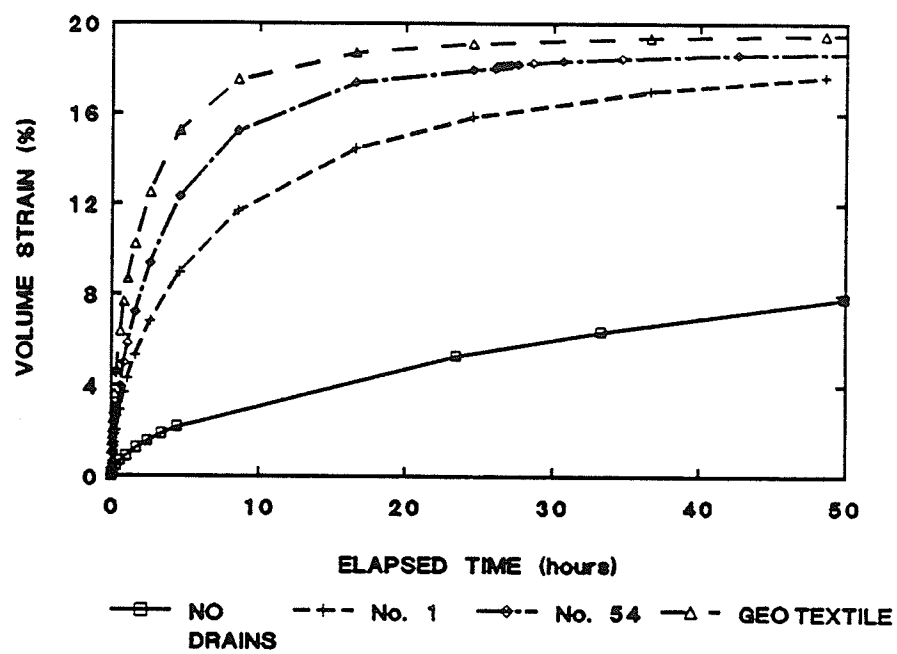


FIGURE 5 Volume strain (consolidation) of Winnipeg clay specimens with and without side drains.

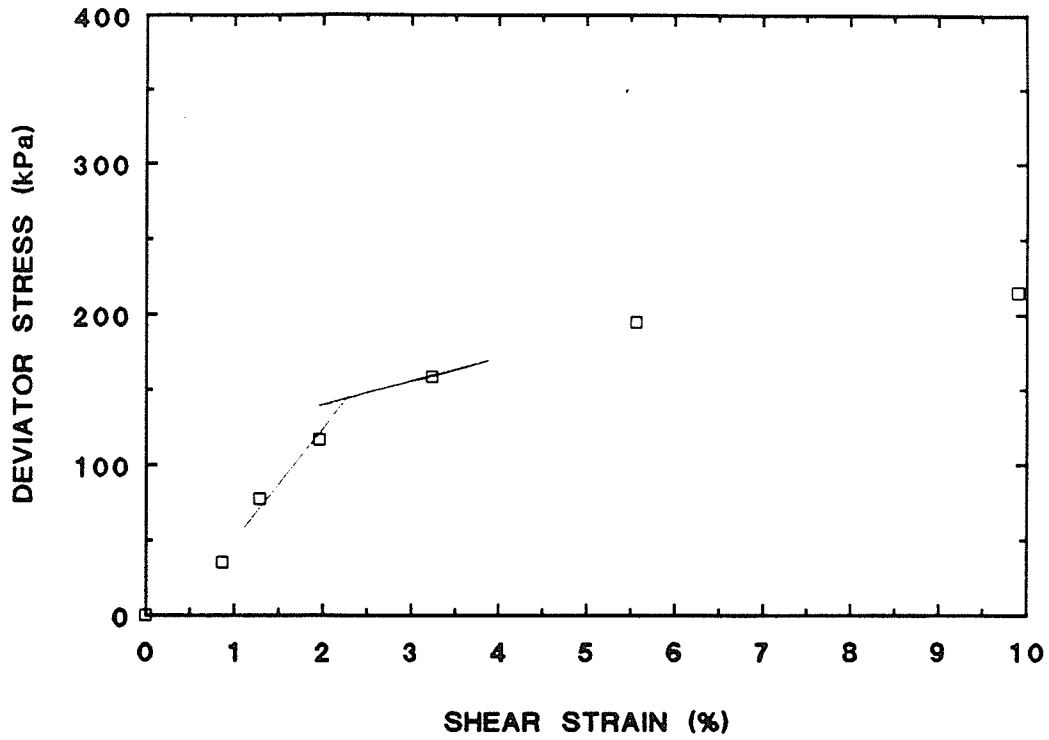
APPENDIX C

This appendix contains stress-strain (deviator stress *versus* shear strain) data for all yielding specimens tested in this program. The tests are arranged numerically. Complete test data for each specimen has been reported by Graham *et al.* (1990), and Graham and Oswell (1991).

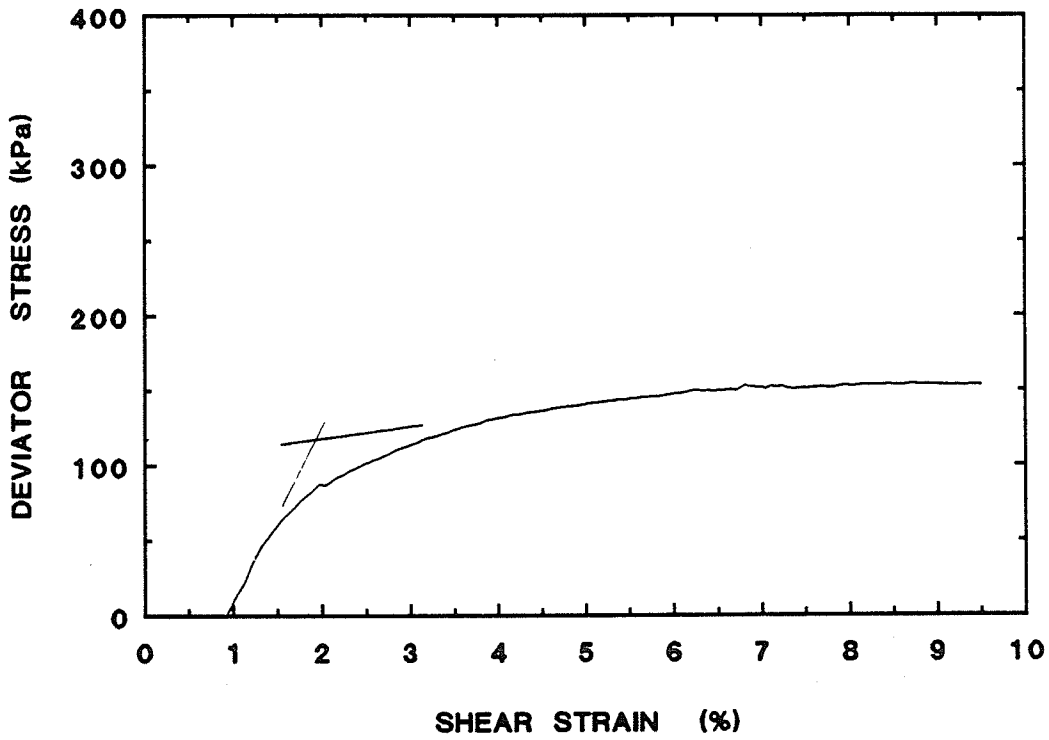
Straight-line pre- and post-yield segments have been added to each stress-strain plot. The intersection of the lines is the interpreted yield stress. In some cases this value will differ slightly from the yield stress reported in Table 5.4. This is because the tabulated yield stresses represent an average yield stress determined from several different stress-strain, or work energy plots.

Data for all tests, except T1138 and T1150 are presented as deviator stress *versus* shear strain plots. Data for tests T1138 and T1150 (isotropic consolidation) are presented as Sum Work *versus* LSSV.

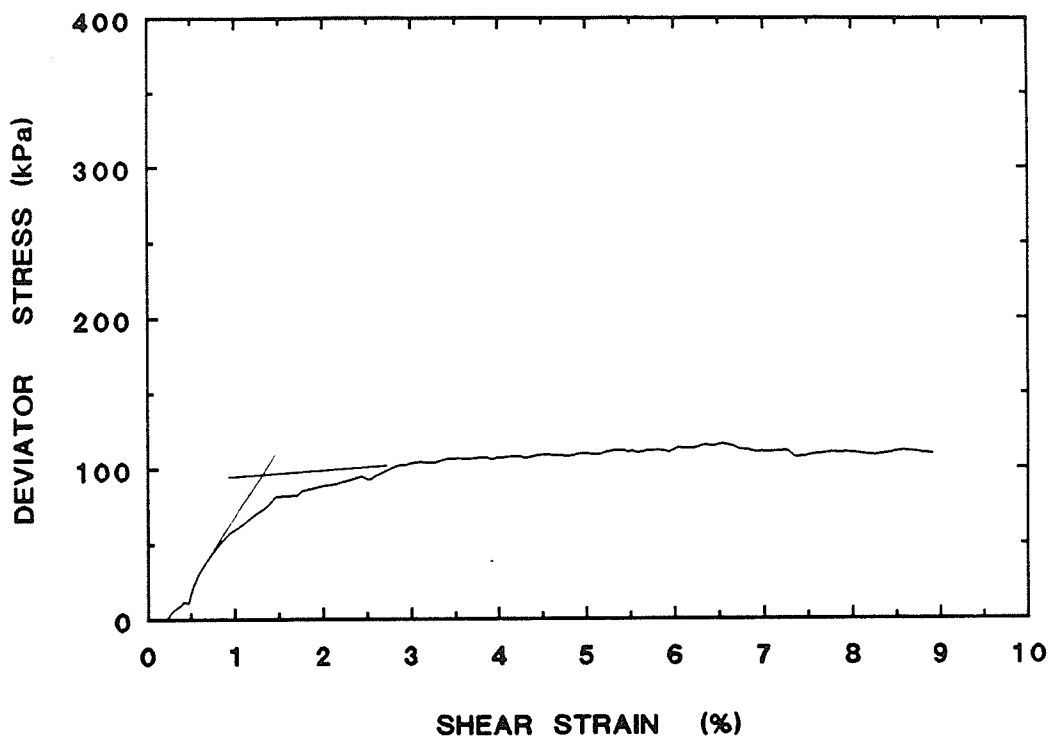
BUFFER SPECIMEN T1114
DRY DENSITY = 1.48 Mg/m³



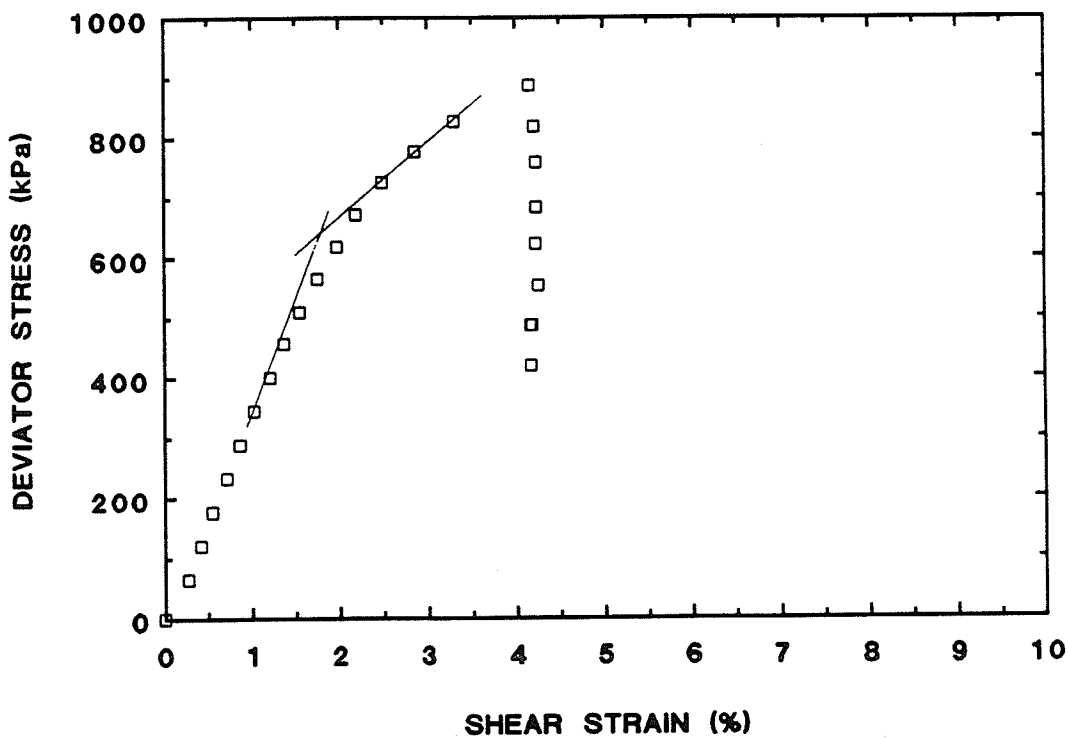
BUFFER SPECIMEN T1116
DRY DENSITY = 1.49 Mg/m³



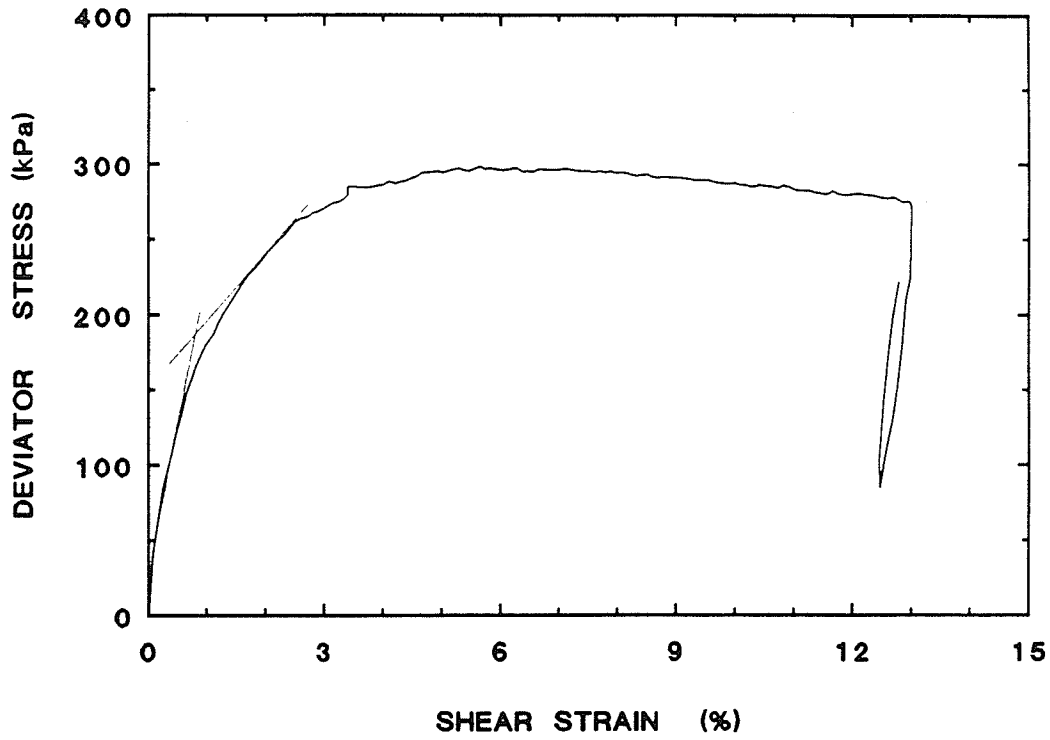
BUFFER SPECIMEN T1117
DRY DENSITY = 1.48 Mg/m³



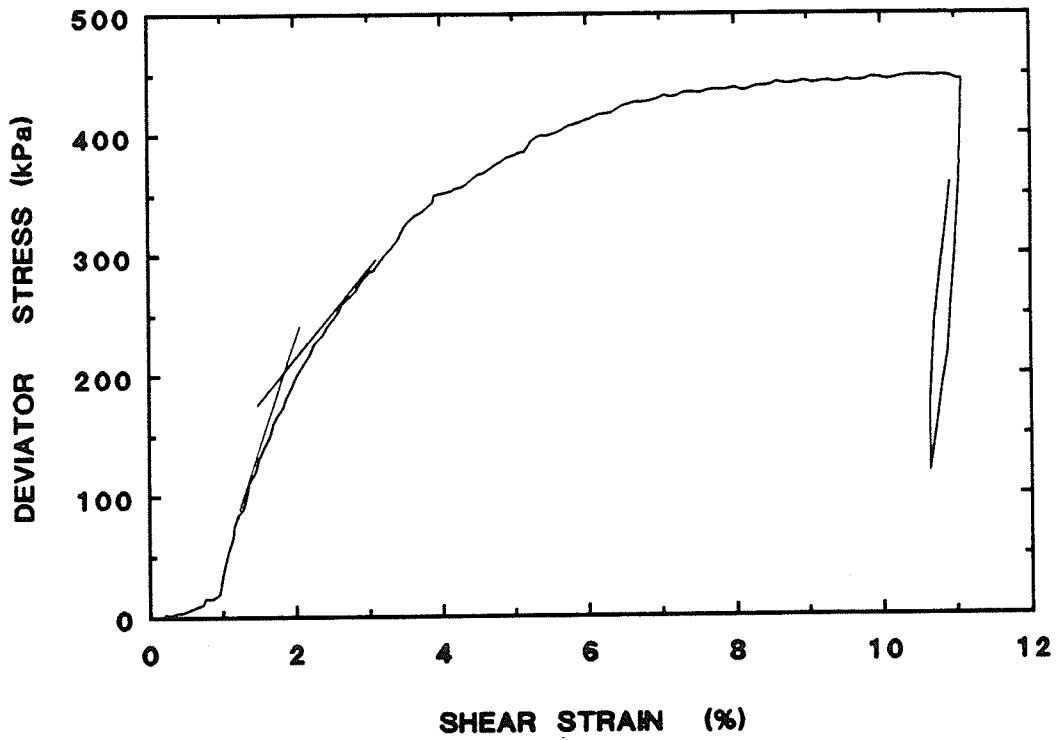
BUFFER SPECIMEN T1118
DRY DENSITY = 1.67 Mg/m³



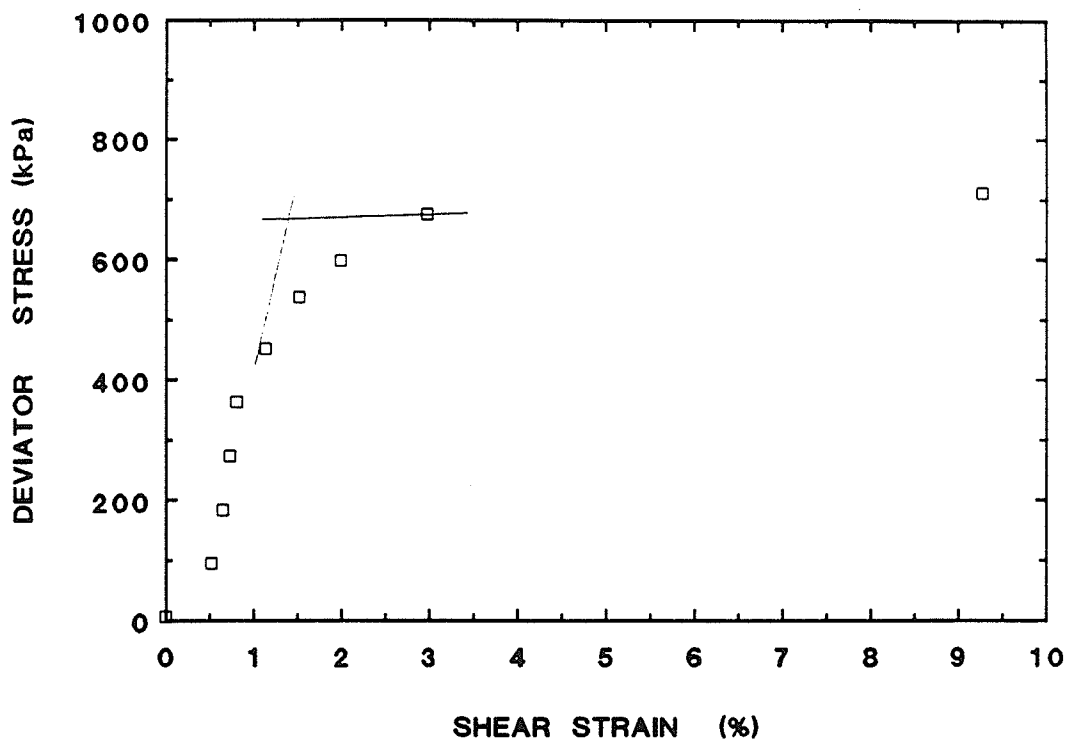
BUFFER SPECIMEN T1120
DRY DENSITY = 1.47 Mg/m³



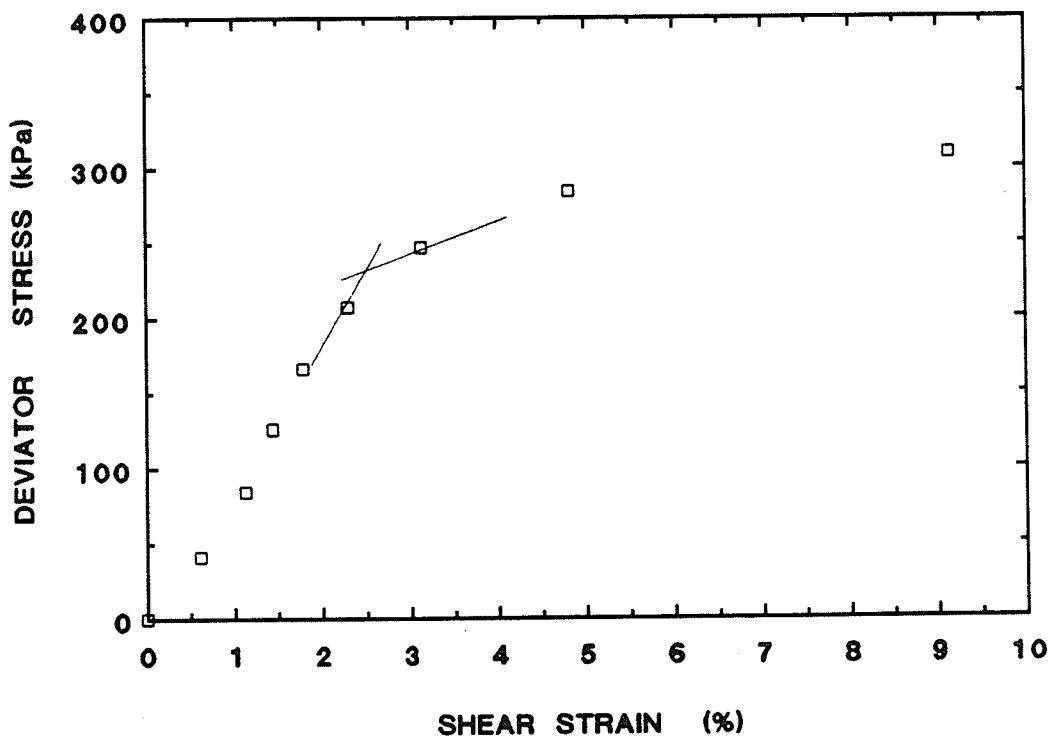
BUFFER SPECIMEN T1121
DRY DENSITY = 1.50 Mg/m³



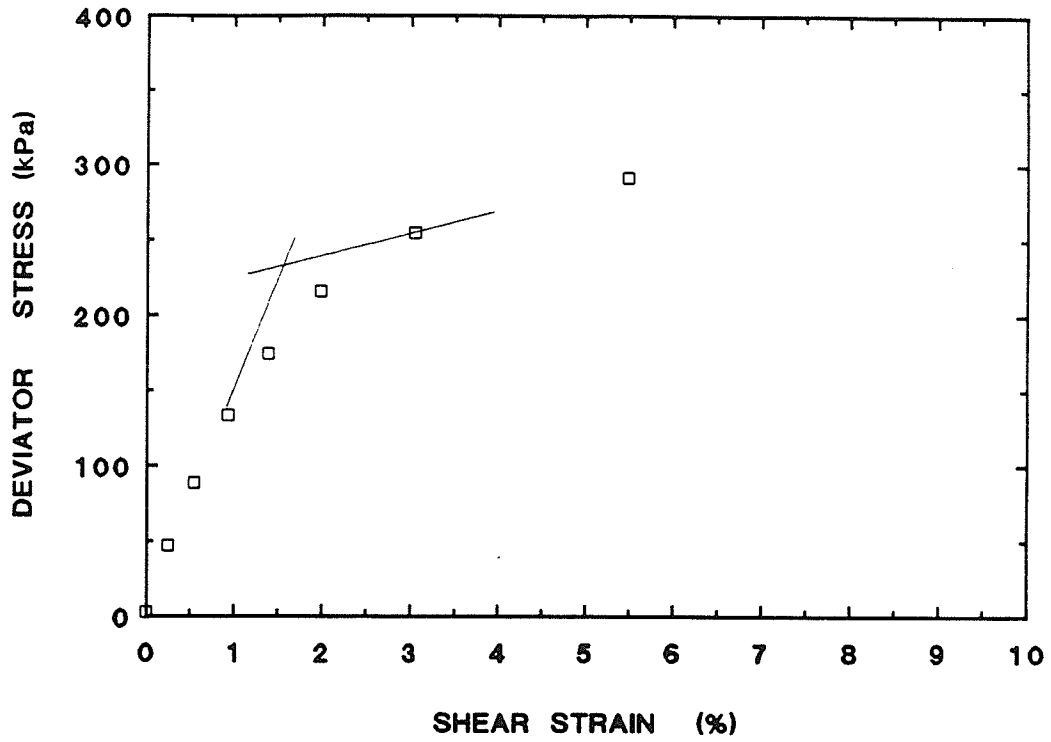
BUFFER SPECIMEN T1122
DRY DENSITY = 1.67 Mg/m³



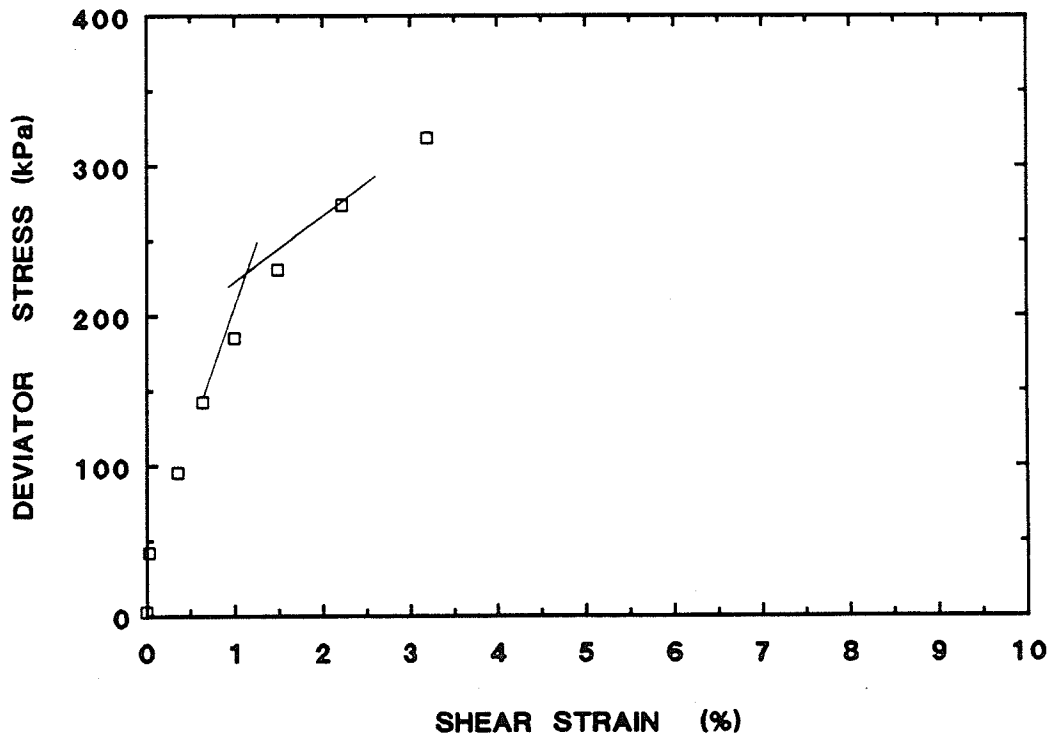
BUFFER SPECIMEN T1123
DRY DENSITY = 1.48 Mg/m³



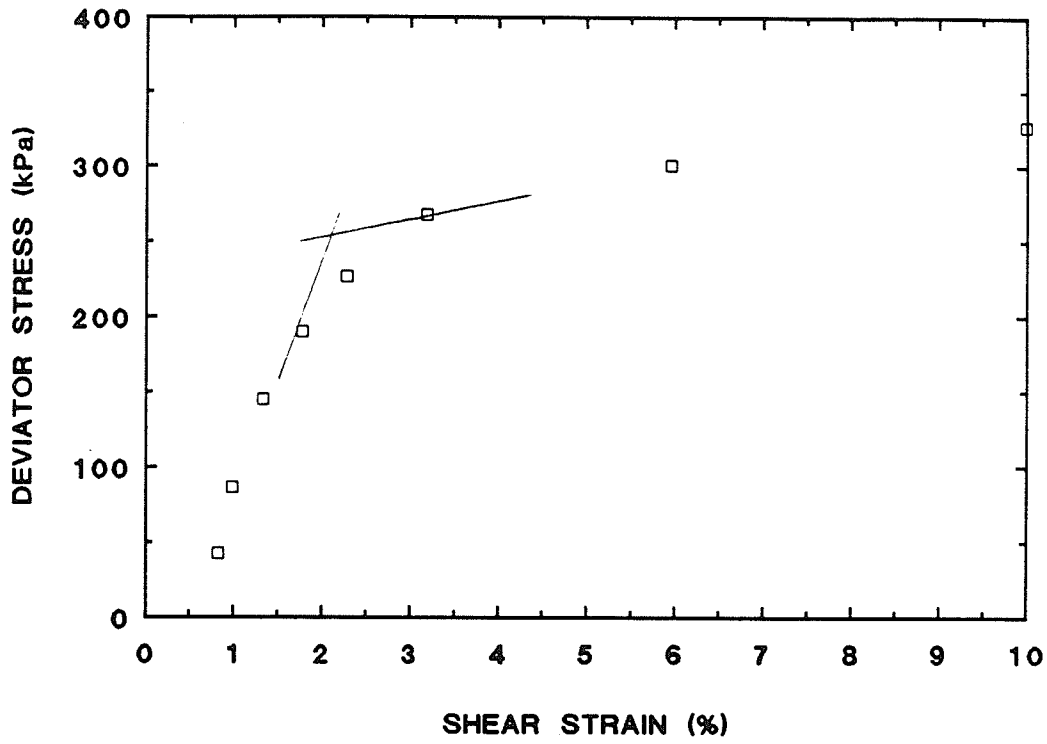
BUFFER SPECIMEN T1124
DRY DENSITY = 1.48 Mg/m³



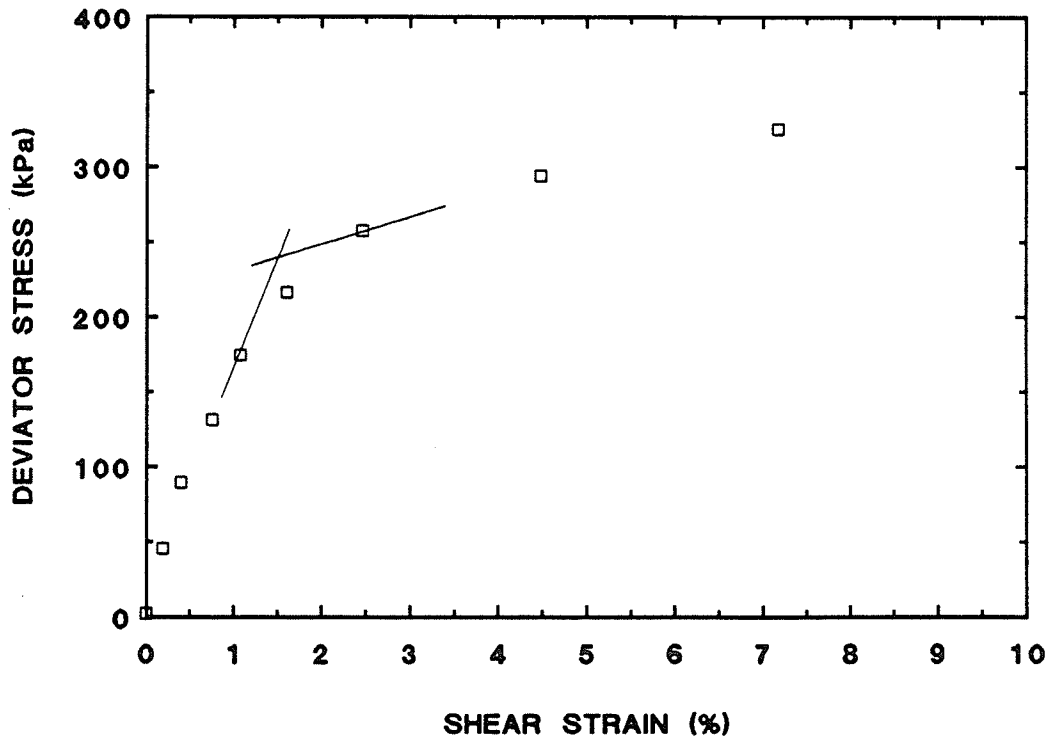
BUFFER SPECIMEN T1125
DRY DENSITY = 1.49 Mg/m³



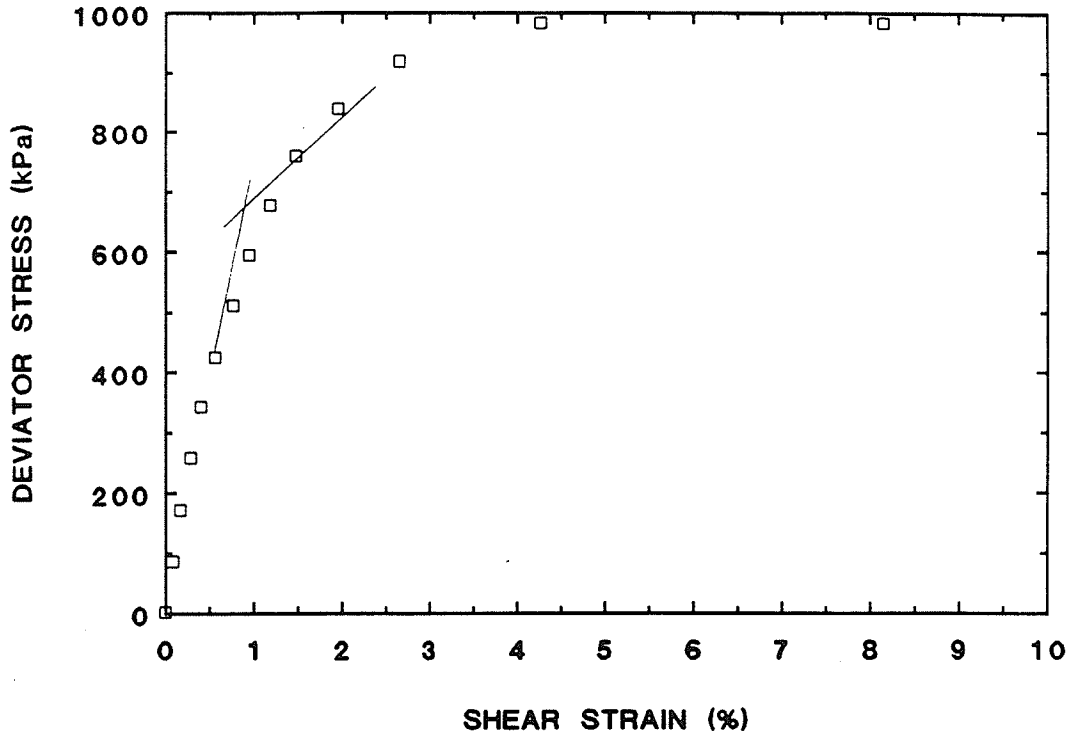
BUFFER SPECIMEN T1128
DRY DENSITY = 1.48 Mg/m³



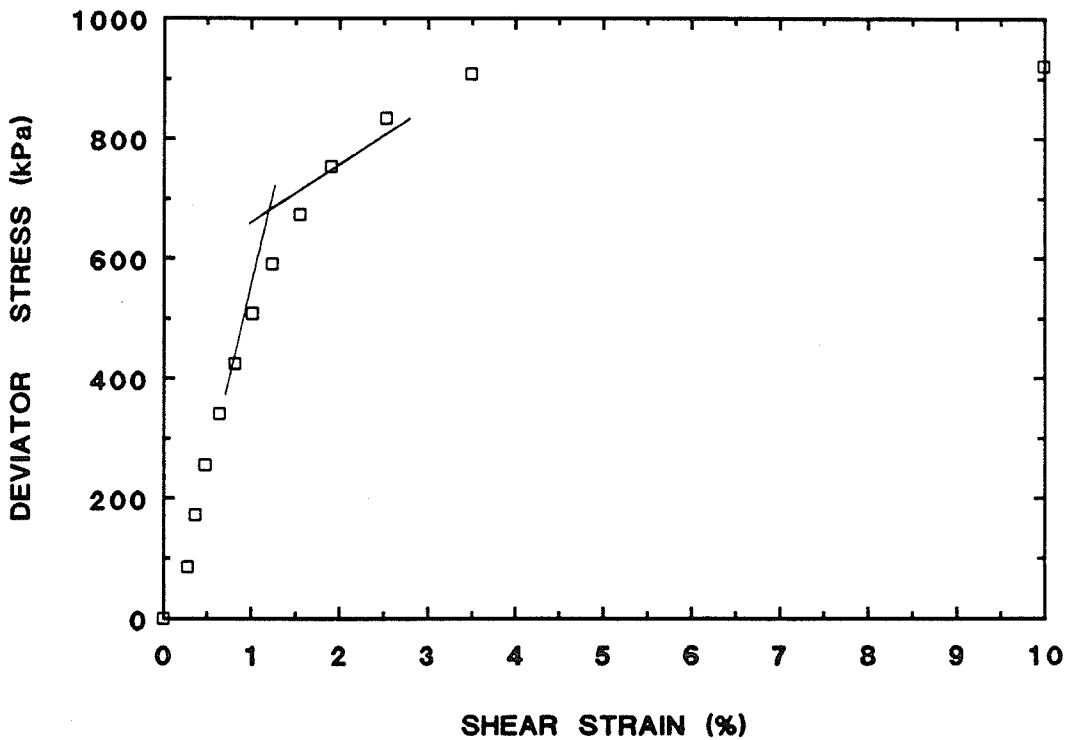
BUFFER SPECIMEN T1129
DRY DENSITY = 1.49 Mg/m³



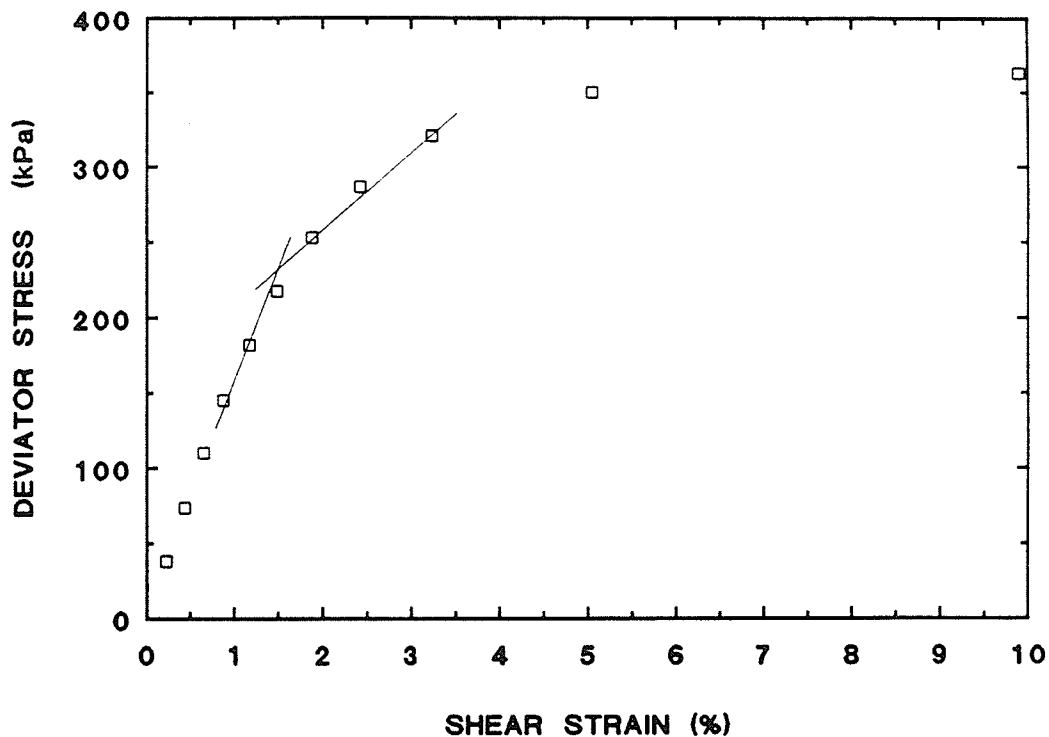
BUFFER SPECIMEN T1130
DRY DENSITY = 1.67 Mg/m³



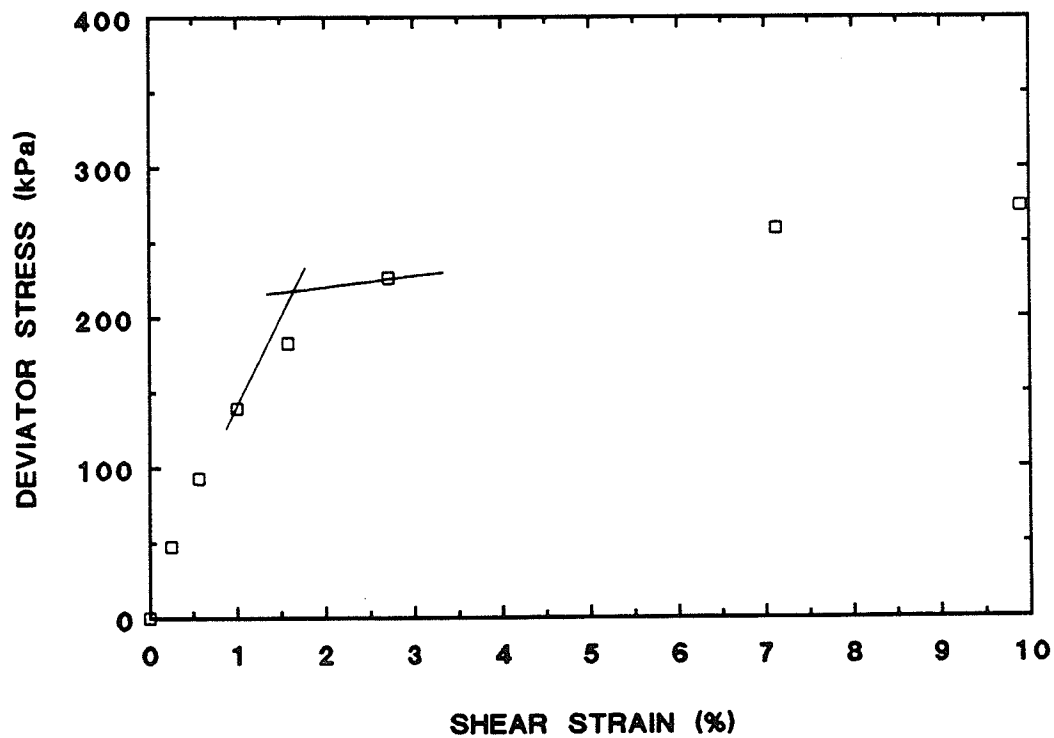
BUFFER SPECIMEN T1132
DRY DENSITY = 1.66 Mg/m³



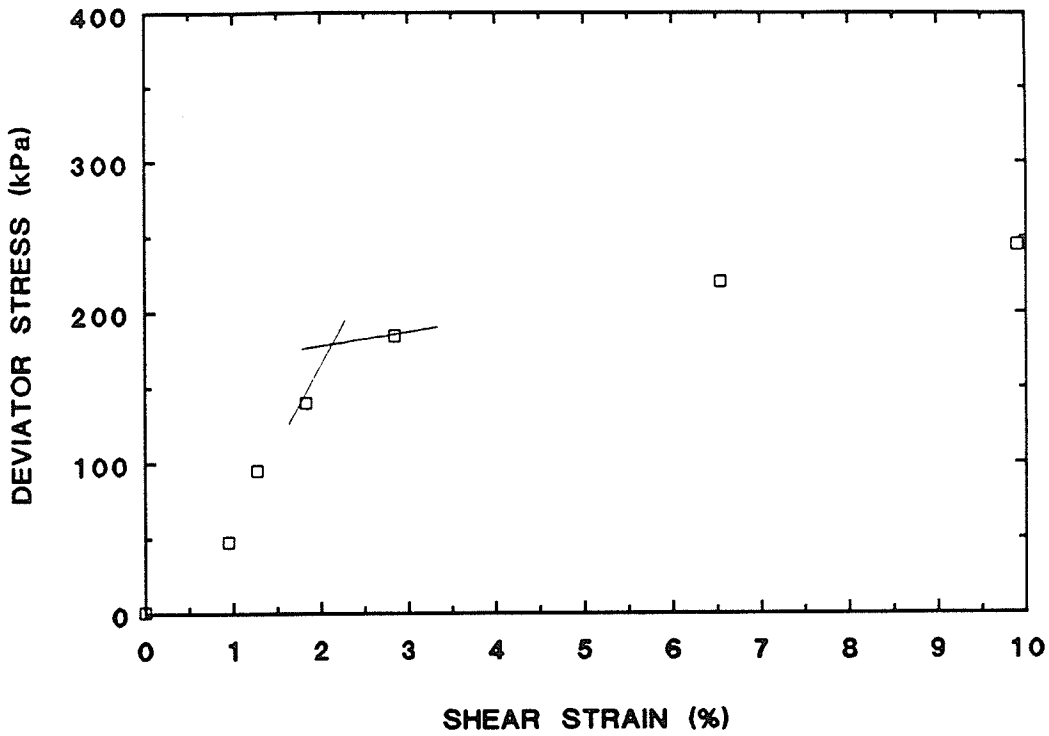
BUFFER SPECIMEN T1134
DRY DENSITY = 1.49 Mg/m³



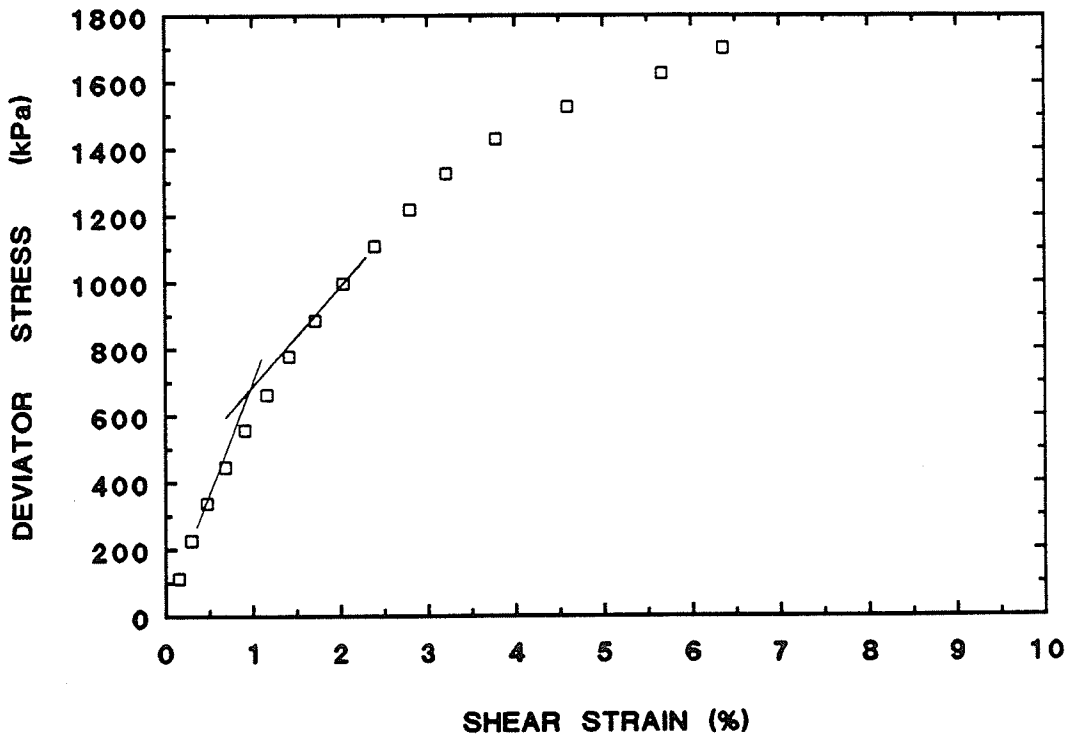
BUFFER SPECIMEN T1135
DRY DENSITY = 1.49 Mg/m³



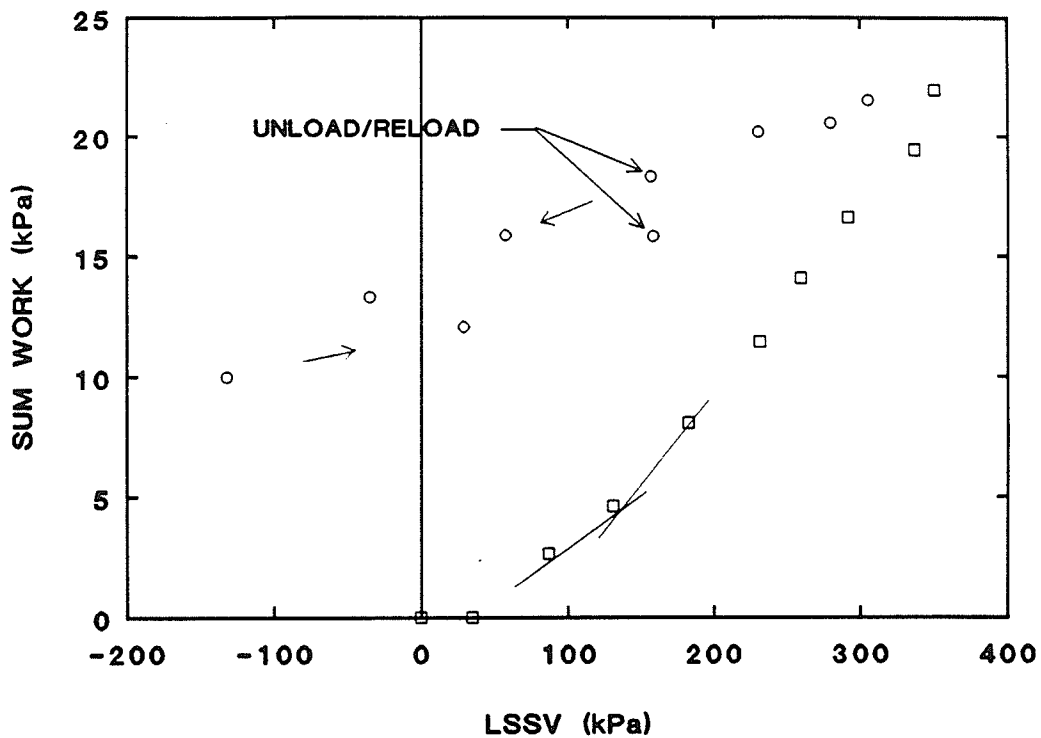
BUFFER SPECIMEN T1136
DRY DENSITY = 1.49 Mg/m³



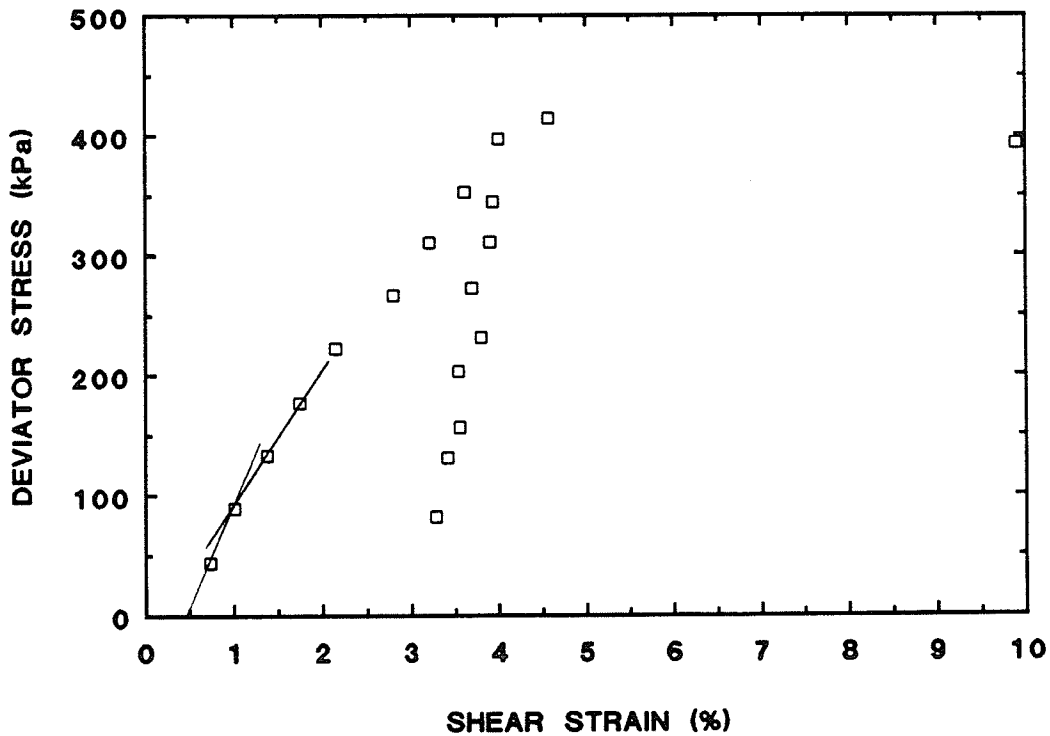
BUFFER SPECIMEN T1137
DRY DENSITY = 1.67 Mg/m³



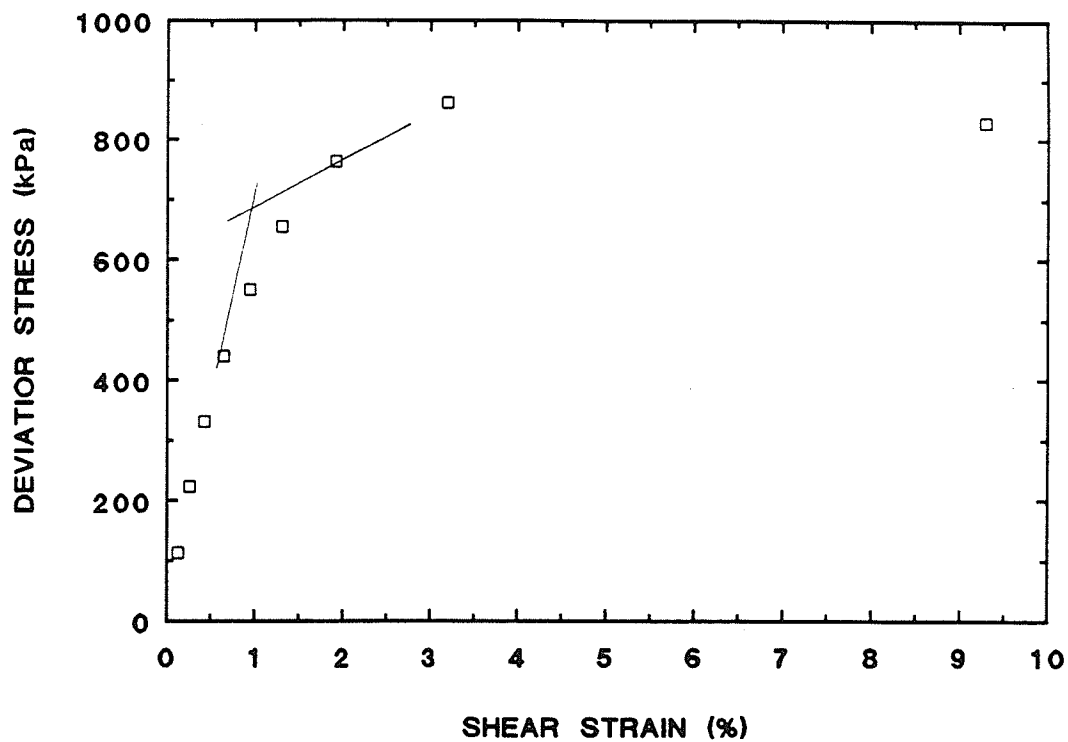
BUFFER SPECIMEN T1138
DRY DENSITY = 1.49 Mg/m³



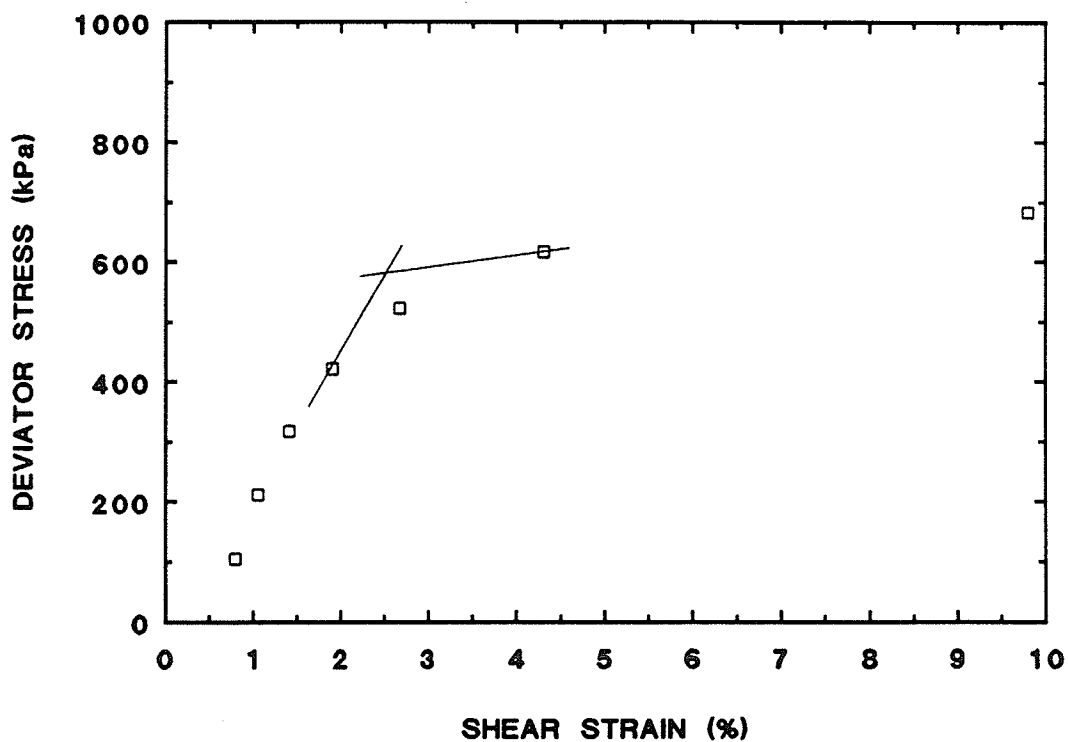
BUFFER SPECIMEN T1139
DRY DENSITY = 1.49 Mg/m³



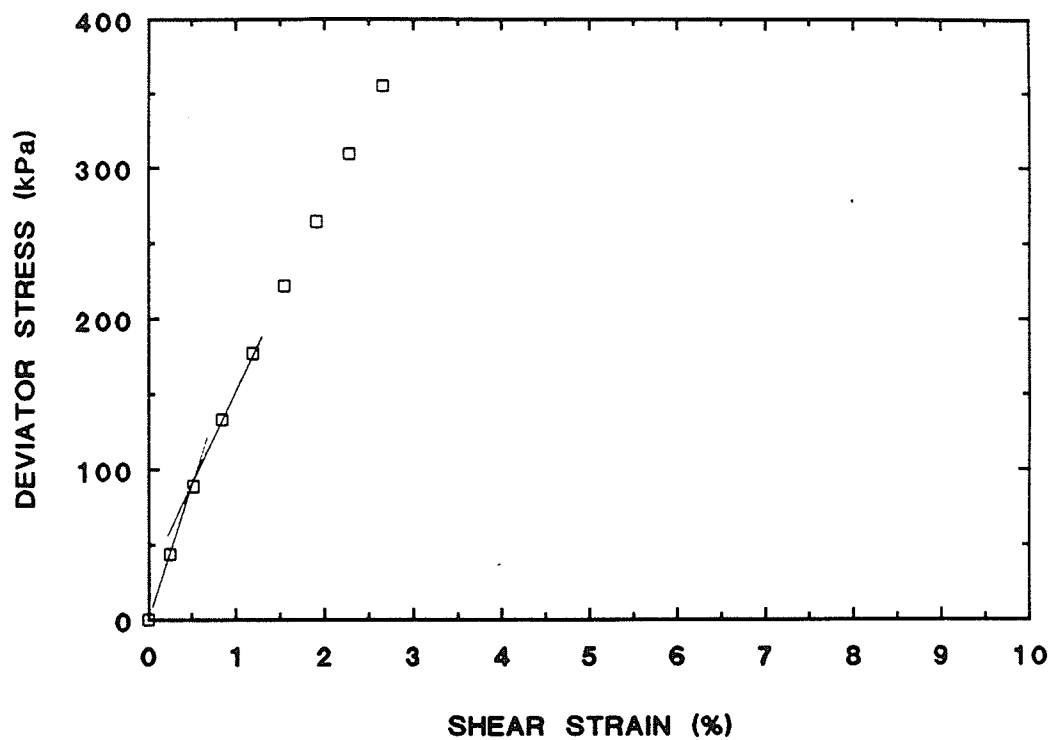
BUFFER SPECIMEN T1140
DRY DENSITY = 1.67 Mg/m³



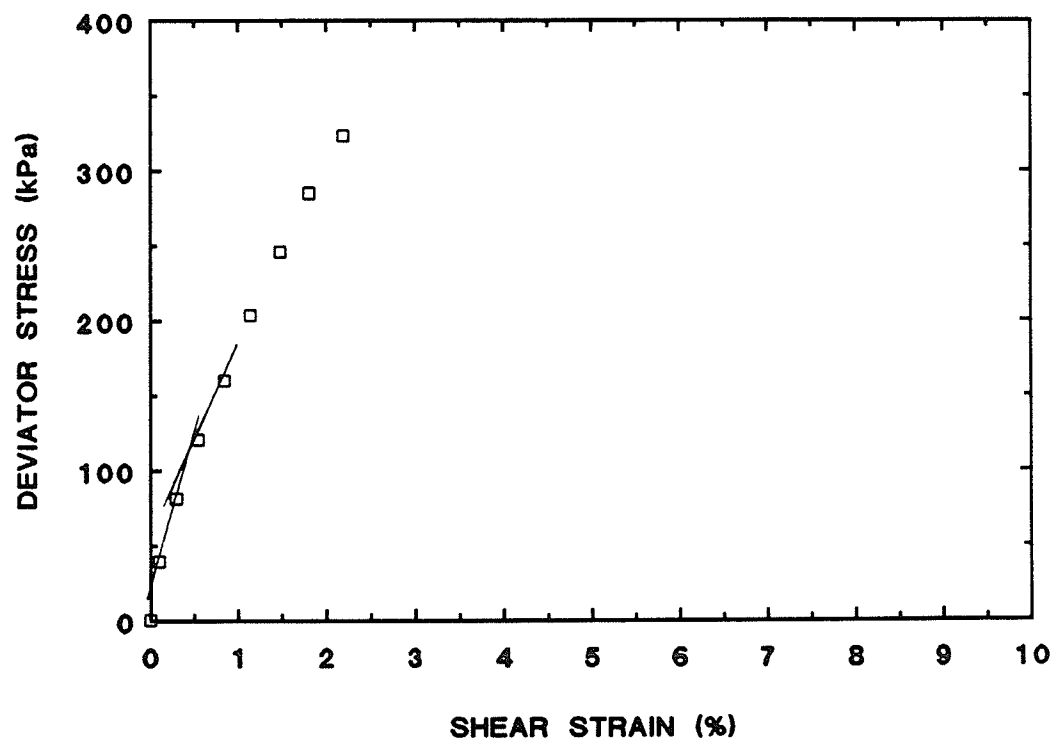
BUFFER SPECIMEN T1141
DRY DENSITY = 1.67 Mg/m³



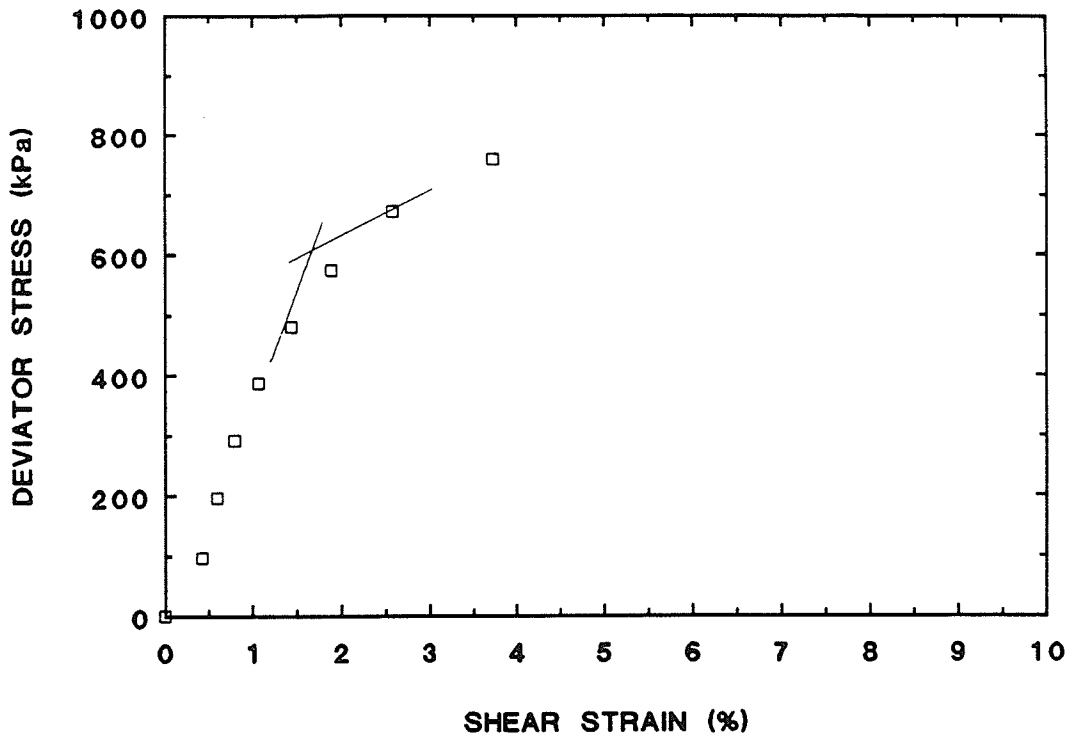
BUFFER SPECIMEN T1144
DRY DENSITY = 1.49 Mg/m³



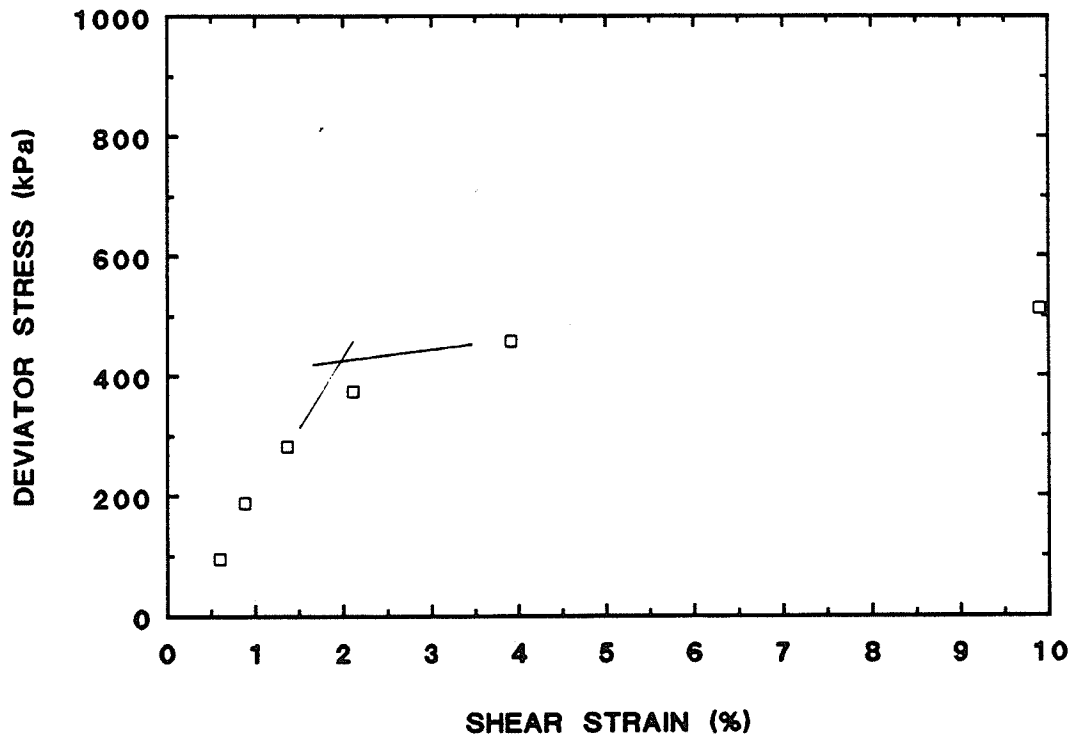
BUFFER SPECIMEN T1145
DRY DENSITY = 1.48 Mg/m³



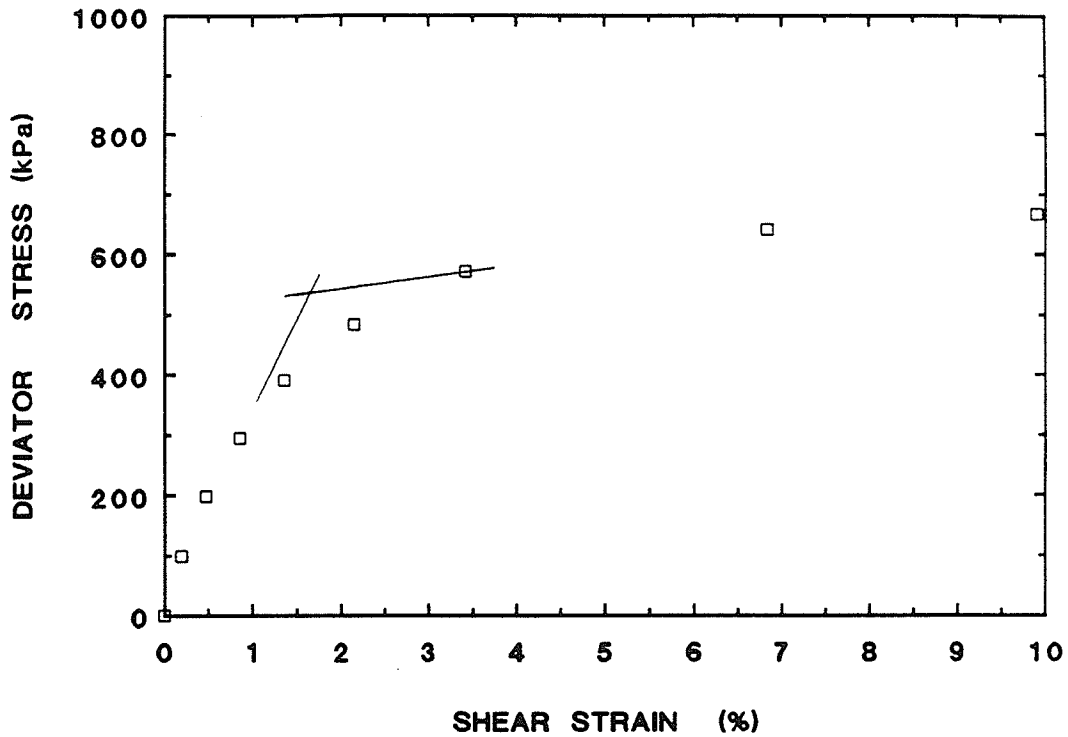
BUFFER SPECIMEN T1146
DRY DENSITY = 1.67 Mg/m³



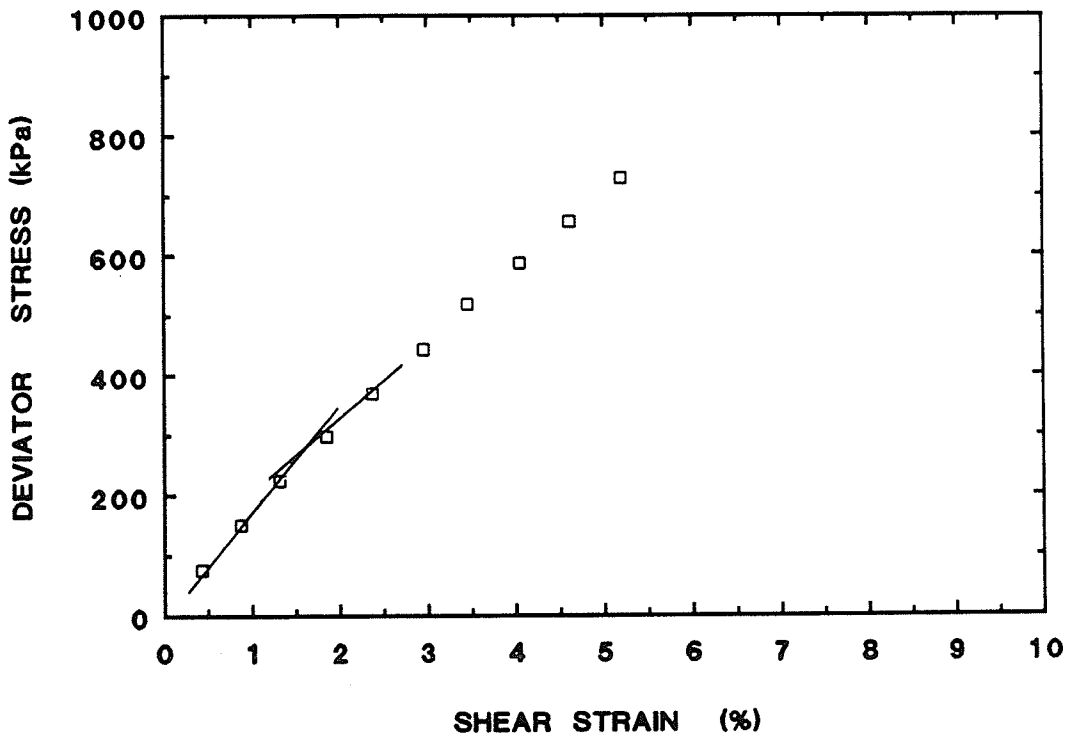
BUFFER SPECIMEN T1147
DRY DENSITY = 1.66 Mg/m³



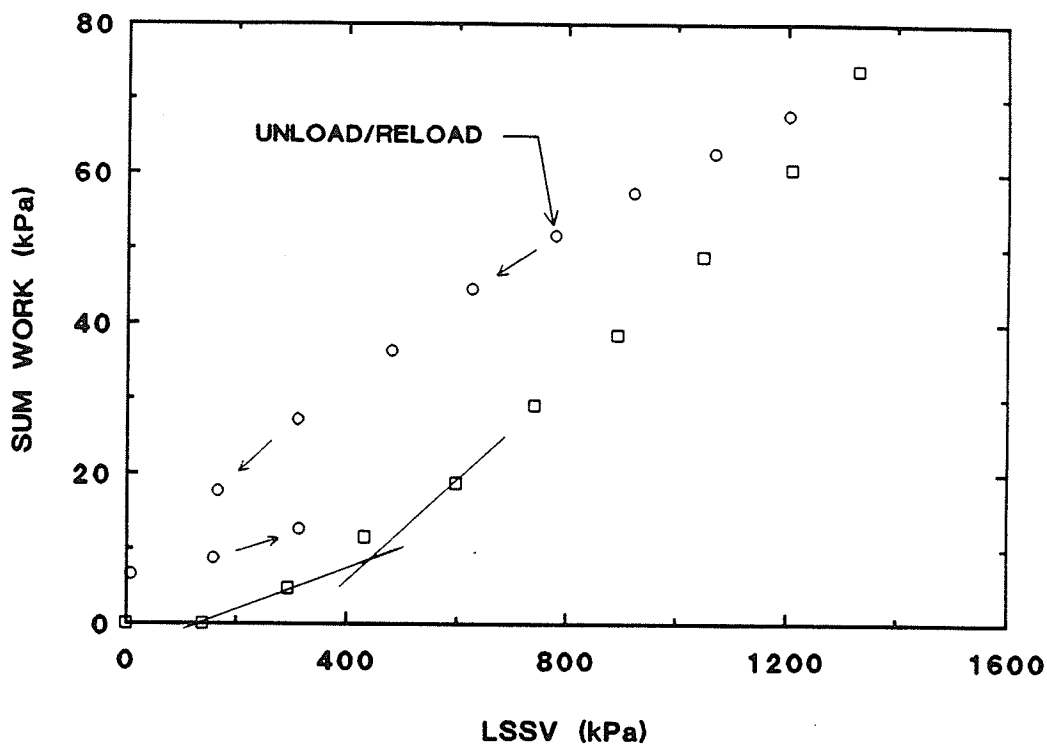
BUFFER SPECIMEN T1148
DRY DENSITY = 1.67 Mg/m³



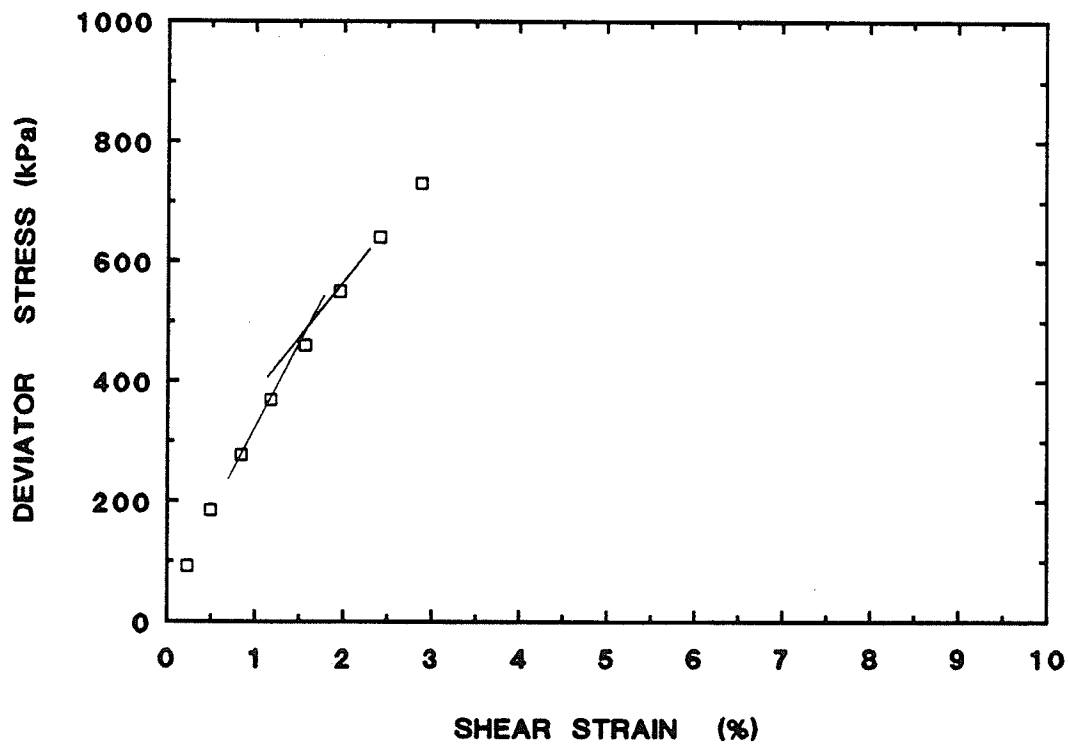
BUFFER SPECIMEN T1149
DRY DENSITY = 1.67 Mg/m³



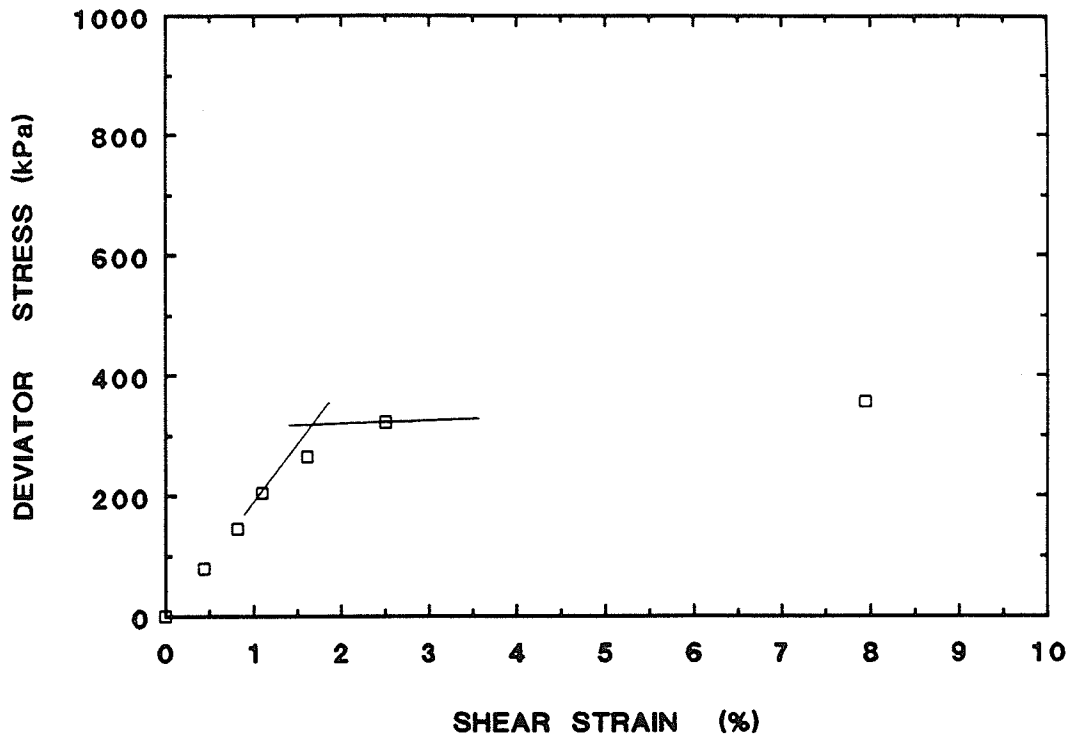
BUFFER SPECIMEN T1150
DRY DENSITY = 1.68 Mg/m³



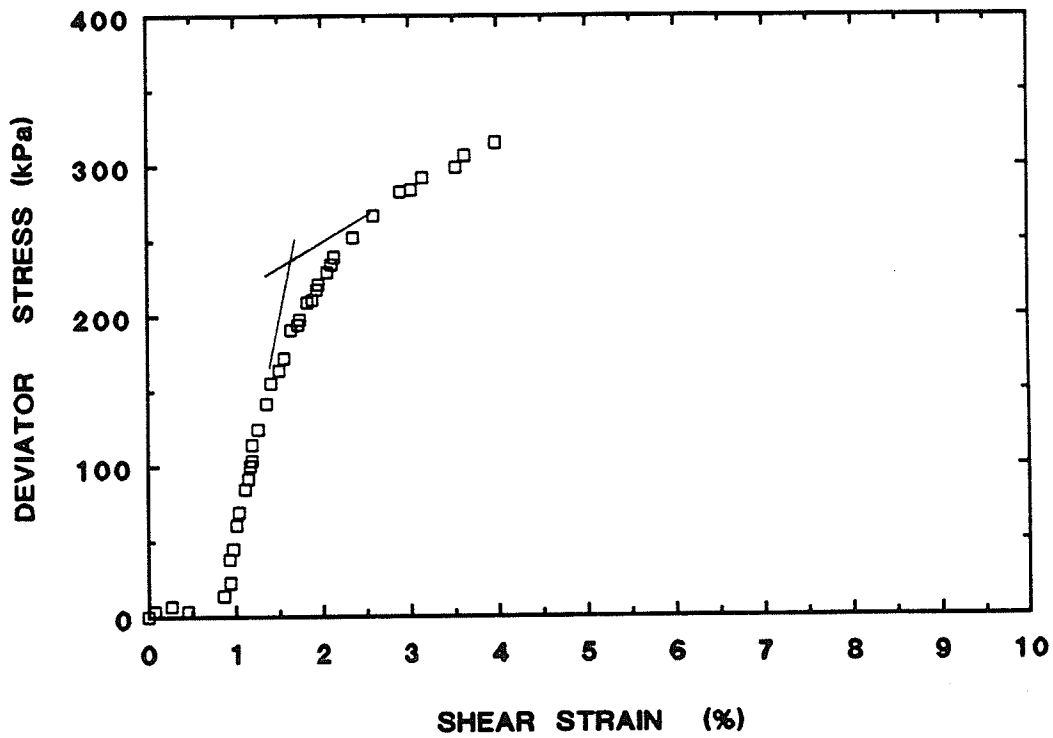
BUFFER SPECIMEN T1151
DRY DENSITY = 1.69 Mg/m³



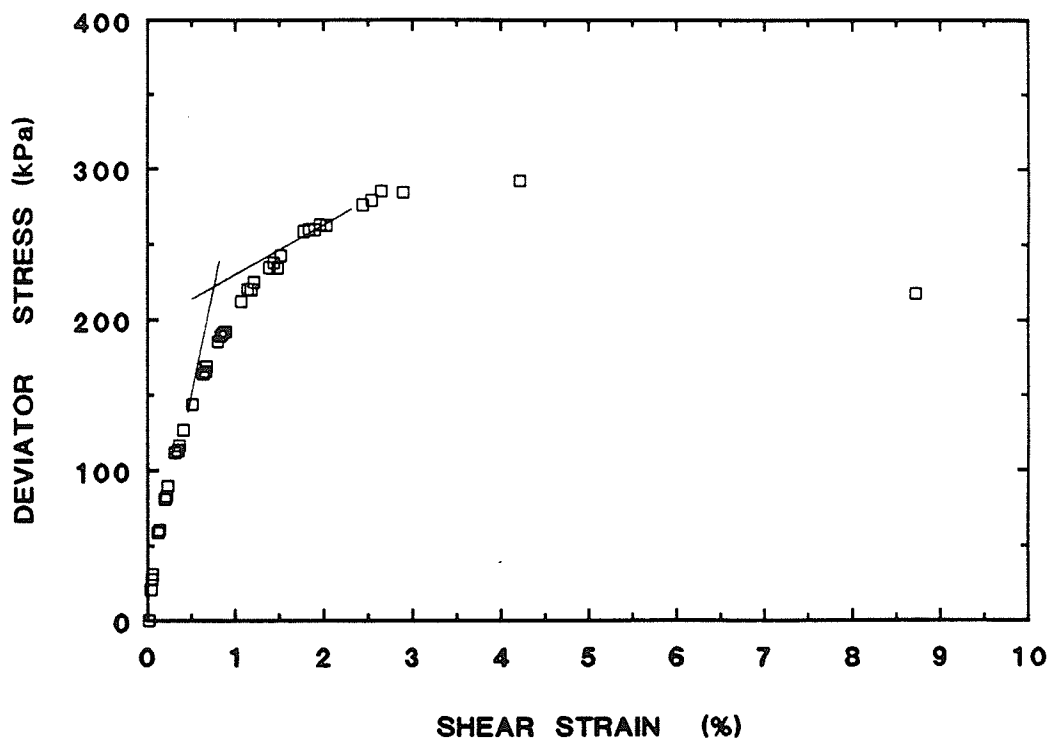
BUFFER SPECIMEN T1152
DRY DENSITY = 1.65 Mg/m³



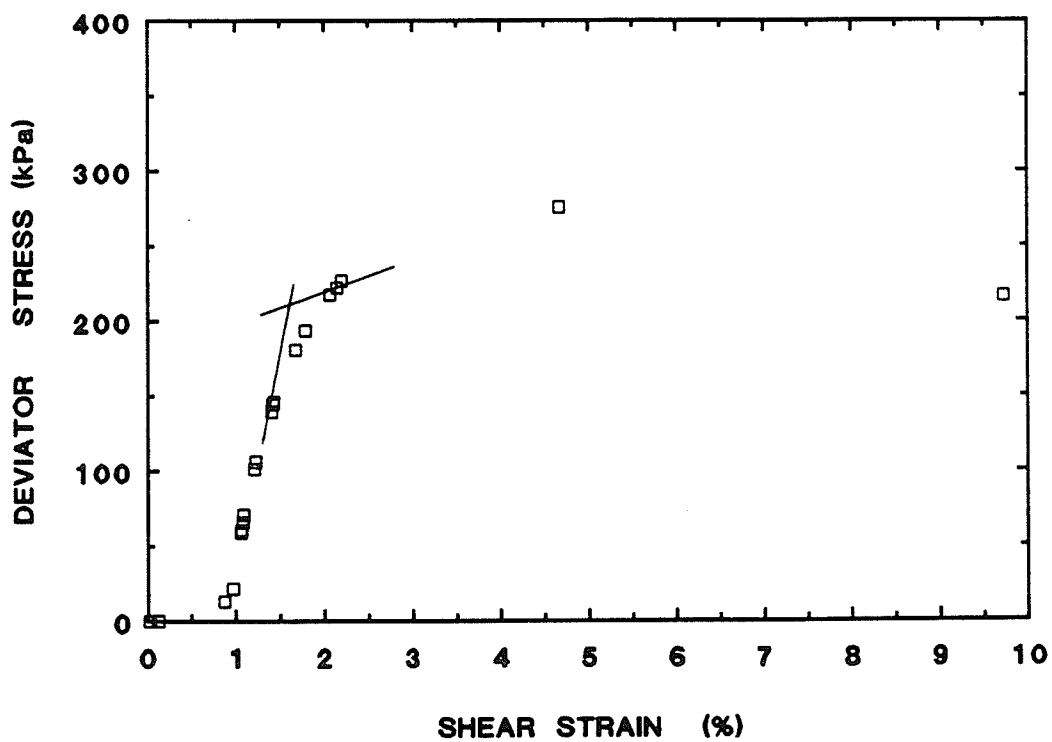
BUFFER SPECIMEN T1153
DRY DENSITY = 1.47 Mg/m³



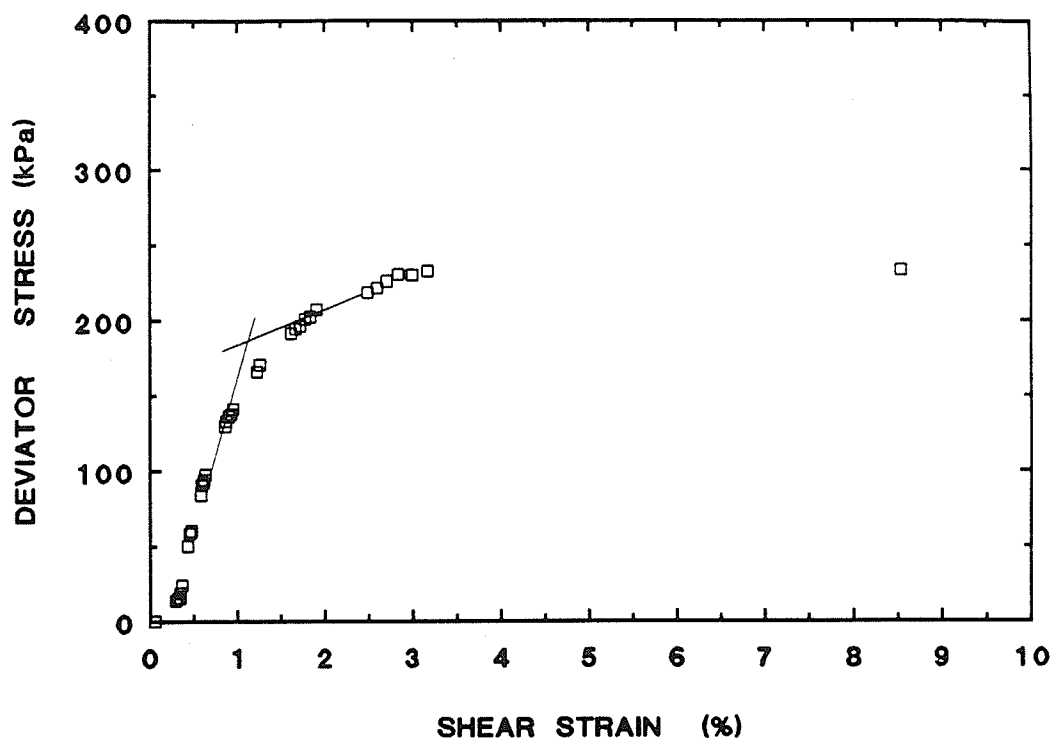
BUFFER SPECIMEN T1154
DRY DENSITY = 1.47 Mg/m³



BUFFER SPECIMEN T1155
DRY DENSITY = 1.48 Mg/m³



BUFFER SPECIMEN T1156
DRY DENSITY = 1.50 Mg/m³



June 1, 1993

Helen Agar, Thesis Officer
Faculty of Graduate Studies
University of Manitoba
Room 500, University Centre

RE: Publication of "Elastic Plastic Behaviour of a Sand-Bentonite Mixture" by
J.M. Oswell (1991)

Dear Helen:

I hereby give my permission to J. Oswell and the Faculty of Graduate Studies to publish the following co-authored paper in Oswell's thesis according to the copyright guidelines set out by the University of Manitoba for publication of theses:

James M. Oswell, James Graham, Brian E. Lingnau, and Martin W. King, "Use of Side Drains in Triaxial Testing at Moderate to High Pressures: Technical Note", ASTM Geotechnical Testing Journal, Vol. 14, No. 3, September, 1991, pp. 315-319

The applicable terms and conditions of publication are given in two documents: (1) the "Thesis Copyright License" form signed by J. Oswell and (2) form NL-0091 "Non-Exclusive License to Reproduce Theses" also signed by J. Oswell.

J. Graham, DSc., PhD.
Professor of Civil Engineering

June 1, 1993

Helen Agar, Thesis Officer
Faculty of Graduate Studies
University of Manitoba
Room 500, University Centre

RE: Publication of "Elastic Plastic Behaviour of a Sand-Bentonite Mixture" by
J.M. Oswell (1991)

Dear Helen:

I hereby give my permission to J. Oswell and the Faculty of Graduate Studies to publish the following co-authored paper in Oswell's thesis according to the copyright guidelines set out by the University of Manitoba for publication of theses:

James M. Oswell, James Graham, Brian E. Lingnau, and Martin W. King, "Use of Side Drains in Triaxial Testing at Moderate to High Pressures: Technical Note", ASTM Geotechnical Testing Journal, Vol. 14, No. 3, September, 1991, pp. 315-319

The applicable terms and conditions of publication are given in two documents: (1) the "Thesis Copyright License" form signed by J. Oswell and (2) form NL-0091 "Non-Exclusive License to Reproduce Theses" also signed by J. Oswell.

Brian Lingnau, M.Eng.

JUL 22 1993



The University of Manitoba
Inter-Departmental Correspondence

DATE: 21 July 1993
TO: Helen Agar, Thesis Officer
FROM: Martin W. King, Clothing & Textiles
SUBJECT: Publication of "Elastic Plastic Behaviour of a Sand-Bentonite Mixture" by J.M. Oswell (1991)

I hereby give my permission to J. Oswell and the Faculty of Graduate Studies to publish the following co-authored paper in Oswell's thesis according to the copyright guidelines set out by the University of Manitoba for publication of theses:

James M. Oswell, James Graham, Brian E. Lingnau and Martin King, "Use of Side Drains in Triaxial Testing at Moderate to High Pressures: Technical Note", ASTM Geotechnical Testing Journal, Vol. 14, No. 3, September, 1991, pp. 315-319.

The applicable terms and conditions of publication are given in two documents: (1) the "Thesis Copyright License" form signed by J. Oswell and (2) form NL-0091 "Non-Exclusive License to Reproduce Theses" also signed by J. Oswell.